Laser Powder Fusion of H13 tool steel using pulsed Nd: YAG laser

by

A. Dwarkanath

Master's thesis

Submitted in partial fulfilment of the requirements for

the award of

Master of Philosophy of Loughborough University

(October 2002)

Abstract

Laser Powder Fusion, has been used to explore the possibility of fabricating 3-dimensional parts from Computer Aided Design (CAD) data, using the underlying philosophy of 'Rapid Prototyping' or 'Freeform fabrication' techniques. Such techniques have emerged in the past decade or so, as a revolutionary way of designing and realising products primarily for form, fit and functionality. Applications have evolved in the areas of automotive, aerospace, medicine to name a few. The Laser Powder Fusion technique, is characterised by the use of a heat source, like a laser or electron beam used for melting or fusing powder material like metal, polymers etc to the required geometry, by tracing and filling in (or rastering) 2-dimensional contours, line by line, layer upon layer, to obtain the 3D geometry.

The motivation for the present work comes from the use of this technique for fabricating components with enhanced functionality, for applications in production and prototype tooling, engine parts etc. The future aim is to incorporate multiple materials fused under the heat of a laser beam. These materials could possibly be dispersed spatially in a graded manner, to aid the realisation of a concept called 'Functionally Graded Materials (FGM)'.

Tracks of fused beads, using Tool steel (H13) material, were processed to a length of 30mm on a substrate plate 40 x 40mm in size. A Nd: YAG laser was used to deliver the required energy, at the focal zone. Process parameters were varied in accordance to data established from initial graphs, which indicated the range of input parameters for which Output could be achieved. Pulse parameters, pulse width, pulse frequency and energy were varied in conjunction with scanning speed in order to complete each individual scan.

Every scan was repeated five times on a substrate plate, for one set of parameters. The entire set of experiments was undertaken for two levels of powder layer thickness, 1mm and 0.4mm respectively. Resultant beads were measured at various points for height, width and the resulting data plotted against variations in pulse parameters and speed.

It was found that both height and the width of a bead varied with pulse parameters, pulse width (or pulse duration) and pulse frequency. At both layer thickness, values of bead width and bead height were generally found to increase along with increasing pulse width and frequency. Maximum values of bead width and height reduced at increasing speeds. The range of bead width and height remained similar for a set layer thickness, for variations in speed and also energy levels.

Acknowledgement

Table of Contents

1. Introduction

Powder fusion of metallic materials, for producing functional parts has evolved as an outcome of recent developments in laser sintering, laser cladding and the field of Rapid Prototyping or Solid Freeform fabrication [1][2][3][4]. The past decade has witnessed growth in a number of processes, that use powder fusion of metallic components using a laser beam and quite a few of them have been reported to produce parts of near-full to full density by the melting process [1]. The parts produced nevertheless require post-processing operations, like machining, to be brought to final dimensions and accuracy. The techniques by and large have looked very promising in application areas for direct fabrication of injection moulding and die-casting tools and also for repair and overhaul of military, commercial aerospace and automobile components where expensive parts can be re-used and their life extended [5][6][7].

The techniques could also be promising for producing thermally efficient and better designed production tools in moulding applications. Fabricating Injection moulding tools having conformal cooling channels could lead to reduction in cycle times and has been a subject of recent exploration [8]. Materials like Copper have been incorporated in the core of the mould with the outer surface being fabricated of a material like tool steel [9]. Such bi-material compositions incorporated in a single component can be described as 'tailoring' of material properties for that particular component. Negative, undesirable effects due to the differences in physical, thermal and chemical properties that may affect service life due to cracking at the interfaces, delamination etc, can be avoided by grading

the material interface. The result being that the material composition gradually changes in profile, across the component [10].

This work in the area of fully dense tool steel fabrication was expected to be an input to future work in exploring the possibility of fabricating materials with graded composition, 'Functionally Graded Materials' (FGM), by fusing multiple materials under the laser beam.

Additive fabrication technologies have emerged in the past decade or so, and are jointly referred to as 'Rapid Prototyping (RP)' or 'Freeform fabrication techniques' [11][12][13]. The techniques are used to construct parts by processing materials into complex geometrical shapes directly with the aid of 3-dimensional (3D) Computer Aided Design (CAD) model data. The process effectively involves splitting a solid 3D CAD model into thin 2-Dimensional cross-sectional layers. These layers are then physically realised using one of the many RP techniques, which carry out the task of building the 3D model as shown in Figure 1.1

One of the well-known processes used to build parts in such fashion is the Laser Sintering (LS) process. In this process, a laser beam is used to selectively sinter materials that range from nylon to thermoplastic binder coated steel powder. The technique makes use of pre-placed powder material deposited or spread on a powder bed or substrate, which is then subsequently sintered or fused by a laser. The laser selectively traces the geometric contour of each layer (slice), which is then filled with hatch patterns to generate an equivalent 2D solid layer of finite thickness. Subsequent layers are deposited or spread and fused on top of the previous layer to realise a three dimensional object.
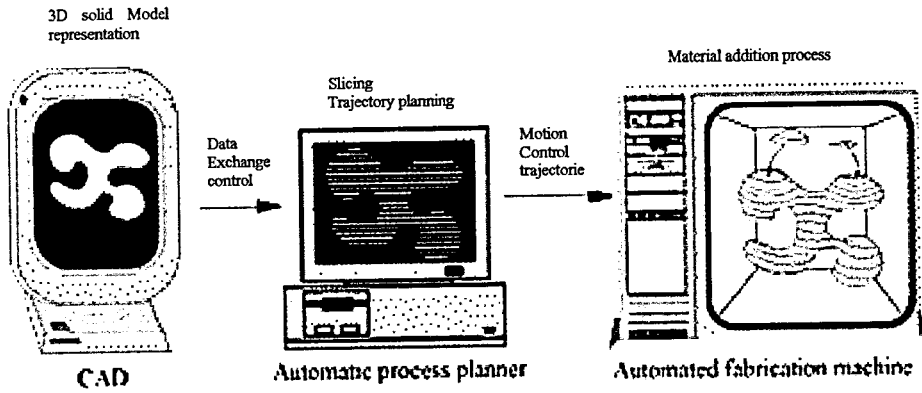
Figure 1.1: Basic Rapid prototyping concept
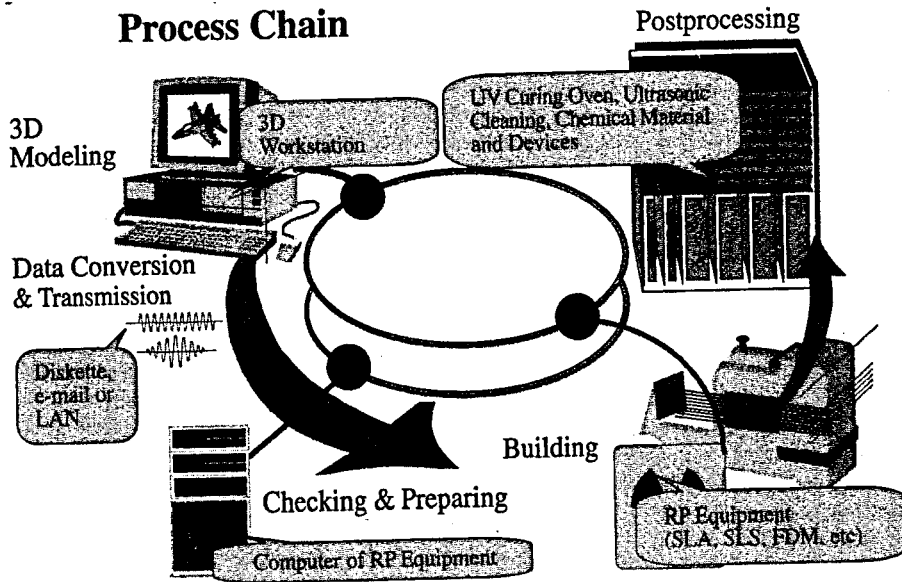
Figure 1.2: Process Chain for the Rapid Prototyping process [14]

The rapid prototyping process chain in highlighted in Figure 1.2 and an overview of Rapid Prototyping technology is represented in Figure 1.3, depicting four major aspects of the technology viz. the solid model input formats, range of materials, the various fields of applications including aspects of engineering and the methods and technologies used by various RP processes.

The technique as mentioned before, can be used to generate metallic parts from materials such as tool steel where the powder melts and solidifies under the influence of a laser beam. It can be used to produce both direct and indirect tooling for small- scale production or prototyping. The ability to construct complex geometry, can effectively be combined with the ability of laser fusion techniques to produce multiple material parts with enhanced functionality. For example, an increase in thermal conductivity of moulds could reduce cycle times and result in less cooling channels being necessary. To achieve this, graded regions of multiple materials with compositionally or structurally varied functionality, within the same component or tool would be necessary. Rapid prototyping and Rapid Tooling are now a novel way of producing near-net shape tools, dies and inserts. Such tools with graded regions of multiple materials could have a high thermal conductivity material close to critical areas, which would effectively enhance the functionality and life of the tool. A similar concept would be true for engines e.g. near the walls of the cylinder. Hence, the idea of producing parts in production grade materials like tool steel in combination with a high thermal conductivity material would become an interesting possibility.

This work undertook preliminary investigations into Nd:YAG laser fabrication of preliminary scan paths for a single material, H13 tool steel. It investigated the parameters that would produce a solidified metal structure (bead) and recommend further work towards the realisation of 3-D blocks (cubes) of the same material.
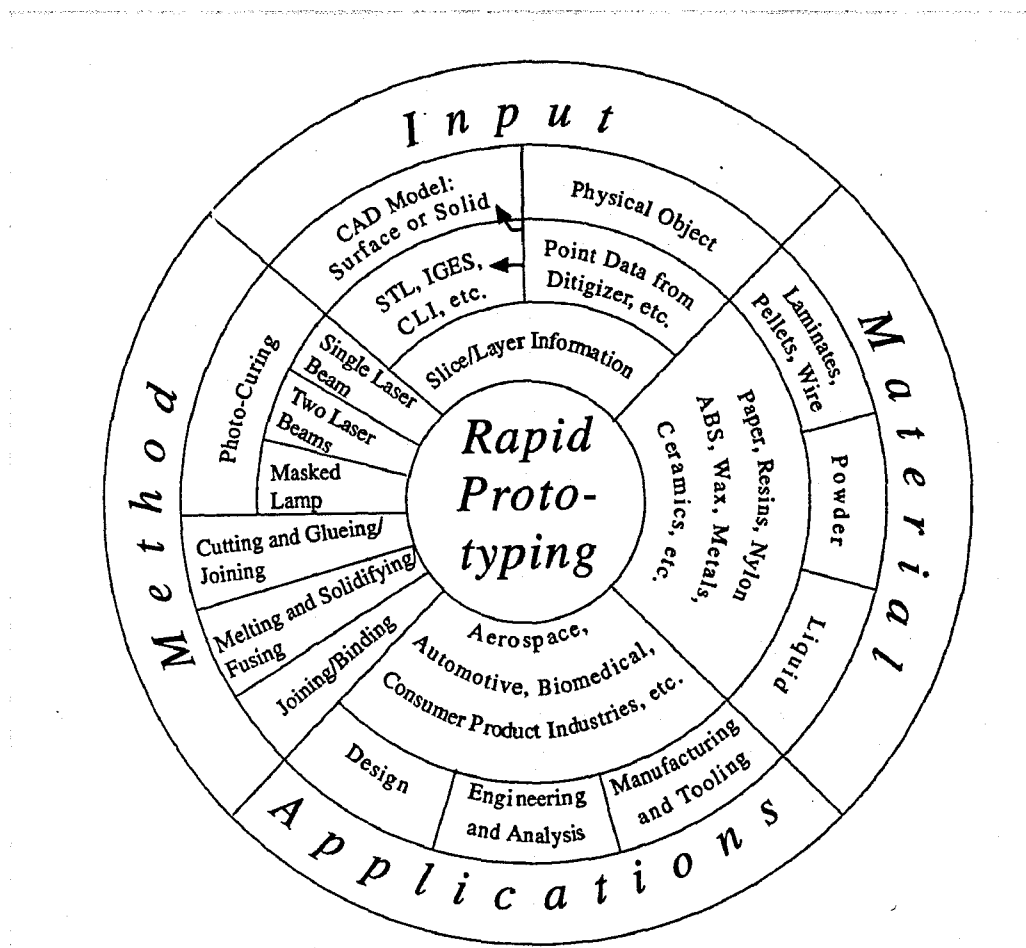
Figure 1.3: The Rapid Prototyping Wheel depicting four major aspects of RP [1]

2. Direct Metal Fabrication

The chapter covers the area of prototyping of metallic parts using Laser based techniques using direct and indirect methods of manufacture. Broadly the chapter focuses on processing by laser sintering and by laser cladding operations.

2.1. Direct fabrication by laser sintering

This section describes two techniques, commonly in use for the processing of metal parts using rapid prototyping principles, Laser Sintering (LS) and Laser Generating (LG).

2.1.1. Pre-placed Powder techniques (Laser sintering)

These techniques are available commercially in the form of Rapid prototyping machines, which generally use proprietary materials. The main processes are Laser Sintering (LS) offered by 3D Systems Inc. USA and Direct Metal Laser Sintering (DMLS) offered by EOS GmbH, Germany [15][16][6][17][18]

A schematic diagram of the LS process is shown in Figure 2.1.
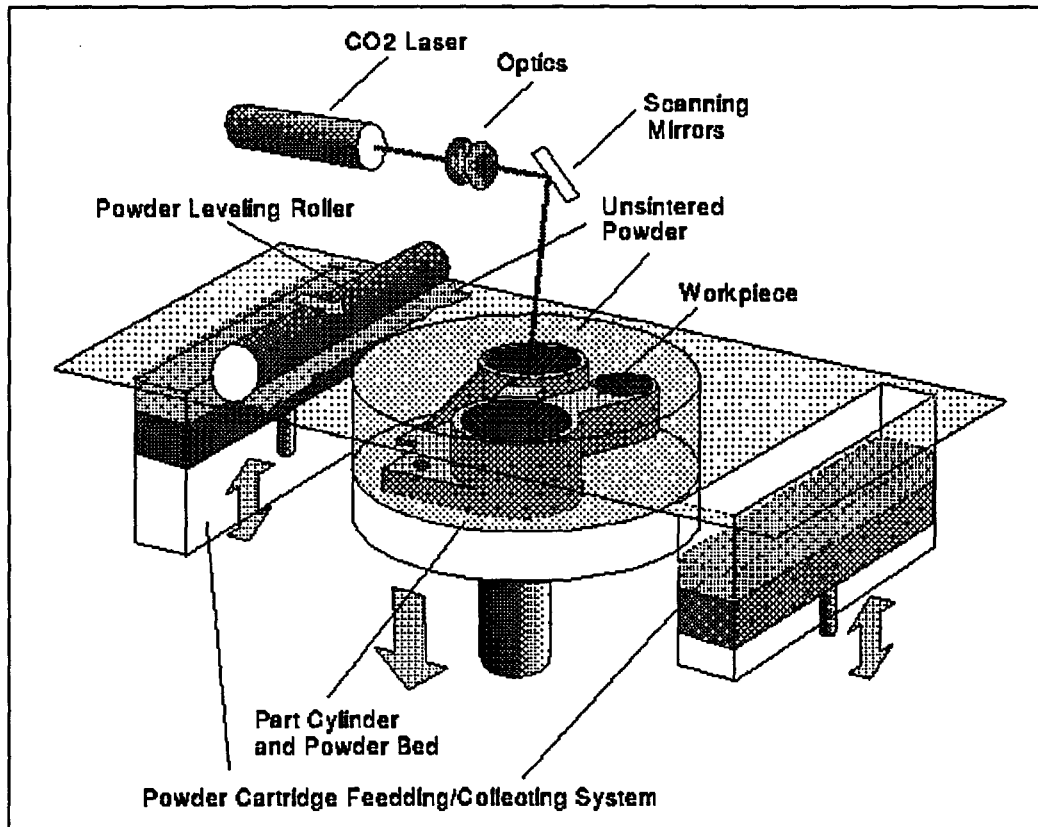
Figure 2.1: Schematic drawing of the LS process [19]

The 3D Systems' LS process involves the use of a high power laser beam, which selectively melts and fuses powder material along a path governed by 3D CAD model data. The process begins with a very thin layer of heat fusible powder deposited by means of a mechanical roller on the work bed and heated to a temperature just below its melting point. The laser then traces the path of the component to be fabricated, raising the temperature of the powder to its sintering point, effecting bonding or consolidation. The table is then lowered through a distance corresponding to the layer thickness e.g. 0.1 mm, before the roller

spreads the next layer of powder onto the previously built layer and the cycle is continued till the component is complete. The powder remains loose in unsintered areas and acts to support the following layers of powder, sintered or loose. The entire process is carried out in an enclosed chamber of an inert gas (nitrogen) to prevent oxidation of the powder. After the fabrication is complete, the excess loose powder is shaken off to reveal the fused component [20].

A photograph of a commercial LS machine offered by 3D Systems is shown in Figure 2.2.

Figure 2.2: The LS machine by 3D Systems Inc.

Some of the materials used in the process are: Wax, engineering thermoplastics such as Polycarbonate and Nylon [21][22], glass filled nylon, polystyrene for investment casting patterns [23], metallic materials such as steel/copper matrix material with a thermoplastic binder. The binder coated metallic powder is used in the patented Rapid Tool™ process (shown in Fig. 2.3) to create mould cavity and core inserts for prototype tooling [24].

The scan pattern and exposure parameters will be major factors in determining part properties [14]. The packing density of the powder is also a crucial factor in

determining the mechanical properties of the part after sintering. Particle packing densities of 50 to 62 percent are reported for commercial sintering process with uniform sized particles [14].

The advantage of sintering or sinter bonding with the aid of a thermoplastic binder over direct melting and fusing is the avoidance of the liquid phase, hence subsequently avoiding associated distortions caused by the flow of molten material. In the fusion of binder coated metallic powder, the binder is later burnt out leaving a porous metal part. The part is later infiltrated with a low melting point material like Copper to achieve a more dense component [14].

One other way of effecting greater density in parts is the use of the principle of Liquid Phase sintering as a means of enhancing the sintering behaviour of a powder material [25]. This could be achieved by using a Liquid Phase metal in a solid phase powder, such as Copper in Nickel. Densities up to 82 % have been achieved [26]. Sometimes the process when used to liquid phase sinter metal powder can be used in conjunction with Hot Isostatic Pressing (HIP) in order to produce a full or near full dense component [27][28] This has been carried at the University of Texas, Austin, where the LS process was first invented.

Materials that were processed included Inconel 625, Stainless Steel, Titanium Ti-6Al-4V and Molybdenum. The LS machine was modified for atmosphere controls and laser systems (a Nd:YAG laser) to process high temperature metals. The concept itself included producing an integral skin and core part, with the skin having almost full density and the core being about 70% dense. This was later subjected to the HIP process and fully dense structures were seen for

Inconel single layers with some porosity for multiple layers. Stainless steel was seen to give a nearly fully dense microstructure [27].
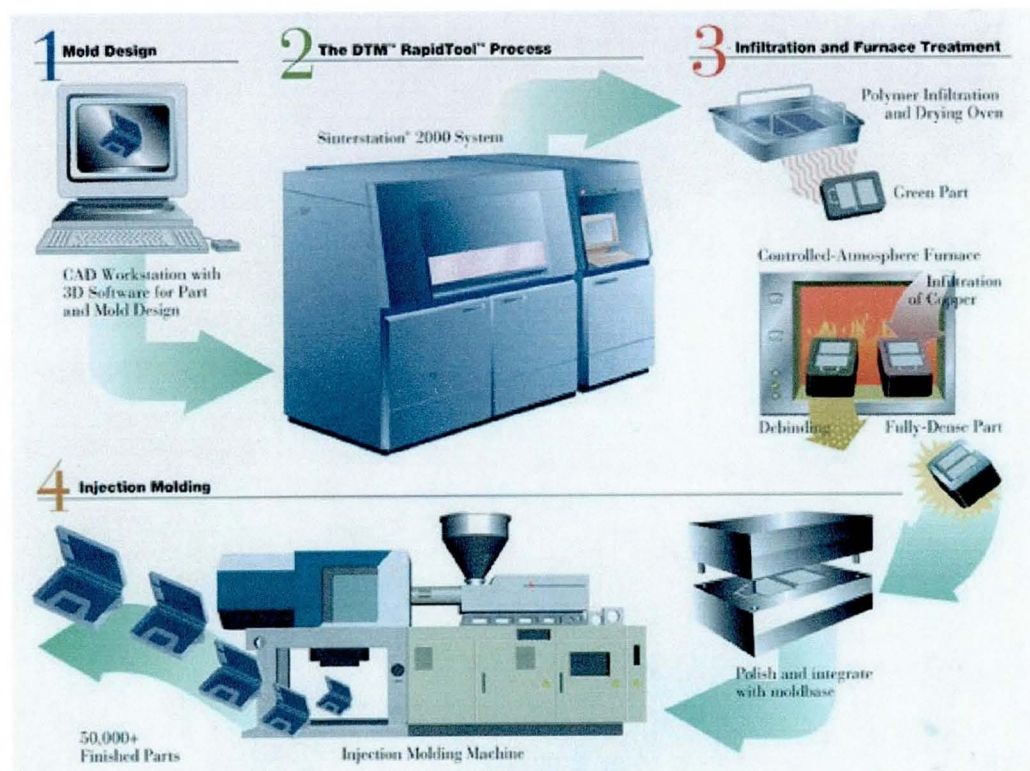
Figure 2.3: The Rapid Tool™ Process [29]

A preliminary study of laser sintering of pure metals has revealed that a copper block produced in a nitrogen atmosphere was consolidated to a density of 52%[30].

2.1.2. Laser Generating (deposition based)

Laser generating (LG) is based on the laser cladding [33] technique. Here metallic powder is delivered into the focal zone of the laser beam as opposed to scanning the surface of a pre placed powder layer. The material melts or fuses due to the intense heat energy of the beam at the focal zone. Figure 2.4 shows the LG process at the focal zone.

Prominent amongst commercial processes that offer this type of rapid prototyping of materials is the LENS™ (Laser Engineered Net Shaping) process [34].

The LENS™ process consists of a high-power Nd:YAG laser, a glove box with controlled atmosphere, a 3-axis CNC positioning system and a powder feeder unit. The powder feeder unit is composed of delivery nozzles (as seen in Figure 2.5a and 2.5 b), which is designed to inject the powder stream directly into the focussed laser beam. The beam creates a weld pool on the substrate into which the powder particles are injected to build up each layer. The substrate moves beneath the laser beam, thus facilitating formation of the required geometry of the part, again from 3D CAD data, as in the case of other Rapid Prototyping technologies. After a single layer has been deposited, the powder delivery nozzle and the focussing lens assembly are incremented in the positive z-direction for generating the next layer. This process is repeated until the part is complete.

Solid parts with complex internal and external features have been built to near-net-shape with this process and subsequently machined to final accuracy and surface finish requirements [35]. Fully dense parts have been obtained using materials like Alloy 625, Alloy 690, 316 Stainless Steel powder [1].

Applications include producing injection moulding and die-casting tools (Figure 2.6) [35][36], along with repair and overhaul of engine components [5]. Materials like H13 tool steel for injection moulding applications as shown in Figure 2.7, Inconel 625 (nickel based alloy) and Titanium alloy (Ti-6Al-4V) are reported to have been used for repair and overhaul of components like turbine blades [5].
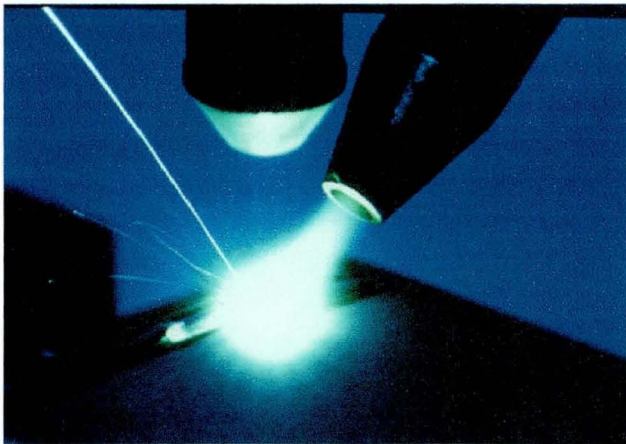
Figure 2.4: The LG process at the focal zone
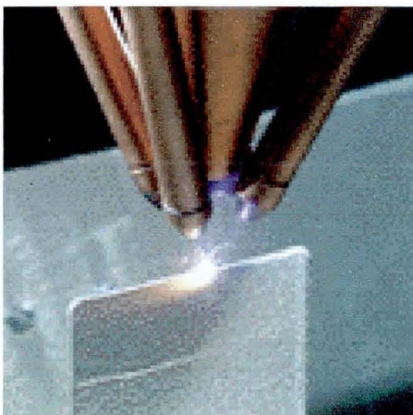
Figure 2.5a: The LENS™ process performing a single line build [31]
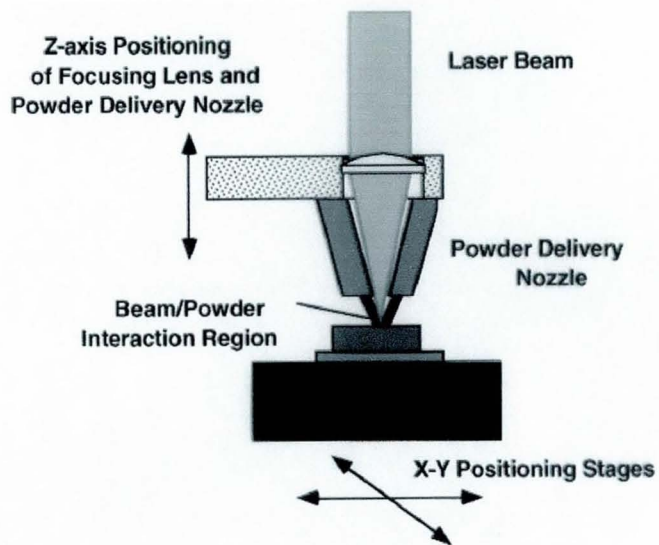
Figure 2.5b: Schematic of a powder deposition process [32]
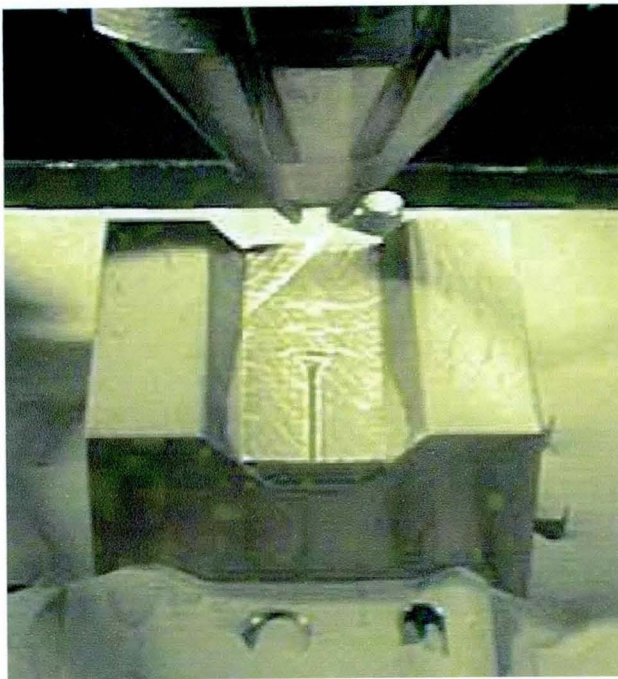
Figure 2.6: H13 tool steel Die Casting Tool using LENS process [37]

Figure 2.7: Injection moulding tool by LENS process [37]

Other processes have evolved which use a similar principle to LENS™, also using Laser Powder Deposition techniques. These are:

Directed Light Fabrication (DLF), invented at the Los Alamos National Laboratory, USA. In this process, metal powder is carried by an argon gas stream, which then enters into the focal zone of a laser beam, where it melts and forms a molten pool of material. The pool moves with the laser spot to create a solidified three-dimensional bead [38][39]. The system has powder feeders attached for co-deposition of multiple materials, to create alloys at the focal zone or form dissimilar metal joint combinations by changing powder composition from one material to another. Iron based materials as well as stainless steels are used in the process[40]

Directed Metal Deposition (DMD) is a process developed at the University of Michigan, Ann Arbor and Stanford University. In DMD, a laser generates a melt pool on a substrate material while a second material is delivered into the melt pool either as powder or as a wire-feed that melts and forms a bond with the

substrate [41][42]. A schematic of the DMD process is shown in Figure 2.8a. The process is shown in its working condition in Figure 2.8b. The technology is now commercialised by the POM group. The process is claimed to be able to generate components like advanced tools with conformal cooling channels (Figure 2.8c) for thermal efficiency, by incorporating materials like Copper chromium at the core and tool steel at the surface [5]. The process is also reported to be used for depositing wear resistant and high temperature materials on to tool surfaces thereby increasing tool life and productivity. A number of cobalt based stellite and nickel based alloys have been used to fabricate bi-metallic tools for elevated temperature applications [5].
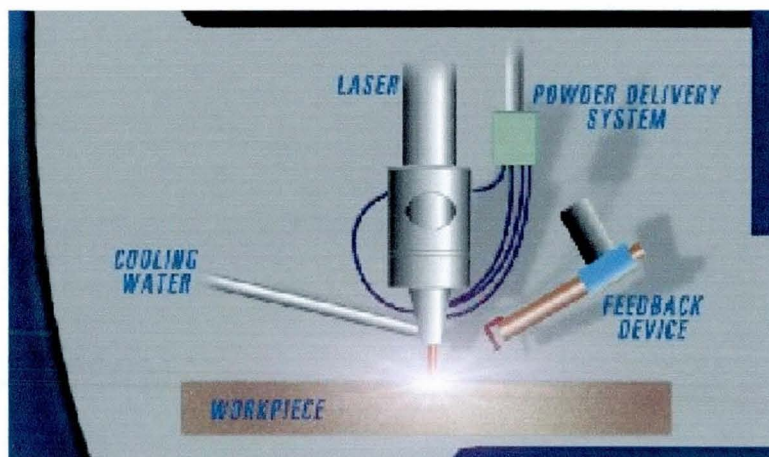
Figure 2.8a: Schematic of DMD [43]
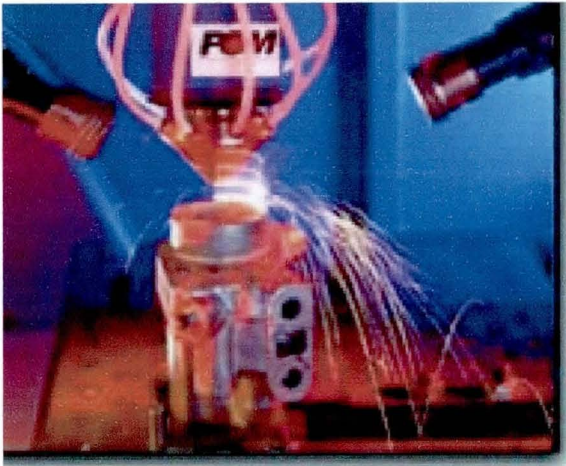
Fig 2.8b: DMD in action   [43]
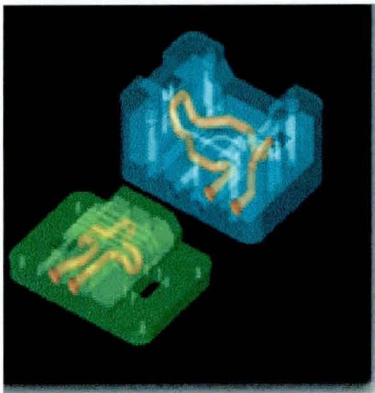
Fig 2.8c: Conformal cooling channels follow cavity of the tool [43]

Controlled Metal Build Up is a technique, which uses laser generating and welding along with conventional $2^{1/2}$ axis milling. This method is being developed at the Fraunhofer Institute in Germany [44].

A process known as " Laser consolidation (LC)" has demonstrated the possibility of producing fully dense metallic parts using Powder Deposition. This has been a result of work undertaken at National Research Council of Canada. Figure 2.9 a, b and c shows some of the parts produced by this technique [45].

In another method of fabrication, parts are built in a layer-by-layer fashion by feeding raw material in wire form into a melt pool maintained by an electron beam [46]. Electron beam Melting (EBM) has now been commercialised by Arcam AB. The materials used by the commercial process are H13 tool steel. Porosities less than 0.5% are reported [47].

Other techniques have been reported where a combination of arc welding [48] and 5-axis CNC machining has been used to produce metal parts [49]
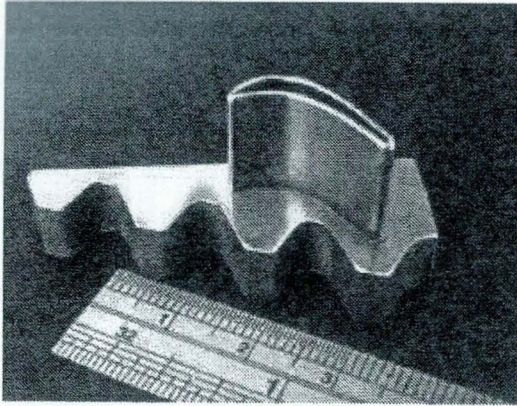
Figure 2.9 a: LC In-738 airfoil built on cast IN-738 substrate [45]
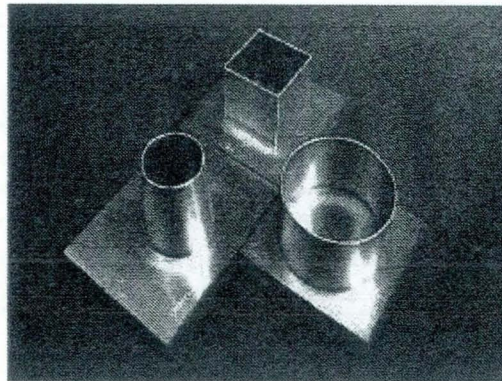
Figure 2.9 b: LC as-consolidated IN-625 samples [45]
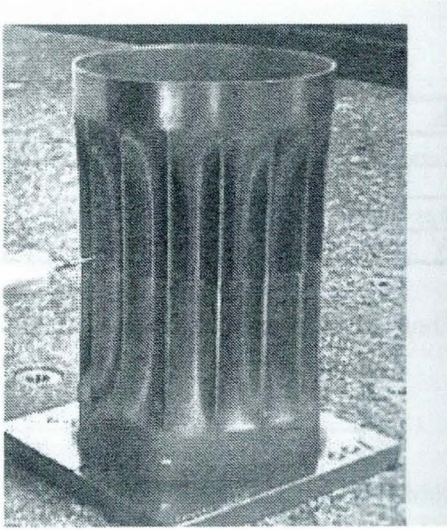
Figure 2.9 c: A complex consolidated IN-625 shell [45]

2.1.3. Other layer manufacturing routes for metals

Exceptions to laser based generating techniques, are those such as Shape Deposition Manufacturing (SDM) developed at Stanford University [50]. A weld-based deposition process was used to deposit material to near-net shape. The part was then transferred to a shaping station where it was machined to net shape using a 5-axis milling machine [51]. Thus the process used sequential steps of material deposition and removal to form 3Dimensional structures. One of the unique features of this process was that it created variable layer thickness dictated by part geometry [52]. Layer thickness ranged, from a few thousands of an inch to the practical limits of deposition and shaping equipment. The adaptive layer (variable layer height) splitting technique reduces the build time by reducing the number of layers to a theoretical minimum.

Other techniques such as 3-D Welding have been reported to produce metallic parts of superior properties but with limited complexity that also required finish machining operations [53].

3D printing is a process, which uses an ink-jet print head to deposit binder material on a layer of powder to selectively bind the material. Similar to how an inkjet printer achieves colour documents a 3D printer can use a print head with several jets to deposit binder and/or slurries of several materials and create controlled composition of the part, effectively realising the concept of FGM manufacture. This process was developed at the Massachussets Institute of Technology, USA [54]

A process called metalprinting™ is in development, which uses the principle of high speed photocopiers viz. photo masking and electrostatic attraction to deposit and consolidate materials of iron powder [55].

2.2. Significance and applications of lasers in manufacturing

Lasers are used in manufacturing today, for various applications including sheet metal cutting, drilling, spot welding, seam welding, surface modification of components and many other applications. They are used because of the tremendous advantages they have to offer. For example advantages in terms of their precision, low heat input capability, ability to be automated and precisely controlled by CNC programming, ability to produce very small heat affected zone producing low thermal distortion, ability to achieve high processing speeds, and of safety and their ease of operation.

The laser was first invented in the 1960's [56]. The acronym 'LASER' means Light Amplification by the Stimulated Emission of Radiation. It was found that certain materials like gases or crystals could be excited and be made to emit a particular light or a type of radiation. The first laser used a rod of ruby crystal as the material to be excited and since then a number of materials have been shown to 'lase' or produce laser light.

The lasing action is produced by excitation of a material and raising its energy state from low to high energy levels. Materials in the excited state show a tendency to return to the lower or ground state. During this process they emit energy in the form of a photon, which consequently results in a particular wavelength of light being emitted. Such photons are known to be mobile and they collide with other excited electrons stimulating them to release identical photon(s). This is known in laser theory as 'stimulated emission'. Continuation of this process, results in the 'amplification' of light energy by simultaneous emission of a number of photons resulting from the collision with excited electrons. The light is known to have a relationship between the photons, which move in step or phase with each other [57]. This is 'coherence' that is exhibited by a laser source. In addition to laser light being coherent in nature, it is known to have low divergence (typically expressed in radians) which means that the beam does not spread out very much. Coherence gives the light beam its ability to be focussed/concentrated to a very small spot size thus producing high heat energy to cut, weld or drill various materials.

The output of laser light is monochromatic, consisting of one or a small number of well defined wavelengths. These characteristics of laser light are considerably

different from an alternative heat source for example a light bulb, which would emit a highly divergent and incoherent light.

The most common lasers used in processing materials are the Carbon Dioxide, Nd:YAG and the Excimer laser. Figure 2.10 gives a diagrammatic sketch of a YAG laser. It consists of a cavity with the active medium Neodymium, Nd^{3+} ions, in a Yttrium Aluminium Garnet (YAG) crystal rod which has polished circular end faces. There are two mirrors positioned on each side of the laser rod. The rear mirror is a total reflector and the front mirror is partially reflecting through which the output beam emerges. In the cavity is also mounted a krypton (flash) lamp, whose emission spectrum suits Nd^{3+}. When an electric current passes through the flash lamp, pulses of white light are emitted. Some of the light, which is coupled into the laser rod, by the reflective pumping chamber is absorbed into the rod. Some of this absorbed light causes excitation of Nd^{3+} causing them to switch from a low energy to a high energy state. In the excited state the atoms are unstable and are accompanied by photon emission as they try to jump to lower energy states. A photon that passes near another excited Nd^{3+} would induce de-excitation with emission of another photon, hence called 'Stimulated emission'. The stimulated photon is coherent with the stimulating photon with the same frequency, wavelength, phase, direction and polarisation [58].

REAR   OPTIONAL   LASER ROD &   FRONT
MIRROR   COMPONENTS   FLASHLAMPS   MIRROR

Energy monitor

VIEWING   BEAM dump
HEAD   PROCESS
SAFETY   SHUTTER
FILTER   SAFETY SHUTTER

FOCUS LENS   B.E.T
                                           (UPCOLLIMATOR)

                                           HE - NE LASER
                                           (WHEN FITTED)
WORKPIECE

Figure 2.10: YAG laser (Working Principle) [58]

The emerging beam path is folded using two steering mirrors, one near the
energy monitor and the other close to the Beam expanding telescope (BET). The
former mirror is partially reflecting and allows for the beam energy to be
monitored, while reflecting most of the beam towards the latter mirror. This
mirror is a total reflector, which directs the beam via the BET and safety
(Process) shutter, the purpose of which is to intercept the laser beam when
output is not required and the flash lamps are energised. The beam is deflected
into the beam dump, by the totally reflecting mirror. When the shutter is 'open'
the BET has the role of increasing the beam diameter, because this has the effect
of reducing the divergence and therefore spot-size at the workpiece [58]. A
second function of the BET is to compensate for differences in the focal length

of the process lens for visible light and light at laser wavelength, thus making it possible that the laser beam focus becomes coincident to the visual focus, seen through viewing optics like a mounted camera.

One of the principal differences in the nature of light radiated from different types of lasers, is that they exhibit different wavelengths. The wavelength of a Nd:YAG laser would fall in the near infrared region of the electromagnetic spectrum. Its value being 1.06 microns. The wavelength of light emitted by a CO_2 laser is in the far infrared region with a wavelength of 10.6 microns. Excimer wavelengths fall in the Ultra-Violet (UV) zone of the light spectrum. The ability of metallic materials to absorb light energy of lower wavelength makes Nd:YAG (henceforth referred to as YAG) a suitable choice of laser for various cutting, drilling and welding applications. YAG lasers can also provide pulsed output – which is emission of energy over a shorter period (typically milliseconds) - giving increased peak power for metal cutting [57]. Carbon dioxide lasers with higher wavelength are known to be absorbed to a lesser extent by metals though their high average power output is known to induce a coupling effect, which increases the temperature to induce melting. They are particularly absorbed well by some materials like titanium and non-metals [57]. Excimer lasers have a limitation of very short pulse durations in the range of a few nanoseconds which restricts their use to applications like surface treatment, ablation of raw materials for thin film deposition, annealing etc [57].

2.3. Laser fusion of metal parts

Laser sintering or melting of metallic particles has been used to produce functional parts for various applications as covered in Section 2.2. The technology promises new applications given its flexibility in accommodating a great variety of materials and also for producing novel material properties for specific applications. The subsequent paragraphs highlight this aspect of using Lasers for part manufacture using the intrinsic philosophy of Rapid Prototyping techniques along with their capability to produce tailored materials, commonly known as Functionally Graded Materials (FGM).

2.3.1. Applications and possibilities

Laser powder fusion is characterised as a welding process, which is uni-directional and enables highly localised areas of a component to be built up of a metal or alloy without overheating the substrate, on which the part is built [59]. The small heat affected zone provided by the focal spot of the laser beam is highly advantageous as compared to excessive temperatures offered by other welding processes such as Tungsten Inert gas (TIG), Plasma and Electron Beam Welding.

Multi-material structures produced by Laser Powder Fusion and applied to areas in injection moulding and die-casting tools and Engine blocks could be an interesting possibility. It could be possible to construct materials like Copper that exhibit high thermal conductivity properties close to the cooling channels or

close to the walls of the cylinder thereby enhancing the heat transfer rate. A layered manufacturing process combined with metallic powder fusion would enable the construction of such components with multi-material properties whose composition, microstructure would be tailored to the desired functionality. An example of this has already been carried out using the Shape Deposition Manufacturing (SDM) process, wherein an injection moulding tool was constructed that transitioned from Invar in the centre to Stainless Steel on the outside of the tool. The resulting tool exhibited minimal distortion from thermal stresses and excellent exterior corrosion resistance [10]. Such tailoring of part for varying functionality over its cross-section has been defined as a Functionally gradient structure, in material terms a Functionally graded material. This topic is further covered in the following chapter.

2.3.2. The laser fusion process

Laser instigated powder melt formation occurs in an area where the beam is focussed to a diameter typically 0.5mm or 500 microns. This gives a melt pool with a diameter typically of 800 to 1000 microns [60]. It is this small diameter of localised heat input, which effectively distinguishes the laser powder fusion process or a laser welding process from other conventional welding techniques. Due to the small diameter of melt pool at the focal zone, the material is brought to its melting point in fractions of a second and also cools as fast. This results in a material that shows uniform distribution of elements in the microstructure

along with fine grains. Such material often has better strength than its equivalent solid parent material [57]. Hence the system could essentially be classified as a Rapid Solidification system where the laser illuminates small areas for definition of the part geometry and where the dwell time per unit area is of the order of milliseconds.

The thermal conductivity of a powder metal in a powder bed is less than its solid equivalent [57]. The heat produced by the beam is hence 'contained' within the small heated zone produced at the focus, causing the material to drastically increase in temperature within a short time and also cool at very high rates. If a molten pool at the focal zone were to be imagined to be spherical, then it would be easy to understand the high solidification (cooling) rates that are achieved at the spot. A sphere would in essence have a very large surface to volume ratio, one that is inversely proportional to the diameter of the sphere (the diameter being less than 1mm e.g. 800 microns) [60]. Tiny spheres would conduct heat from the surface, which in effect would have a very large in area in comparison to the small volume of the sphere where the heat was stored, hence resulting in high solidification rates. In reality, the molten pool is known to have a complex shape but is small nevertheless, with high solidification rates. Solidification proceeds from the bottom of the molten pool to its surface. This is due to the high thermal conductivity of the solid substrate in contact with the bottom of the pool and the low thermal conductivity of the powder bed, which makes the cooling rate slower at and around the pool surface [3].

Rapid solidification in itself imparts certain qualities to the metals and alloys that undergo such phenomenon. More uniform and size-refined solidification microstructures, largely eliminating the detrimental effects caused by segregation are formed [61]. Other literature on Rapid solidification processing suggests that it is a means of producing beneficial effects like chemical homogeneity, fine microstructures, extended solid solutions and metastable phase formation in metallic alloys [62].

To generate a three dimensional part by layerwise manufacturing, the process includes successive addition of layers on top of the previous, which in turn requires that sufficient adhesion/bonding be achieved to the substrate. It is also necessary that adjacent lines of solidified material, have a sufficient degree of overlap to ensure lack of porosity [3]. Dilution with the substrate or previously solidified layer can be kept very low as the beam can only act on the substrate through the powder, which has a low thermal conductivity and therefore melts first [63].

Dilution would be more of a concern where the parent material is different from the base material as in a coating by the laser cladding process, where it may be inadvisable to mix the two materials due to undesirable property alterations at the interface.

2.3.3. Possibility of Functionally Graded Materials (FGM) manufacture

The concept of Functionally Graded Material (FGM) generation is made more possible by the use of Laser Sintering and Laser Generating techniques.

2.3.3.1. Definition

A Functionally Graded Material has been defined as a material exhibiting spatially inhomogeneous properties and microstructure [63]. These materials are produced by gradually varying the composition of two or more materials across the surface, interface or bulk of the material. The materials are consequently able to exhibit the characteristics and functionality of the individual materials plus additional functionality derived from the graded composition.

2.3.3.2. Background

Functionally graded materials in the form of graded multi-layers have been the focus of considerable interest owing to their use in diverse applications as thermal-barrier and wear resistant coatings, thin film stacks or patterned lines in microelectronics, optoelectronics and magnetic storage devices, and also laminated composites [64]. Many components are subjected to mechanical, thermal or chemical loads which are unevenly distributed across the section. As an example, a turbine blade during the course of its service life will have to withstand high non-stationary heat fluxes and centrifugal accelerations. An ideal

structure for this application would consist of a tough metal core and a corrosion resistant ceramic at the hot surface of the blade (Figure 2.11). Where the ceramic is to be directly bonded to the metal, spalling may occur during thermal cycling, as very high stresses occur at the interface. In such a case, a gradient material, which has a smooth transition from the ceramic surface to the metal core, can avoid thermo-mechanical stress concentration at the interface [65].

The concept of FGM has also been applied to develop sintered hard materials for the metal cutting industry as opposed to the normally used cemented carbide and cermets. The aim here is to distribute the functionality of the material between the surface and the core and to use the thermal stresses actively to improve performance through grading the composition (Figure 2.12) [66].

FGM made using 3D printing techniques were investigated for wear resistance and increased strength of a mechanical part [67]. Variation of medicine placement within an FGM pill was used to optimally deliver drugs to a patient through controlled release over a period of time [68].

Most Laser Generating methods that have had been introduced earlier, have been reported for their potential to produce graded material or multiple material parts. There are other techniques that are used conventionally in order to generate a FGM, some of which are produced by the powder metallurgy route, thermal spraying route and various coating and infiltration techniques [69]. However, many of these techniques are unable to cost-effectively produce graded parts. Laser processing exemplifies those techniques that are capable of producing the thicker functionally graded regions. In combination with RP techniques, it promises to be an efficient method [70].

A target for work at Loughborough University, aims at incorporating materials of high thermal conductivity properties, close to the cooling channels of injection moulding and die-cast tooling for faster heat removal, higher efficiencies and longer life.
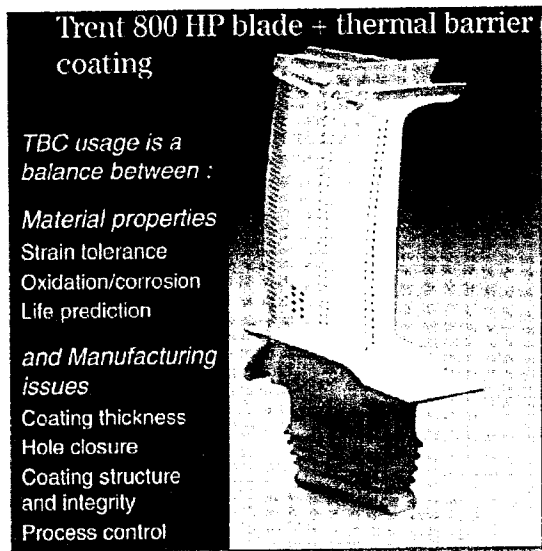
Figure 2.11: High Pressure Turbine Blade with Thermal barrier coatings [71]
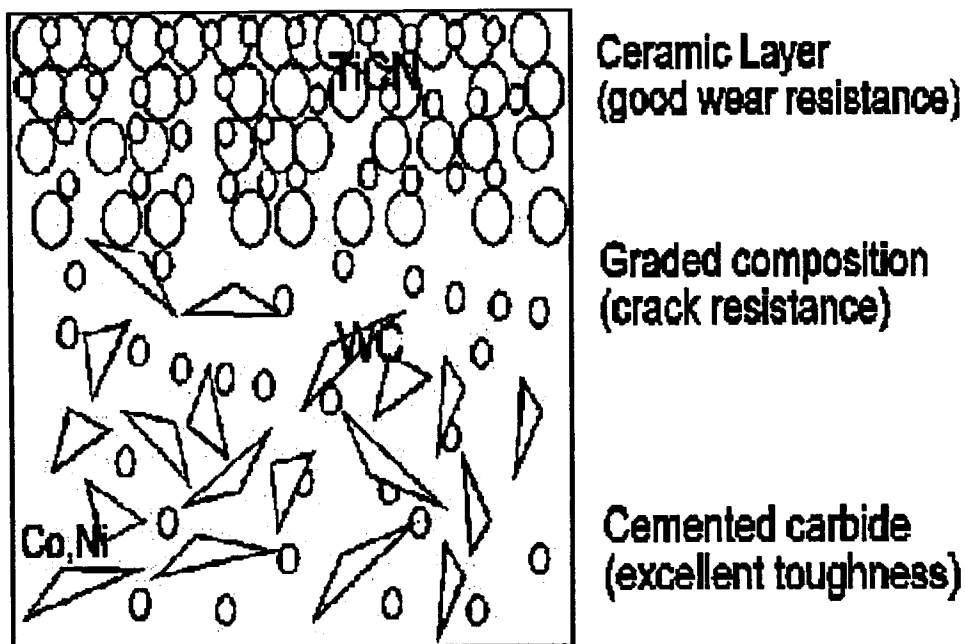
Figure 2.12: FGM for wear and toughness combined [72]

Work with a single material using Laser Powder Fusion was undertaken as a part of a European BRITE EURAM project [73]. The project named PROMET, was carried out during 1993-97 and showed that H10 tool steel powder could be successfully melted into a consolidated part of near-net shape resulting in 100% density using a high power Carbon Dioxide (CO_2) laser beam [74].

An example of this work was demonstrated by producing a forging tool of reasonably simple geometry (Figure 2.13). It was noted though, that it might be possible to use this process more efficiently or to better advantage if it could be used to produce components of multiple materials or graded materials. The use of high speed machining is better at fabricating single material tool steel shapes of reasonable size and complexity to a high geometric accuracy as compared to a Powder fusion process, which required post processing in addition to initial near-net shape fabrication.

Generation of graded cross-sections using a powder-bed or pre placed powder technique for Laser Fusion would require a mechanism to deposit or pre place alloys or powder blends in a pre determined compositional profile on the powder bed. This would then be scanned by a laser beam, which would trace the path of the slice contour for a given cross-section of the part and follow it up with hatch patterns to fill or solidify the material within the contour. The pre placed method, could use a multiple hopper configuration that would deposit spatially controlled compositions on the powder bed.

Fig 2.13: H10 tool produced during PROMET [73]

Exploration into the possibility of fabricating such structures could also be begun using a manual discrete banding technique. This technique involves mixing powder blends with differing ratios of the two FGM materials and then manually laying the blends out in bands to create a gradual change in material composition [9].

It could also be possible to produce a vertical FGM in the feed cylinder of a Laser Sintering machine either manually with discrete layers or by using vibration to induce segregation of the powder particles, resulting in a continuous FGM. The change in composition is then effected only in the Z-direction.

2.3.3.3. FGM's and their types

FGM's may be classified according to the size and position of graded regions leading to three main categories:

1) Interface FGM- An interface FGM, is a layer of graded material situated at the interface between two materials with different properties [69].

2) Surface FGM- Surface FGM's whose progressive change in composition and structure eliminate the significant discontinuities in properties that occur across well defined interfaces, have been proposed as an alternative to conventional coating systems [69].

3) Bulk FGM- The aim of a bulk FGM is to give the different property requirements at the surface, over a reasonable volume beneath the surface and at the core of a component [69].

2.3.3.4. Techniques for producing FGM parts

There are a variety of processing techniques currently practised.

The conventional techniques being practised are:

1) Powder processing using conventional sintering as in powder metallurgy.

2) Thermal spray using a gun to spray molten metal onto a substrate.

3) Vapour Deposition where a thick or a thin film coating is applied onto a substrate to form a gradient [69].

4) Thin sheets of materials bonded together usually mechanically to form the graded component

There are other non-conventional techniques like:

5) Infiltration of a porous base material with the required filler to form the graded component

6) Laser cladding techniques.

7) Plasma spraying and laser processing [69].

Plasma spraying is similar to spray metal processing where the raw material passes through a plasma gun and turns molten and is deposited onto a substrate.

8) Microwave sintering [75].

3. Processing by laser fusion – Issues and considerations

The following chapter focuses on processing and control issues while attempting to fabricate parts using laser fusion. The more material property specific issues, determining the process are considered in the subsequent sections.

Direct laser sintering of metal parts is a complex metallurgical process, which can be influenced by several phenomena that are commonly found in laser welding and liquid phase sintering applications [76]. A number of aspects determine the nature of parts obtained from the use of laser fusion.

3.1. Processing aspects and issues for laser fusion of metallic material

3.1.1. Importance of having a homogenous mixture

One of the process issues is the mixing of metallic powders (alloys, alloy blends) for laser deposition e.g. in LG, or whether a homogenous material is formed during solidification [10].

The resulting material could be comprised of isolated islands of one material in the matrix of the other material and this may happen because of inadequate mixing or melting. This would result in material properties significantly different than that expected for a full alloy. It is said that deposits which transition from 100% bronze to 100% stainless steel show visible segregation of the two materials into distinct bands and have significant cracking [10]. X-ray diffraction

of a Shape Deposition Manufacturing sample showed multiple phases present in the material. Such segregation was not seen as surprising, considering that copper and iron have very low solubility below 1400°C at any concentration indicating inadequate melting [10].

3.1.2. Surface tension

If melting occurs, the process relies on surface tension driven melt displacement to distribute the molten volume and bond the nearest particles into a conglomerate that is near full-density or significantly less than full-density, depending upon the interaction parameters. Fusion based processes of this kind are very susceptible to unwanted thermal gradients which reduce the chance of wetting leading to balling phenomena and poor layer properties [77].

Liquid metal surface tension, which plays a part in influencing the wetting angle between the solid and liquid phases as the melt pool progresses, can disrupt bonding between rastered lines and individual layers [47]. Certain scanning and atmospheric conditions allow surface tension phenomena to dominate, causing the melt pool to solidify into a series of balls.

It is also well known that surface tension forces play an important role in shaping the melt beads that are generated in direct LS of metals. Increasing the bed temperature to several hundred degrees celsius will increase wetting and melt ball beading will be reduced thereby allowing greater control over the part geometry [77].

3.1.3. Vaporisation

In Electron Beam melting the vaporisation from the surface of the melt pool is expected to be a major factor limiting the productivity of the process. Excessive vaporisation not only reduces the amount of thermal energy available in the melt pool for deposition, it also lowers the material yield. Furthermore, if any alloy constituents have very dissimilar vapour pressures, significant differences between the composition of feedstock material and the part may result. Damage to the equipment for electron-beam generation, vacuum production, wire feeding and part positioning may also occur. It is therefore of the utmost importance to be able to accurately predict the amount of vaporisation for various operating conditions [46]. Volatalisation can lead to problems with alloy depletion and laser energy inconsistencies over long periods of time [7].

3.1.4. Porosity

Porosity is still a major problem for metal building and a number of solutions have been proposed. These include infiltration with low melting point alloys or direct fusing with binary powder mixtures. Neither of these solutions allows one to build components without compromising part strength and functionality [77]. Generally, gas atomised powders are used as materials in processes like LS, LG etc. The atomisation can induce small pores within individual powder particles. These pores or voids are mostly produced by entrapment of atomising gases (e.g. argon) and could be present in different amounts depending upon the alloy

composition, particle size or atomisation conditions used by the producers [78]. Apart from gases contained within the powder, other sources could be from a contaminated surface, entrainment of turbulent impact of particles into the molten pool as in a powder-feed LG process, and also vaporization of alloy constituents.

A study of the LENS powders and deposits showed that the voids within the powders and within deposits are generally spherical in shape [78][79]. Powders with large voids/particle size ratios may result in less deposit porosity. Regardless of the process parameters chosen, powders with lowest porosity were recommended, in order to minimise LENS deposit porosity.

A fundamental problem arises with density of components in pre-placed powder processes, due to the inherent low density of the powder beds [80]. It is important that the powder is optimised for its shape and size distribution in order to increase the density of non-packed powder beds. This is decisive for the quality of the finished component [81]. The density of powder beds can be increased by optimising particle shape and surface state. Smooth particles can move easily, leading to higher density. Regular equiaxed particle shapes tend to arrange more efficiently. Therefore spherical grains are preferred.

Energy input into the system by vibration of a powder bed can further increase density. Suitable powder size ratios including addition of fines can increase density.

3.1.5. Marangoni forces

Marangoni forces, which are recognised in laser Welding and which are a result of steep temperature gradients across the melt bead could also form a natural force leading to the modification of the melt bead shape. These forces generate surface tension gradients across the melt bead, which in turn generate convective mass transfer and local reciprocal stirring of the melt volume thus having a significant effect on the melt geometry [71]. Effects of Marangoni convective flow within the melt volume causes cylindrical shaping of the melt bead, resulting in areas of porosity between scan lines [80]. A flatter, wider profile of the melt bead is necessary so as to increase final part density.

3.2. Control issues in laser fusion

3.2.1. Laser Beam Quality

In methods based on laser treatment, the "quality" (mode) of the laser beam is of high importance. Nd:YAG (wavelength= $1.06\mu m$) laser sources provides beams with high absorptances on powders, but with lower beam quality because of loss in optical fibres. CO_2 laser beams (wavelength= $10.6\mu m$) have a better mode but the absorption of the radiation is lower [82].

3.2.2. Laser Beam Absorption

Absorption of laser energy by the powder plays a key role not only in the process efficiency, but also in the part accuracy, since thermal gradients cause residual stresses in the part, and thermal diffusion can induce sintering of particles not situated directly under the beam [82].

3.2.3. Importance of Powder Properties

Powder properties are also important. Powder particles must not be too fine, so that the powder still "flows" well under the delivery device; particle size also limits the minimal height of a layer, hence accuracy and surface roughness, especially in slanted planes [82].

Fine powder becomes difficult to spread on the working area and laser/powder interaction efficiency decreases when the particle diameter goes below the laser wavelength.

Granulometry is an essential factor affecting roughness, together with parameter optimisation. The preparation of a smooth and level powder layer may be hindered by electrostatic and magnetic properties of powders: meanwhile, such features could be exploited to compact the powder bed, for example [82].

3.2.4. Control of thermal behaviour

It is important to control the thermal behaviour as a means of controlling part fabrication. Geometric properties like accuracy, surface finish, low warpage as well as materials properties e.g. strength and ductility, could be controlled with appropriate parameters. Each subsequent pass is known to have a reheating effect on its preceding passes. Initial laser passes, produced during the making of a H13 thin wall using the LENS process, have been seen to bear a region with different microstructure as compared to the regions produced by more recent laser passes [83]. Scanning speeds have been reported to have a direct effect on the hardness of materials like H13 tool steel. Higher speeds were reported to produce more hard material because at higher speeds preceding layers receive a temperature rise in a shorter time thus reducing ageing or tempering effects caused by the thermal cycling.

A thermal gradient is known to exist across the molten pool and then subsequently in the bulk of material, in a process like LENS. To optimise mechanical properties, which are a function of microstructure, which in turn is a function of thermal history during solidification, an understanding of gradients by techniques such as thermal imaging is deemed to be useful [83].

3.2.5. Controlling the temperature profile to affect microstructure

Simulation work done at Sandia National Laboratories on Laser Engineered Net Shaping (LENS) shows how grains of very different shapes and sizes form

within the same deposition line. It also shows that relatively minor changes in the dynamic temperature profile results in microstructures with very different characteristics. The implication of this work for LENS™ fabrication is that controlling the temperature profile is essential to tailoring the microstructure of a component to its application [84]. Some of the work on this process also suggests the role of thermodynamic enthalpy (heat) of the powder blend during the mixing and melting process at the focal zone, whose exothermic or endothermic characteristic would determine the homogeneity of the deposited alloy as well as the rate of solidification [85]. This would consequently affect the microstructure and properties of the deposit.

3.2.6. Control of residual stresses

Direct metal sintering relies on laser induced melting to couple powder particles together. Significant thermal gradients exist using this route unless the powder bed temperatures are controlled to a value just short of the powder melt temperature [77].

The knowledge of the magnitude and distribution of residual stresses is important for its effect on structural behaviour [83]. Thermal gradients during part fabrication (build up of layers) could lead to differential shrinkage [86]. This could induce residual stresses, which can be very high and cause warping, cracking and failure [87][86]. When a sintered part is exposed to relatively high temperatures, residual stresses are relaxed leading to geometrical deformations

and loss of tolerances. This can be a limiting factor for such processes/materials combinations that aim to produce products like tools for applications such as injection moulding, where structural and geometrical changes would occur at normal operating temperatures. Metal parts from the Direct Metal Laser Sintering (DMLS) process indicated an upper limit of 300°C existed for practical use [87].

Residual stress accumulation during material build up could cause layer delaminations in addition to part warping and cracking as mentioned before [88]. Such stresses arise from the contraction and expansion associated with layer deposition causing distortions. A few methods are known to lessen thermal distortions and cracking like use of powder-bed preheating, aimed at homogenising temperature distributions [89]. Laser sintering of stainless steel powder at room temperature indicated for single and multiple layers that short bead lengths of less than 15 and 12 mm respectively, significantly reduced warping and stress cracking [89].

3.2.7. Effect of Atmospheric control

A study conducted on laser sintering of stainless steel 314S showed that the degree of oxygen present during the heating, melting and fusing of metal powder strongly limited the range of laser powers and scanning speeds for successful processing [89]. Reduced oxygen and oxidation levels lowered absorption of laser energy as well as balling and other detrimental surface phenomena.

Oxygen in general can be present in the surrounding atmosphere, contained within the porosity of the powder bed and in the form of a passive layer of oxide on the surface of particles prior to sintering [90]. However it is also possible that surface oxides can increase absorption of laser light when using a CO_2 laser beam. Normal conditions would strongly reflect $10.6\mu m$ radiation. Experiments were carried out by Hauser et.al [90] by varying atmospheric conditions of air, air/argon mixture and argon. Changes in melt quantity and quality, oxidation and oxidation related phenomena were observed. Conditions for sintering successful single lines for stainless steel 314S with an air atmosphere were found to be limited. When increasing the net energy density (a function of both power and speed), small droplets (balls) of liquid metal were observed and these were covered by a surface oxide scale. Such balling and breakage was observed as being widespread for air sintering, presumably due to large melt volumes and the influence of the surface scale [90]. At low speeds less than 8 mm/sec and high powers (125 to 200W) with a CO_2 beam, surface tension forces appeared less dominant and the melt pool began to flow more freely and continuously to form a solidified shape.

In a pure argon atmosphere, a wider process map for successful scanning of flatter and well-bonded solidified layers existed, though porosity was seen to exist resulting in densities of 40-50%. Even with high energy densities e.g. 185W at 1mm/sec, full melting did not occur with air, air/argon sintering.

High temperature oxidation of a resolidified powder layer is also known to reduce wetting and can prevent bonding between layers [80][91]. Laser Sintering of iron powder in an inert argon atmosphere with a 50 Watt CW, Nd:YAG laser

indicated that satisfactory single layers were produced. Unfortunately, bonding between successive layers was still not complete. It was theorised that a period of oxidation growth during the cooling of the layer to room temperature could have affected sintering and wetting characteristics [91]. In a single layer, adjacent scans carried out relatively fast by the laser beam, were able to reduce the chance of oxide formation and hence were found satisfactory. Between layers where the material was allowed to return to room temperature, each layer ran through a temperature cycle that was conducive to oxide formation. Though the atmosphere itself was free of oxide, enough residual oxygen was present on the powder, to form an oxide layer on the upper surface and prevent good bonds between the layers [91]. Densities up to 35 % were produced.

In a study of Direct metal laser sintering of cermet superalloy, it was found that oxygen present in the process caused balling, separation and tearing due to surface tension effects [7]. It was found that a high vacumn atmosphere resulted in relatively uniform surface features, no cracking, tearing or separation when experimentation was conducted within an acceptable window of parameters. It was also noted that preheating of the powder bed was beneficial due to outgassing of the powder that takes place, thus preventing further contamination [7]. It also improved the uniformity of flow and solidification of the molten material, thus enhancing the surface finish and uniformity of the component. Preheating to appropriate temperatures was also known to reduce hot-tearing, hot-cracking and balling of the molten material. Controlling energy density (power, spacing) and speed, were crucial to achieving the same end.

3.3. Material and property specific issues

The use of laser fusion to process a wide variety of materials and also combinations of two or more materials brings with it a unique set of challenges that require the understanding of material and its interaction with laser light along with other issues that may arise due to material property based interactions itself. Some of the issues that could be faced during processing are highlighted in the following sections, most of which could generally be related to problems faced during conventional welding techniques.

3.3.1. General issues

Problems can result from sharp interfaces between dissimilar materials. Thermal stresses due to co-efficient of thermal expansion mismatches can result in delamination and a sharp interface can act as an initiation site for fracture [10].

One of the most important properties with respect to bond formation is the co-efficient of thermal expansion (CTE) [9]. By combining materials severe stresses may build up because of the mismatch of the co-efficient of thermal expansion [63]. The mismatch in CTE's, normally present in a metal/ceramic bond lead to destructive thermal stresses during thermal cycling or shock loading. Metal/Ceramic bonds are frequently created at an elevated temperature and then cooled. The large CTE mismatch coupled with this large change in temperature will create a residual thermal stress in the component, which may weaken the

bond. An FGM component allows the CTE value to change gradually from a low value to a high value. This distribution of CTE values will tend to spread the thermal stresses out over a volume of material instead of concentrating them at the interface [9].

The importance of interfaces between dissimilar materials is connected primarily to their inherent inhomogeniety i.e. the fact that physical and chemical properties may change dramatically at or near the interface itself. It should be realised that physical properties like elastic moduli, thermal expansion or electrical resistivity may differ near interfaces by orders of magnitude from the bulk regions. As a result these sharp gradients may change an isotropic bulk solid locally into a highly anisotropic medium [63].

Dissimilar metal welding essentially consists of joining two metal components having different (but individually specific) properties and rendering the weldment at least as strong as the weaker of the two metals, ensuring no failure at the weld [92].

This could be considered as similar to the issue of being able to laser-weld two dissimilar metal powders in-order to create a functionally gradient material rendering high thermal conductivity and hence heat-removal properties.

Some of the important issues that need to be considered while trying to weld two such materials are covered in the following section.

3.3.2. Material property specific issues

3.3.2.1. Melting point

For successful joining the differences in melting points of the two materials should be low [92]. This is of prime importance while employing such welding processes as one of the metals may be in molten state long before the other. The joining of copper to steel is difficult as their melting points are 1080°C and 1500°C respectively. But if welding by fusion between these is essential, then a process with high and concentrated heat input is advised which requires less joining time [92].

3.3.2.2. Solid-Solubility

There should be a certain amount of solid solubility between the concerned metals at ambient as well as welding temperatures. Joining is difficult if there is little or no solubility. As an example, copper and steel are difficult to be welded due to poor solubility whereas joining of nickel and steel is easier as they have good solubility [92].

In the development of FGM's for metal-ceramic combinations by laser beam, solid solubilities of the two materials plays a very important role. Since metals and ceramics are quite different in their chemical properties, in addition to their

thermal and mechanical properties, the solid solubility of ceramic in metal or that of metal in ceramic is extremely limited [93]. So it may prove very difficult to obtain a well-graded metal-ceramic material using laser beam processing.

3.3.2.3. Intermetallics

When different metals are welded under certain conditions of composition and temperature they may form phases other than solid solutions, which are called intermediate phases or intermetallic compounds [93].

Intermetallics at the transition zone may have properties other than the base metals, thus causing a hindrance at the welding zone. It is therefore suggested that information should be obtained as to what intermetallics would be formed (from phase diagrams) [93]. Information on their ductility, crack sensitivity, corrosion susceptibility etc. as well, are helpful.

For example the study of aluminium-iron phase diagram reveals the presence of a number of complex intermetallics, a few which are known to be brittle. This suggests that in general a weldment of aluminium and steel would be poor in quality [92].

22Ti	40 Zr	72 Hf	90 Th	**Group B**
23V	41 Nb	73 Ta	91 Pa	
24C	42 Mo	74 W	92 U	

25 Mn	43 Tc	75 Re	93 Np	
26 Fe	44 Ru	76 Os	94 Pu	
27 Co	45 Rh	77 Ir	95 Am	**Group A**
28 Ni	46 Pd	78 Pt	96 Cm	
29Cu	47 Ag	79 Au	97 Bk	

Figure 3.1: Table illustrating formation of intermetallics for metal-metal combinations [94].

In Figure 3.1, the metals in group A will mix together forming perfect solid solutions and are thus readily weldable in combination. For the metals in group B, this is only partially the case. The group A metals form intermetallic phases with the group B metals and so they are not suitable for welding together [94]. This is also the case for combinations of group A or B metals with other metals not listed in either of the two groups such as aluminium, beryllium, magnesium etc. In this scheme, details of 46 of the most important metals together with the weldability of over 1000 potential material combinations, are stored in a computer database [94].

3.3.2.4. Thermal expansion and Thermal conductivity

Large internal stresses would be generated at a weldment during any change in temperature, if the differences in CTE are large, as in the case of aluminium and mild steel which have a CTE of 23 and 12 respectively. This might lead to cracks. A similar thing may happen with stainless steel (whose CTE is twice that of mild steel) when it is to be welded to mild steel [92].

A high thermal expansion co-efficient is usually a disadvantage in design and other considerations being equal, a material with low thermal expansion co-efficient is preferred. Thermal expansion interacts with thermal conductivity and specific heat to generate thermal and residual stresses when a component is heated non-uniformly [95]. Also, one metal may transmit or conduct heat from the weld area much faster than the other. The thermal conductivity of copper: aluminium: steel: is 1.00:0.52:0.17 as can be seen in Figure 3.2. Thus the metal with higher thermal conductivity will require more heat to come to the welding temperature than the one with lower conductivity [92].

In developing metal/ceramic FGM's by laser beam processing problems might occur due to differences in thermal expansion co-efficient, the melting point and the thermal conductivities. Most metals have larger co-efficient of thermal expansion and thermal conductivities than ceramics [93]. Also most metals are ductile while most ceramics are very brittle. Due to rapid heating and cooling rates in laser materials processing cracks are formed more easily, not only in the metal-ceramic boundary region but even in the ceramic part during rapid cooling [93].

	Density ρ (g/cm³)	Specific heat (C) (J/kg per K)	Thermal conductivity λ (W/m per K)	Thermal diffusivity (λ/ρ per C)	Thermal expansion coefficient (10⁻⁶/K)	Electrical resistivity (μΩcm)
Aluminium Aluminium alloys	2.70 2.46–2.93	900	239 88–201	0.098	23.5 16.5–25	2.68 3.5–8.6
Copper Copper alloys	8.94 7.57–8.94	385	399 21–397	0.12	17.7 16–21.2	1.7 7–35
Magnesium Magnesium alloys	1.74 1.75–1.87	1050 960–1050	167 79–146	0.091	27 26–27.3	3.9 5–14.3
Nickel Nickel alloys	8.89 7.85–9.22	456 373–544	74.9 9.1–21.7	0.019	13.3 7.6–14.9	9.5 51–139
Titanium Titanium alloys	4.51 4.42–4.86	528 400–610	16 4.8–16	0.0067	7.6 6.7–9.8	48.2 70–170
Zinc Zinc alloys	7.13 5.0–6.7	389 109–123	113 26–28	0.04	39.7 27.4	6

Steels
  Carbon steels
  Low alloy
  Stainless
	
	7.83–7.87
	7.83–7.87
	7.42–8.69
		
		435–494
		452–494
		402–519
			
			45.2–65.3
			33.1–48.6
			12.1–26.8
				
				0.015
				0.010
				0.005
					
					10.6–12.62
					10.55–12.8
					9.3–18
						
						12–19.7
						20–37
						48.6–122

Aluminas	3.45–3.99	730–1100	13.8–43.2	0.008	4.5–8	
Beryllias	2.8–2.93	1020–1090	270–300	0.09	5–8	
Titanias	3.5–4.13	690	2.5–5	0.001	5–8.5	
Zirconias	3.5–5.9	450–750	0.9–2	0.0005	7–9	
Porcelains (oxide compounds clay based)	1.8–3.8	850–1100	1.1–6.2	0.0013	1–11	
Porous oxide ceramics (electrical refractories)	1.9–4.4	1100	0.3–3.7	0.0006	-0.05–7	
Silicon carbides	2.2–3.2	600–700	12.6–200	0.06	2.8–12	10⁵–10¹¹ᵃ
Boron nitrides	1.9–2.1	780	1.5–250ᵇ	0.0007–0.16ᵇ	-2–4.1	
Silicon nitrides	1.9–3.3	700–1100	7–43	0.01	1.5–3.6	
Sialons	3.3	600	21.3	0.01	1.5–1.7	
Cemented carbides	10–15.3		25–120		5–7	
Glass ceramics	2.4–2.6	500–900	1.3–3.6	0.0013	-0.25–9.7	
Carbons, graphites	1.6–2.2	700–800	5–121ᵇ	0.003–0.08ᵇ	1–8.3	90–450
Glasses	2.18–2.50	710–830	1.1–1.2	0.0006	0.013–7.8	10¹⁴–10¹⁶

ᵃ Other ceramics have resistivity 10^9–10^{17} Ωcm. Plastics 10^6–10^{18} Ωcm.
ᵇ Depending on direction of heat flow.

Figure 3.2: Thermal properties of some important materials [95]

3.3.2.5. Specific Heat

In dissimilar metal welding, the knowledge of specific heat is very important as it provides an indication of the amount of heat required to raise any of the metals to its melting point [92].

For practical purposes it should be noted that a metal having low melting point (m.p.) and relatively high specific heat, like aluminium with m.p. 660°C and specific heat 900 J/kg per K may require as much or even a higher quantity of heat to reach the point of fusion as compared to another metal with higher m.p. and lower specific heat like, stainless steel with m.p. 1395°C and specific heat 402 J/kg per K as shown in Figure 3.2 [92].

3.3.2.6. Chemical Stability

A large separation of metals in the electrochemical series implies larger susceptibility to corrosion at the interface (more attack on the active metal) [92]. The galvanic series for some common weld-base metals and alloys are shown in Figure 3.3. Thus metals having large difference in their galvanic potentials and which are involved with service environments of strong electrolytes may have problems of localised corrosion at the joints. It is possible that two base metals, which may be compatible in one corrosive atmosphere may not be acceptable in a different corrosive atmosphere. Hence, a knowledge of the ultimate use of the

component is important to retain the chemical stability at the joints of the concerned materials [92].

Corroded End (Anodic or Least Noble)
Magnesium and its alloys
Zinc
Aluminium 6053
Aluminium 3003
Aluminium 2024
Aluminium
Mild Steel
Wrought Iron
Cast Iron
Ni-resist
Lead
Tin
Muntz Metal
Naval Brass
Yellow Brass
Admiralty Brass
Aluminium Bronze
Red Brass
Copper
Silicon Bronze
70-30 cupronickel
Nickel (passive)
Inconel (passive)
Monel
18-8 Stainless type (304)
18-8-3 Stainless type 316 (passive)
Protected End (Cathodic or most noble)

Figure 3.3   Galvanic series for some common metals and alloys [96]

3.3.2.7. Electrical Conductivity

With dissimilar metals, the differing resistances to current flow results in a problem of unequal heating of the parts to be welded. This is true for resistance welding. For example the electrical conductivity of copper, aluminium and stainless steel are relatively 100%: 59%: 16% as seen in Figure 3.4 [92].

In resistance welding where the resistance of the metal to current flow is used to increase a small area of it to a high temperature, electrical conductivity is of special importance.

Metal	Relative Electrical Conductivity	Relative Thermal Conductivity
Silver	100	100
Copper	96	94
Gold	69.5	70
Aluminium	59	57
Magnesium	41	40
Beryllium	40	40
Tungsten	29	39
Zinc	27	26.5
Cadmium	22	22
Nickel	23	21
Iron	16	17
Platinum	15	17
Tin	12.5	15.5
Lead	7.7	8.2
Titanium	2.9	4.1
Mercury	1.6	2.2

Figure 3.4: Relative Electrical and Thermal conductivities of some metals [96]

The electrical and thermal conductivities of metals follow roughly the same order. This is to be expected since both the flow of electricity and heat depend upon the ability of electrons to move freely within the metallic structure [96]. Thermal conductivity goes hand in hand with electrical conductivity and is usually required in all conductors operating in the high ampere range [97].

3.4. Some Issues in welding with a high intensity beam

3.4.1. The case of Electron Beam Welding

Electron beam welding has found wide application in dissimilar welding because of its high density energy source and fast welding speed which easily overcomes the thermal conductivity difference of the metals. However, diffusion, percussion and laser beam welding processes are still widely used for making dissimilar joints in aerospace industries, joining of wires and welding of very thin sheets etc. [92].

Figure 3.5 gives the suitability of various combinations of materials for Electron beam welding [94].

Solid lines = Suitable for welding together
Broken lines= suitable for welding together under certain conditions
No line= Not suitable for welding

Material group

1. Unalloyed and low alloyed low carbon steels, in particular structural steels, not free machining steels.
2. High alloy steels, high carbon contents, in particular ledeburitic tool steels.
3. High alloy very low carbon steels, in particular corrosion resistant steels.
4. Cast irons with lamellar or spheroidal graphite, black tempered cast iron.
5. Aluminium alloys with the exception of those containing zinc.
6. Pure copper, low alloy copper.
7. Copper alloys with the exception of those containing large amounts of zinc (brass, nickel silver).
8. Nickel and nickel alloys
9. Cobalt alloys with the exception of hard materials containing large amounts of carbides.
10. Titanium and Titanium alloys

Figure 3.5: Suitability of various material combinations for Electron beam welding [94]

3.4.2. Laser Welding

Laser Welding is normally a liquid-phase welding process, which joins metals by melting their interfaces causing the mixing of the molten metal which in turn solidifies on removal of the laser heat source [98]. The most suitable metals for laser welding are those, which have the same or overlapping liquid temperature ranges and are soluble in one another, assuming that they are good absorbers of laser light [98]. Pure metals, which have one definite melting temperature, can usually be readily welded to themselves, but not always to a different pure metal. They will however usually weld to an alloy, which has the same base metal element. The Figures 3.6 and 3.7 show the weld suitability of various pure metal combinations. Figures 3.8 and 3.9 show the suitability of welding certain specific alloy materials.

	Silver	Aluminium	Gold	Beryllium	Cobalt	Copper	Iron	Magnesium	Molybdenum	Nickel	Platinum	Rhenium	Tin	Titanium	Tantalum	Tungsten
Aluminium	B															
Gold	A	E														
Beryllium	E	B	E													
Cobalt	C	E	B	E												
Copper	B	B	A	E	B											
Iron	C	E	B	E	B	B										
Magnesium	E	B	E	E	E	E	C									
Molybdenum	C	E	B	E	E	C	B	C								
Nickel	B	E	A	E	A	A	B	E	E							
Platinum	A	E	A	E	A	A	A	E	B	A						
Rhenium	C	D	D	E	A	C	E	D	E	C	B					
Tin	B	B	E	C	E	B	E	E	C	E	E	C				
Tantalum	E	E	D	E	E	C	E	D	A	E	E	E	E			
Titanium	B	E	E	E	E	E	E	E	C	A	E	E	E	E	A	
Tungsten	C	E	D	E	E	C	E	E	C	A	E	A	E	C	A	B
Zirconium	E	E	E	E	E	E	E	E	C	E	E	E	E	B	A	E

Note:
Those combinations which have poor thermal conductivity will probably be good absorbers of laser light. Good thermal conductors will be more suited to short wave length light such as from Nd:YAG lasers.

A — Good (solid solubility achieved
B — Acceptable (doubtful weld structures are possible)
C — Weld with caution (unacceptable data available)
D — Take extreme caution (no data available)
E — Undesirable combination (intermetallic compounds formed)

Figure 3.6: Fusion weldability of pure metal combinations [98]

Table 4.8	Laser Weldability of Dissimilar Metal Combinations (4)																		
	W	**Ta**	**Mo**	**Cr**	**Co**	**Tl**	**Be**	**Fe**	**Pt**	**Ni**	**Pd**	**Cu**	**Au**	**Ag**	**Mg**	**Al**	**Zn**	**Cd**	**Pb**	**Sn**
W																				
Ta	■																			
Mo	■	■																		
Cr		P	■																	
Co	F	P	F	G																
Tl	F	■	■	G	F															
Be	P	P	P	P	F	P														
Fe	F	F	G	■	■	F	F													
Pt	G	F	G	G		F	P	G												
Ni	F	G	F	G		F	F	G	■											
Pd	F	G	G	G	■	F	F	G	■	■										
Cu	P	P	P	P	F	F	F	F	■	■										
Au	-	-	P	F	P	F	F	F	■	■										
Ag	P	P	P	P	P	F	P	P	F	P	■	F	■							
Mg	P	-	P	P	P	P	P	P	P	P	P	F	F	F						
Al	P	P	P	P	F	F	P	F	P	F	P	F	F	F	F					
Zn	P	-	P	P	F	P	P	F	P	F	F	G	F	G	P	F				
Cd	-	-	-	P	P	P	-	P	F	F	F	P	F	G	■	P	P			
Pb	P	-	P	P	P	P	-	P	P	P	P	P	P	P	P	P	P	P		
Sn	P	P	P	P	P	P	P	P	F	P	F	P	F	F	P	P	P	P	F	

Legend: ■ Excellent · G Good · F Fair · P Poor

Figure 3.7: Diagram of laser weldability of dissimilar metal combinations [98]

Material	Comments
Aluminium alloys	Laser welds in aluminium alloys generally have poor quality and caution is necessary for applications where high reliability is required.
Copper	Only suitable for micro-spot welding applications.
Cast Iron	Nodular cast iron can be welded using a nickel filler wire to overcome weld cracking
Nickel base and high nickel alloys (C263, Hastelloy, Inconel, Incoloy, Kovar, Monel, Nimonic, PK33, Waspaloy)	Some of these alloys weld extremely, however those without a number are available in different grades which produce quite different weld qualities. Therefore the material manufacturer should be consulted with respect to weld properties, in case a filler material is required to improve them.
Steels:	
Low carbon and high strength low alloy (HSLA) forming grades.	Very good quality welds can be achieved provided sulphur and phosphorous levels are kept low.
Medium and high carbon	Weldable, but special precautions are necessary to ensure acceptable weld properties.
Alloy steels	Satisfactory laser welds have been made in numerous pipeline, shipbuilding and structural steels. High weld hardness can be a problem due to fast cooling rate.
Stainless Steels	
Austenitic	Very good quality welds can be achieved in most grades except free machining.
Ferritic	Grades with low carbon and chromium levels will weld best. Weld toughness is affected by grain coarsening.
Martensitic	Welds and their HAZs are hard and brittle due to the high carbon content
Titanium and alloy 6Al-4V-Ti	Good quality welds with fine grain structures can be achieved, but material cleaning just prior to welding and high quality weld pool gas shielding are essential.

Figure 3.8: A guide to engineering materials which can be laser welded [98]

	Laser Welding Characteristics of Different Alloy Steels
Alloy	**Notes**
Al Alloys	Problems with: 1.Reflectivity – requires atleast 1kW 2. Porosity 3. Excessive fluidity –leads to drop out
Steels	O.K.
Heat resistant alloys: e.g. Inco 718, Hastelloy	O.K. but: 1. Weld is more brittle 2. Segregation problems, 3.Cracking
Ti alloys	Better than slower processes due to less grain growth
Iridium Alloys	Problem with hot cracking

Figure 3.9: Laser welding characteristics of various alloys [96]

3.4.3. Absorptivity and Reflectivity of metals

This aspect may be important especially during laser sintering of a Metal-Ceramic system to form a Functionally Graded Material.

The absorptivity of a CO_2 laser beam on metals is in the range of 5%-10%, while that on the ceramics exceeds 90%. Thus if the laser beam is irradiated on the metal-ceramic mixture simultaneously, the ceramic part can be evaporated while the metal part is not even melted due to their differences in absorptivity [93].

Figure 3.10 describes, some characteristics of absorptivity and reflectivity of metals when subjected to laser irradiation.
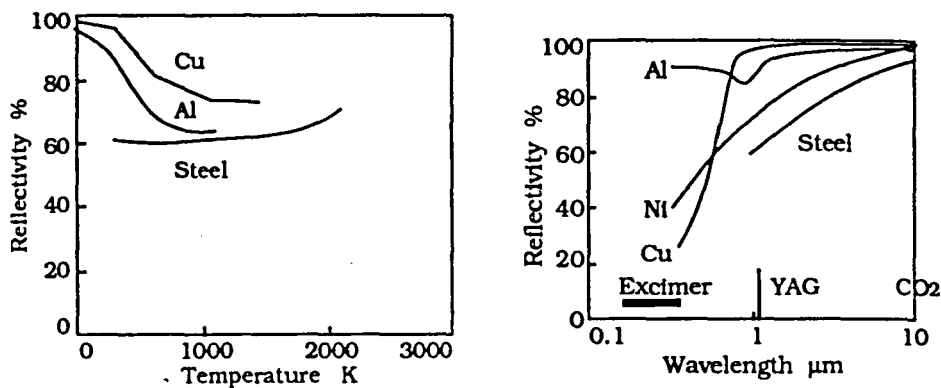
Figure 3.10: Diagram of reflectivity of a number of metals as a function of temperature and wavelength of the laser [99]

Type	Wavelength (μm)
Carbon Dioxide	**10.6**
Carbon Monoxide	**5.4**
Nd-YAG	**1.06**
Nd-Glass	**1.06**
Excimer(KrF)	**0.249**

Figure 3.11: Wavelengths of laser beam [99]

From Figure 3.10 it is seen that reflectivity falls at shorter wavelengths. The wavelength for a Nd:YAG laser is 1.06μm which is ten times less as compared to that for a CO_2 laser whose wavelength is 10.6 μm (Figure 3.11). Thus as seen in Figure 3.10, the curve for materials e.g. Nickel and Steel, shows lower reflectivity at Nd: YAG wavelength and higher reflectivity for CO_2 wavelength. The reflectivity is not only a function of the material but also the surface shape, surface films (such as oxides), and plasmas [99].

4. Experimental program and objective

Based on the literature survey and work undertaken, the interesting possibility of using the Laser Fusion process to produce tooling with graded compositions was regarded as the main objective and was used for determining the program of experiments. The experiments were designed, based on the pre-placed powder or powder bed method of producing parts as opposed to the laser cladding technique. The pre-placed powder technique in addition to being able to construct multiple material geometry, will give the added advantage of being able to support overhanging geometry by virtue of the loose unprocessed powder from the previous layers. This would help in the creating aspects of a tool, like cooling channels, which could be made conformal to the cavity and also can be of any shape thus effecting faster heat removal. A Nd:YAG laser was chosen for the program of experiments which gave better or improved absorptivity for the metallic material and the powder bed as governed by its wavelength. H13 grade tool steel was chosen as the base material due to its well known application in injection moulding and die casting tools.

Investigating the shape of a bead as a basic building block was considered an initial step in the experimental program. It was thus necessary to investigate how the cross section of the bead defined by the width and height varied with the laser parameters. Other aspects including shape description of the cross-section and the surface profile could be measured.

A 550W pulsed Nd:YAG laser from GSI Lumonics Ltd. was used to perform single line scans in pre-placed powder. Laser output from the Nd:YAG laser can

be controlled by controlling the width, height and shape of the pulse and by

choosing the required frequency of output. This will consequently determine the

pulse energy and average (mean) power at the output.

The laser allows variations in these input values to an extent that is limited by

the flash lamps 'pump output limit' and the maximum 'laser power output limit'.

According to machine specifications this has a maximum of 550W. It is thus

possible to define an area of laser output usage that could be used, to study the

effects on the ability to generate fused beads. The combination of parameters

able to achieve a bead of solidified material would be compared against bead

geometry.

5. Experimental Set-up and Methodology

5.1. Powder material

The material chosen was H13 tool steel supplied by Osprey Metals Ltd., UK. This material was to be investigated, as the 'single' material composition, which could be later used as a base for FGM manufacture. The material is a hot-work tool steel, for applications that experience high temperature or heat loads. These are typically used for die-casting and injection moulding tools [100].

The material specifications and properties are shown in tables 5.1, 5.2 and 5.3. Scanning Electron Microscope (SEM) images of the H13 powder Figures 5.1 and 5.2 highlights the largely spherical shape of the individual granules with an average diameter of 145 to 150 μm. A general indication of the porosity for a single layer was given to be approximately 50 % of the density of H13, tap density as 66% of the bulk material. The oxidation level in the powder was indicated at 250ppm [101].

Component	Weight percent
Chromium (Cr)	4.9
Molybdenum(Mo)	1.7
Vanadium(V)	1.0
Silicon(Si)	0.93
Carbon(C)	0.38
Manganese(Mn)	0.32
Iron(Fe)	BALANCE (90.77)

Table 5.1: Composition data for H13 tool steel [101]

Powder Sizing data	
Powder sized to –212 microns	
Particle size data	
+212 µm	1.5%
-212 µm + 150µm	13.2%
-150µm + 106 µm	14.0%
-106µm + 75µm	15.6%
-75µm + 38µm	26.5%
-38µm	29.2%

Table 5.2: Powder sizing data for H13 tool steel [101]

Physical Properties	Metric	Imperial	Comments
Density	7.8 g/cc	0.282 lb/in³	
Thermal Properties			
CTE, linear 20°C	11 µm/m-°C	6.11 µin/in-°F	25 - 95°C
CTE, linear 250°C	11.5 µm/m-°C	6.39 µin/in-°F	25 - 205°C
CTE, linear 500°C	12.4 µm/m-°C	6.89 µin/in-°F	25 - 540°C
Heat Capacity	0.46 J/g-°C	0.11 BTU/lb-°F	from 0-100°C (32-212°F)
Thermal Conductivity	24.3 W/m-K	169 BTU-in/hr-ft²-°F	at 215°C; 24.4 W/m-K at 350°C, 24.3 at 475°C, 24.7 at 605°C
Descriptive Properties			
Annealing Temperature	850 - 870°C for 4 hours	furnace cool 20°C per hour max.	
Stress Relieving Temperature	600 - 650°C for 2 hours (approx.)	cool in still air; to be stress relieved (always) before hardening.	

Table 5.3: Physical and thermal properties for AISI type H13 tool steel [102]
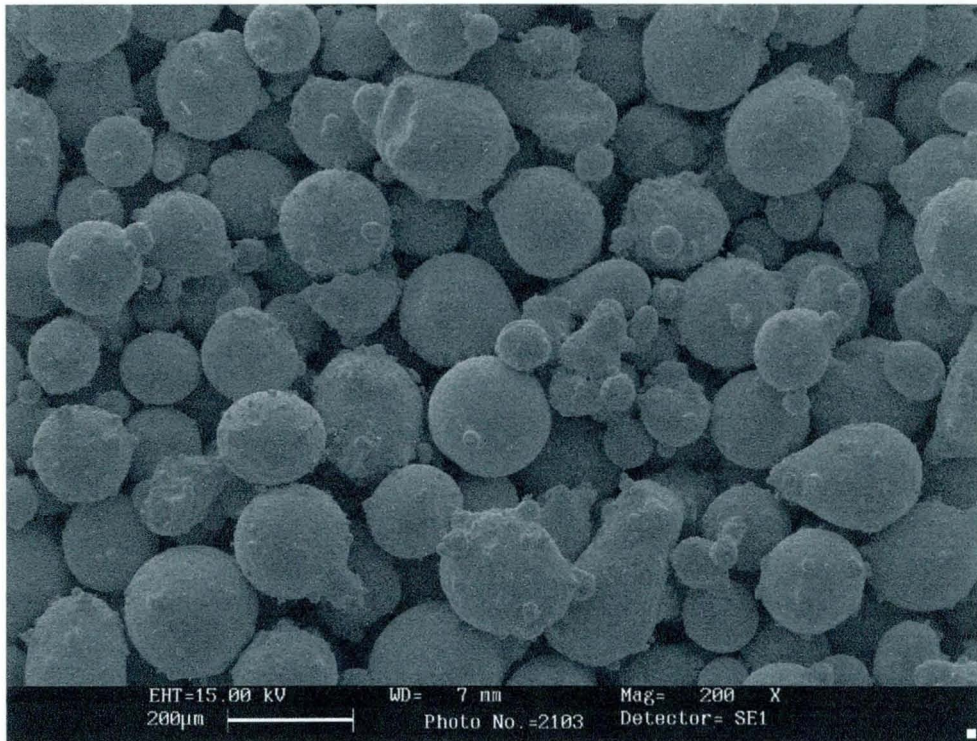
Figure 5.1: SEM of H13 powder at 200X magnification
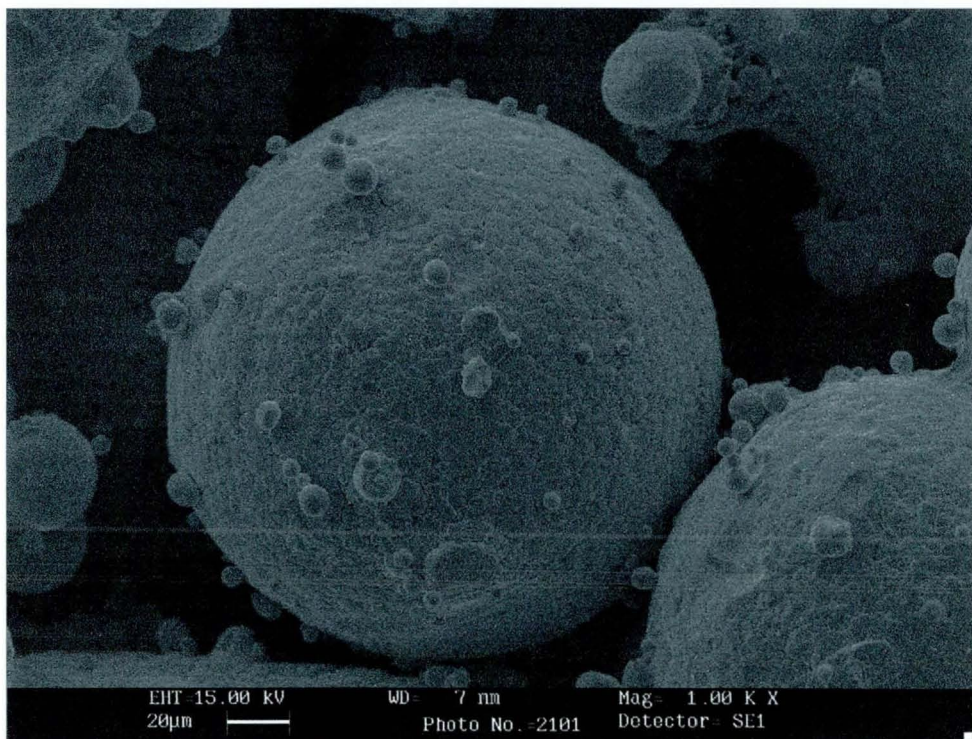
Figure 5.2: SEM of H13 powder particle at 1000X magnification

5.2. Experimental equipment

The set-up for the experiment consisted of a simple fabricated powder bed assembly, with a top plate having a number of slots, hand movable in the z-direction. The slots were to accommodate, small square substrate plates (40mm x 40mm x 1mm) in dimensions on which powder was spread and levelled to the required thickness. The substrate was intended as a base for eventual building of tooling and which would reduce distortion of the part. In case of single linear beads the plates were considered also to be useful for sectioning and handling of the beads. The top plate was movable on four tie-rods fitted to the rest of the fixed assembly as shown in Figure 5.3. The entire assembly was mounted on the machine translation bed, which could move in the X, Y axes and a 360° rotational axis.

The pulsed output of the laser beam, was focussed on to the surface of the metal powder by a focussing head which could move in the Z-direction. A camera fitted to the focusing head assembly, which housed the lens, was able to image the process as it happened and aided focussing of the beam. A sharp image of powder bed on a Black and White television screen mounted on the outside of the Laser Unit, indicated the beam was in focus.

Experiments were divided into three stages:

1) Establishing a set of laser output limit graphs.

2) Using the output limit graphs to determine a set of parameter combinations, for producing single fused beads.

3) Measuring the beads for their height and width.

Powder
Bed with
slots
mounted
on XY -
bed

Focussing
head moves
in the z –
axis
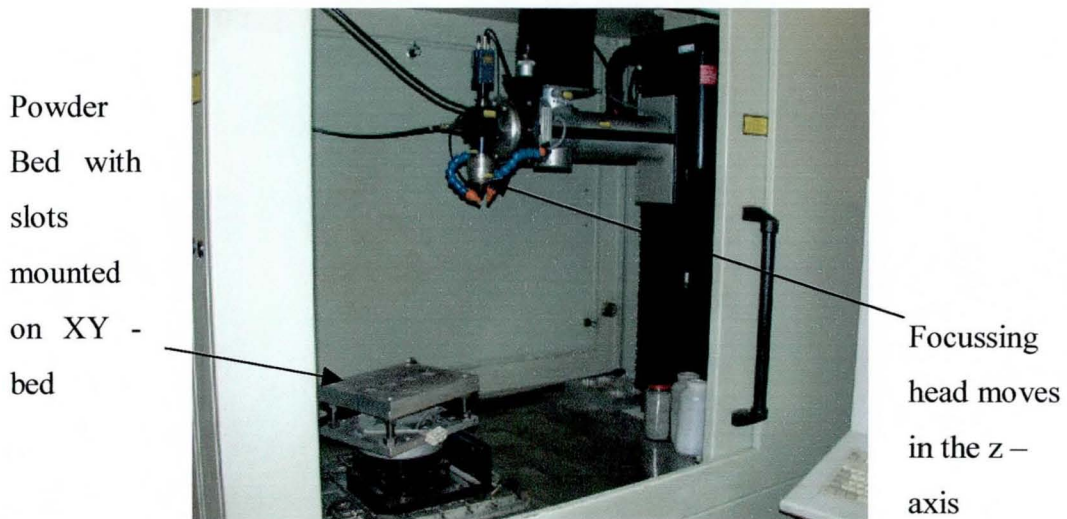
Figure 5.3: The Nd:YAG Processing station showing the laser

5.3. Determining laser output limits

As a first stage, laser output from the Nd:YAG was characterised into 'Output limit' graphs, which demonstrated the range of parameter combinations for which a predetermined level of output (pulse energy) could be attained, using a combination of input parameters i.e. pulse width and frequency.

The output limit graphs were determined as follows:

The first step involved manually setting laser parameters, pulse frequency and pulse width. The pulse height was then adjusted to give as close an energy level as possible to the required energy level. The laser either produced energy output or it gave an error message due to the maximum specifications on the laser being reached as driven by a incompatible combination of parameters.

If the laser produced output then the energy level was noted.

Plots of pulse width or duration of pulse (defined in milliseconds) versus Frequency (in Hertz) were plotted for pulse energy levels from 5J to 70J, with 70 Joules being the maximum pulsed energy achievable on the laser.

Pulse width variations had a upper limit specification of 20 milliseconds on the laser and frequency could be increased up to a maximum of 100Hz.

Hence, for each of the Pulse Energy value 5,10, 20, 30 and 60 J a corresponding plot of pulse width versus frequency were made. The pulse width was set at 0.5, 2, 6, 10, 14, 18 and 20 milliseconds and frequency was set at 5, 10, 30, 50, 70, 90 and 100 Hz.

5.4. Producing single beads

The possible input parameter combinations were combined with various scanning speeds. Speeds were set at the following levels: 1mm/sec, 5mm/sec, 10mm/sec and 20mm/sec. Available literature for laser scanning using a focussed YAG beam and other general laser welding related literature reported the use of similar speed levels [56]. Other fixed parameter values were inert gas flow rate, which was set at 15 litres/min and the focal length of the lens at 80mm, giving a spot size of 0.8mm.

Two values of powder layer thickness of 1mm and 0.4 mm were chosen. A 1mm layer height for tooling manufacture would result in a faster overall build rate. Also for building tooling using laser fusion, the surface finish would not be as important, since the part will be machined later to the required finish. A layer

thickness of 0.4mm will be the minimum feasible layer height to recoat with the existing powder size given that it is roughly twice the maximum particle size. This was also recommended during a preceding Brite/ Euram project (PROMET) carried out in the years 1993-97 indicating the use of layer thickness 1.2mm, 0.6mm, and 0.4mm [103].

For each individual combination of pulse width, frequency, pulse energy and scan speed at any given thickness there were produced 5 equidistant beads. This was to account for repeatability and averaging the measurements of bead width and height.

The beads were produced by running a laser beam on a layer of powder spread and levelled to the required thickness. The substrate plate 40 x 40 mm, is first dropped into the slots provided in the top plate of the powder bed assembly. The thickness gauge is then placed on the substrate plate following which the powder material is manually deposited and spread on the substrate and levelled to the gauge height (thickness) of 1mm or 0.4mm as the case may be. The levelling itself could be done manually using any plate material of the appropriate size. The focussing head is then positioned at a start point about 5mm and 8mm distance from the edges forming the corner of the substrate. The XY bed is programmed to impart linear motions at the required speed, to generate 5 equidistant beads 5mm apart, each being scanned in the same direction. The program at the laser control module co-ordinates the XY bed with the shutter at the laser head, causing it to open and close at the beginning and end of each linear scan. Between scans the traverse of the table is rapid (approximately 1 to 2 seconds) and there is a default dwell time of 1 second at the beginning of each

scan. Increasing the dwell time at the program end, will allow a level of delay between individual scans. In order to lessen overall experimental time, two or more substrate plates or parameter combinations were processed at a given time by making use of the multiple slots available on the top plate.

5.5. Measurement of beads

The 5 equidistant beads were subject to height and width measurement at fixed points. The height and width of the bead as indicated in Figure 5.4 provide a useful measure of describing the shape of the bead and bead quality. Ratios of height to width could be calculated to indicate the suitability of bead profile while building overlapping beads, horizontal and vertical layers. Also a flatter semi-circular bead indicated in Figure 5.4 would be preferable over a more cylindrical bead shape, due to less percentage overlap between adjacent beads being necessary and also to reduce the possibility of porosity formation due to the undercut at the point where the bead joins the substrate.

Beads on a H13 substrate (H13 chosen to avoid dilution of the powder material) were kept at a length of 30mm. Width measurements were taken by a vernier at 5 equidistant points 6mm, 12mm, 18mm, 24mm and 30mm from the start point of the beads.

Height was measured at these points using a micrometer. The height was measured along with the plate. The thickness of the plate was later subtracted to give the bead height. The average of the width measurements at points on each track were further used to give an average of all 5 tracks on a single substrate

plate. These values were then plotted on graphs representing the average width or height of a single bead fused to the substrate, for varying parameter combinations.

Top View of bead	Cross-section
Uniform bead at low energy, high frequency and moderate speed Parameters: 0.4mm layer, 5J, 10mm/s, 6ms, 50Hz	Bead width = 0.77mm Bead height = 0.62 mm
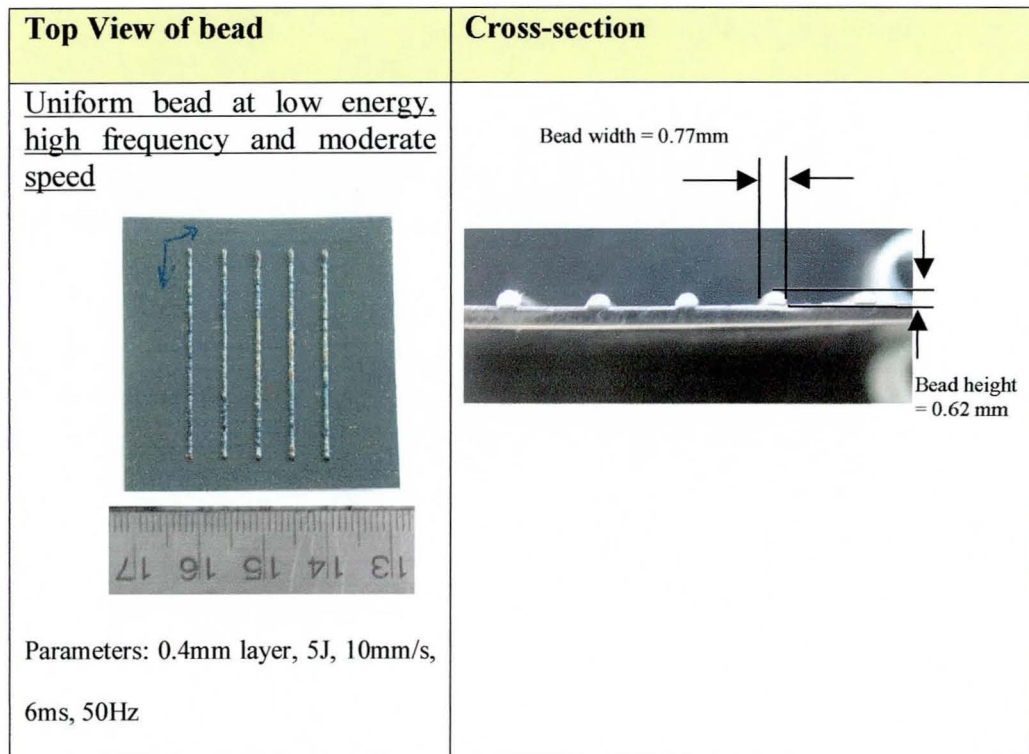
Figure 5.4: Beads fused to substrate and their cross-section

6. Results and Observations

6.1. Effect of variation of pulse parameters (energy, pulse width, frequency) on the laser power 'Output limits'

Laser 'output limit' graphs for incremental pulse energy levels are as shown in Figures 6.1 to 6.5. The graphs show whether the laser was able to generate any output power whilst reaching the predetermined pulse energy levels. Ability to produce the sufficient maximum energy and its corresponding maximum average output power is denoted by a circle (○) symbol and cross (x) symbols indicate where it was not possible to generate any output power and/or where insufficient energy and its corresponding low average power is produced. Insufficient energy is produced normally at very low pulse widths (e.g. 0.5, 2ms) and low frequencies (e.g. 5 and 10 Hz). Where no energy, power was generated at high frequency levels the laser automatically generated a fault condition statement 'Laser Output over limit'. Where at sufficiently low frequency levels no output was generated the fault condition statement ' Calculated pump power limit' was generated. This was seen to occur at higher pulse width values (e.g. 18, 20ms). Reasons for the error statements occurring outside an acceptable envelope would be discussed in Chapter 7 in 'Discussions'. Figures 6.1 to 6.5 show a trend where, increase in pulse energy levels from 5J to 60J progressively reduces the number of parameter combinations (pulse width, frequency) capable of generating output and hence their availability to process. The area marked by the circular symbol (○) is progressively seen to reduce as the energy levels increase.
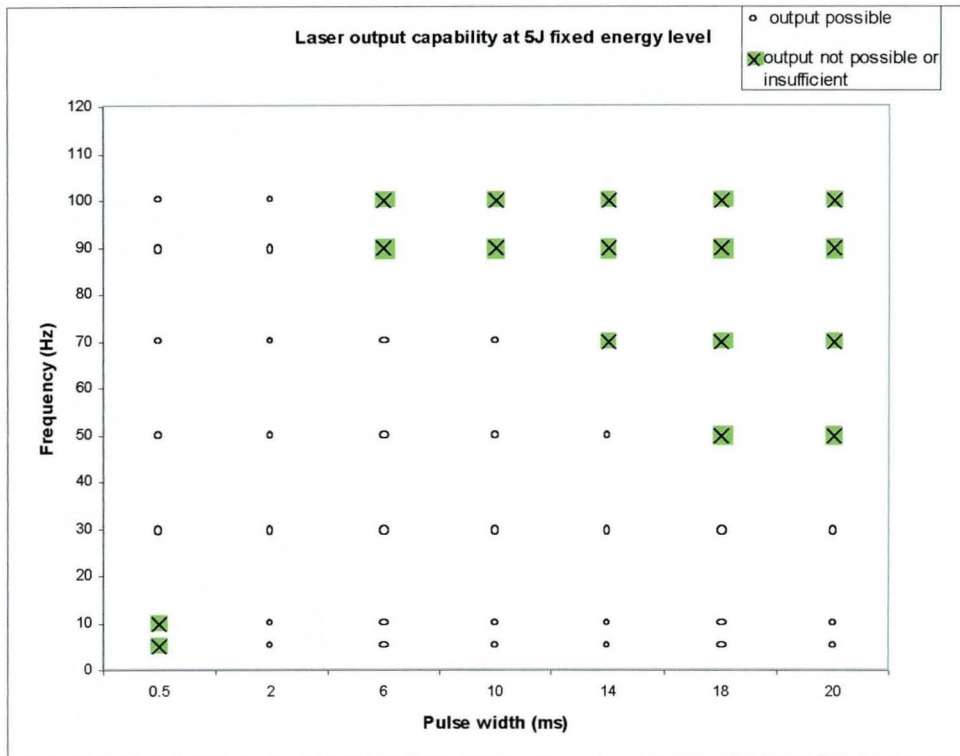
Figure 6.1: Laser output power limits at pulse energy 5J

The graph indicates a decrease in high frequency output for increasing pulse widths. Also at a very low pulse width (0.5 ms) and low frequency (5 and 10Hz) the required output energy level (5J) was not achievable.
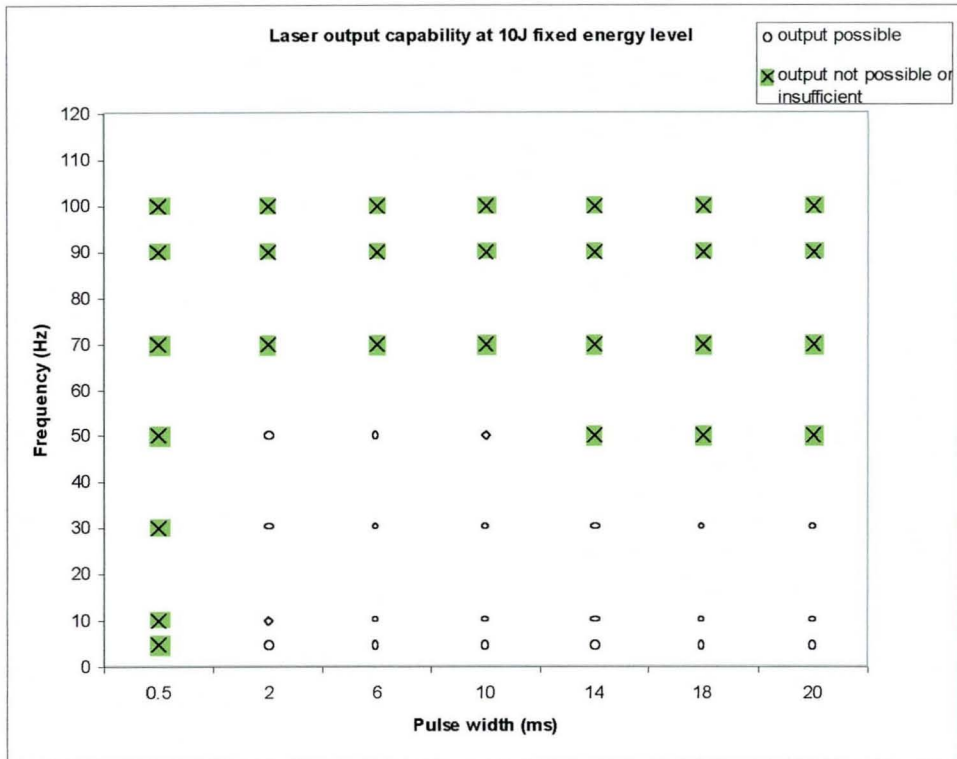
Figure 6.2: Laser output power limits at pulse energy 10J

Similar to the graph for energy of 5J, the number of output combinations at higher frequency levels reduces, this time for the entire range of pulse widths. No sufficient output was possible at the low pulse width of 0.5 ms for low frequency.
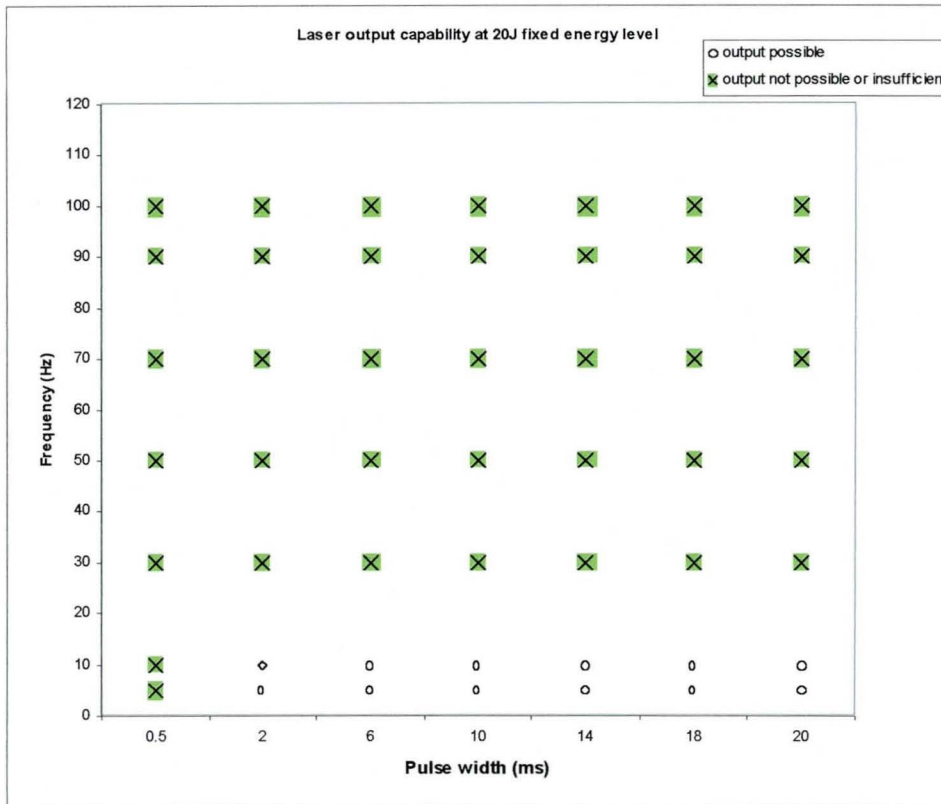
Figure 6.3: Laser output power limits at pulse energy 20J

At 20 J, the trend continues with no output combinations available at frequency

levels at or above 30 Hz, for any given pulse width. There are no output options

for very low pulse widths (0.5ms) for any frequency.
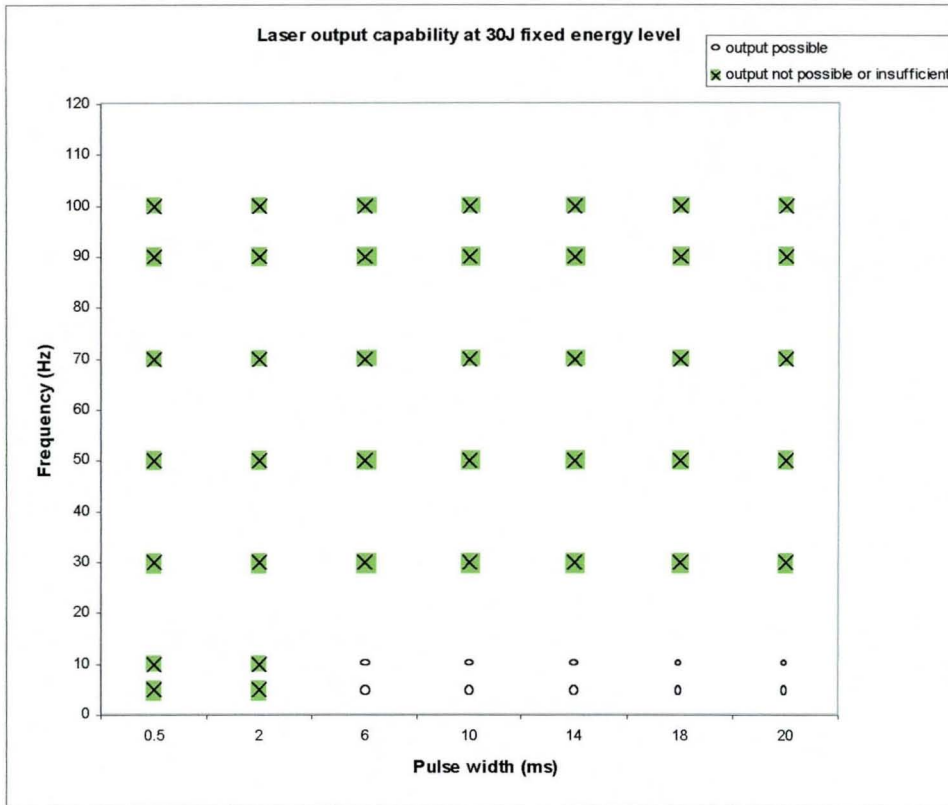
Figure 6.4: Laser output limits at pulse energy 30 J

At 30J, the usable output area of the graph is reduced further. For the frequency levels chosen, an output of 30J is only possible at 10Hz or less. A pulse width of 0.5 and 2ms does not give output at any frequency.
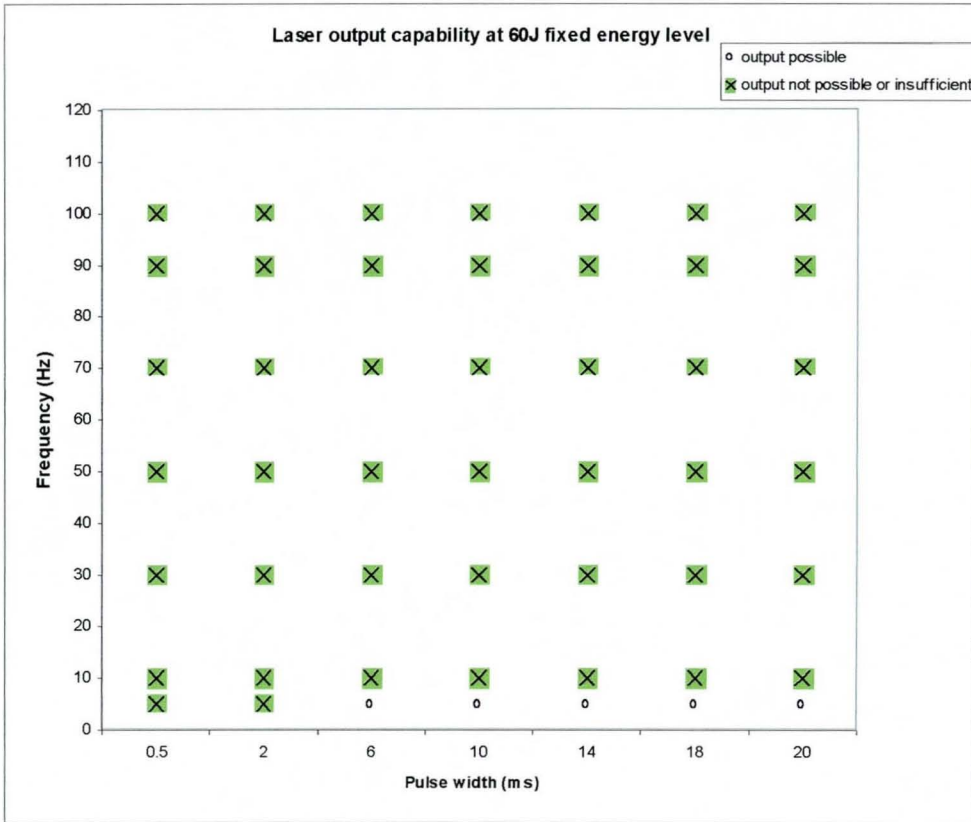
Figure 6.5: Laser output power limits at pulse energy 60J

At 60J, only the lowest frequency (5Hz) chosen, was able to generate output and pulse widths up to 2ms are excluded from the usable area of the graph.

The graphs in Figures 6.1 to 6.5 thus show a decreasing range of available output parameter combinations with an increase in energy levels.

6.2. Producing the single beads

The combination of parameters used in the production of beads, are shown in appendix A. A typical set of continuous beads are shown in Figure 6.6a

Such beads, also shown in Figure 5.4 previously would have a defined width and height. For example the continuous beads shown in Figure 6.6a was a result of a compatible set of parameters, which included the laser parameters and the scanning speed. Besides formation of such beads, it was very often found that the solidified mass of metal powder disintegrated into a discontinuous mass of ball like spherical structures when incompatible parameters were used, (e.g. a low energy level in combination with a relatively high scan speed).   This constituted of a non-bead that was not measured for the analysis. Other non bead scenarios that occurred were, the formation of highly irregular beads where the dimensions could not be measured reliably, lack of bead formation because of the powder being blown away, beads that were partially discontinuous or had broken off due to loose bonding at the substrate for their great part, undercut formed at the substrate with no bead being formed. Such non-bead scenarios were discarded as they could not produce reliable measurements. Only beads that were continuous, fixed to the substrate plate and uniform were therefore chosen for measurement. A number of beads, which resulted from an incompatible set of parameters are covered in section 6.4.2. Figure 6.6 a to c, shows a typical set of cross sections resulting from different types of beads produced by different parameter sets.
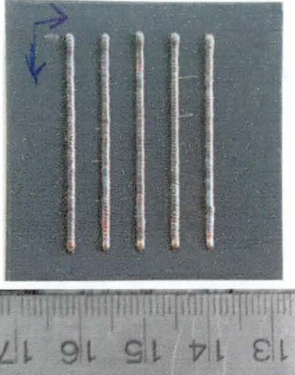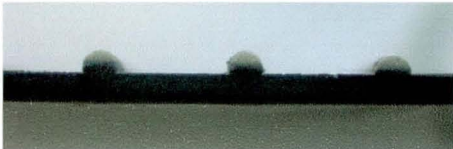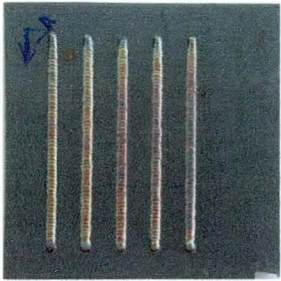
Top view of beads	Cross section
a) Uniform bead at greater layer thickness	Height = 0.866 mm Width = 1.246 mm
1mm layer, 30J, 5mm/s, 14ms, 10Hz	
b) Flattened bead at high energy, low layer thickness (undesirable due to high heat generated at the substrate plate)	Height = 0.33mm Width = 0.83 mm
0.4mm layer, 30J, 5mm/s, 14ms, 10Hz	
c) Irregular beads at low speeds	Height =1.364 mm Width = 1.762 mm
1mm layer, 10J, 1mm/s, 14ms, 30 Hz	

Figure 6.6: Typical cross sections of different beads.

6.3. Dimensions of beads

The following section presents the data that shows the effect of variation in process parameters pulse energy, pulse width or duration, pulse frequency and speed on the width and height of the bead.

6.3.1. Effect of Pulse parameters (pulse energy, pulse width or pulse duration and frequency) and speed on average width of a bead

6.3.1.1. Results of bead width for a layer height of 1mm

Graphs are plotted for an energy level of 5J at fixed speeds in order to understand the effect of process parameters (pulse width and pulse frequency) on the average width for a single bead. The graphs are presented separately for speeds 1mm/s, 5mm/s, 10mm/s, 15mm/s and 20 mm/s.

Figure 6.7 shows a graph at a speed of 1mm/s, indicating an increase in average width for a single bead, with increase in pulse width (or duration of pulse) and also frequency of pulse. Thus pulse width and frequency, both affect the average bead width. At an increased speed of 5mm/s, Figure 6.8 shows a similar rising trend in average bead width with an increase in pulse width (duration) and pulse frequency. An exception is the bead width at value 10ms at frequency 70 Hz, where the average width is seen to drop. Average widths greater than those for 1mm/s are seen, presumably due to the high frequency, which would result in higher average power input.
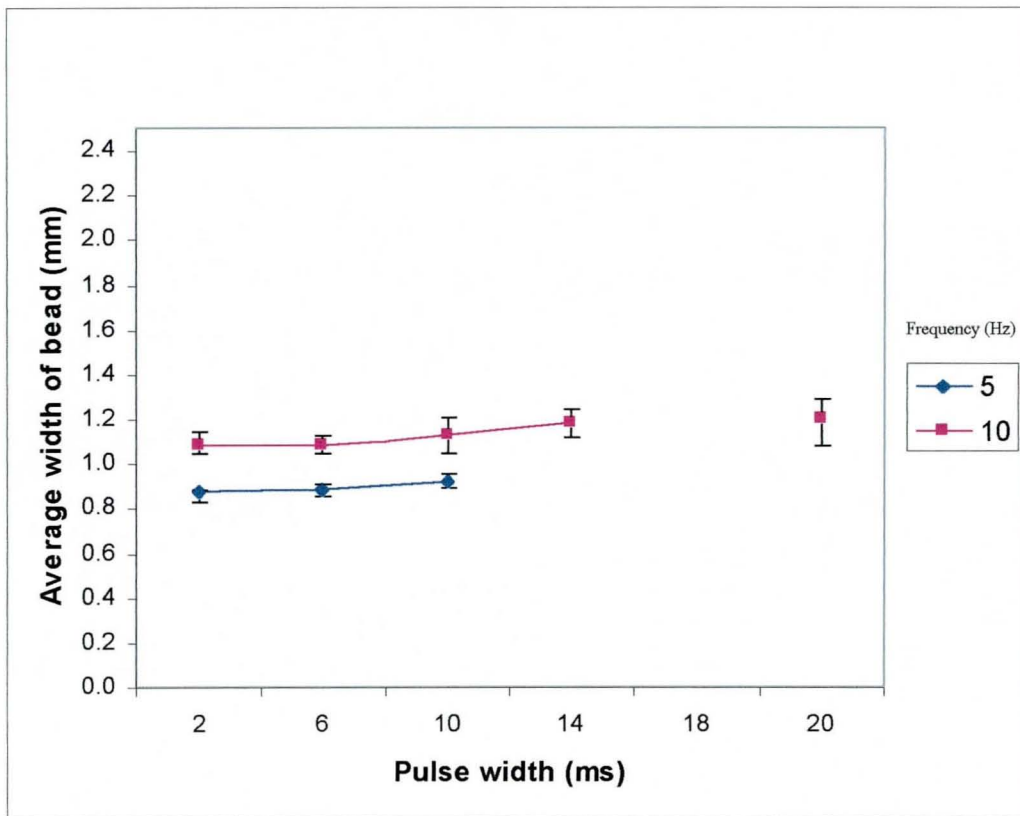
Figure 6.7: Graph of pulse width versus average bead width (1mm/s, 5J)

The effect of increase of pulse width in Figure 6.8 is seen to be somewhat proportional for frequency 30 and 50 Hz, indicating that factors may be acting independently for these frequency levels. Interactions seem to be present at higher frequency (70Hz) as indicated by the intersecting lines between 6 and 10ms pulse duration.
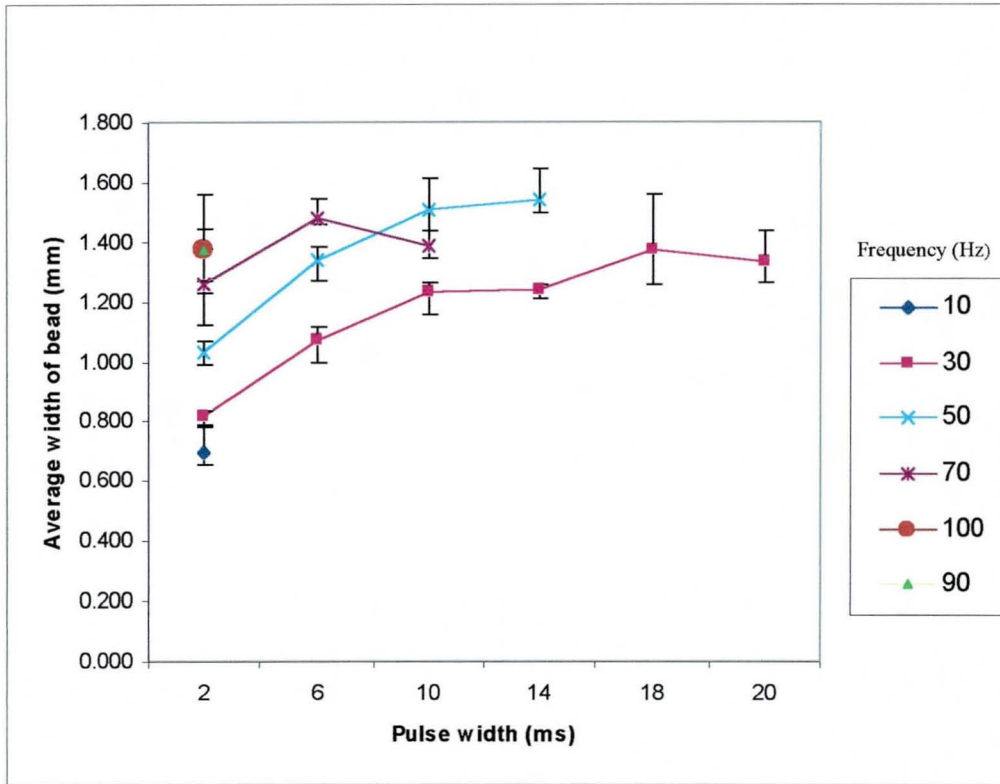
Figure 6.8: Graph of pulse width versus average bead width (5mm/s, 5J)

In Figure 6.9, uniform increasing trends are not present and there is both an increase and decrease in average widths as a result of variation in pulse width. An increase in speed (to 10mm/s) is also coupled with a decrease in number of beads possible for frequency 30Hz and less. This was due to the formation of balling, which were found weakly fused to the substrate plate. No output is available at 18, 20ms for beyond 30Hz. Error bars overlap in areas of low pulse width (0.5, 2ms), indicating that the significance of effect of frequency (for those pulse widths) on the average bead width, is unclear. It is possible to use the lowest pulse width (0.5ms) at this speed (10mm/s) compared to lower speeds. At 15 and 20 mm/s, Figure 6.10 and 6.11 indicate bead formation for very low pulse widths at high values of frequency.
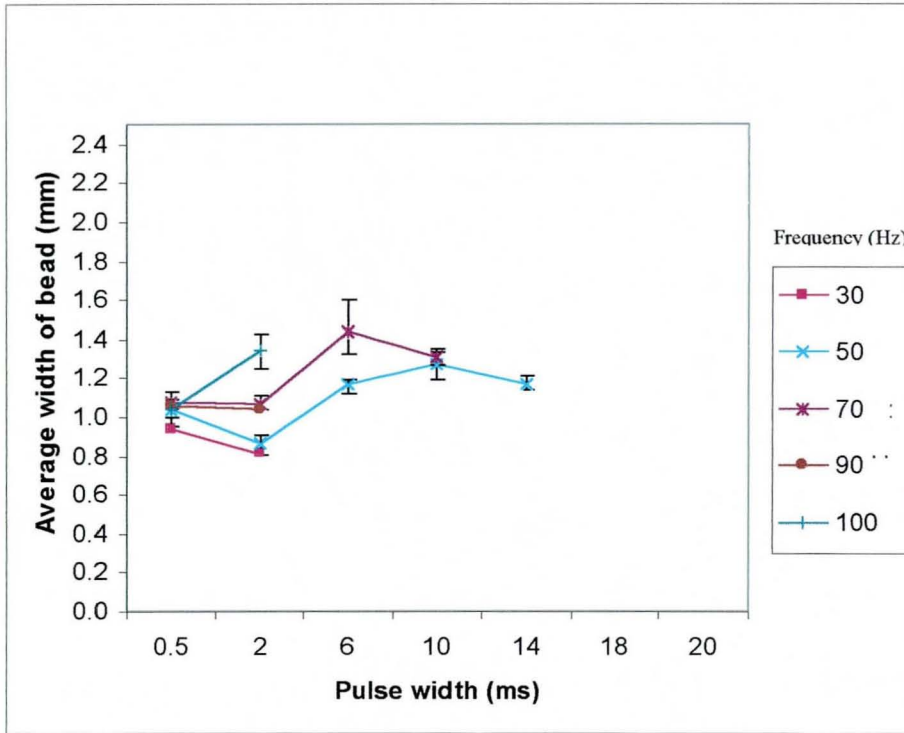
Figure 6.9: Graph of pulse width versus average bead width (10mm/s, 5J)
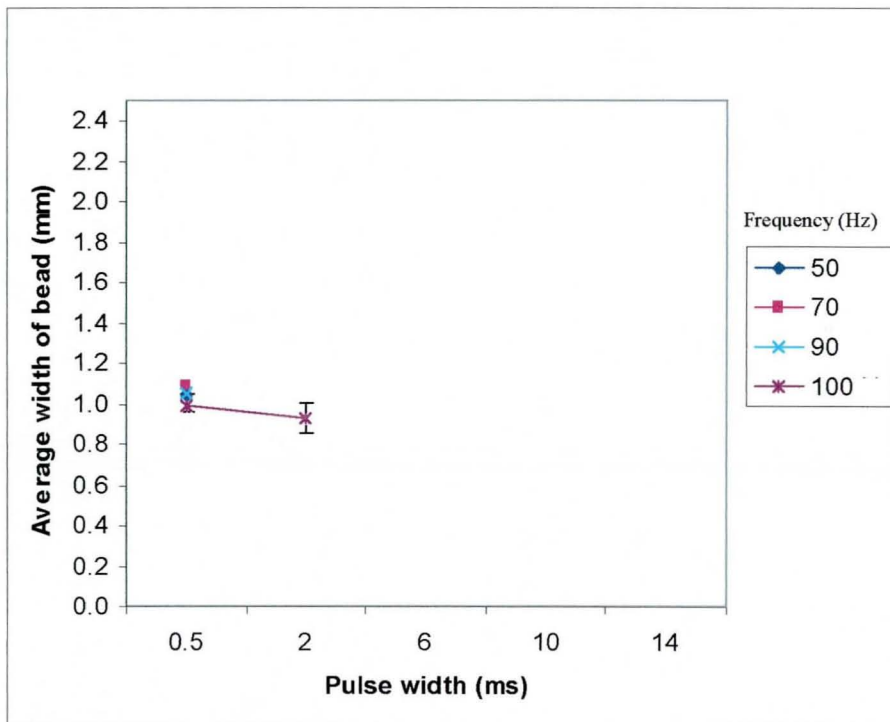
Figure 6.10: Graph of pulse width versus average bead width (15 mm/s, 5J)
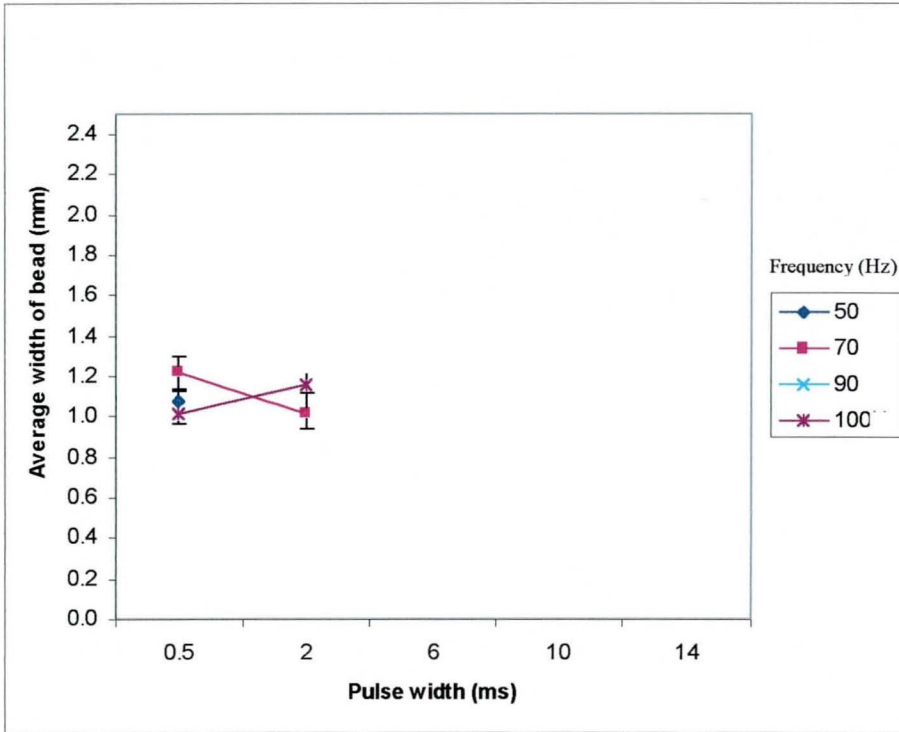
Figure 6.11: Graph of pulse width versus average bead width (20 mm/s, 5J)
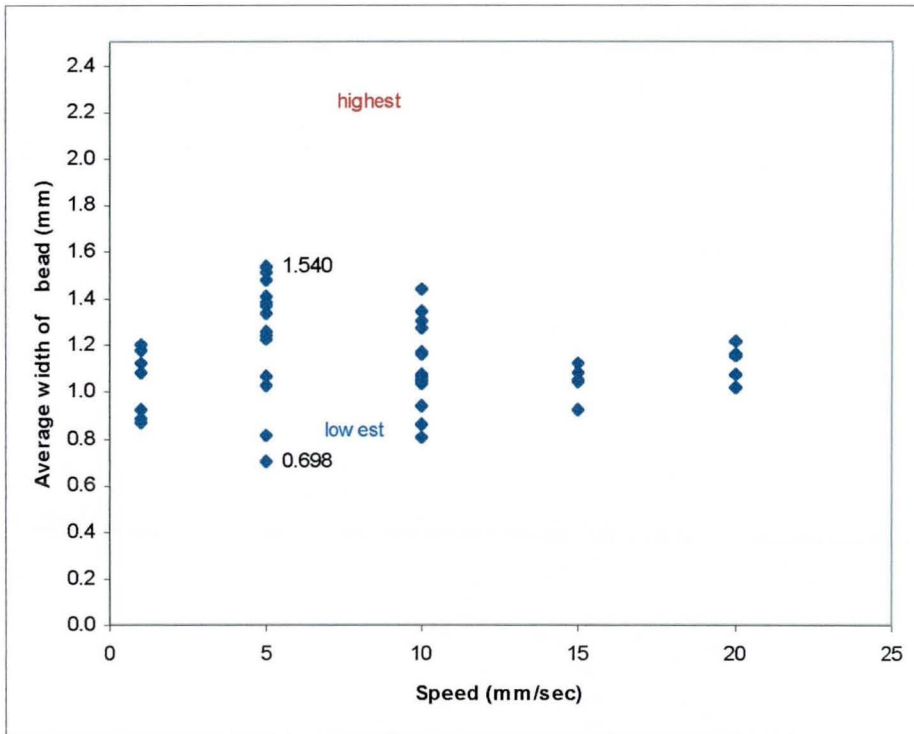
Figure 6.12: Graph of speed versus average bead width (5J)

In Figure 6.12, the graph shows some unclear variation as observed by the variation in highest and lowest, width values. It can be seen that highest and lowest values of bead width are seen at speeds 5 and 10mm/s. The number of observations (or beads), are highest for speeds 5 and 10mm/s.
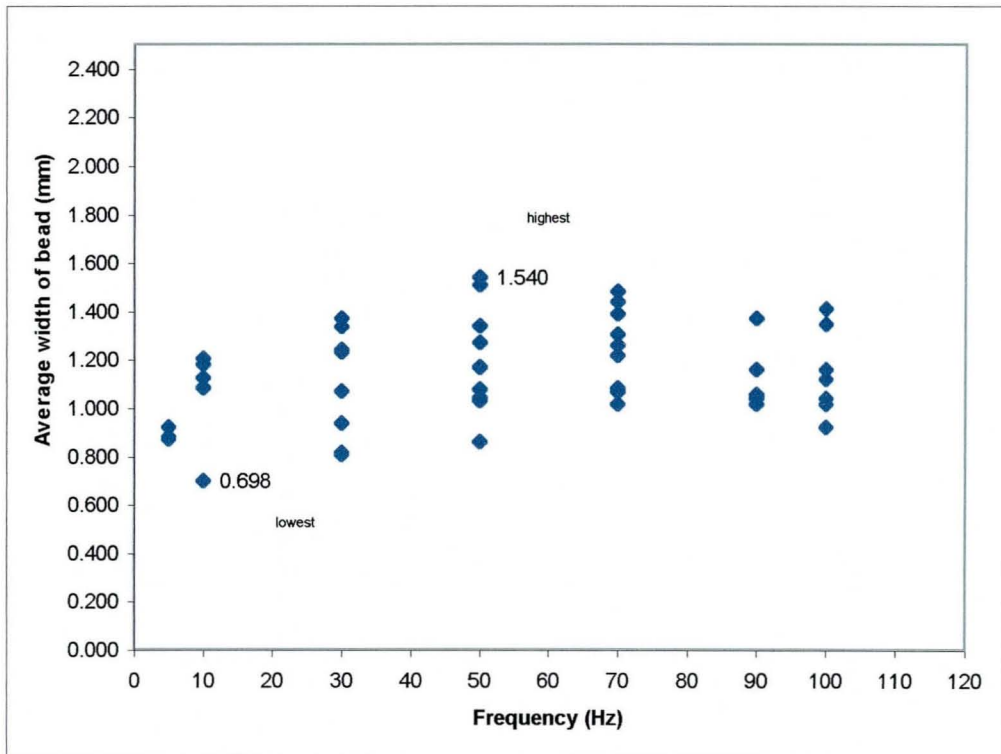
Figure 6.13: Graph of frequency versus average bead width (5J)

At 5J (Figure 6.13), frequencies 30, 50 and 70 Hz are observed to give a reasonably higher number of measurable beads also showing that the lowest value is greater for a higher frequency.
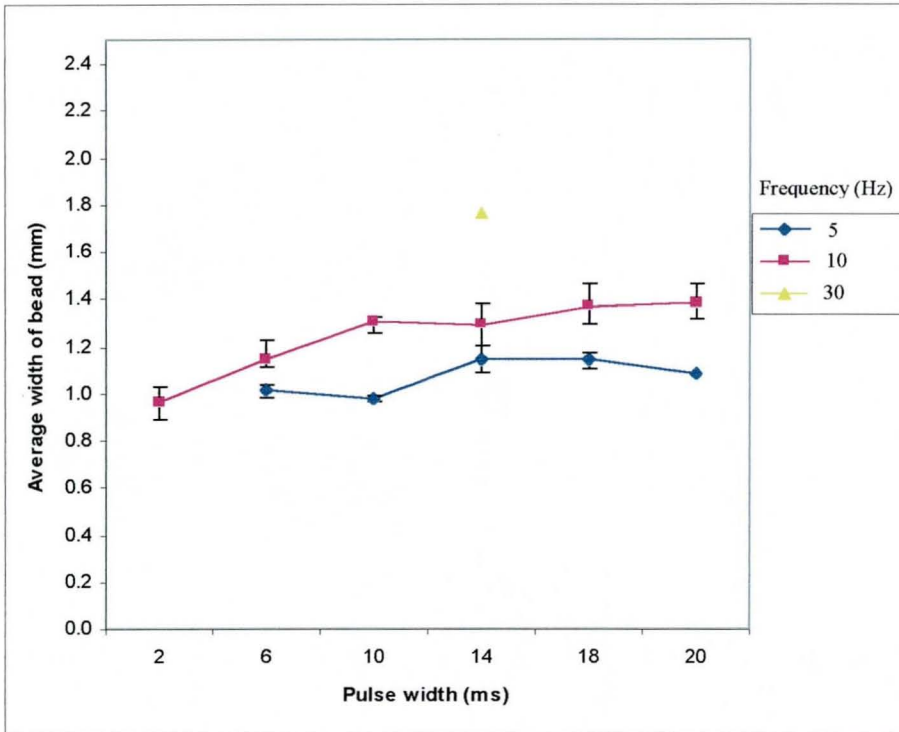
Figure 6.14: Graph of pulse width versus average width of a bead (1mm/s, 10J)

As with the graphs at 5J energy, the graph (10J) in Figure 6.14 shows an increase

in the average width for a single bead with increase in pulse width for value 10

Hz. For 5 Hz the trend is less clear and a decrease is seen at pulse widths for 6 to

10 and 18 to 20 ms. There is only a single bead possible at a higher frequency

level of 30 Hz, which shows a high average value. A comparison with graph

(Figure 6.7 for 10 Hz) at 5J, shows a general increase in width measurements at

10ms and above. Also more beads are seen possible at low frequency (5Hz) for

10J (Figure 6.14) as compared to Figure 6.7.

Figure 6.15: Graph of pulse width versus average width of a bead (5mm/s, 10J)
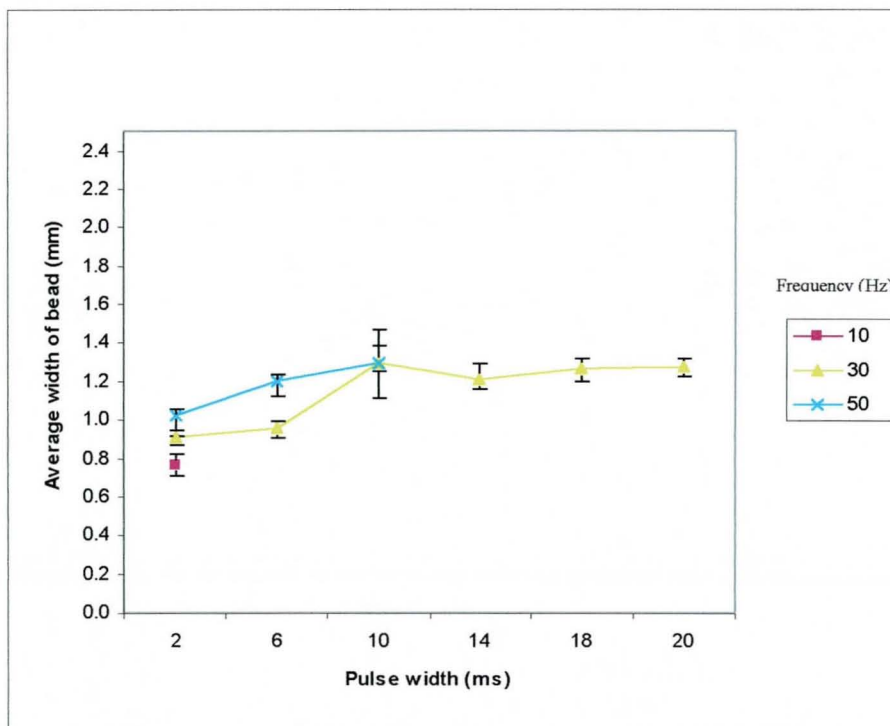
Figure 6.16: Graph of pulse width versus average width of a bead (10mm/s, 10J)

An increase in speed to 5mm/s (Figure 6.15) shows increase in the average width values at pulse width levels up to 14ms (frequency 30Hz), after which the average width drops. Frequency too produces an increase in the average width. It can be seen that a frequency of 30 Hz gives more results as compared to the previous graph at 1mm/s. Low frequencies 5Hz and 10 Hz yield very few results. This is also summarised in Figure 6.20.

A further increase in scan speed (Figure 6.16) to 10mm/s, gives an equal number of results as for 5mm/s. The average width is seen to increase with pulse width for frequency 30 and 50 Hz. In general, for both Figures 6.15 and 6.16, the lines for frequencies 30 and 50 Hz intersect at pulse widths 10ms, indicating that an increase in pulse widths may cause interactions at higher frequency levels. A similar effect is seen to occur at 5J, 5mm/s (Figure 6.8). At speeds 15 and 20 mm/s, Figure 6.17 and 6.18 continuous beads are formed at high frequencies and also overall there are less number of beads formed.

An analysis of all data obtained for an energy of 10 J at varying speeds (Figure 6.19) indicates that average lowest widths tend to decrease with increase in speeds (up to 10mm/s), which may be expected due to reduced line energy available to melt the powder. At higher speeds there are lesser beads.

Figure 6.17: Graph of pulse width versus average width of a bead (15mm/s, 10J)

Figure 6.18: Graph of pulse width versus average width of a bead (20mm/s, 10J)

Figure 6.19: Graph of scan speed versus average width of a bead (at 10J)
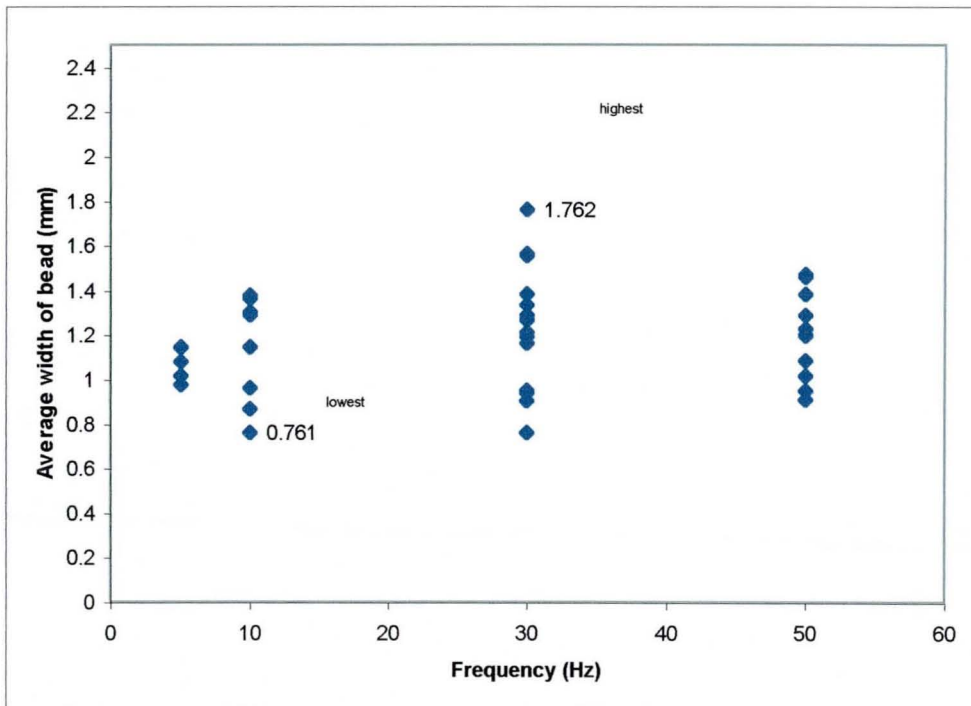
Figure 6.20: Graph of frequency versus average width of bead (at 10J)

The graph for 20J (Figure 6.21) shows no appreciable difference in characteristics from those at energy 10 J and 5J (Figures 6.7 and 6.14). There are increasing bead widths for increasing pulse widths and frequency too has an effect. There were no beads possible with low pulse widths at 0.5 and 2ms. At 0.5ms the laser produces no output and at 2ms the substrate was seen to be burnt and the powder blown, presumably due to the relatively high energy level of 20J giving high peak power.

Nevertheless, comparing Figures 6.21 and 6.14, it is evident that there is a general overall increase in average width of beads as can be expected due to an increase in energy.

It is interesting to see a similar trend marking the gradual rise and fall of bead widths values in Figures 6.15 and 6.22, although at different frequency levels (30 and 10Hz respectively). This indicates that choosing a different energy level could result in similar trends as would result by changing the frequency (at a different energy level), in terms of its effects on the metal powder.

Higher speeds require higher frequency, in order to obtain similar bead widths. Comparing across energy levels Figure 6.23 and Figure 6.19 (20 and 10J respectively), the widths seem to fall within a similar range 0.8mm to 1.6mm. At 20J, Figure 6.23 the number of beads progressively reduce, with increasing speed and beyond 10mm/s beads are not possible. It is clear, this is perhaps due to the lack of frequency levels greater than 10Hz available for 20J with most beads occurring at 10Hz (Figure 6.24).

Figure 6.21: Graph of pulse width versus average width of bead (1mm/s, 20J)
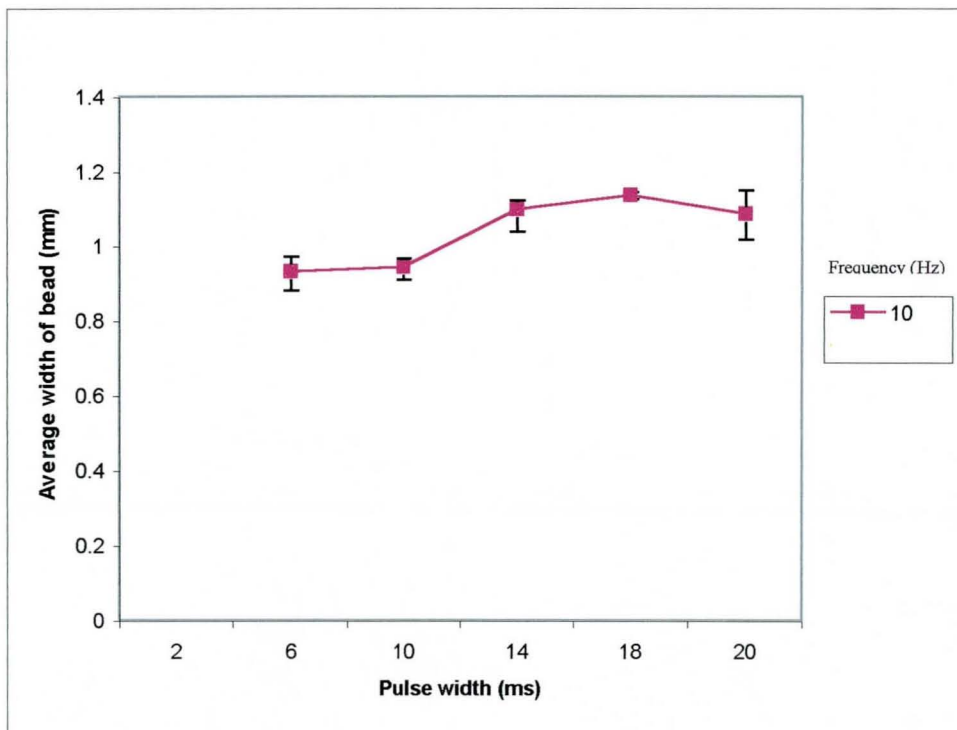
Figure 6.22: Graph of pulse width versus average width of bead (5mm/s, 20J)
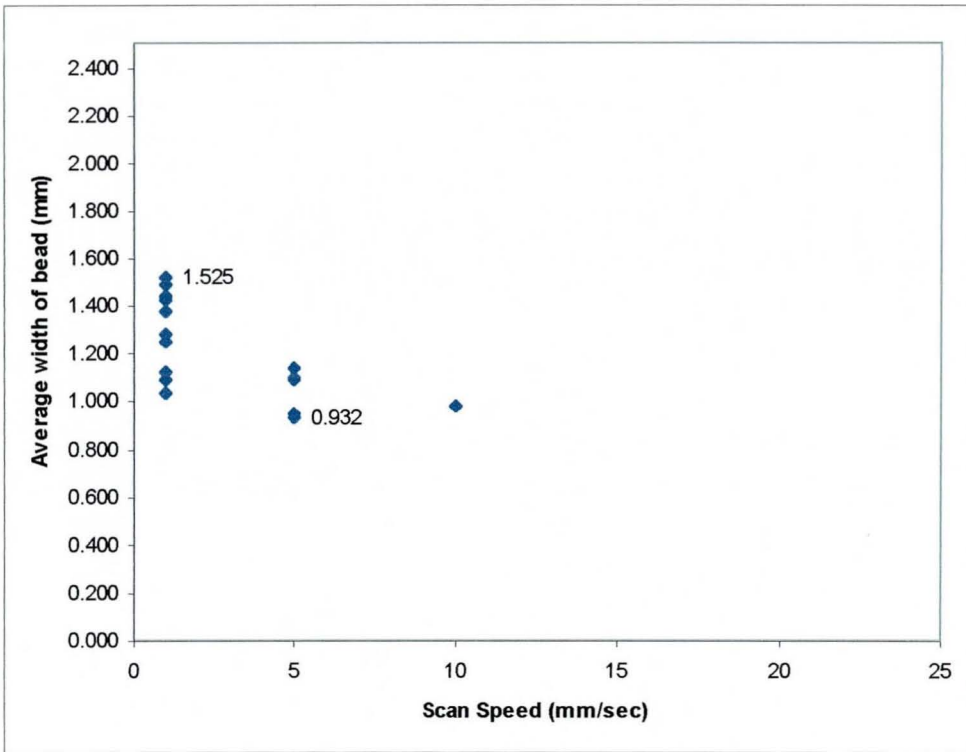
Figure. 6.23: Graph of scan speed versus average width of a bead (20J)
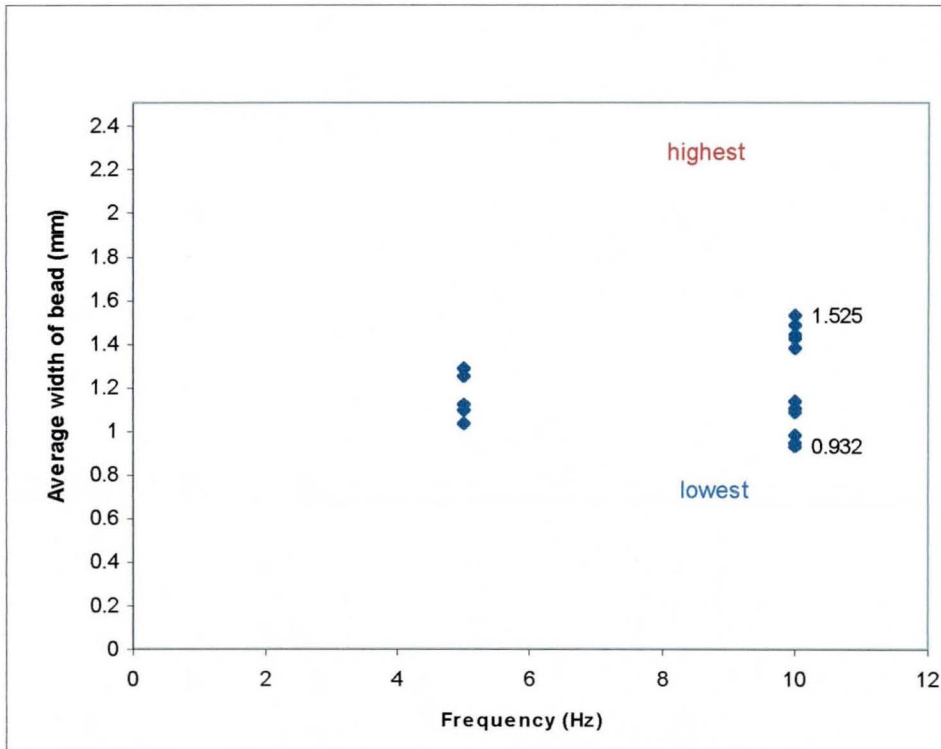
Figure 6.24: Graph of frequency versus average width of a bead (20J)
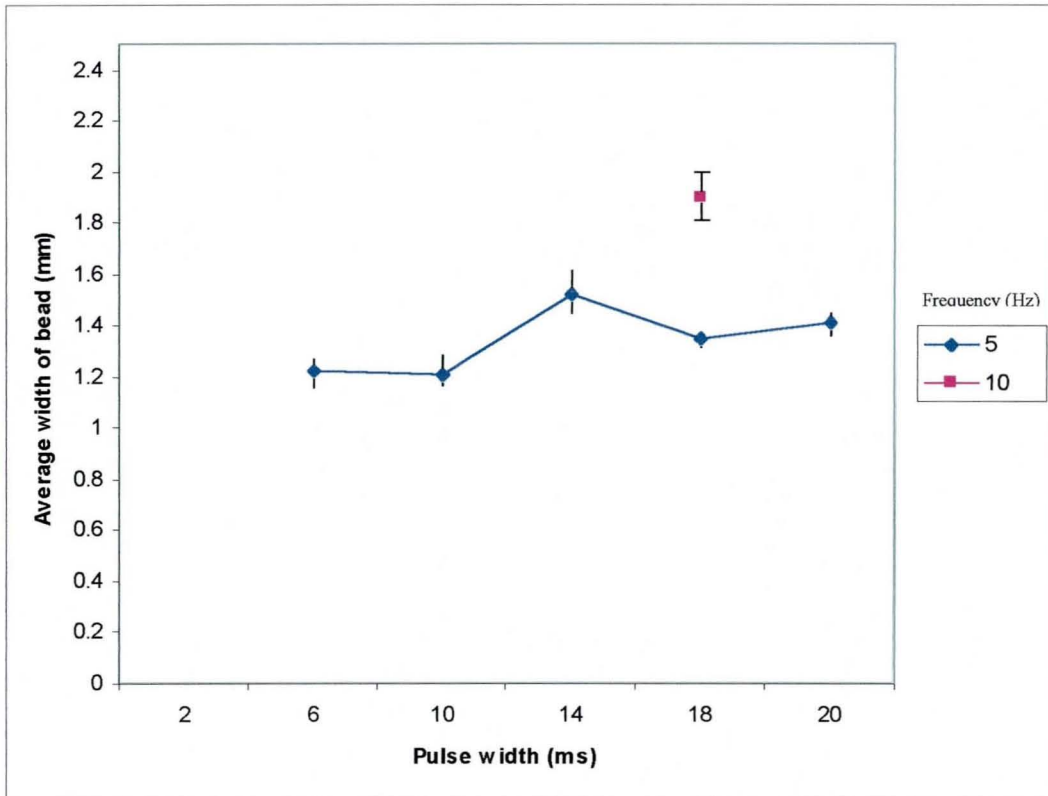
Figure 6.25: Graph of pulse width versus average width of a bead [1mm/s, 30J]

The graph in Figure 6.25 shows an increasing trend common to other graphs at lower energy levels (5J), at the same speed. Widths obtained are higher than those seen for energy level of 20J (Figure 6.21) and 10J (Figure 6.14) for the same frequency and speed.

An increase in scan speed to 5mm/s produces more beads (Figure 6.26) for a frequency of 10 Hz than for 5Hz. As in most graphs the bead width generally increases with an increase in pulse width.

Figure 6.26: Graph of pulse width versus average width of a bead [5mm/s, 30J]
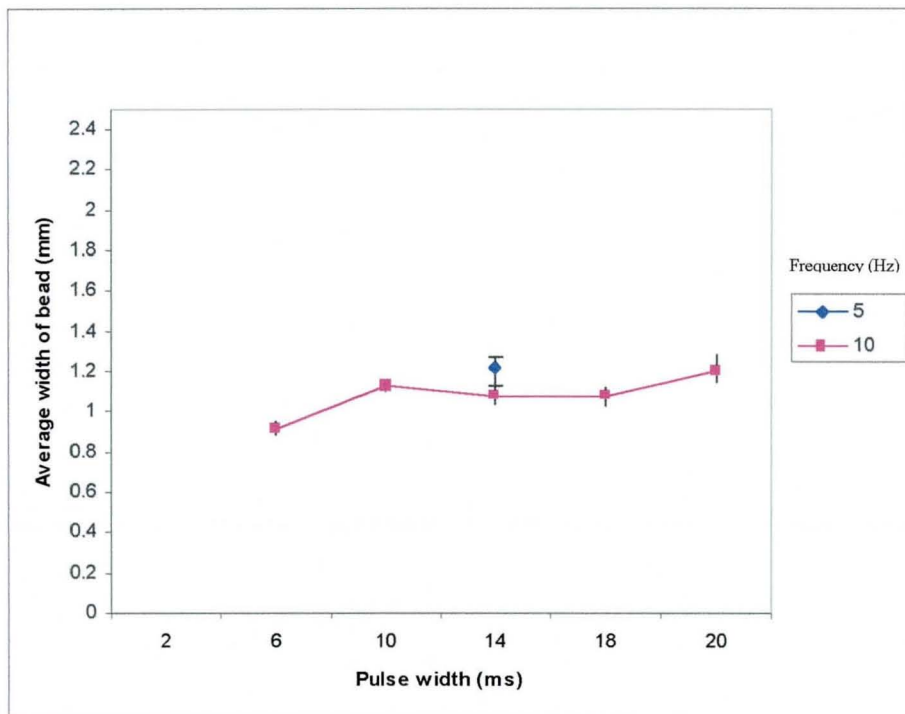
Figure 6.27: Graph of pulse width versus average width of a bead [10mm/s, 30J]

It is interesting to see in Figure 6.27 for a speed of 10mm/s, that only one bead is seen produced at a low frequency at a pulse width of 14ms. This has a width higher than those produced at higher frequency. At a frequency of 5 Hz it is seen not possible to produce beads, due to balling presumably resulting from a combination of relatively lower average powers and high speeds. Generally width values are comparable to those produced at 20J, 5mm/s at 10 Hz (Figure 6.22)

The graph (Figure 6.28) for 30J shows little change in bead widths from frequencies 5Hz to 10Hz.
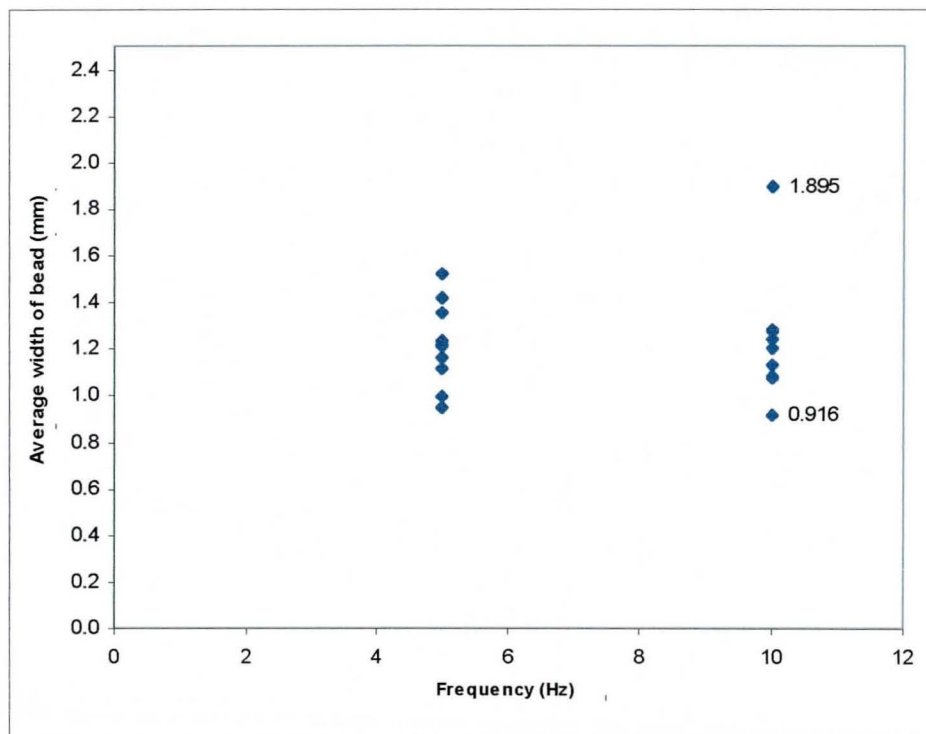
Figure 6.28: Graph of frequency versus average width for a bead [30J]

A graph of scan speed versus average width (Figure 6.29) of a bead for 30J, shows that it is possible to produce more beads at a higher speed e.g. 10mm/s, as compared to that for 20J (Figure 6.23).

Figure 6.30 and Figure 6.31, indicates few beads at pulse energy 60J.

Figure 6.29: Graph of scan speed versus average width of bead [30J]

Figure 6.30: Graph of pulse width versus average width of a bead (1mm/s, 60J)
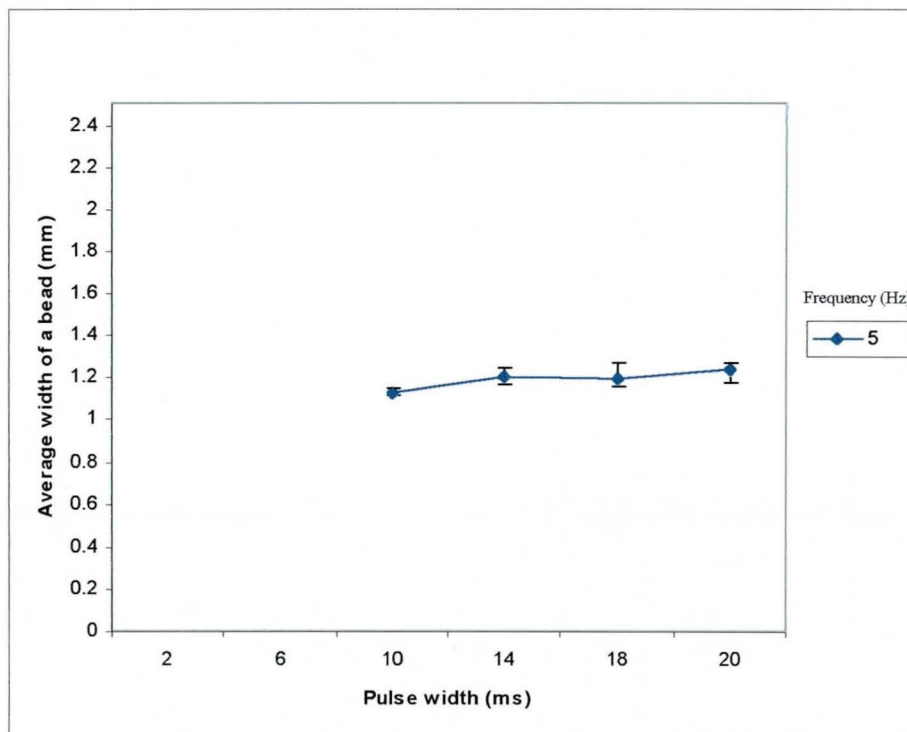
Figure 6.31: Graph of pulse width versus average width of a bead (5mm/s, 60J)

6.3.1.2. Results of bead width for a Layer height of 0.4mm

Figure 6.32 and Figure 6.33 shows no appreciable increase in average bead width with an increase in pulse width. Also frequency series lines are stacked in increasing order of frequencies (as for 1mm layer in Figure 6.8) though much closer with error bars for 5 and 10 Hz overlapping in Figure 6.32 and 30, 50 and 70 Hz overlapping in Figure 6.33. This indicates no significant effect of frequency at those values. In general the increase in speed permits the use of greater frequency values to produce beads. Very low pulse widths (0.5ms and 2ms) produce greater bead widths at high frequencies (90 and 100 Hz) and for these values the results are similar to those with a 1mm layer.

Figure 6.32: Graph of pulse width versus average width of a bead (1mm/s, 5J)

Figure 6.33: Graph of pulse width versus average width of a bead (5mm/s, 5J)

Figure 6.34: Graph of pulse width versus average width of a bead (10mm/s, 5J)

At increasing speeds 10mm/s, 15 mm/s and 20 mm/s (Figures 6.34, 6.35 and 6.36 respectively) the average bead width values are generally seen to be similar. It is observed from a comparison of graphs, that speeds greater than 10mm/s require frequencies starting at 30Hz in order to produce beads and low frequencies 5Hz and 10 Hz are suitable for speed of 1mm/s.

Width values are generally seen to lie between 0.6 and 1mm as evident in Figure 6.33. Figure 6.37 in comparison with Figure 6.12 (at 1mm layer thickness) shows reduced widths with 0.4mm layers.

Figure 6.35: Graph of pulse width versus average width of a bead (15 mm/s, 5J)

Figure 6.36: Graph of pulse width versus average width of a bead (20 mm/s, 5J,)

Figure 6.37: Graph of speed versus average width of bead (5J)
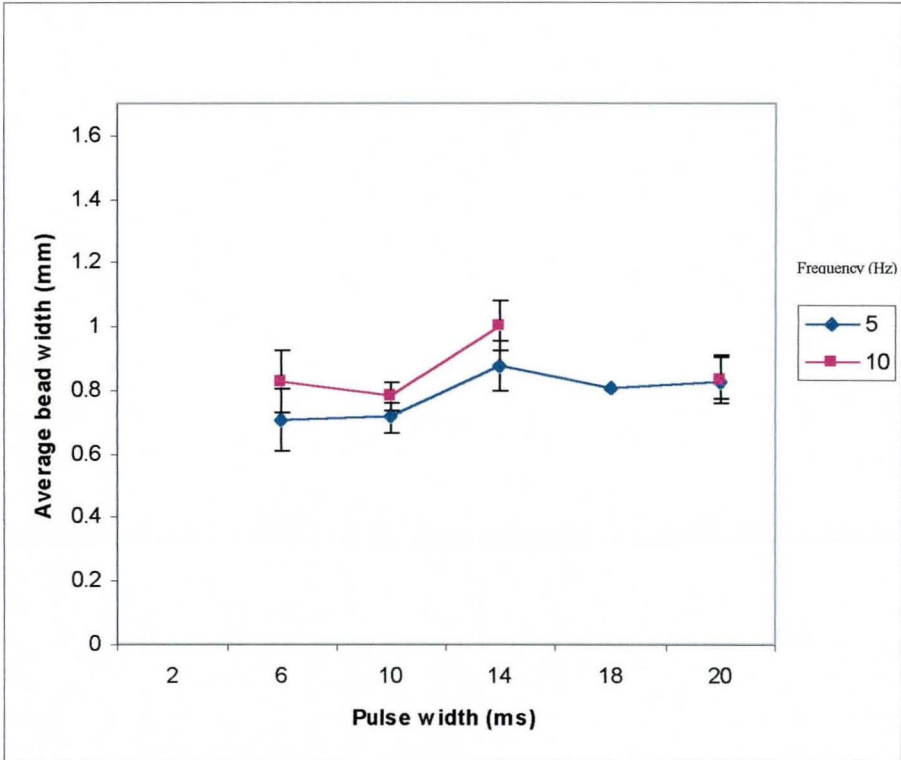
Figure 6.38: Graph of pulse width versus average width of a bead (1 mm/s, 10J)

Similar results are observed at a higher energy level of 10J as shown in Figures 6.38, 6.39, 6.40, 6.41, 6.42 for speeds 1, 5, 10, 15 and 20mm/s respectively. The range of average bead widths, are not changing with scan speed, as seen in Figure 6.43.
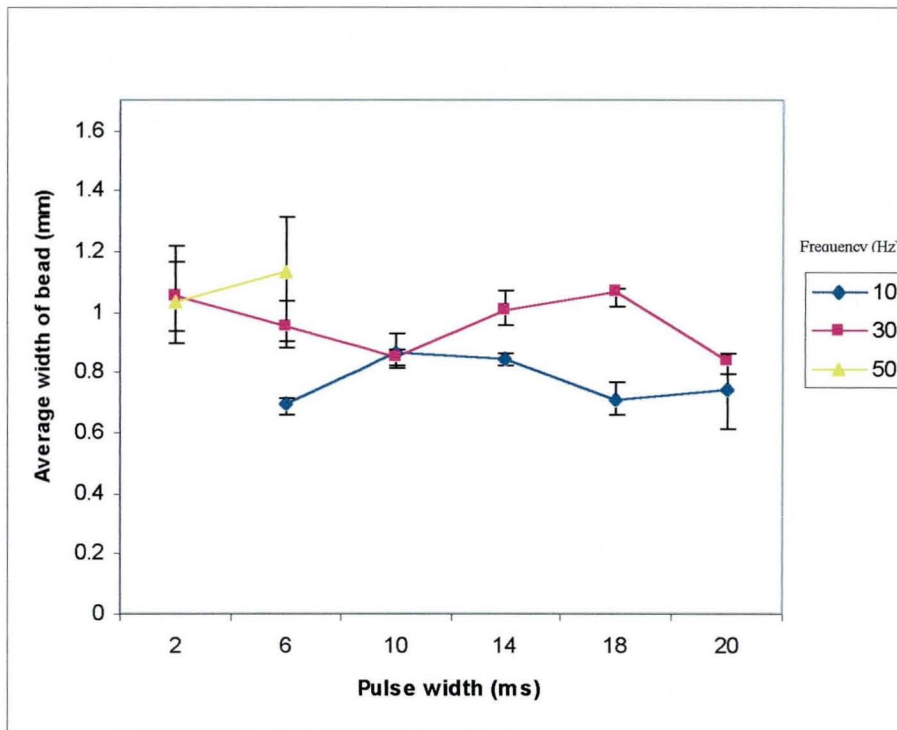
Figure 6.39: Graph of pulse width versus average width of a bead (5mm/s, 10J)
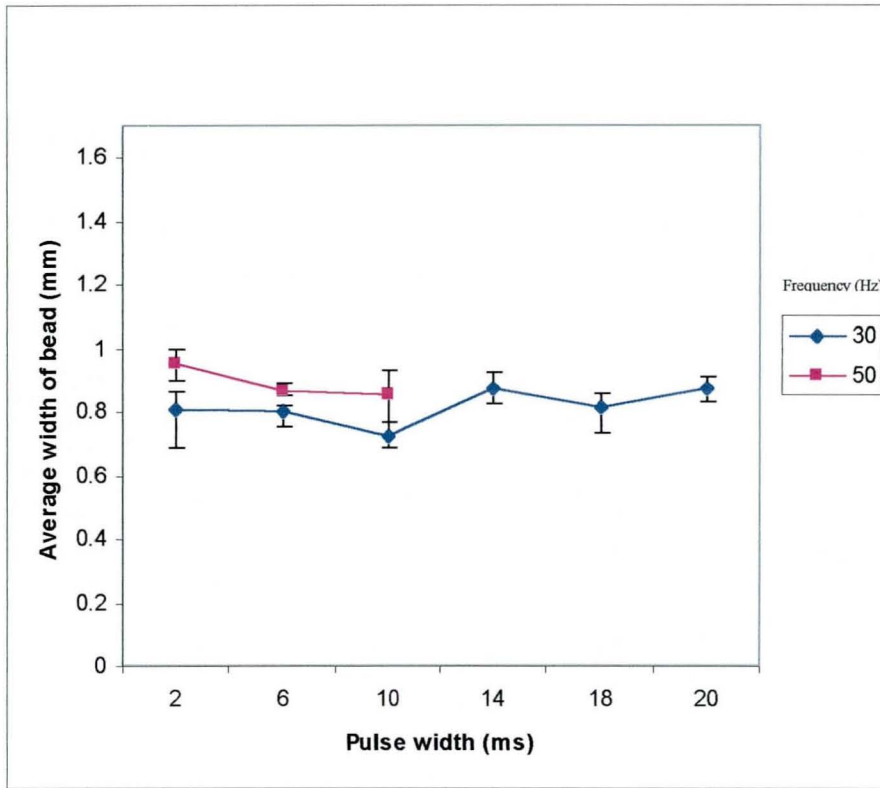
Figure 6.40: Graph of pulse width versus average width of a bead (10mm/s, 10J)
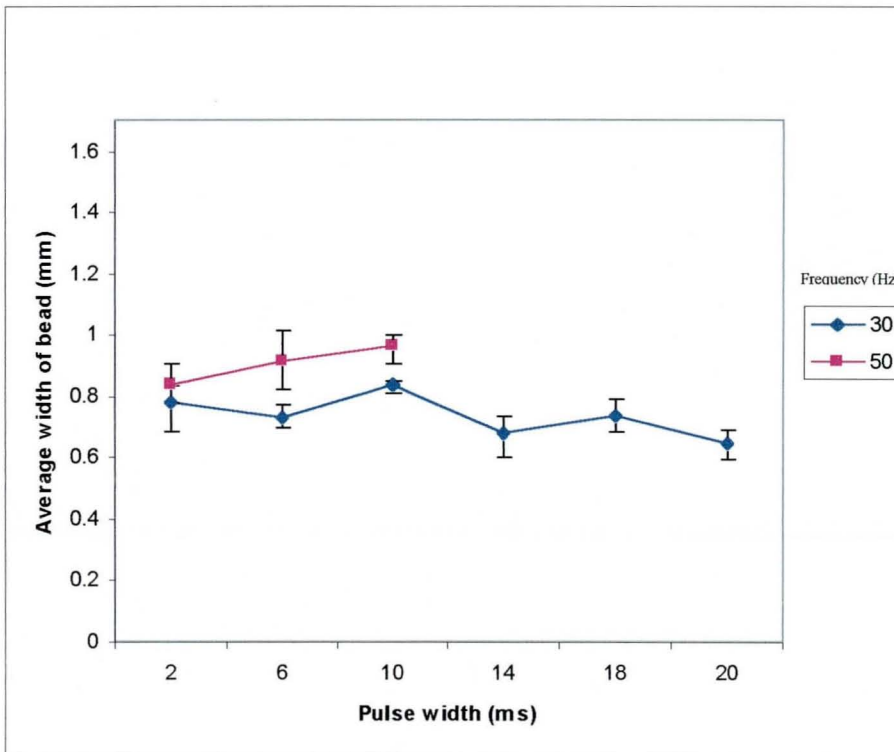
Figure 6.41: Graph of pulse width versus average width of a bead (15mm/s, 10J)
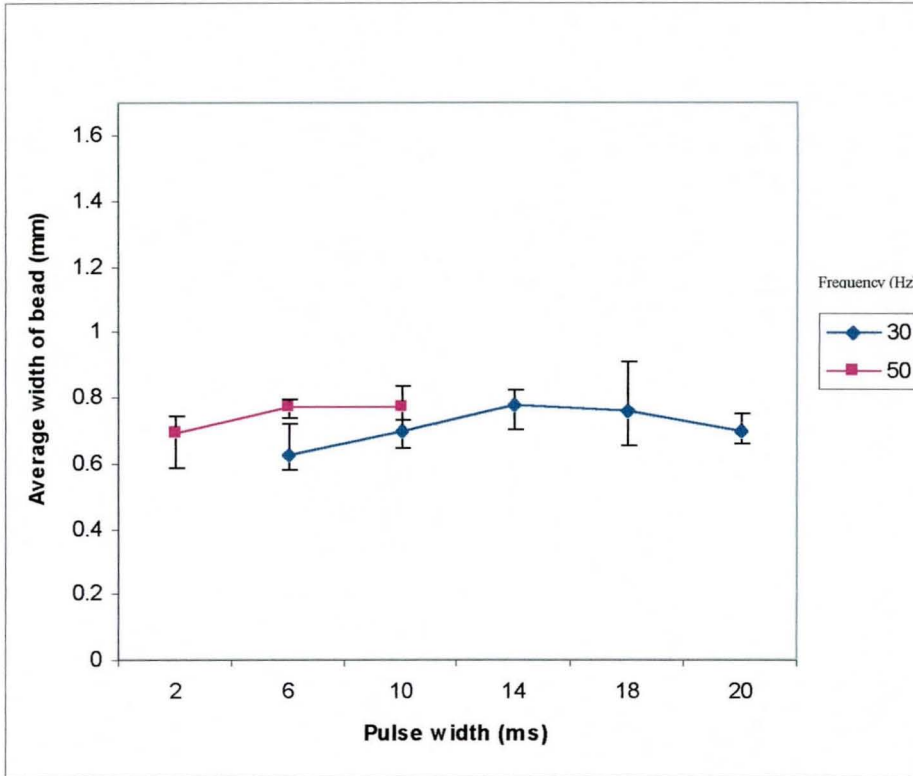
Figure 6.42: Graph of pulse width versus average width of a bead (20mm/s, 10J)
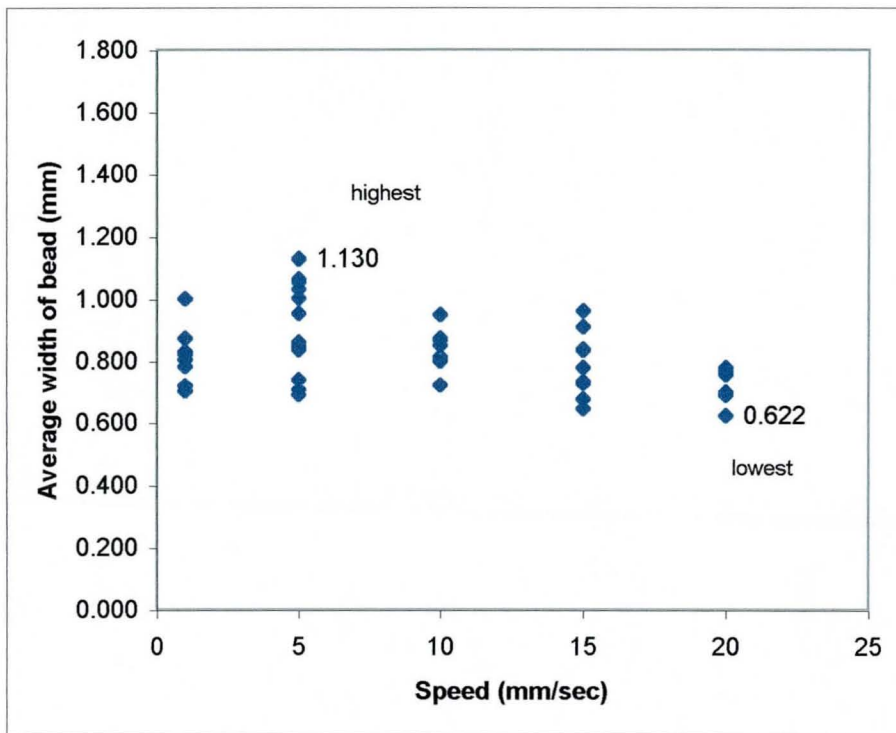
Figure 6.43: Graph of speed versus average width of a bead (10J)

At 1mm/s for 20J, Figure 6.44, there is noted relatively high variation in average width values. Figures 6.45 and 6.46 for 5mm/s and 10mm/s respectively, show little variation in average widths with increasing pulse widths.

There is a reduced number of beads (Figure 6.47) at higher speeds, with the highest being 10mm/s. Figure 6.47 shows the decreasing value of maximum widths obtained at each level of increasing speed. Also there are comparatively fewer beads at 1mm/s as compared to Figure 6.23 (20J, 1mm/s, 1mm layer).

It should be observed that a higher energy level, the choice of which limits high frequencies due to equipment limitations would result in lesser number of parameters and hence possible beads. This is seen comparing graph shown for 30 J and 20J, Figure 6.52 and Figure 6.47.with graph for 10J (Figure 6.43) where greater number parameters result in greater number of beads.
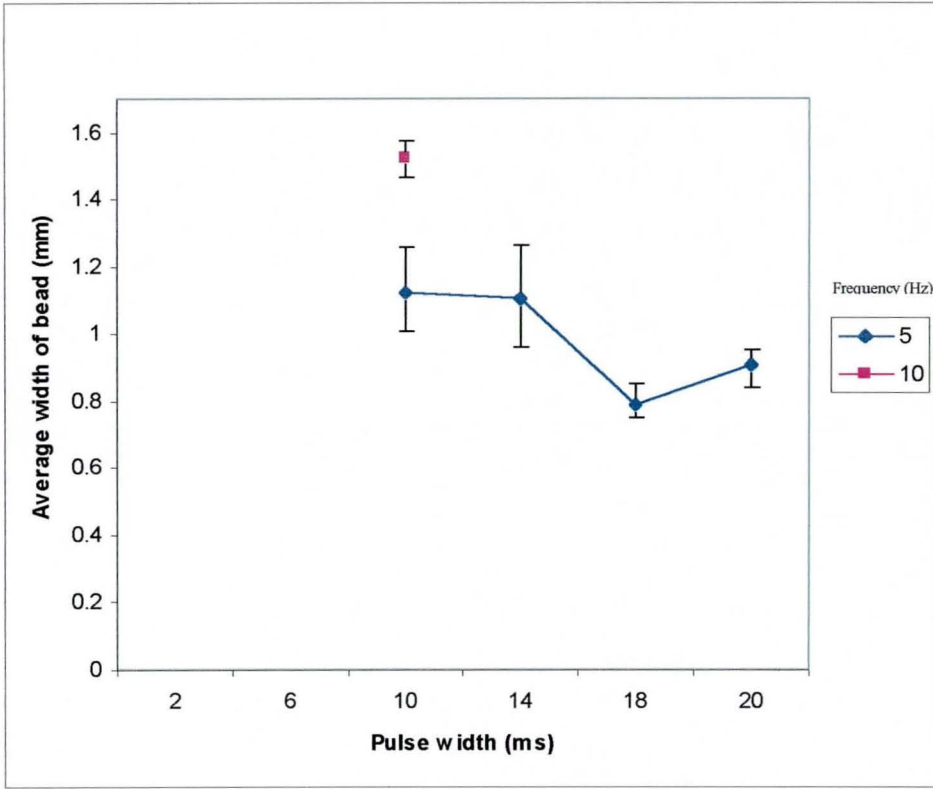
Figure 6.44: Graph of pulse width versus average width of a bead (1mm/s, 20J)
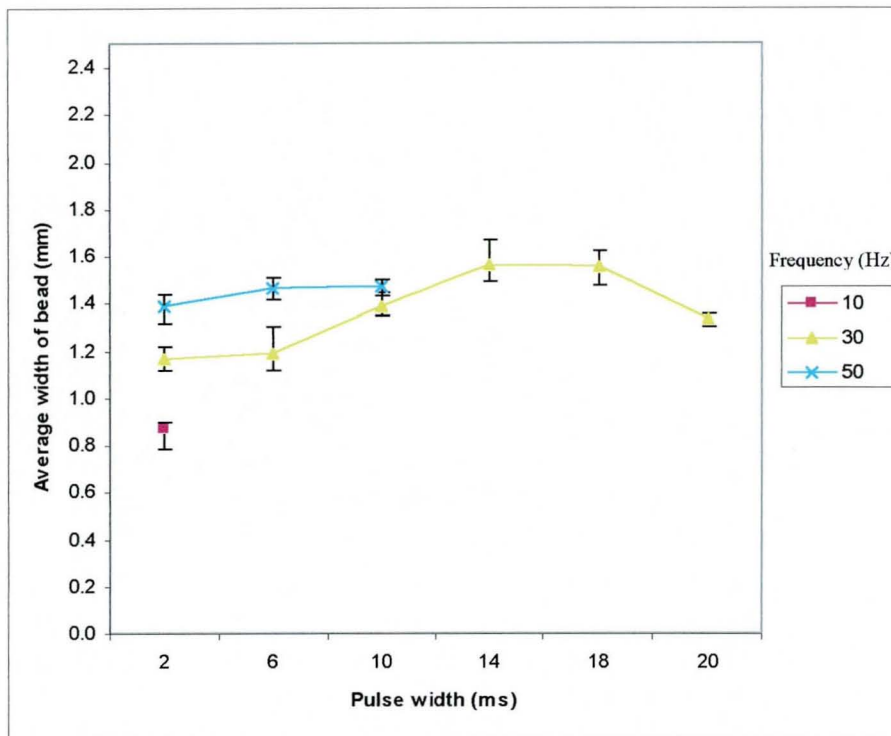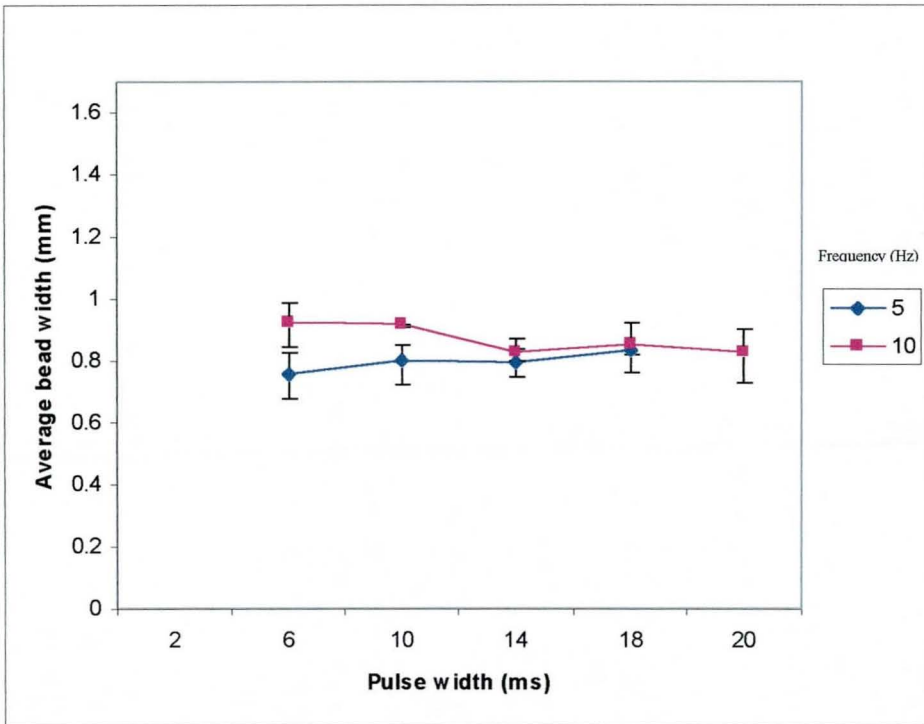

Figure 6.45: Graph of pulse width versus average width of a bead (5mm/s, 20J)
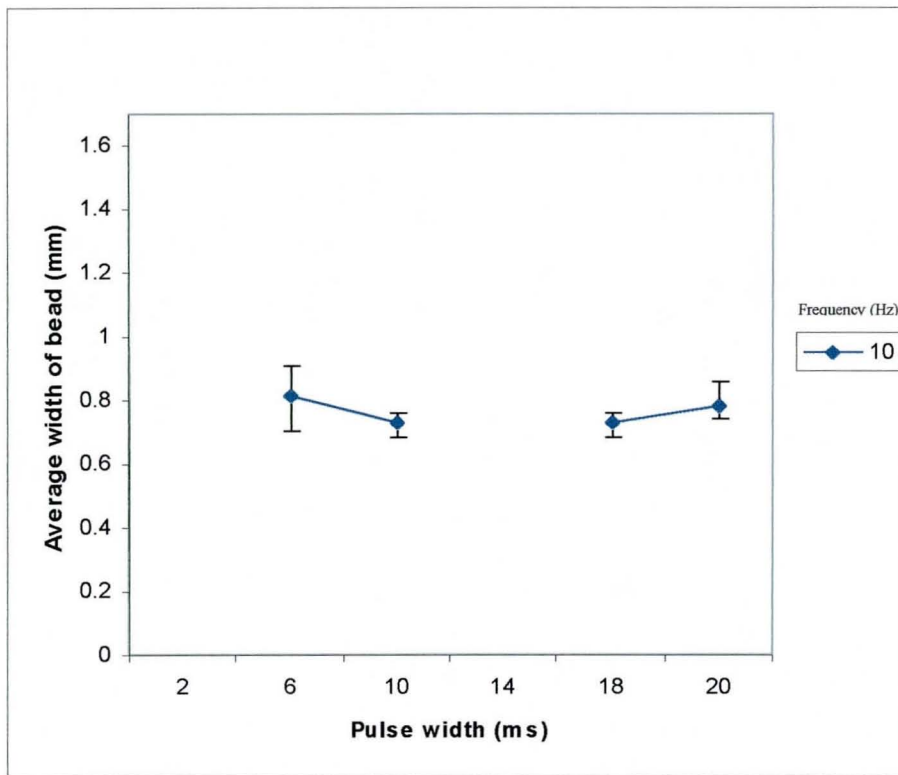
Figure 6.46: Graph of pulse width versus average width of a bead (10mm/s, 20J)
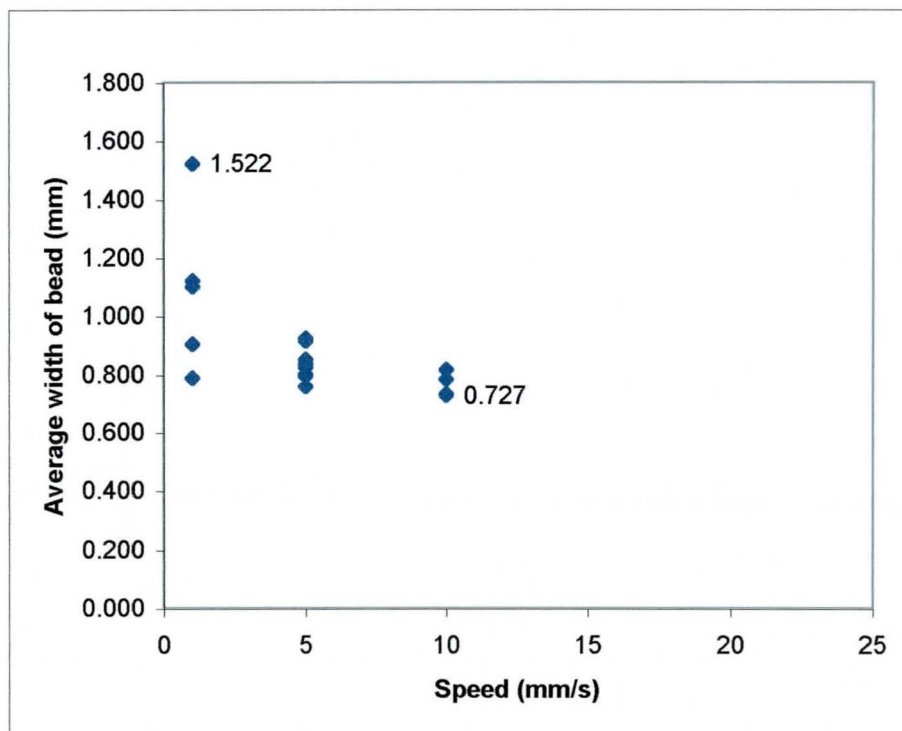
Figure 6.47:Graph of speed versus average bead width (20J)

At 30J a speed of 1mm/s gave a large variation in average beads widths with increasing pulse widths (Figure 6.48). This is somewhat similar to the variation seen in Figure 6.44 at 20J. There is also a peak for 5 and 10mm/s at pulse widths of around 14ms (Figure 6.49, 6.50). With 30J and 15mm/s few results were achieved as shown in Figure 6.51. Figure 6.52 shows similar results to those found for other energy levels.
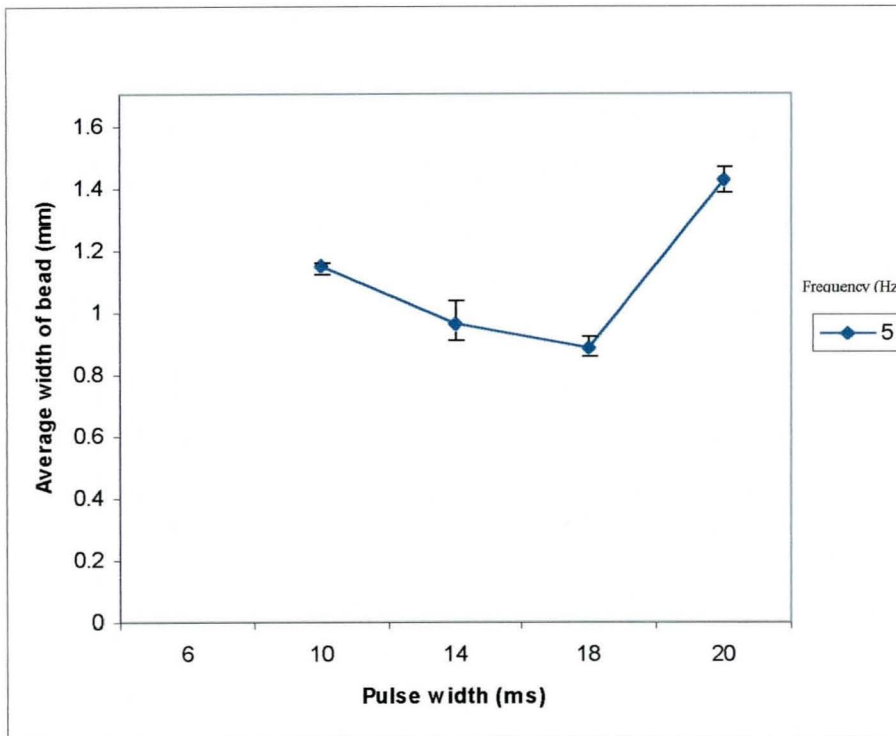
Figure 6.48: Graph of pulse width versus average width of a bead (1mm/s, 30J)
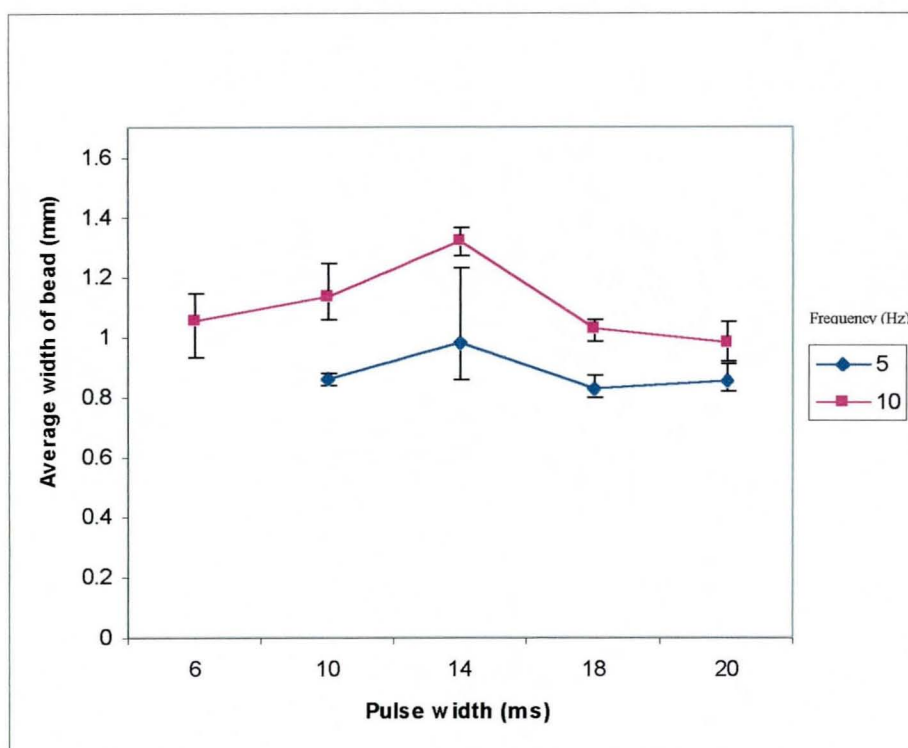
Figure 6.49: Graph of pulse width versus average width of a bead (5mm/s, 30J)
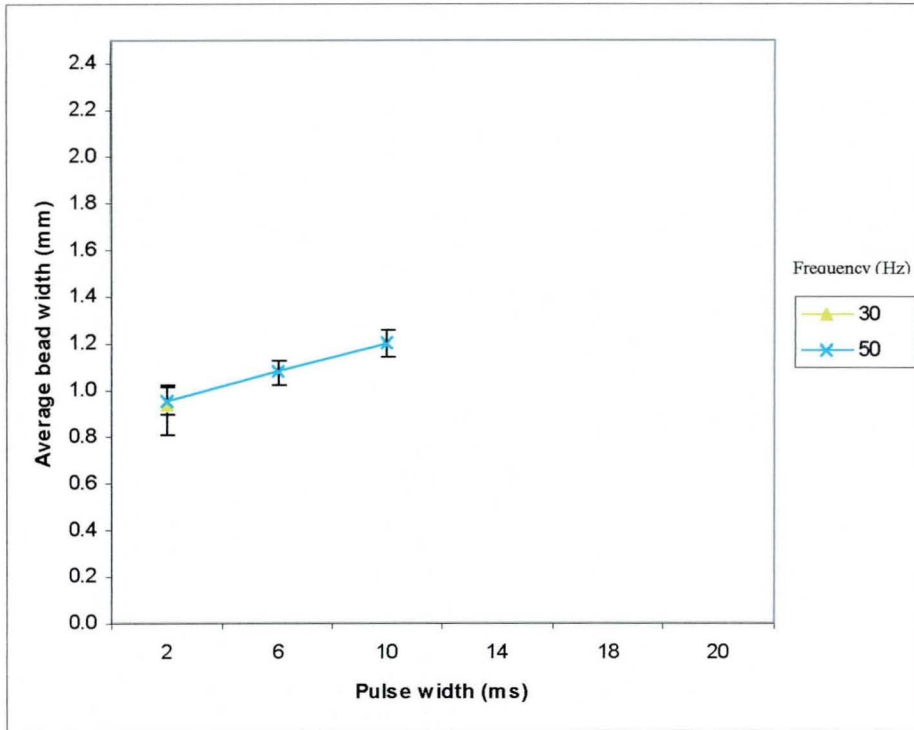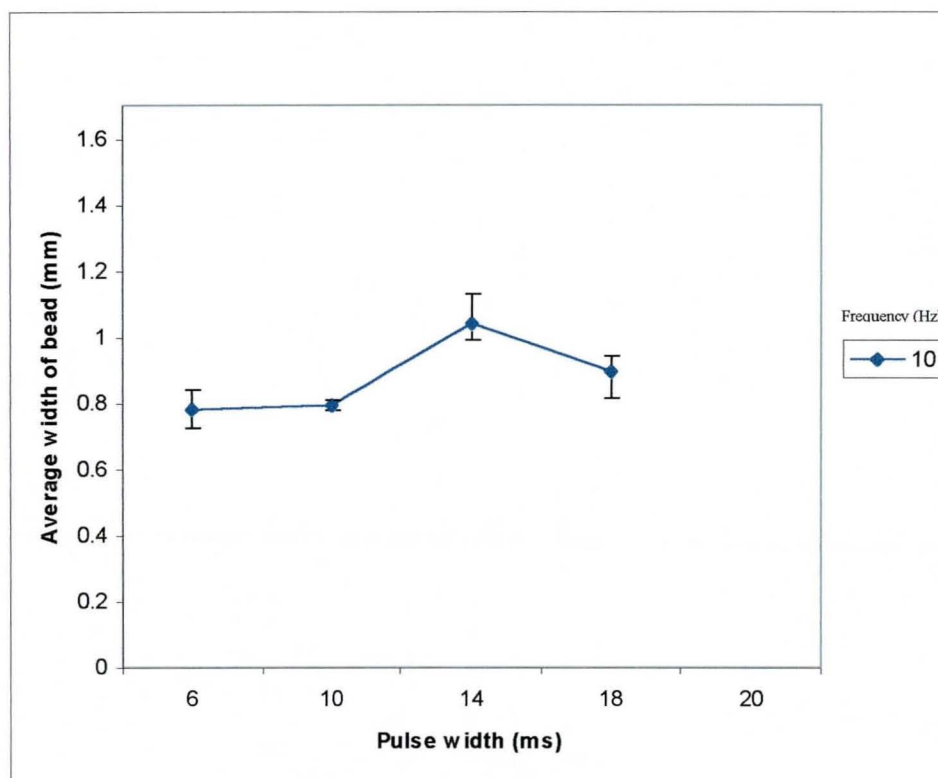

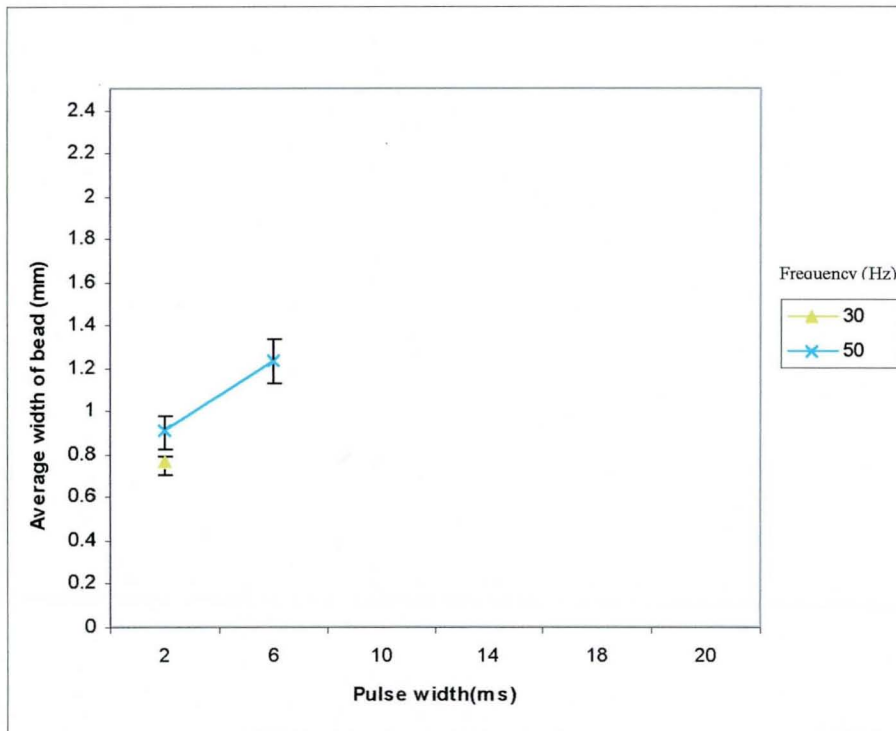Figure 6.50: Graph of pulse width versus average width of a bead (10mm/s, 30J)
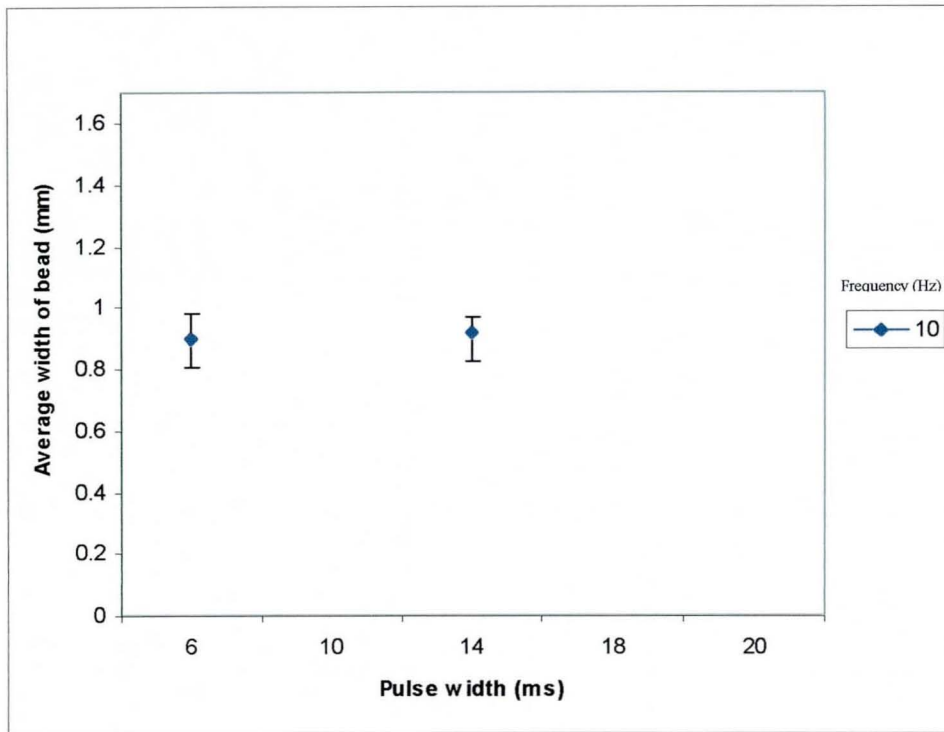
Figure 6.51: Graph of pulse width versus average width of a bead (15mm/s, 30J)
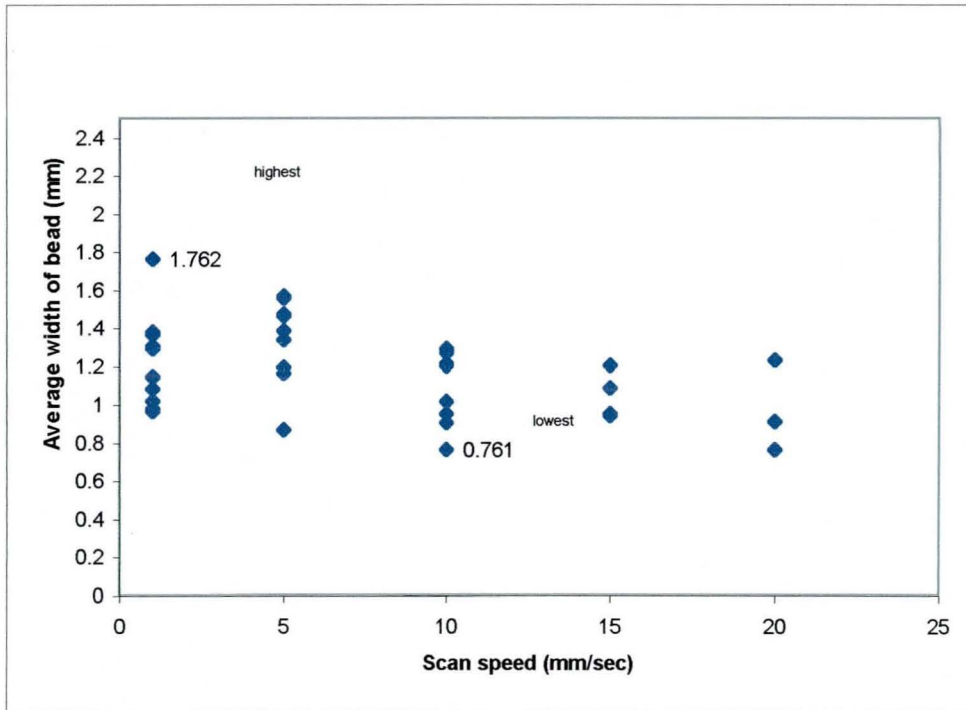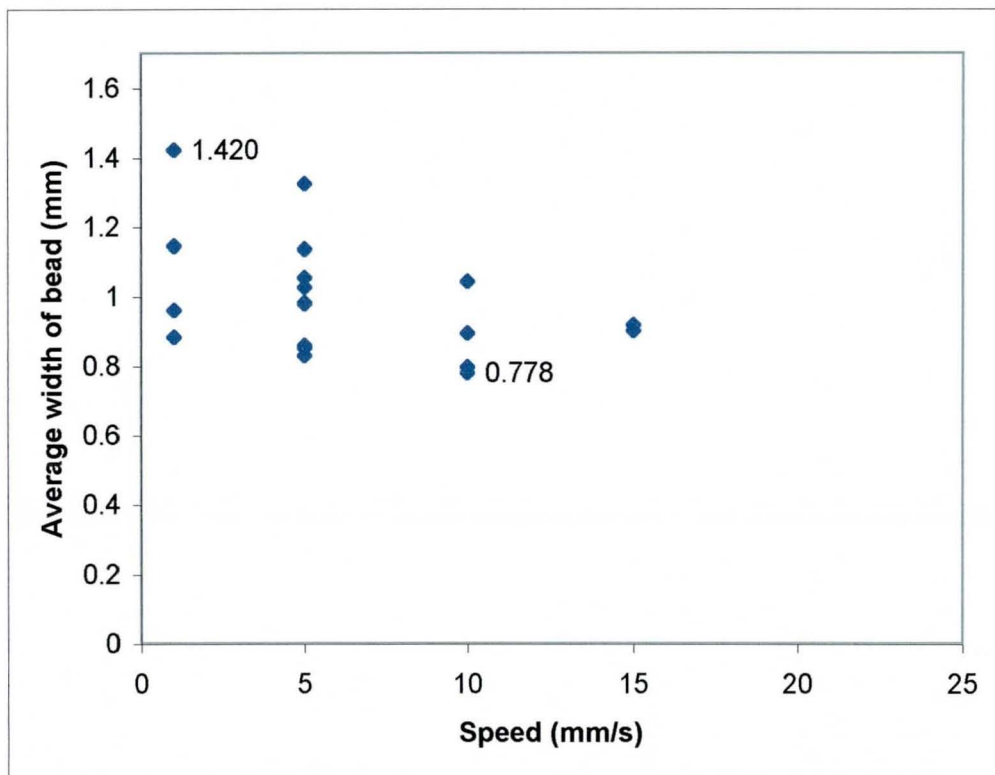

Figure 6.52: Graph of speed versus average width of a bead [30J]
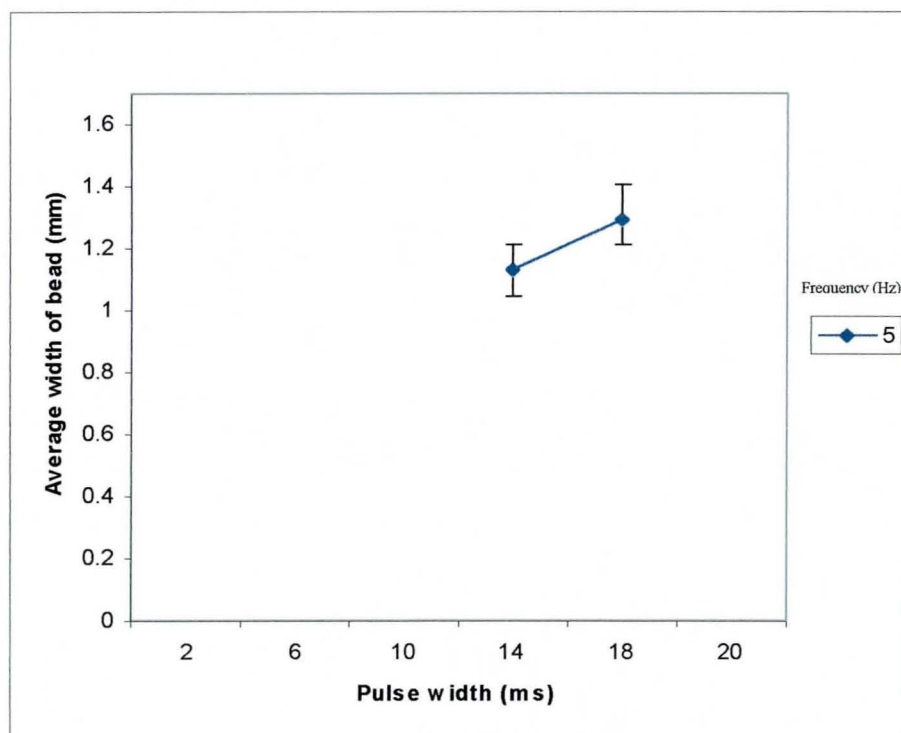
Figure 6.53: Graph of pulse width versus average width of a bead (5mm/s, 60J)

Figure 6.53 shows that beads were only produced in a few instances at 60J.

6.3.2. Effect of pulse parameters (pulse energy, duration and frequency) and speed on average height of a bead

6.3.2.1. Results of bead height for a layer height of 1mm
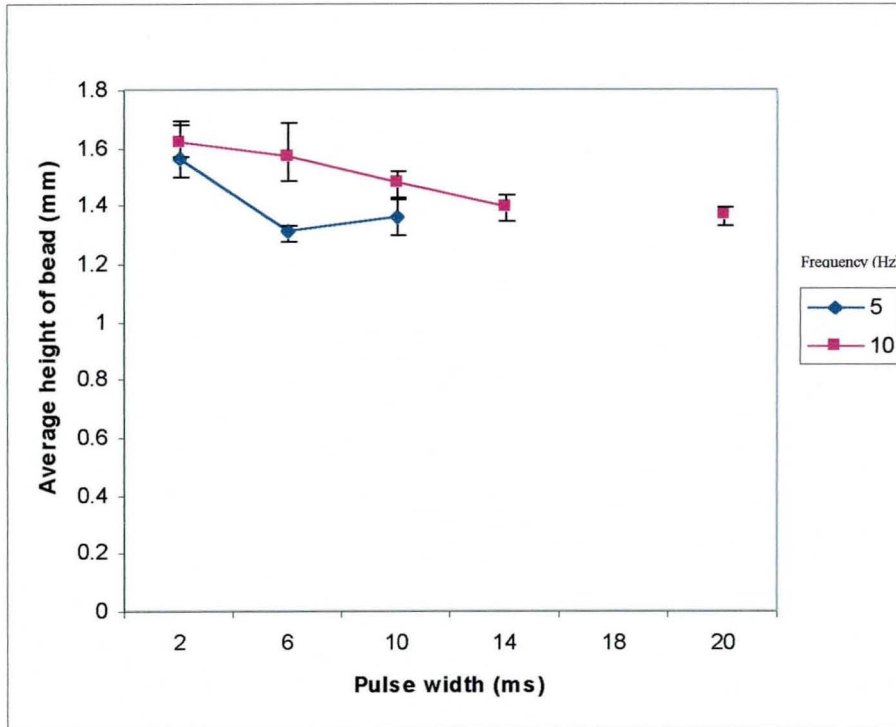
Figure 6.54: Graph of pulse width versus average height (1mm/s, 5J)

In contrast with average bead widths showing an increase with increasing pulse widths, the graph for bead height in Figure 6.54 shows a decrease in average height with an increase in pulse width. The bead height itself is generally higher for a higher frequency. Also the heights are seen as higher than the layer height of 1mm. For a speed of 5mm/s, the height increases with an increase in pulse width and frequency (Figure 6.55). Again bead height is generally greater than the layer height of 1mm, the exception being at certain low pulse widths.
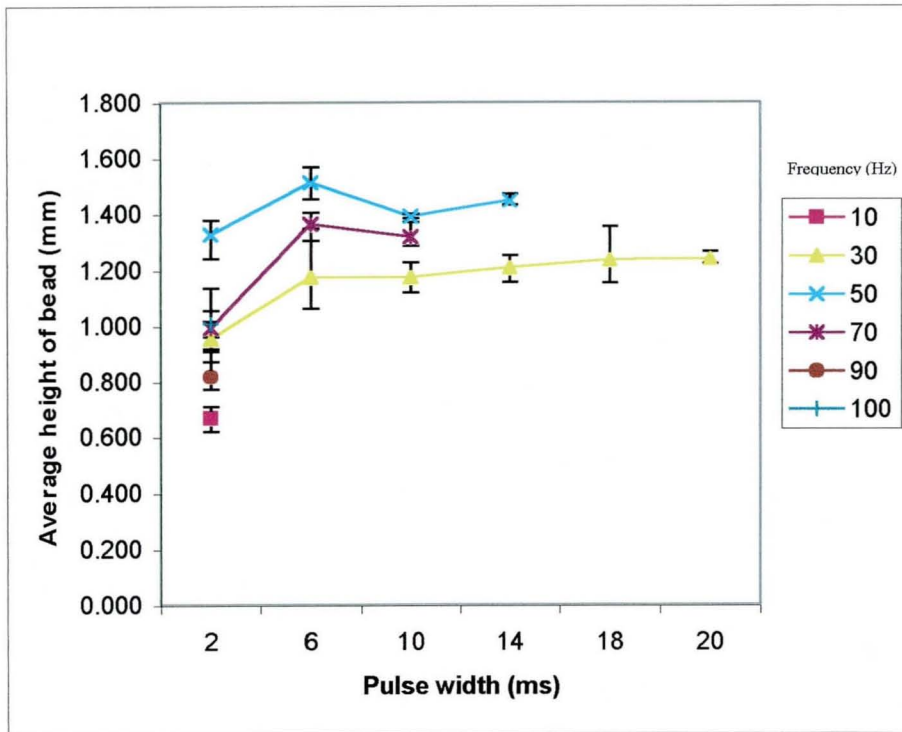
Figure 6.55: Graph of pulse width versus average height of bead [5mm/s, 5J]

At a speed of 10mm/s (Figure 6.56) a higher frequency is generally required for bead formation. Figure 6.55 shows that a frequency of 30 Hz gave most beads while Figure 6.56 shows most bead formation at 50 and 70 Hz.

Pulse widths beyond 14ms did not produce beads. That was due to the beads being discontinuous and poorly bonded to the plate.
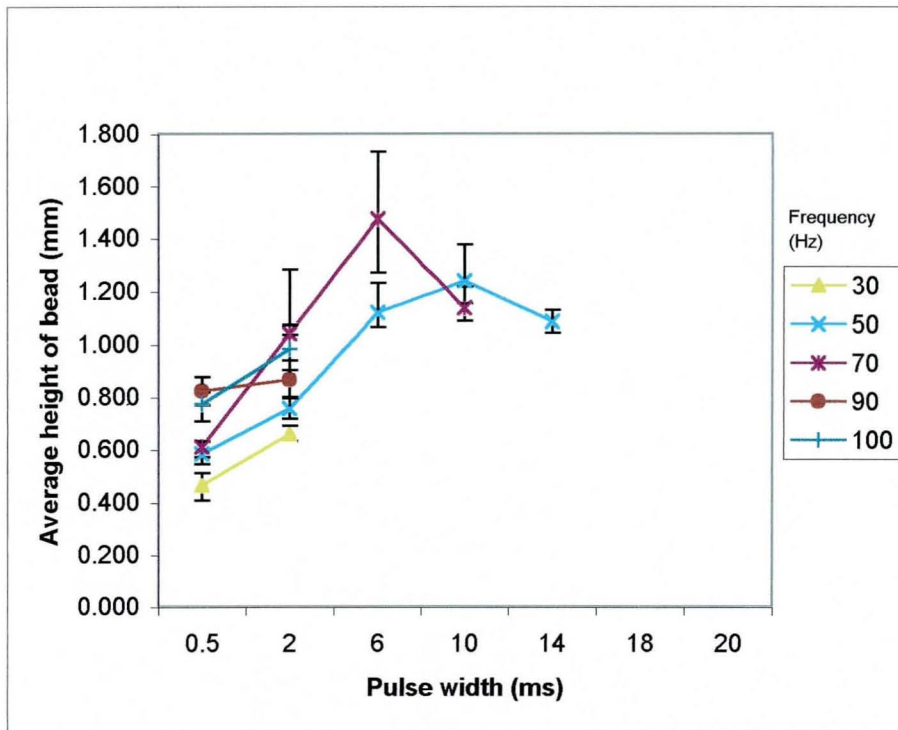
Figure 6.56: Graph of pulse width versus average height of bead [10mm/s, 5J]

Comparing Figure 6.55 and 6.56, it is seen that bead heights are lower at low pulse widths and low frequencies for a higher speed of 10mm/s. The same is seen in the case of increasing speeds for Figure 6.57 and Figure 6.58 at 15mm/s and 20 mm/s respectively. This decreasing trend in bead height with increased speed is more clearly seen in Figure 6.59, which shows a progressive reduction in the maximum and minimum levels at each increasing speed, apart from a few results at 20mm/s. Balling is seen to occur beyond 2ms for Figure 6.58, 6.59. Many bead height values shown in Figure 6.59, exceed the layer height of 1mm, by about 50 to 60 % whereas some values are lower by about 65 to 70%. Such low values are generally observed for speeds above 10mm/s.
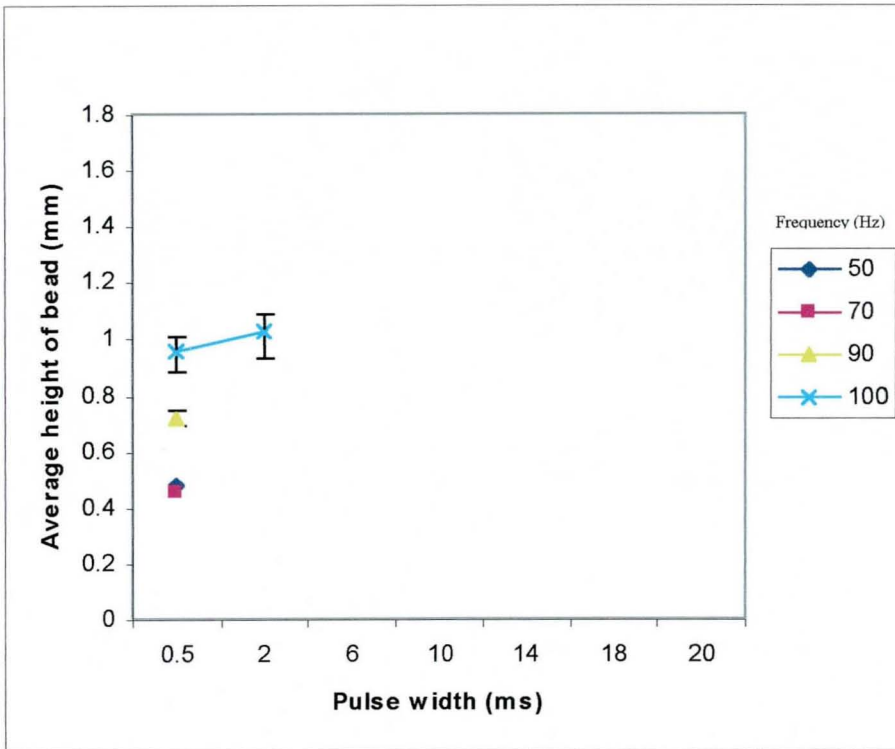
Figure 6.57: Graph of pulse width versus average height (15mm/s, 5J)
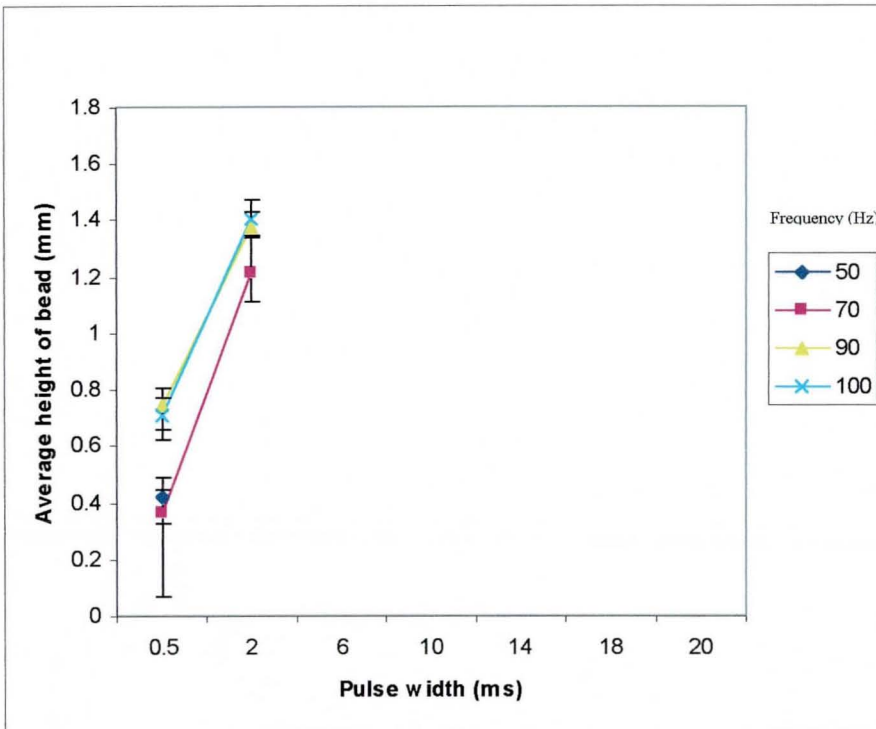
Figure 6.58: Graph of pulse width versus average height (20mm/s, 5J)
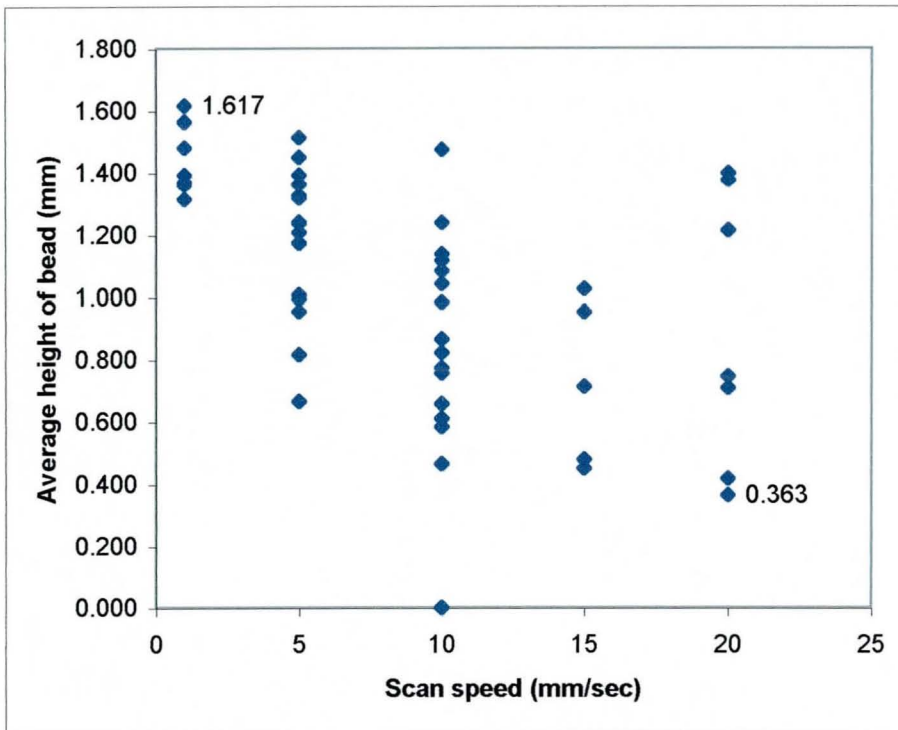
Figure 6.59: Graph of scan speed versus average height of bead [5J]

At a higher energy level of 10 J at 1mm/s (Figure. 6.60), the bead height increases with pulse width for a frequency of 10 Hz.

Error bars overlap in most cases between 6 and 18ms (Figure 6.60) and may indicate that changes in frequency may not significantly affect the average bead height. Increasing bead heights are seen for increasing pulse widths at other speed values (Figures 6.61, 6.62, 6.63, 6.64). The number of beads formed, progressively reduce with higher speeds.
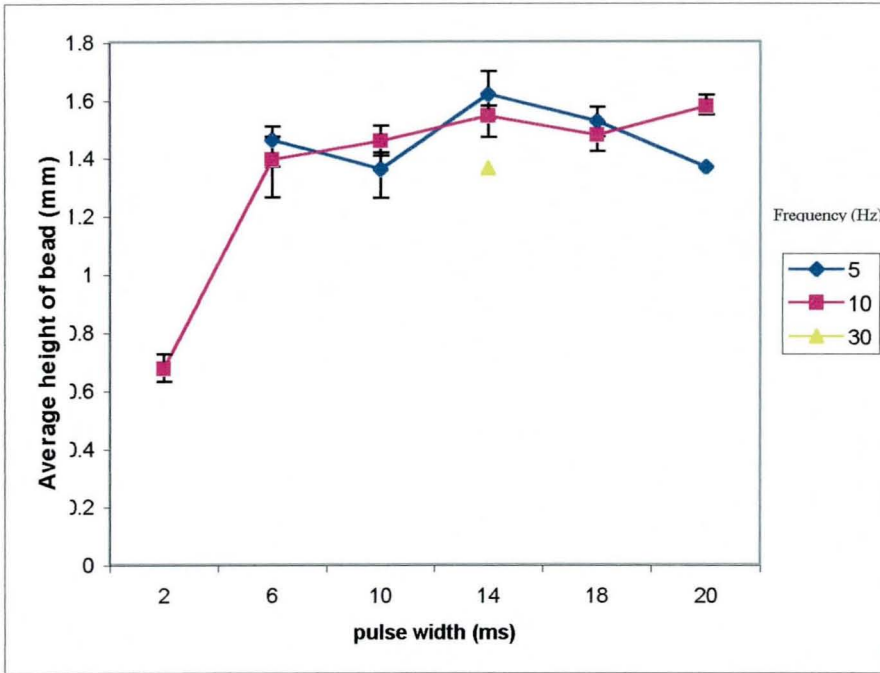
Figure 6.60: Graph of pulse width versus average height of bead (1mm/s, 10J)
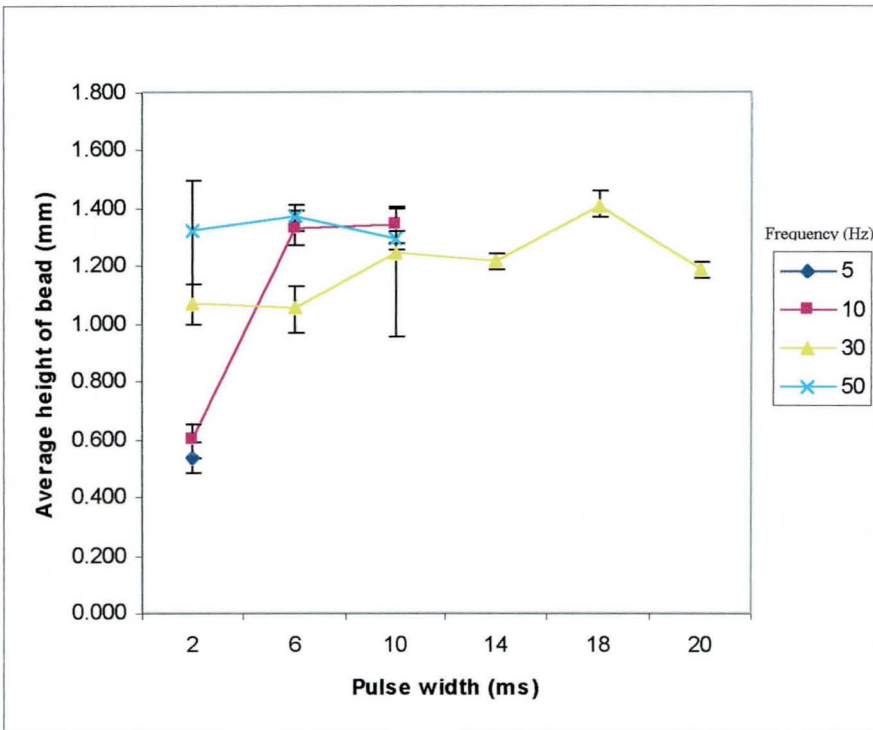
Figure 6.61: Graph of pulse width versus average height of bead (5mm/s, 10J)
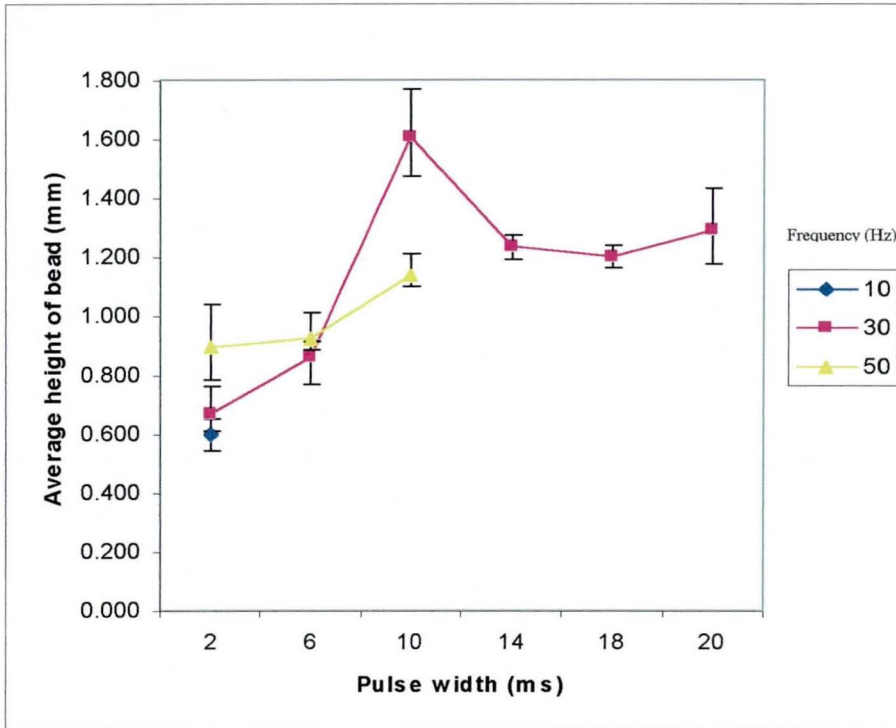
Figure 6.62: Graph of pulse width versus average height of bead (10mm/s, 10J)
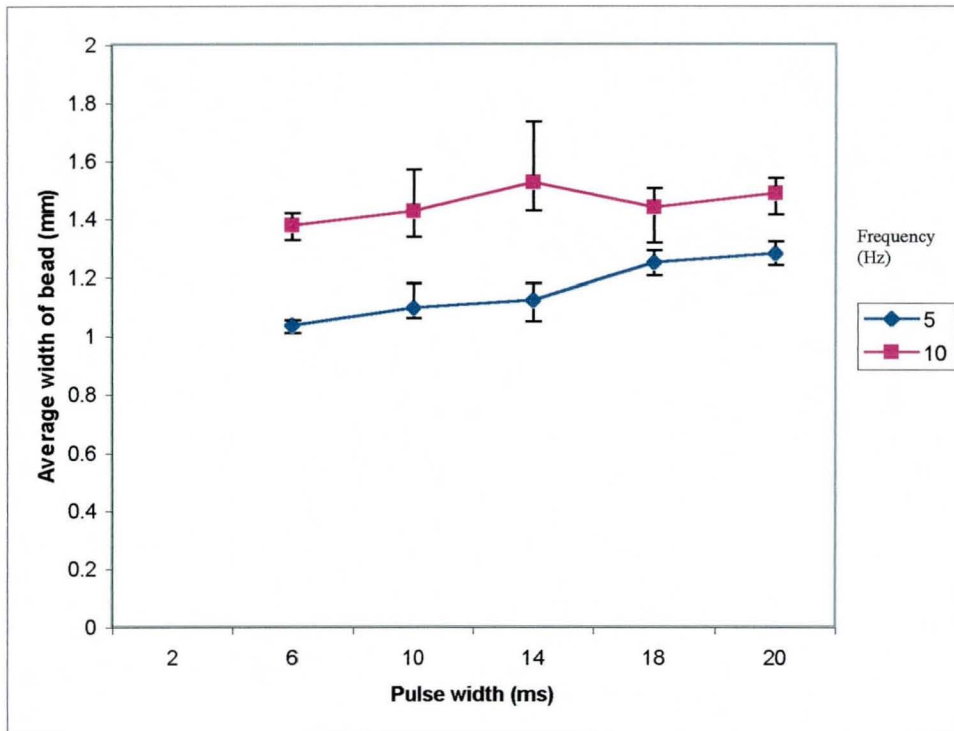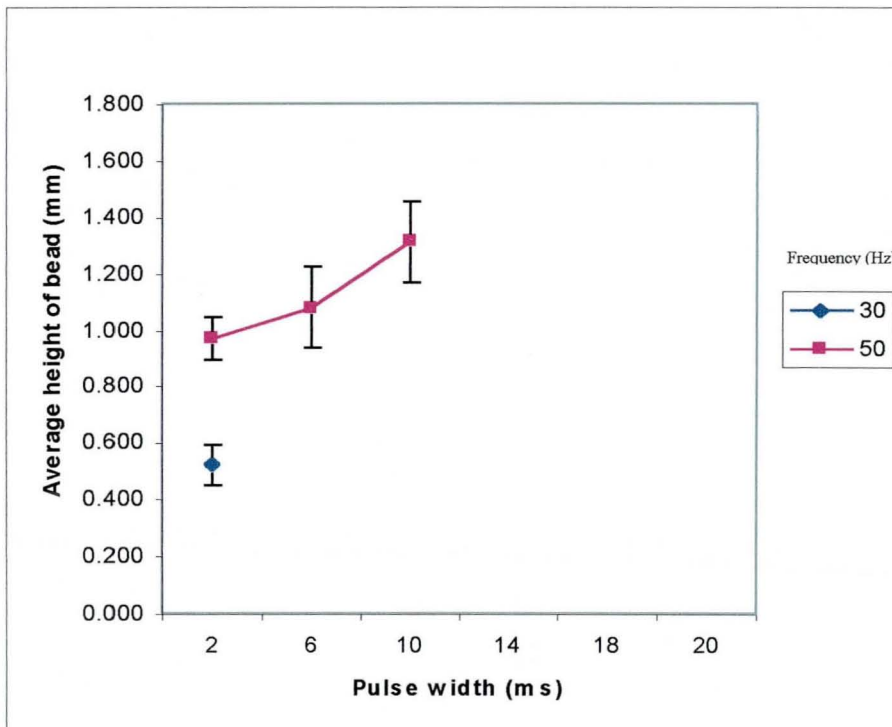

Figure 6.63: Graph of pulse width versus average height of bead (15mm/s, 10J)
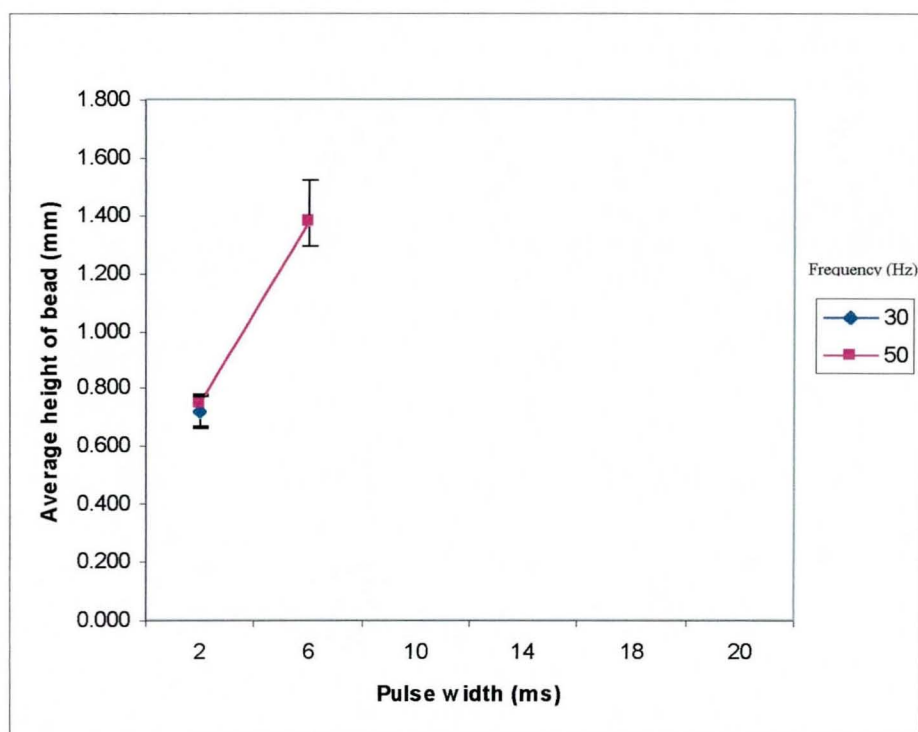
Figure 6.64: Graph of pulse width versus average height of bead (20mm/s, 10J)
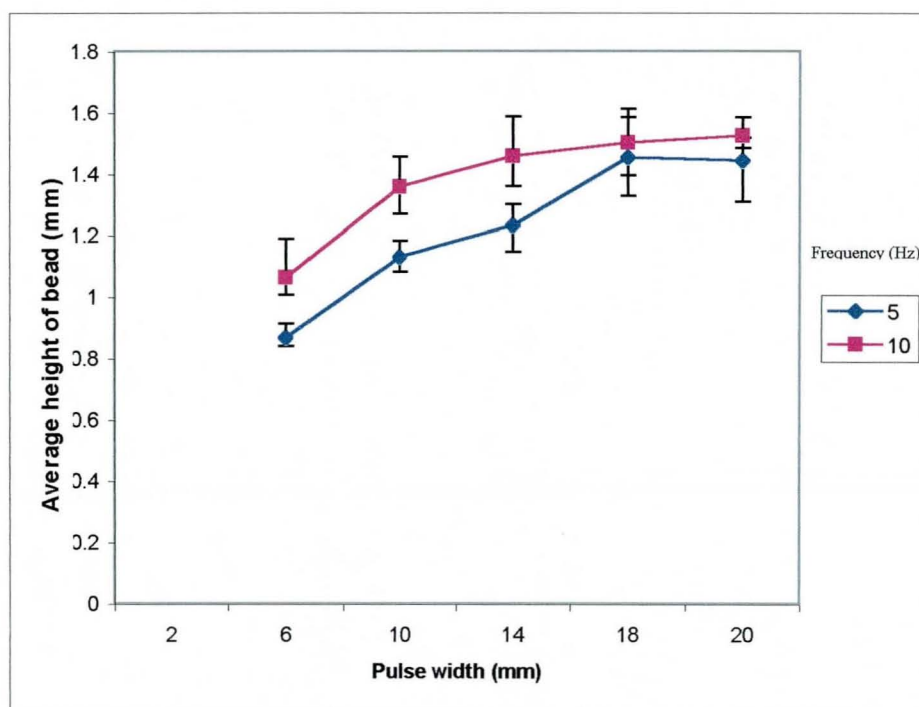
Figure 6.65: Graph of pulse width versus average height of a bead (1mm/s, 20J)

An increase in energy level to 20J at 1mm/s, shows a clearer trend of increasing bead height with an increase in pulse width and frequency (Figure 6.65). This can be compared to Figure 6.60, where the trend is less clear and the results are closer. At 5mm/s in Figure 6.66, the result shows a similar increase though to a lesser extent, with increase in pulse widths. Also at this speed only a frequency of 10Hz generally produced beads at different pulse width settings. With 10mm/s only one set of parameter combination produced beads (Figure 6.67).
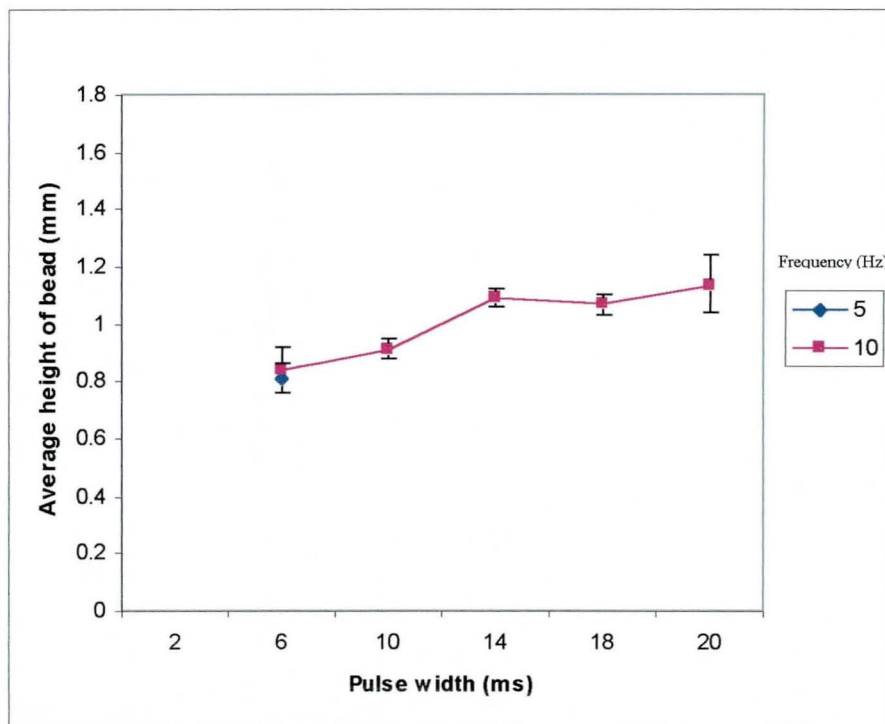
Figure 6.66: Graph of pulse width versus average height of bead (5mm/s, 20J)
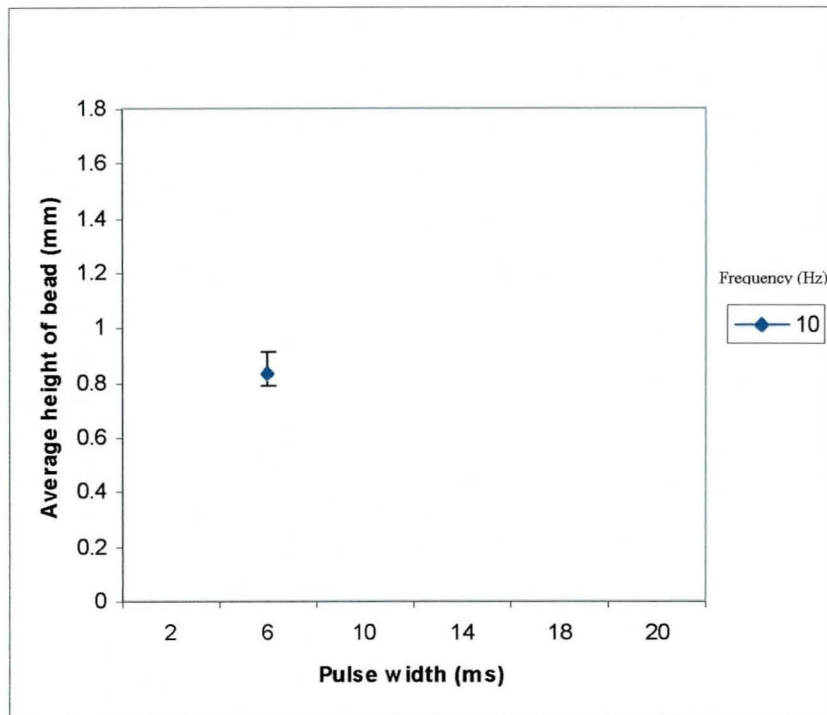
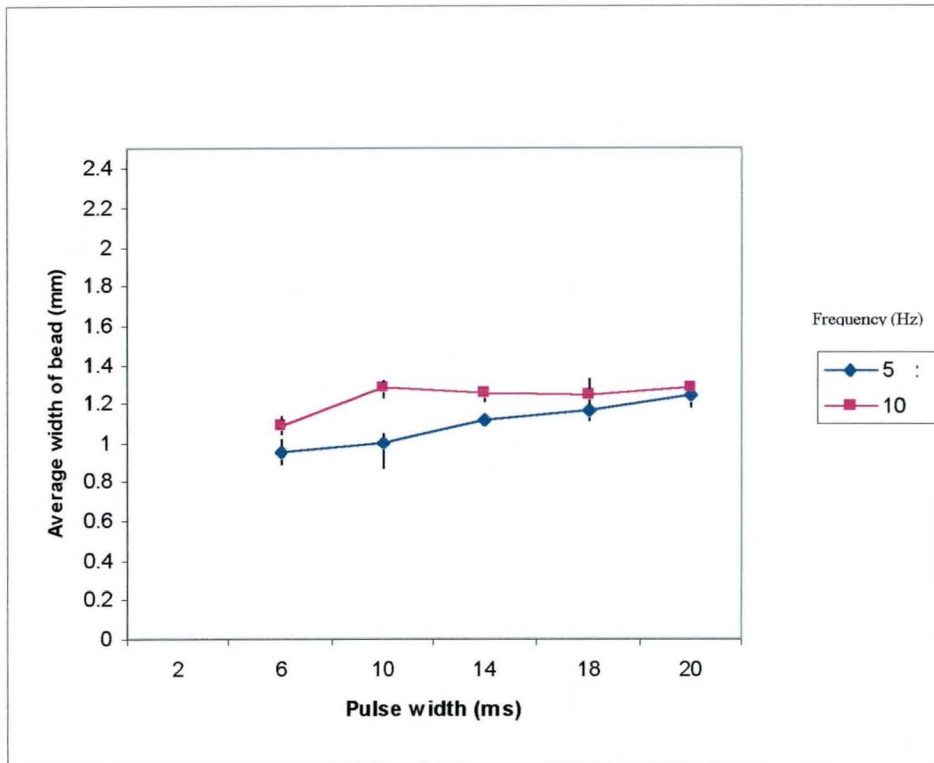Figure 6.67: Graph of pulse width versus average height of bead (10mm/s, 20J)

Figure 6.68 at 30J 1mm/s shows increasing frequencies produce an increase in average bead heights. For 5mm/s at 30J, too an increase in average bead height is observed at increasing pulse widths (Figure 6.69). Average height values are closer at 5mm/s, their error bars showing overlap. This could mean less significant effect of frequency change on average bead height. Most values remain below the powder layer thickness of 1mm, indicating a flatter bead produced due to the high energies involved. The increase in energy to 30J produces beads at a lower frequency of 5Hz, which is not possible for an energy level of 20 J at 5Hz, for the same speed levels (5mm/s) (Figure 6.66 and Figure 6.69). This is due to an increase in average power at higher energy levels (for the same frequency), which in the above cases are 150W for 30J and 100W for 20J. At 10mm/s beads could mainly be produced at a frequency of 10 Hz (Figure

6.70). No bead was produced at a frequency of 5 Hz for a speed of 15 mm/s (Figure 6.71). This figure also shows only one bead produced at 10 Hz. This is in contrast to the far higher number of beads produced at a lower energy level of 5J. This is observed in Figure 6.72 for 30J and Figure 6.59 for 5J. In Figure 6.73 for an energy of 60J, the average bead height was constant with increasing pulse width.
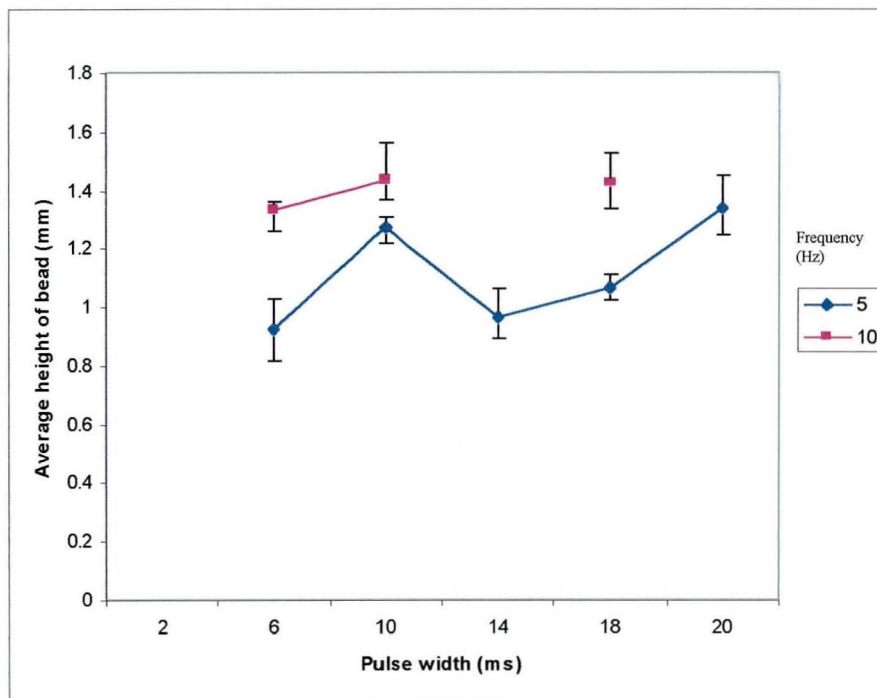
Figure 6.68: Graph of pulse width versus average height of bead (1mm/s, 30J)
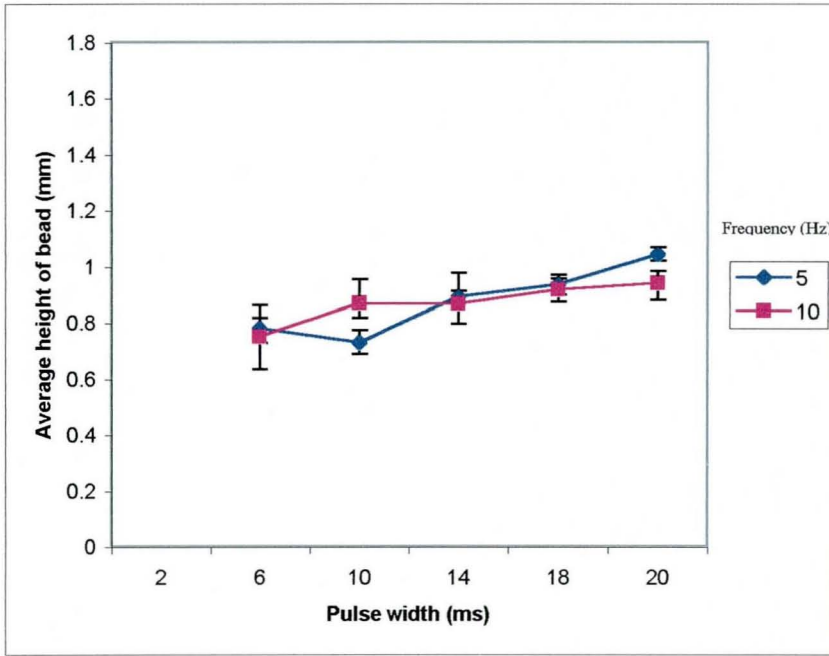
Figure 6.69: Graph of pulse width versus average height of a bead (5mm/s, 30J)
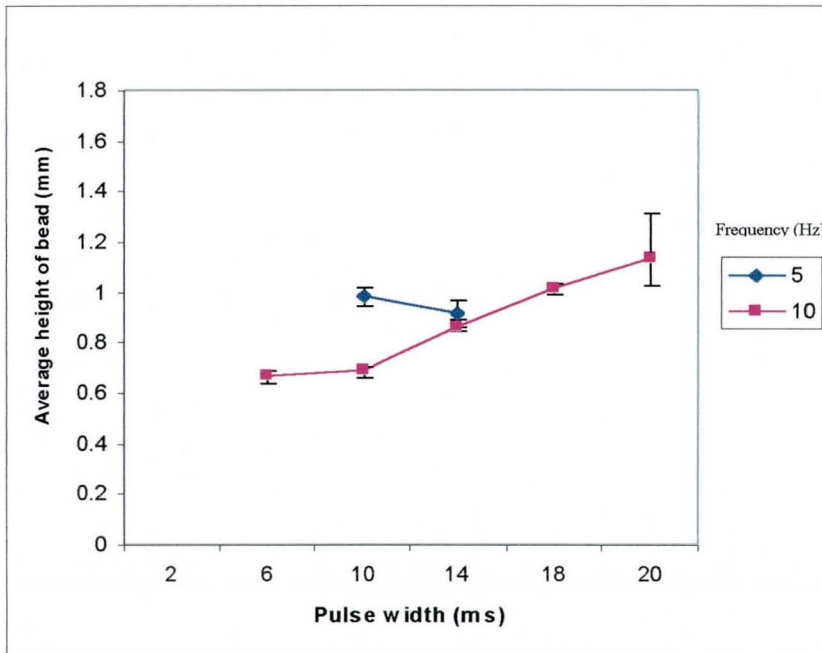
Figure 6.70: Graph of pulse width versus average height of bead (10mm/s, 30J)
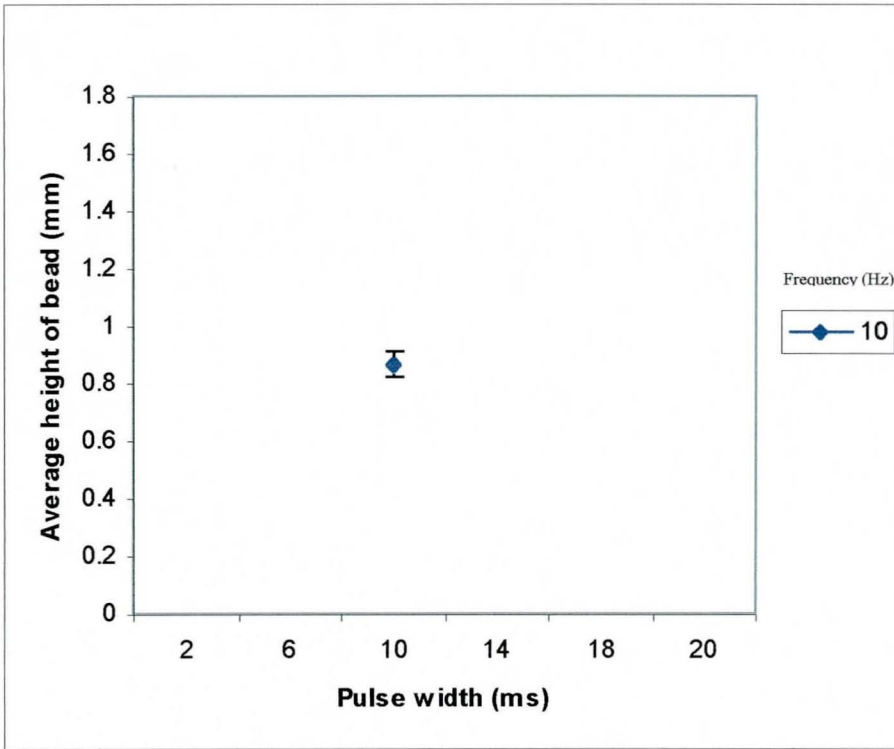
Figure 6.71: Graph of pulse width versus average height of bead (15mm/s, 30J)
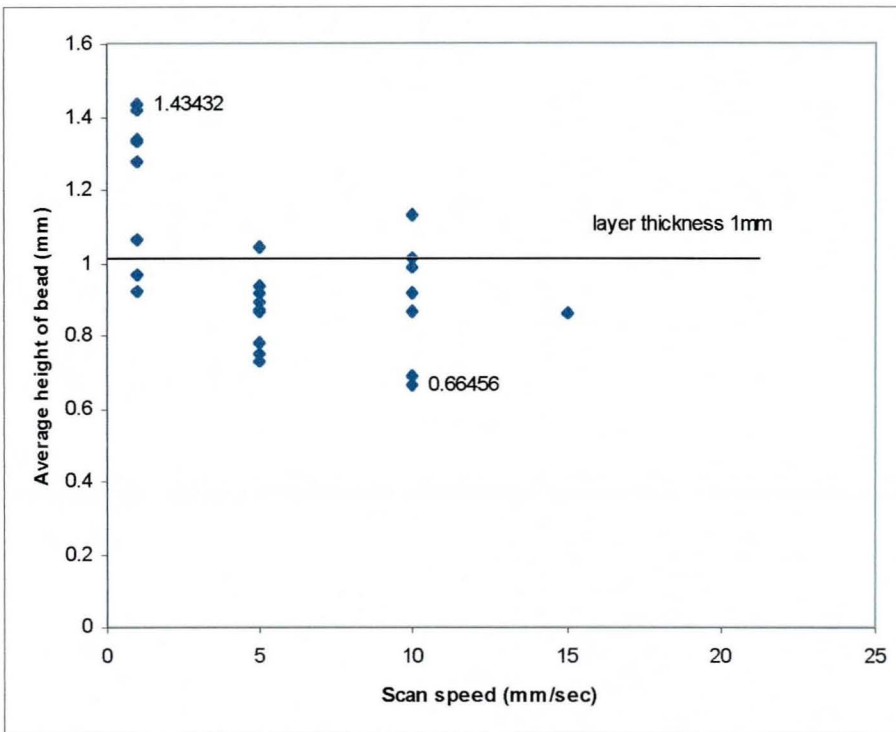
Figure 6.72: Graph of speed versus average height of bead (30J)
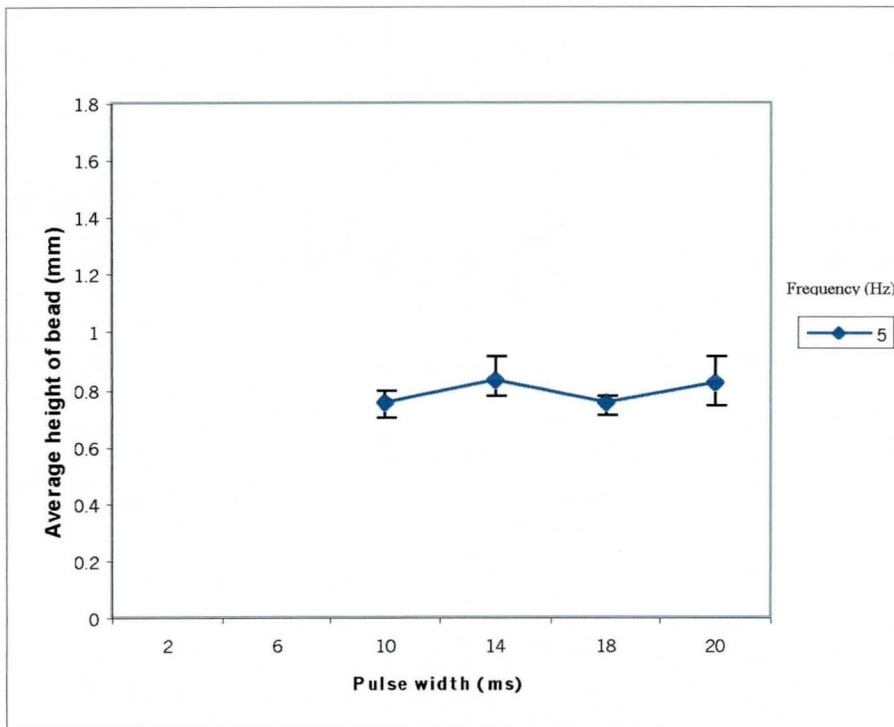
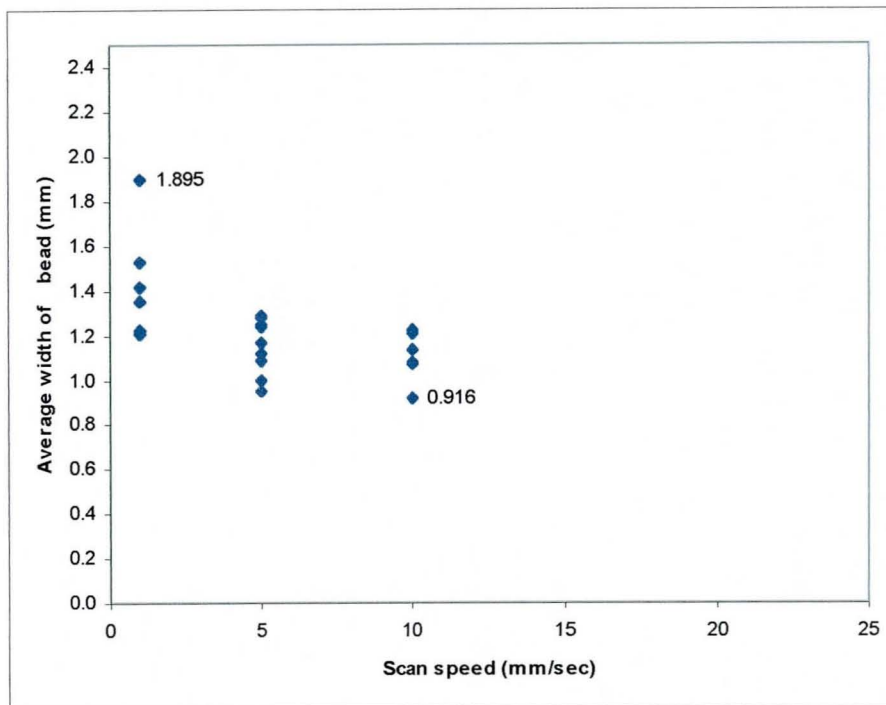Figure 6.73: Graph of pulse width versus average height of bead (5mm/s, 60J)

6.3.2.2. Results of bead height for a layer height of 0.4 mm layer
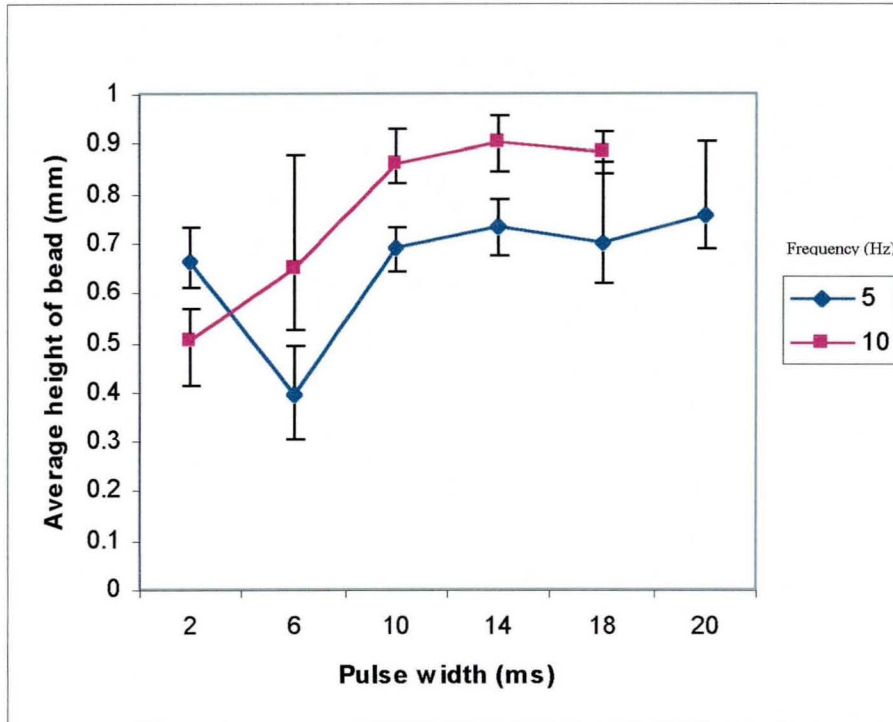
Figure 6.74: Graph of pulse width versus average height of bead (1mm/s, 5J)

The graph in Figure 6.74 for speed 1mm/s, is indicative of an increasing trend in the average bead height, with increasing pulse widths. Figure 6.75 shows a general increase in bead height with increase in pulse widths and higher frequencies at a higher speed of 5mm/s. Also at 6ms, 10Hz maximum and minimum values are seen to randomly high.
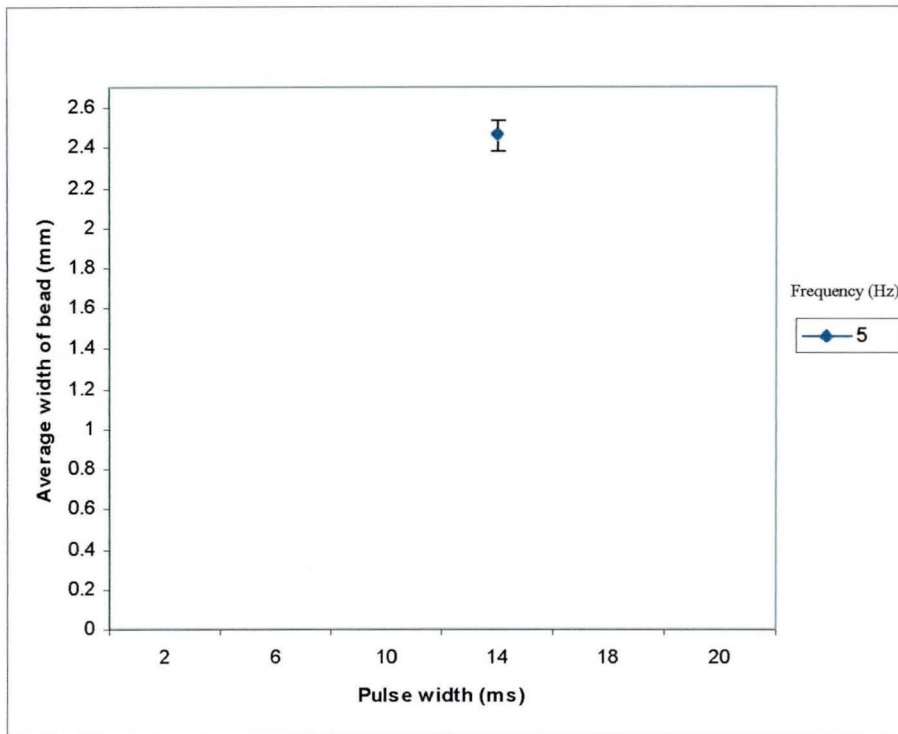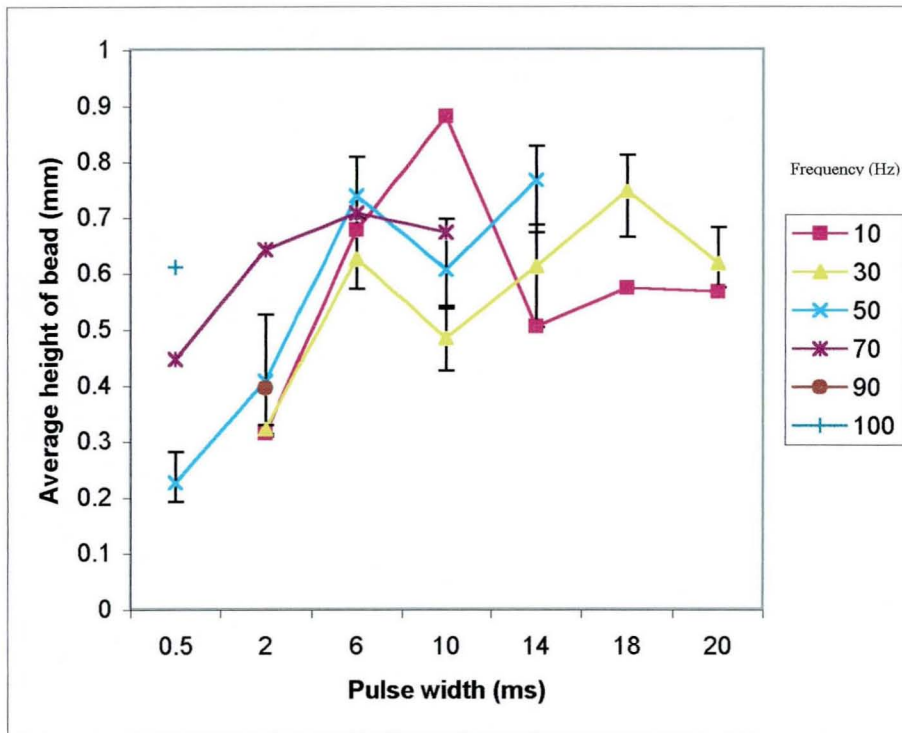
Figure 6.75: Graph of pulse width versus average height of bead (5mm/s, 5J)
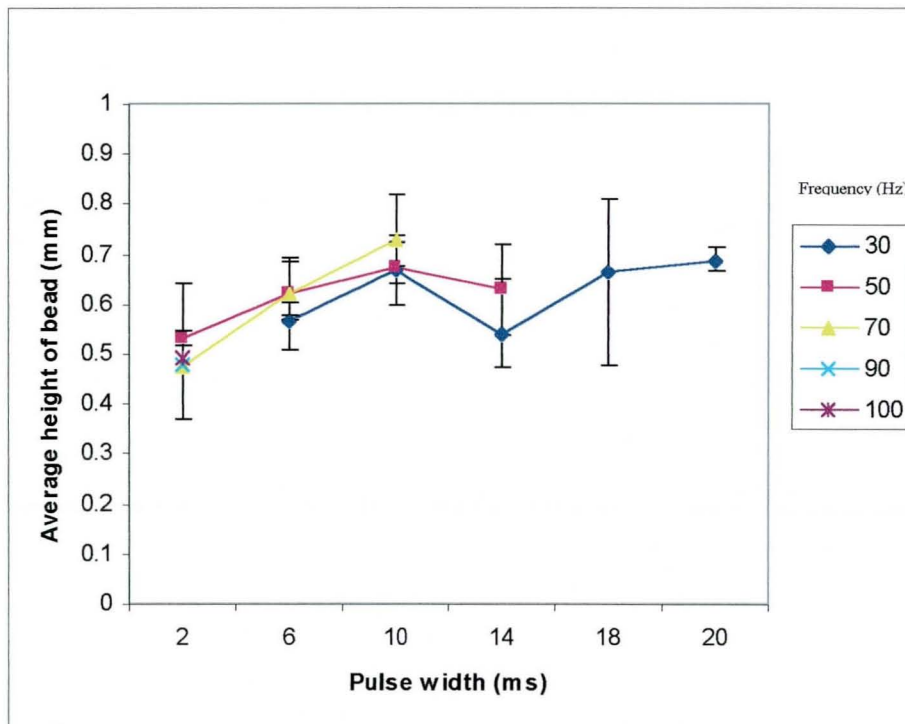
Figure 6.76: Graph of pulse width versus average height of bead (10mm/s, 5J)

At 10mm/s there is less increase in bead height with increasing pulse widths (Figure 6.76). Generally the average bead heights are seen to be higher than the layer thickness (0.4mm) for all three speeds. An increase in frequency also gives a higher average bead height for the same pulse width value. This is less clear for a speed of 15 mm/s (Figure 6.77) where a low frequency (30 Hz) produces higher average bead height compared to frequency (50 Hz). At a speed of 20 mm/s (Figure 6.78) the bead height generally increases with increasing frequency.
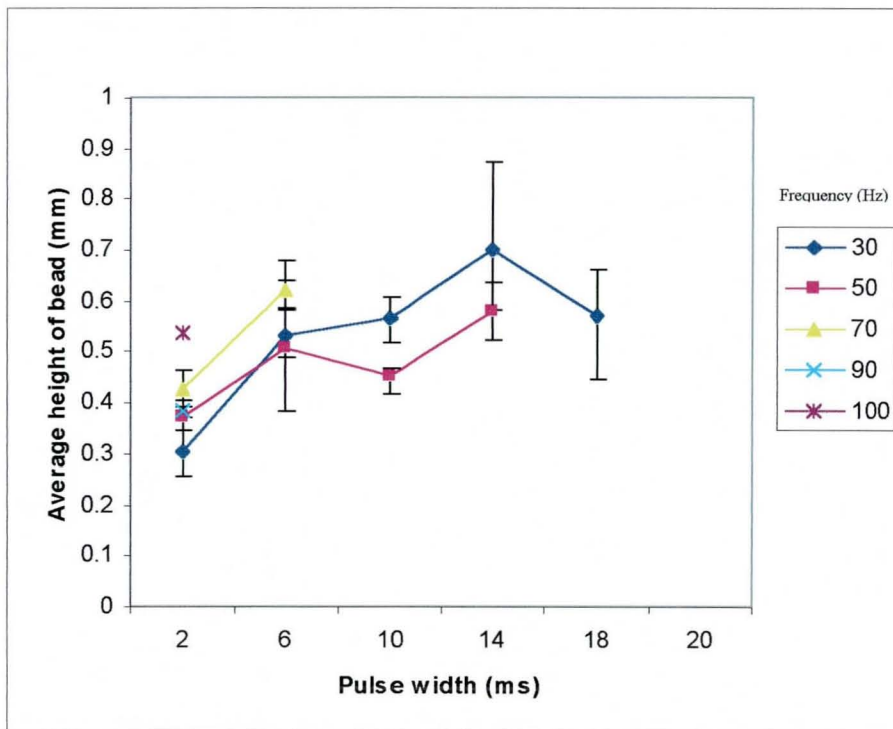
Figure 6.77: Graph of pulse width versus average height of bead (15mm/s, 5J)
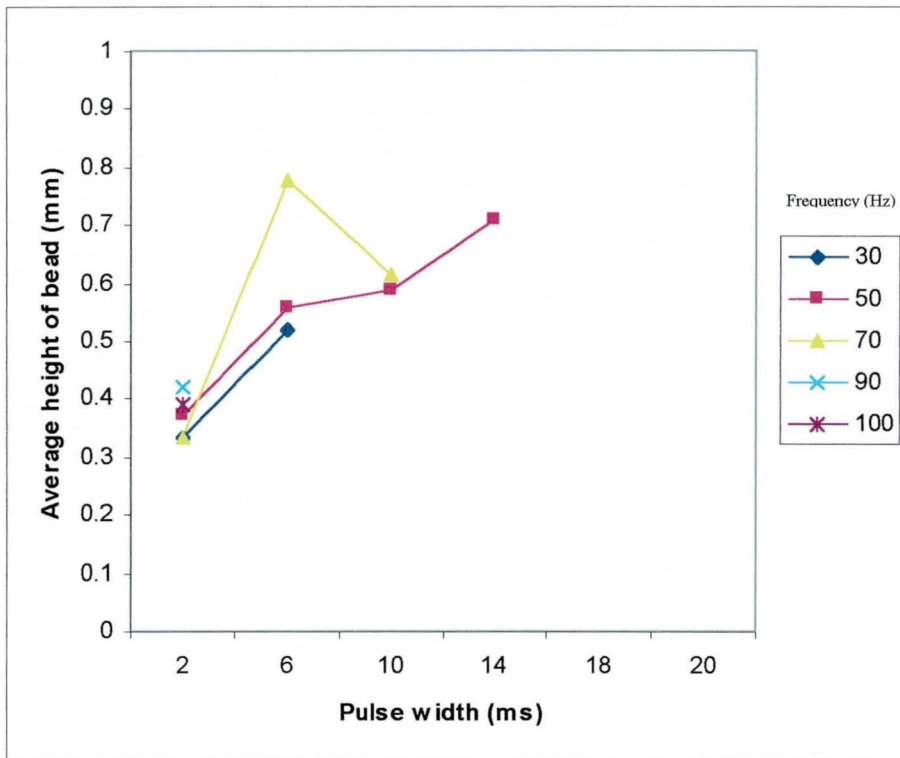
Figure 6.78: Graph of pulse width versus average height of bead (20mm/s, 5J)
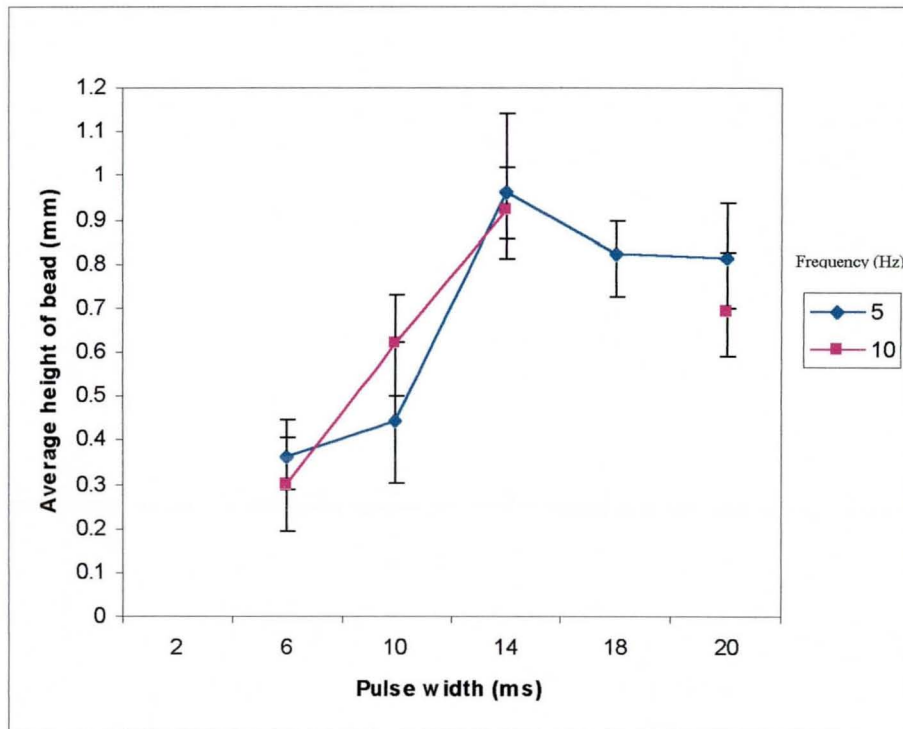
Figure 6.79: Graph of pulse width versus average height of bead (1mm/s, 10J)

At a energy level 10J, a linear increase in average bead height is observed for frequency 10 Hz, Figure 6.79.At a speed of 5mm/s the effect of frequency on the bead height is erratic. The lower frequency levels appear to produce greater average bead heights as noted in Figure 6.80. This erratic behaviour is also observed at 10mm/s (Figure 6.81). At 15 mm/s there is a general increase in average bead height with increasing pulse width and frequency (Figure 6.82). At 20mm/s the results are also erratic (Figure 6.83). Figure 6.84 shows little variation of bead height with scan speed.
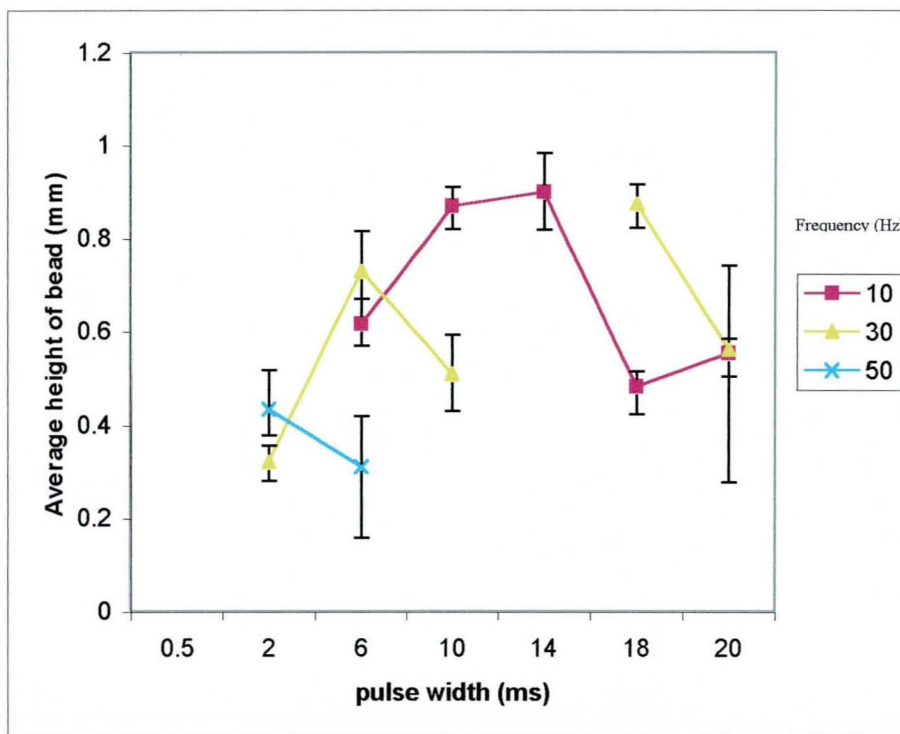
Figure 6.80: Graph of pulse width versus average height of bead (5mm/s, 10J)
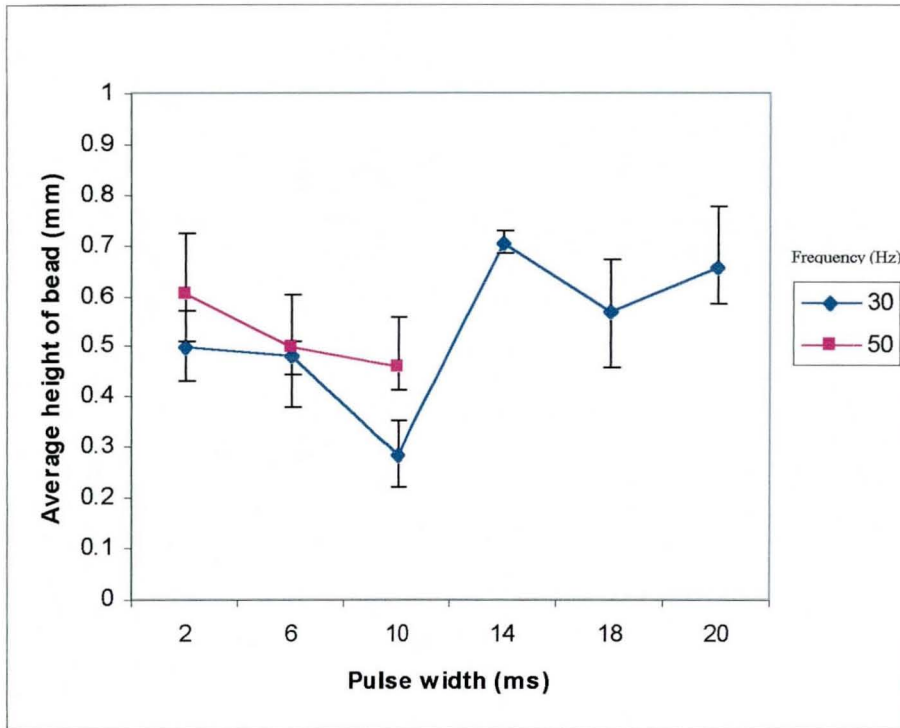
Figure 6.81: Graph of pulse width versus average height of bead (10mm/s, 10J)
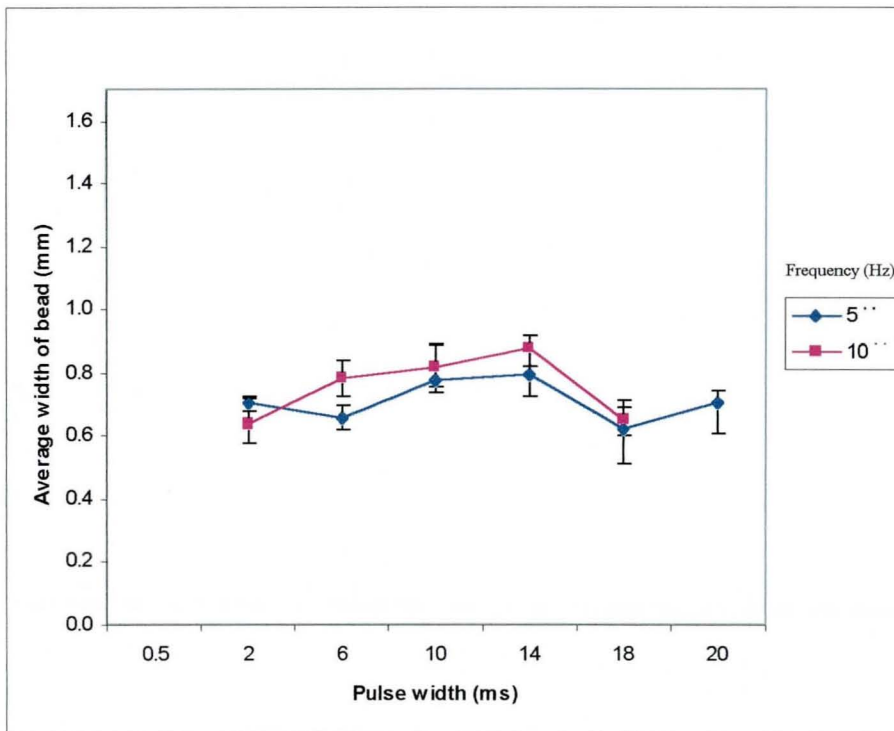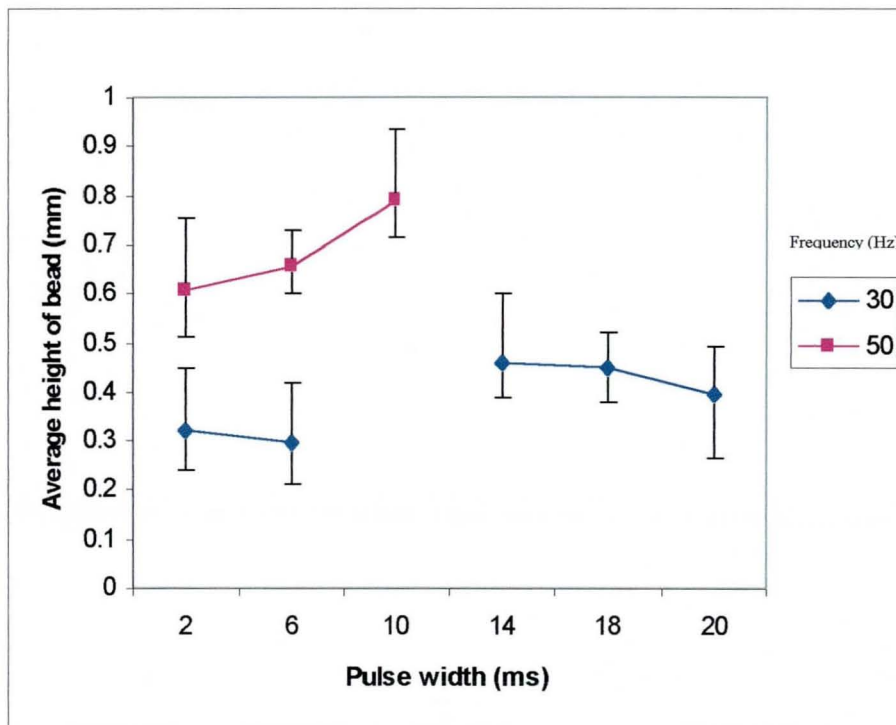

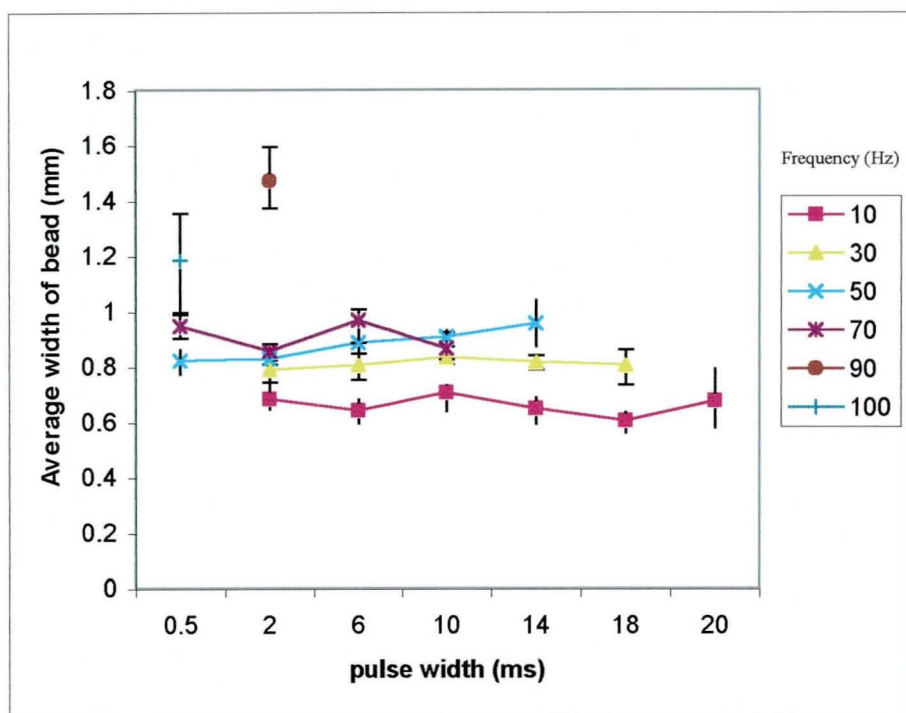Figure 6.82: Graph of pulse width versus average height of bead (15mm/s, 10J)
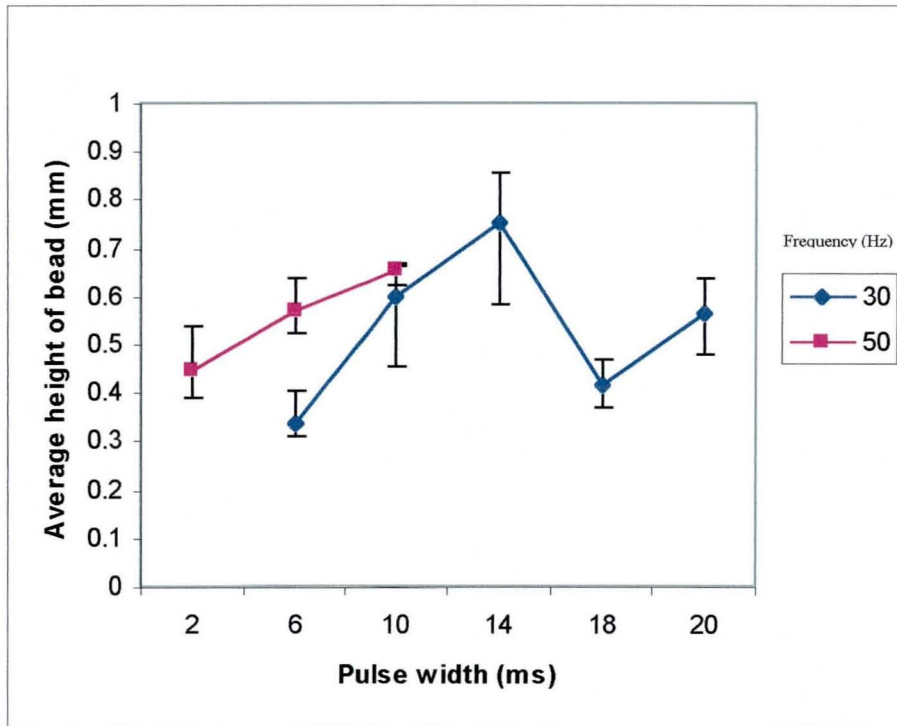
Figure 6.83: Graph of pulse width versus average height of bead (20mm/s, 10J)
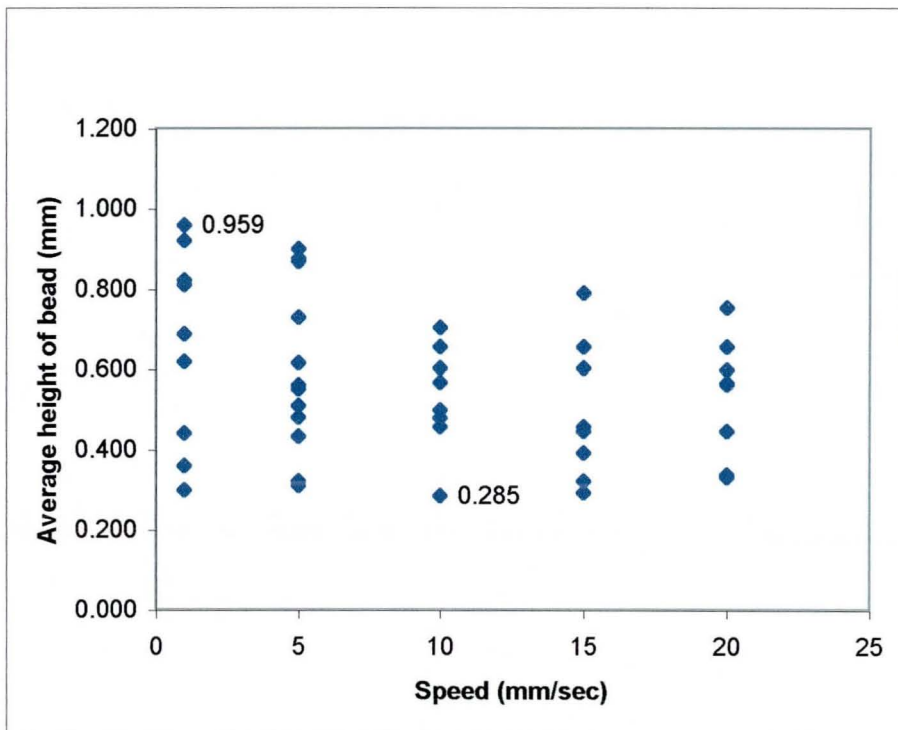
Figure 6.84: Graph of speed versus average height of bead [10J]

At a 20J energy level the trends are unclear (Figures 6.85, 6.86, 6.87).

Figure 6.88 shows that the number of beads produced at 20J are fewer than that

produced at a lower energy setting 5J (Figure 6.75).
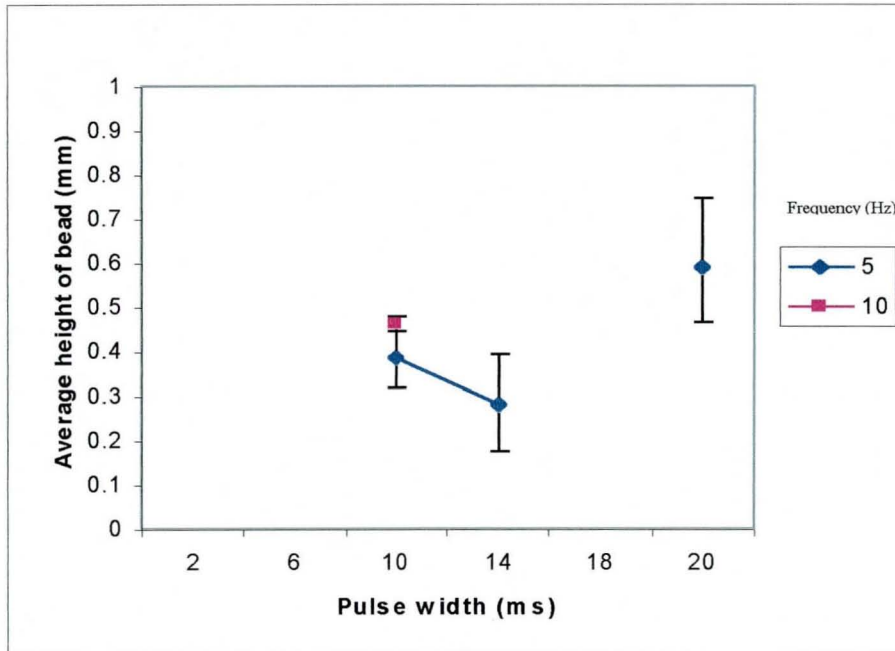
Figure 6.85: Graph of pulse width versus average height of bead (1mm/s, 20J)
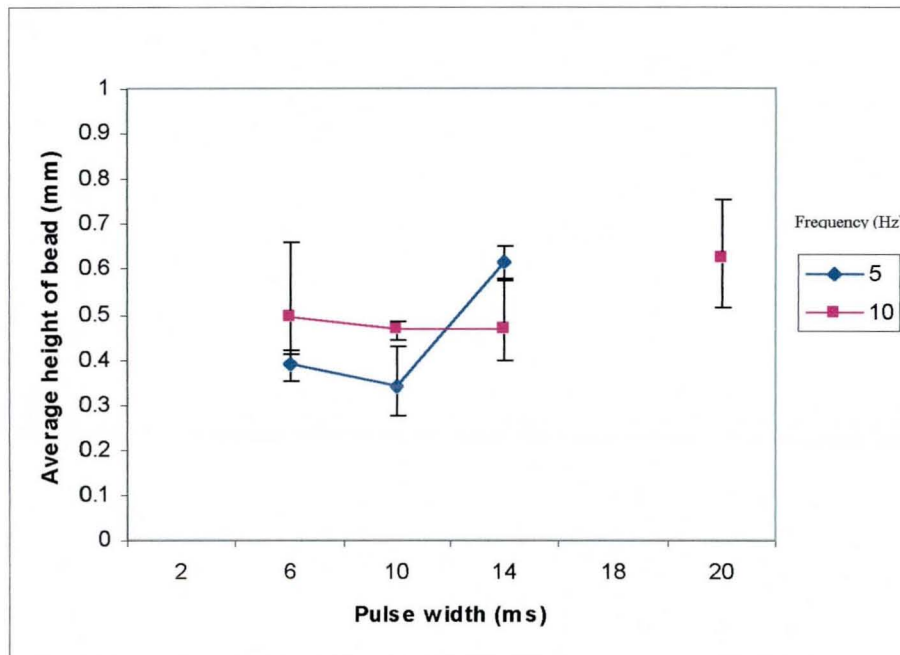
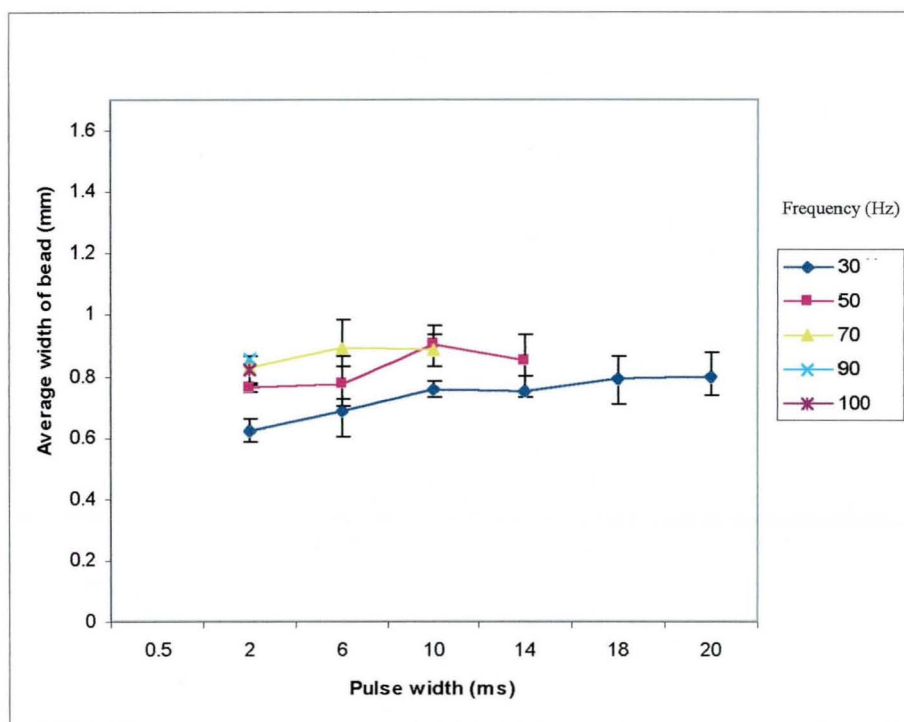Figure 6.86: Graph of pulse width versus average height of bead (5mm/s, 20J)
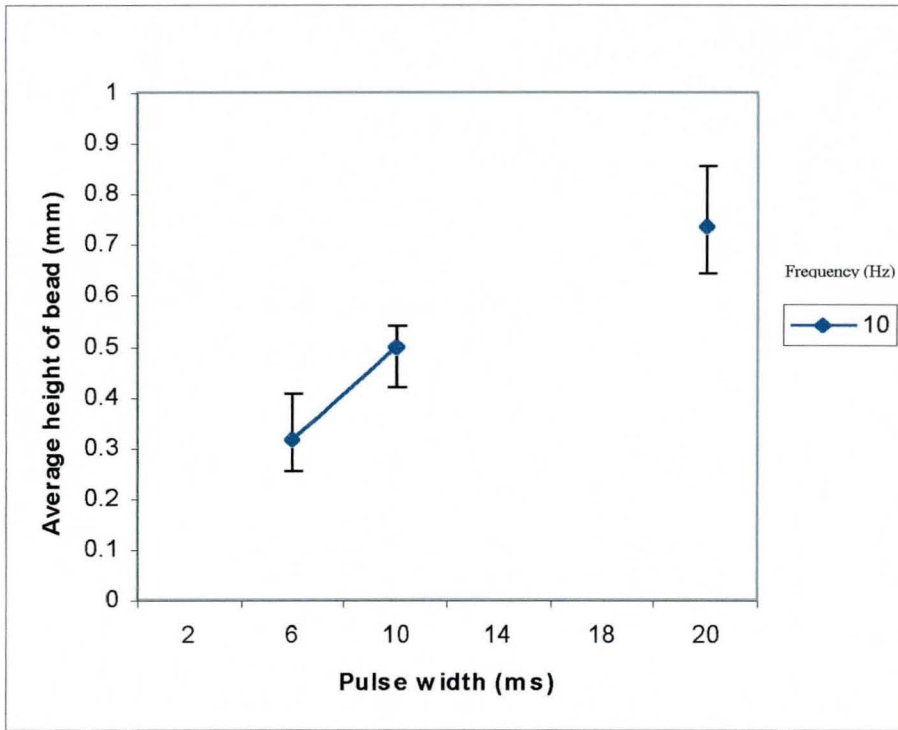
Figure 6.87: Graph of pulse width versus average height of bead (10mm/s, 20J)
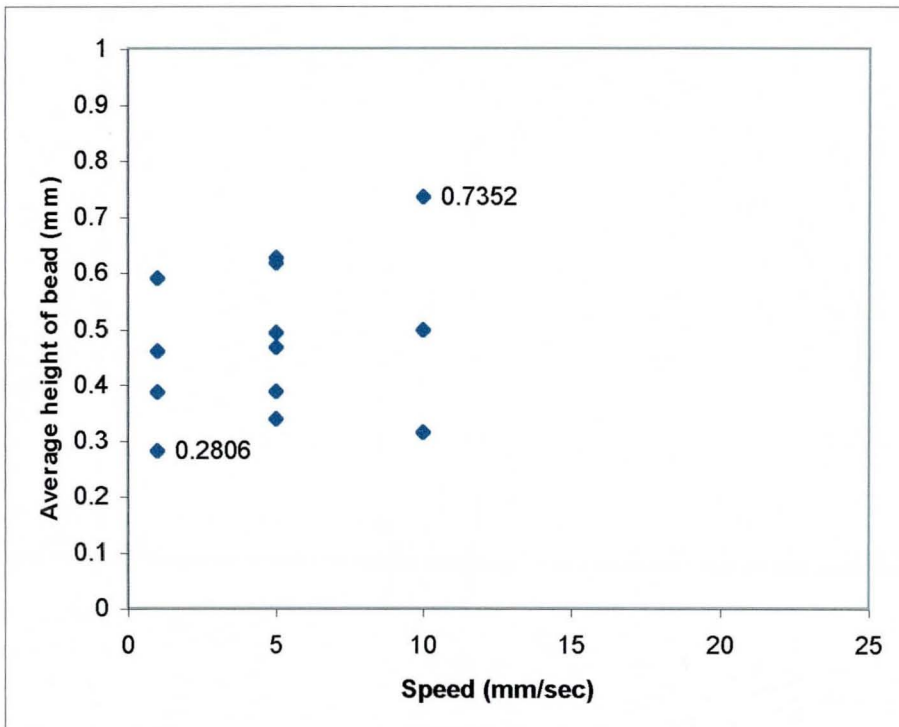
Figure 6.88: Graph of speed versus average height of the bead [20J]

In Figure 6.87, the beads progress from spaced balling to joint of almost continuous appearance fused to plate from 14 to 20ms.

At an energy level of 30 J and 60J there are very few results. Trends are unclear for Figures 6.89, 6.90, 6.91, 6.92, 6.93 for 30J and Figure 6.94.
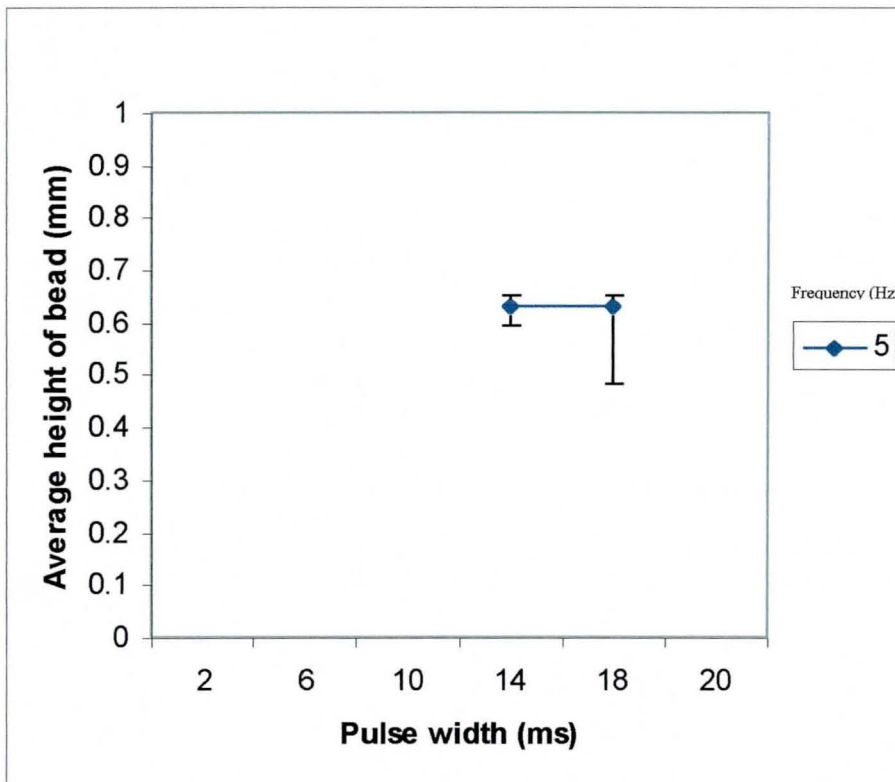
Figure 6.89: Graph of pulse width versus average height of bead (1mm/s, 30J)
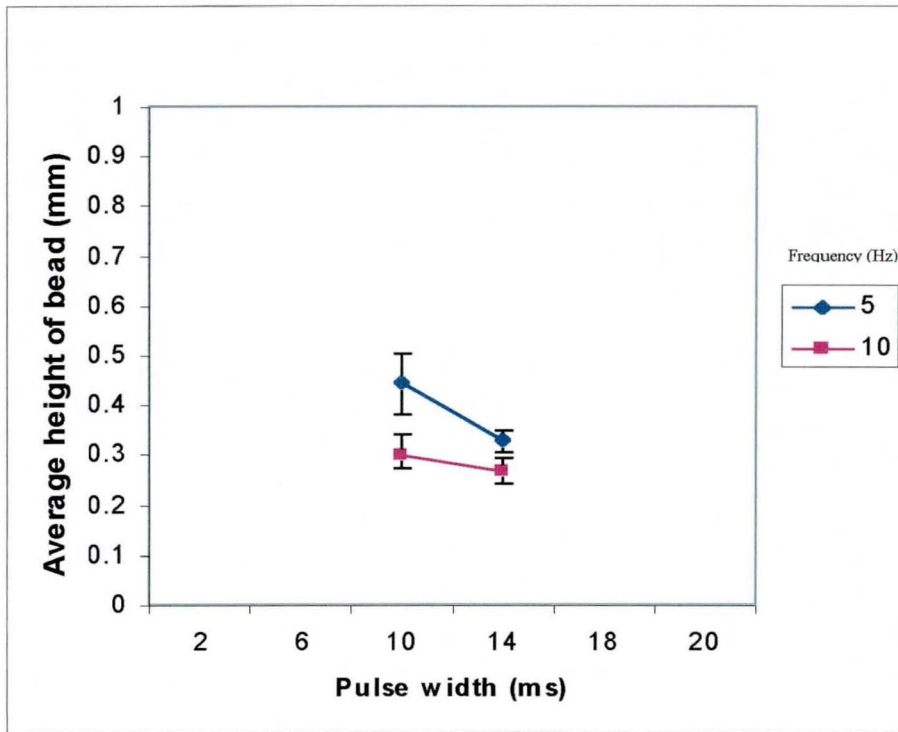
Figure 6.90: Graph of pulse width versus average height of bead (5mm/s, 30J)
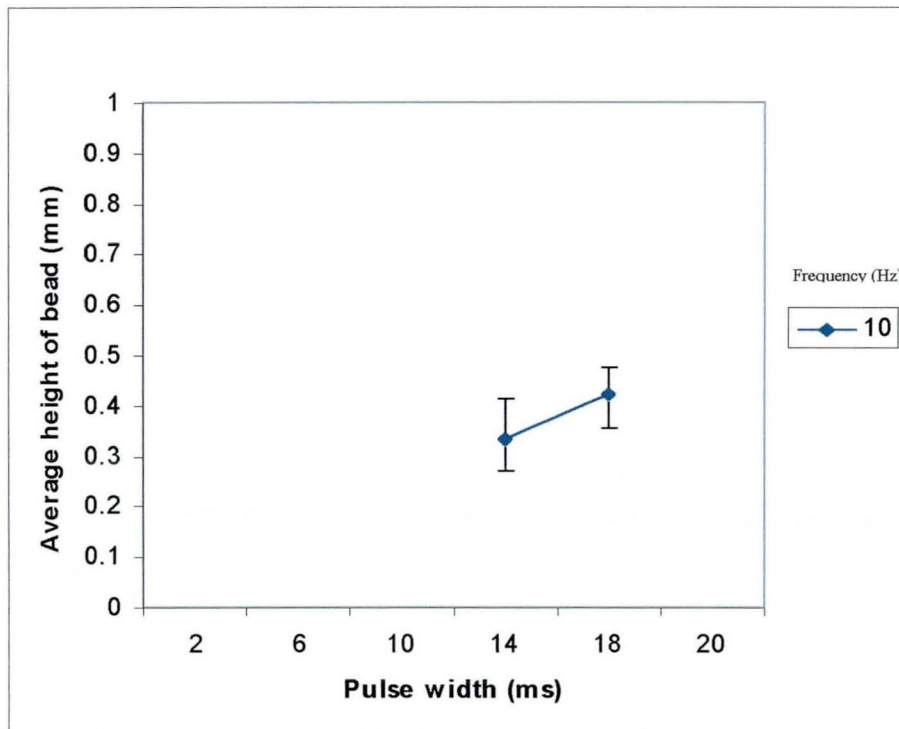
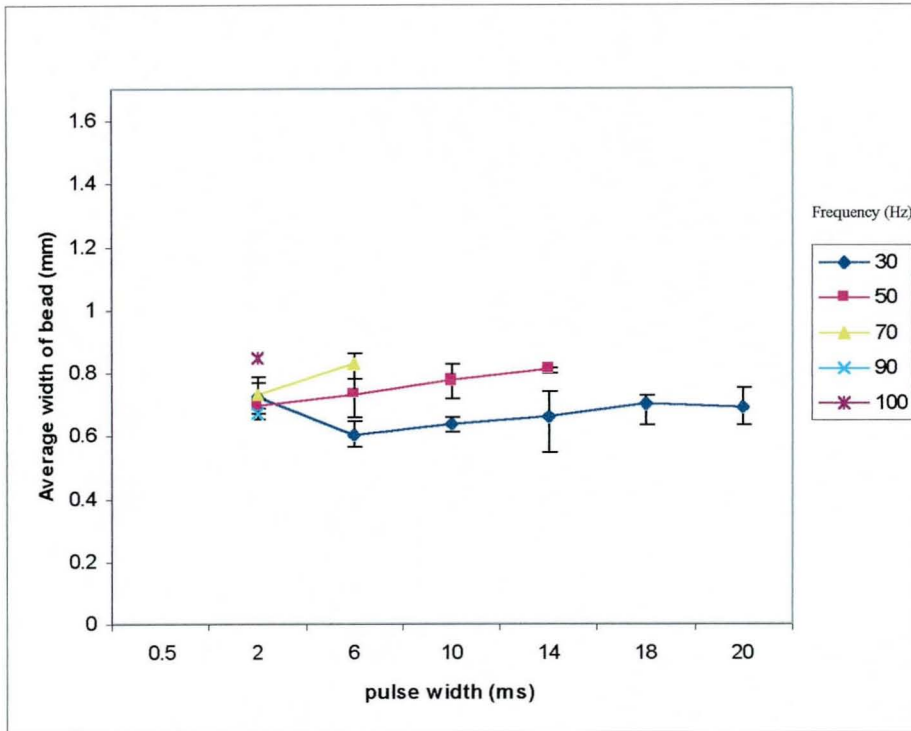Figure 6.91: Graph of pulse width versus average height of bead (10mm/s, 30J)
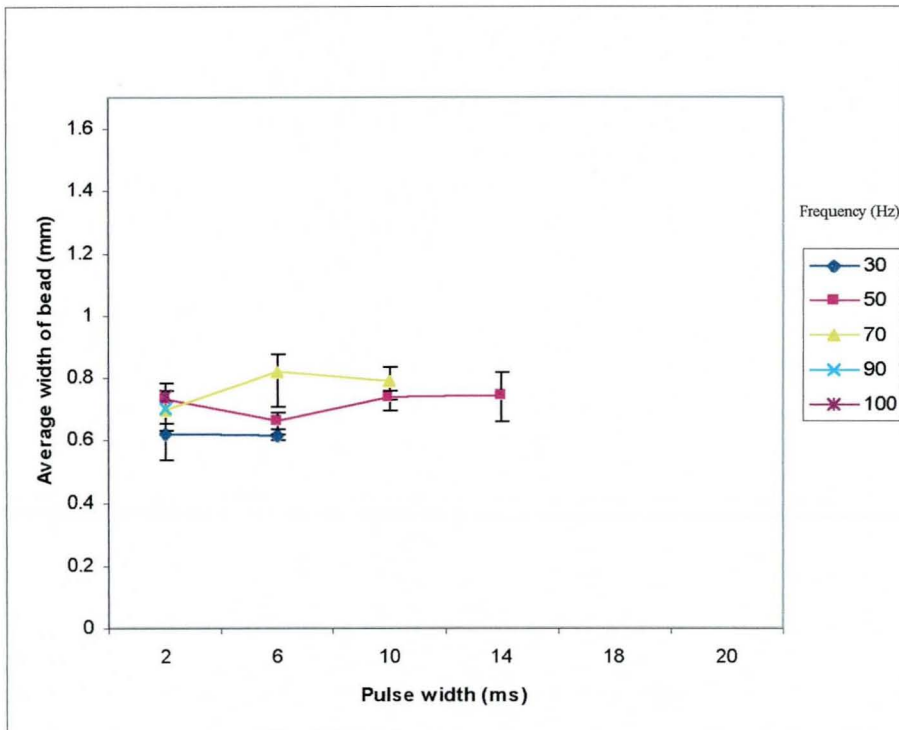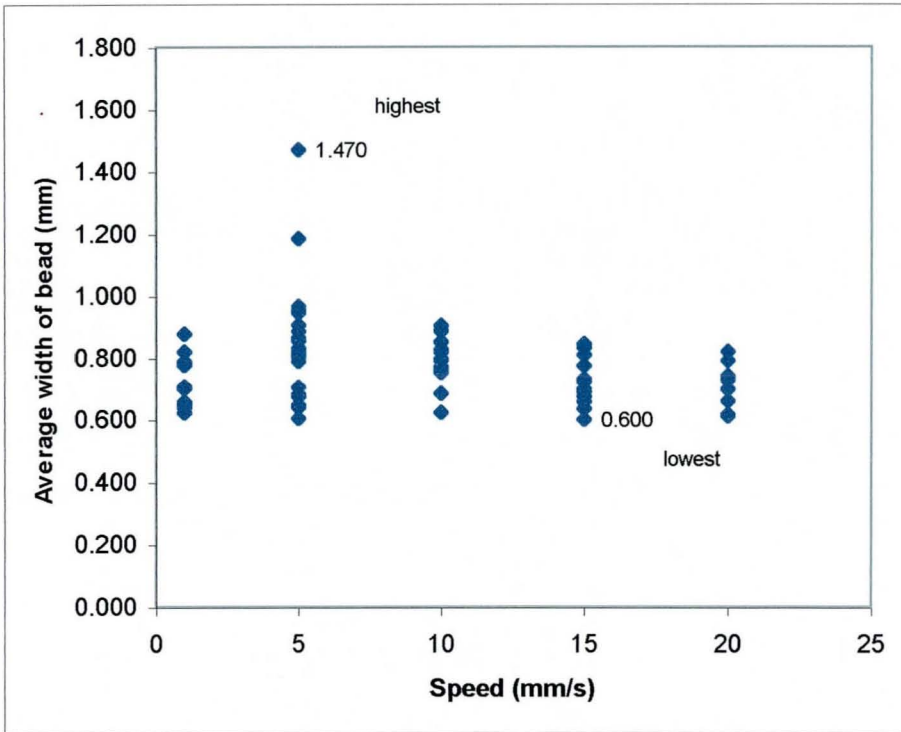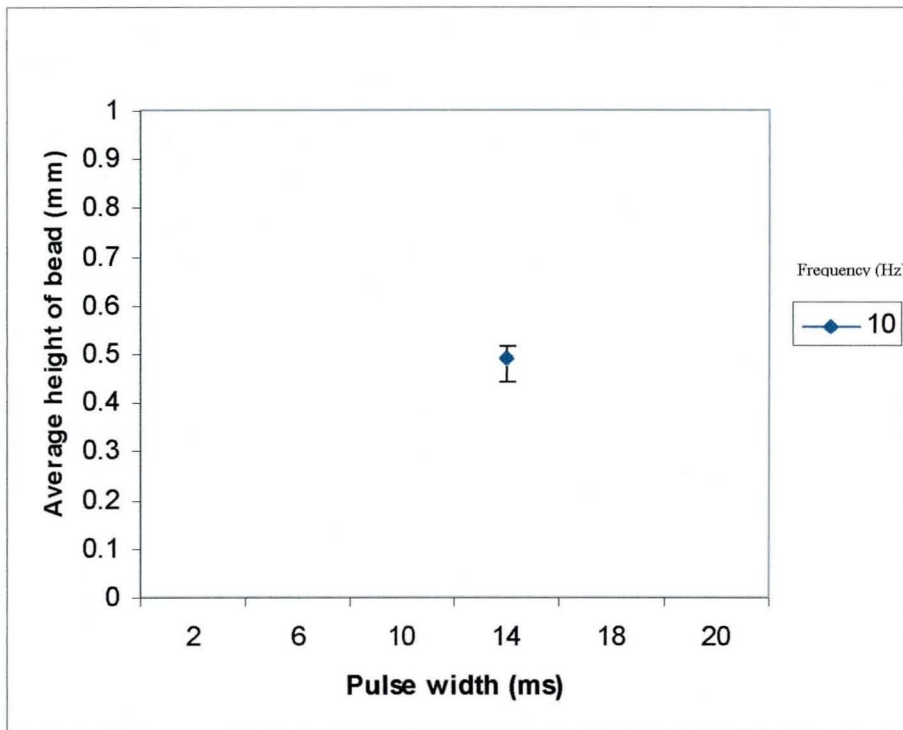
Figure 6.92: Graph of pulse width versus average height of bead (15mm/s, 30J)
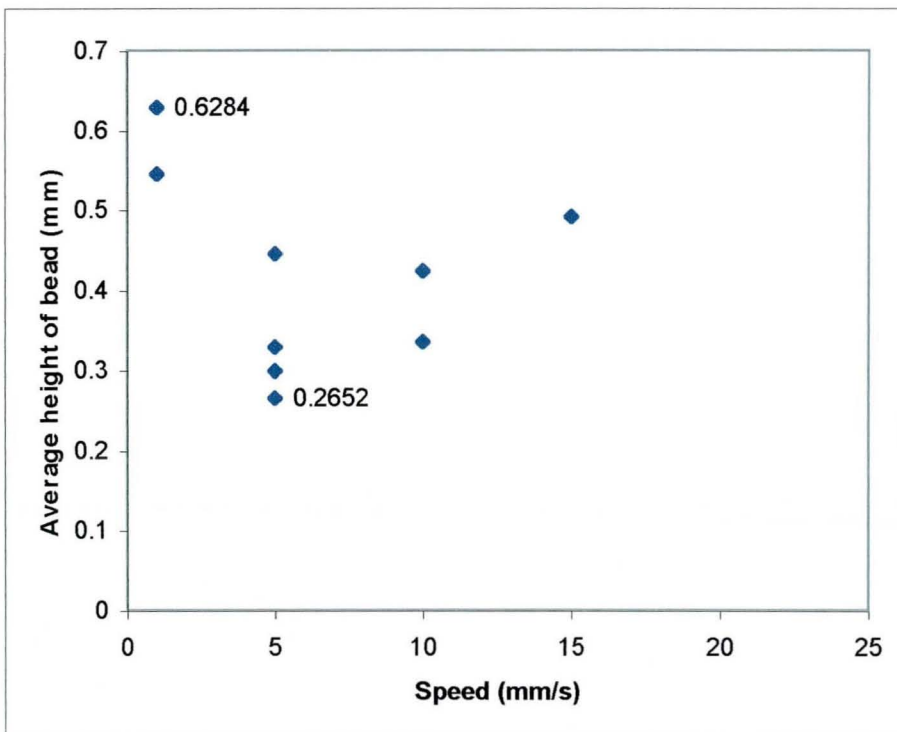
Figure 6.93: Graph of speed versus average height of a bead (At 30J)
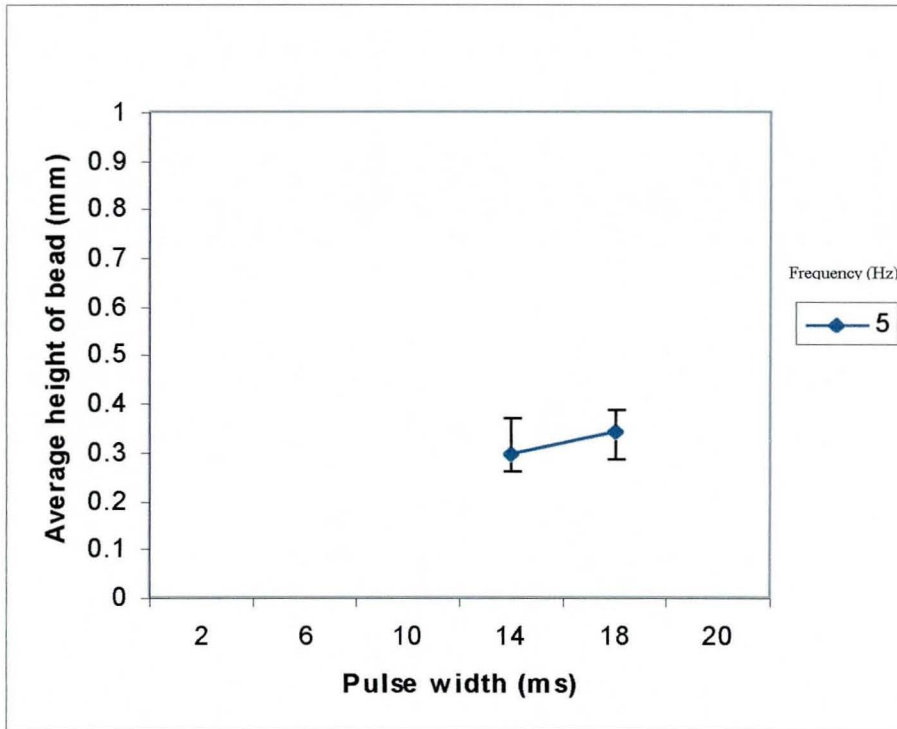
Figure 6.94: Graph of pulse width versus average height of bead (15mm/s, 60J)

6.4. Physical observation of results at various processing parameters

6.4.1. Effect of process parameter variation on the nature of variation in beads

Comparisons are made between the physical appearances of beads and trends exhibited by the graphs in the previous section.
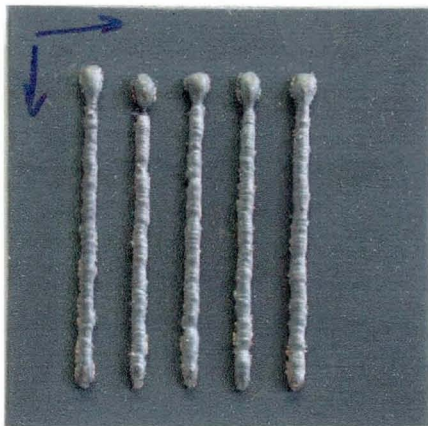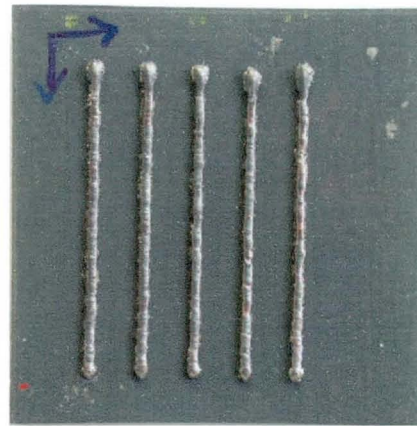
(a) 5mm/s   (b) 10mm/s

Figure 6.95 (a,b) : Figure showing effect of variation of speed (1mm layer height, 5J, 14ms and 50Hz)

Figure 6.95 shows a clear variation in the width of the beads as the speed increased. Figure 6.8 and Figure 6.9 show similar differences.
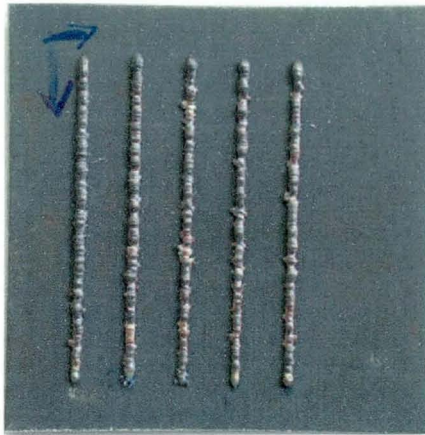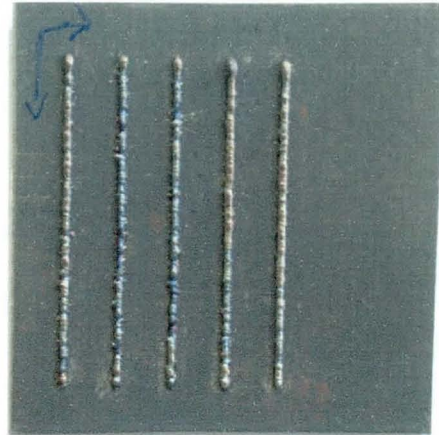
(a) 5mm/s   (b) 10mm/s

Figure 6.96 (a, b): Figure showing effect of speed increase (0.4mm layer height, 5J, 14ms, 50 Hz)

The differences in widths, is not so apparent for 0.4 mm layer height.
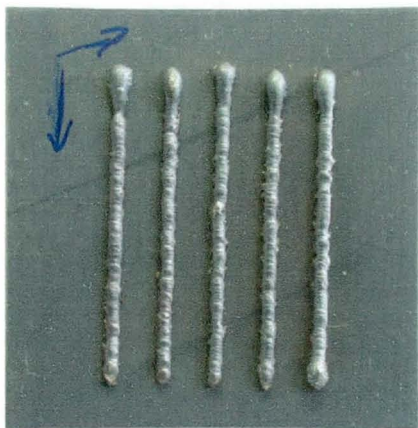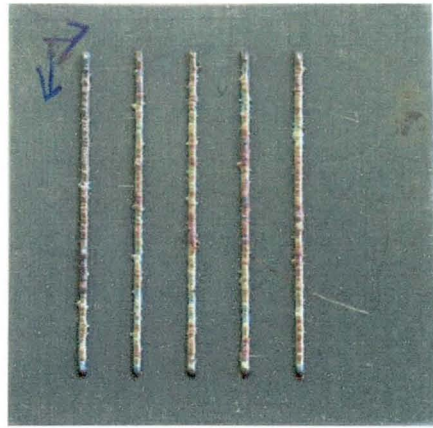
(a) 1mm layer   (b) 0.4mm layer

Figure 6.97: Effect of variation in layer height on the bead (10J, 5mm/s, 10ms, 30 Hz)

Figure 6.97 shows a more regular and thinner bead with a smaller layer height (Figure 6.97 b) for the same parameters.

(a) 1mm/s   (b) 5mm/s   (c) 10mm/s
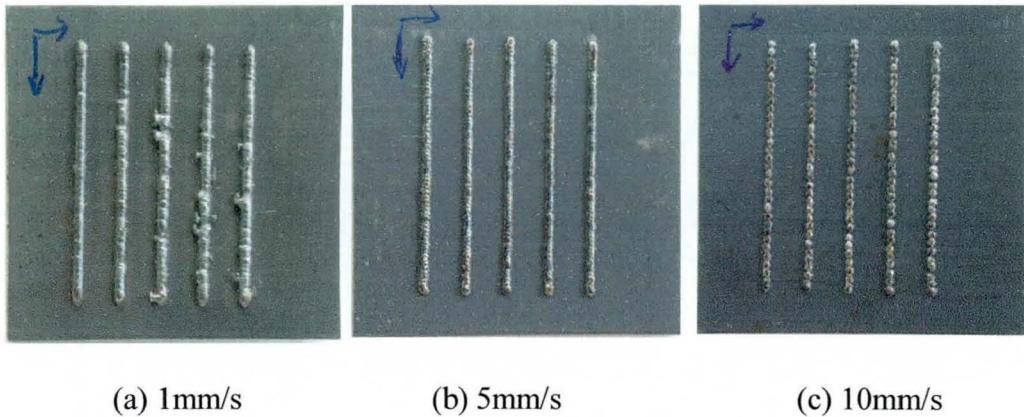
Figure 6.98 (a, b, c): Effect of variation of speed (1mm layer height, 20J, 6ms, 10Hz)

From 1 to 10mm/s the beads vary in size, from being wide and irregular with additional fused metal powders, appearing like outgrowths (fin) along the bead, at 1mm/s to a more regular bead at 5mm/s (also see Figure 6.21 & 6.22). At 10mm/s balling occurred.
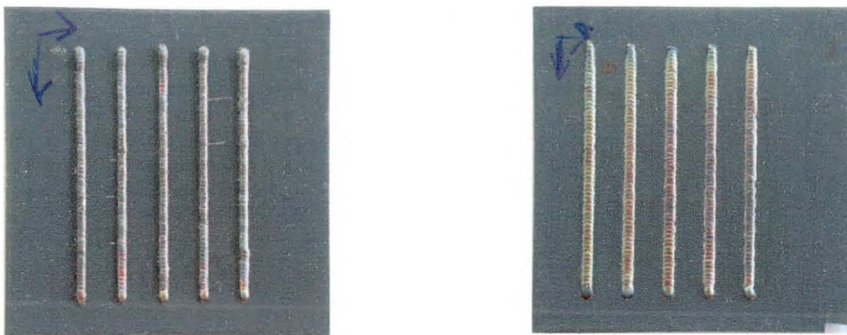
(a) 1mm layer at 30J   (b) 0.4mm layer at 30J

Figure 6.99 (a, b): Comparison of high energy beads at differing layer heights (14ms, 10Hz, 5mm/s)

The beads at 0.4mm layer height are somewhat flatter than those produced with a 1mm layer.
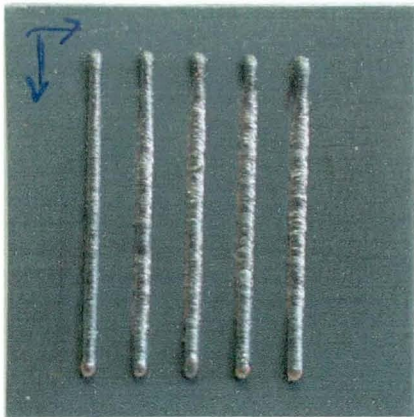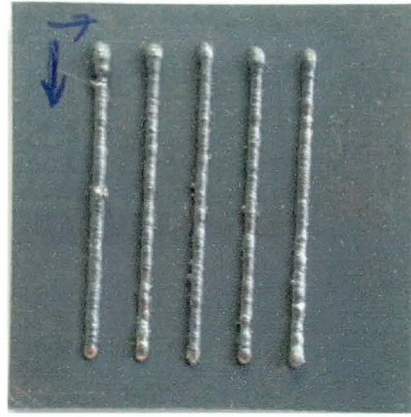
(a) At 14 ms   (b) At 18 ms

Figure 6.100: Effect of change in pulse widths (1mm layer height, 30J, 1mm/s, 5Hz)

At 14 ms the beads along their central part (excluding the bead that was scanned first) were pushed into plate surface, and were also visible on the other side of the plate, indicating penetration through the 1mm thick substrate (Figure 6.100 a).

At 18ms the penetration through the plate was not present. The bead was more regular without the depression (Figure 6.100 b). This was due to a 20 second wait time given between each scan, allowing the substrate the cool down. The improvement in height of the bead or the lack of flattening of the bead onto the substrate is evident.

6.4.2. Effect of process parameter variation in producing undesirable bead quality

These could be defined as problem areas in bead processing where the effect of certain parameter combinations produce results that may not be desirable.
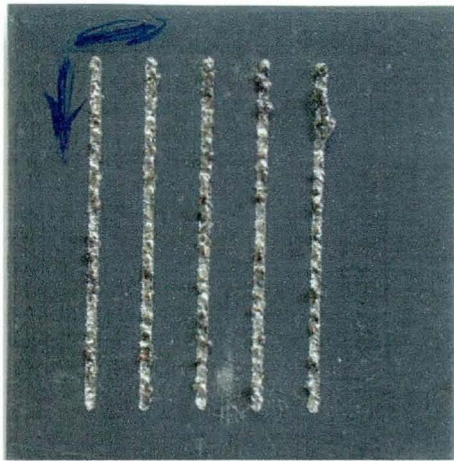
Figure 6.101: Effect of low pulse width (2ms) and speed (1mm/s) [1mm layer height, 10J, 5Hz]

Figure 6.101 show that no bead was formed. At this combination the powder was blown away due to low pulse widths, low speeds causing impact on the substrate and powder bed.
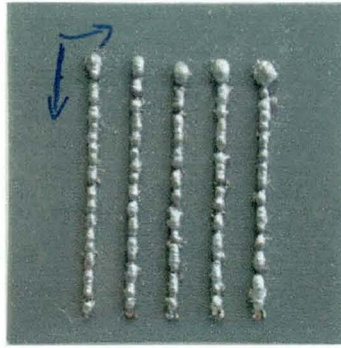
Figure 6.102: Linear irregularity or waviness (1mm layer height, 10J, 1mm/s, 18 ms and 10Hz)

Figure 6.102 show the wavy nature of the bead with some metal powder fused as lateral outgrowths giving its rough nature. This could be due to the low speed involved.
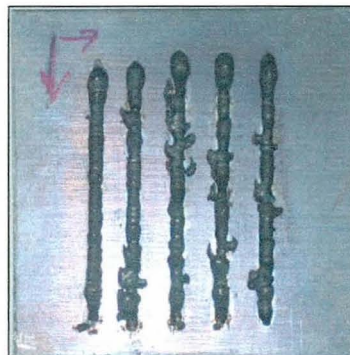
Figure 6.103: Rough Irregular beads with lateral fused metal outgrowths (1mm layer height, 10J, 1mm/s, 14ms, 30 Hz)

The scans were performed at relatively high frequency, high pulse width and low speeds.

7. Discussion

7.1. Effect of variation of pulse parameters (energy, pulse width, frequency) on the Laser Power 'Output Limits'

The Power or Output Limit graphs established at various energy levels (Figure 6.1 to 6.5) show the effective operating range of the laser set-up that was used. The limitations of the laser related to three factors:

a) Maximum mean power output

b) Frequency limits, which also reduced with increasing pulse width

c) At low pulse durations and frequencies the sensors did not register an output due to insufficient power.

As the energy levels increase the area of the graph where sufficient output is obtained reduced. The frequency options reduce with high energy levels.

The YAG laser used was known to have a maximum Mean Power output of near 550W. It is known that Mean Power is a product of the energy and frequency thus expressed as: $P = E \times f$ (1)

Where, P= Mean (average) power (Watts), E= Energy (J), f = frequency (Hz)

Therefore, as frequency increases, the mean (average) power increases. Thus, assuming a maximum output of 550W at the energy levels shown for Figure.6.1 to 6.5, the maximum frequencies possible reduce in accordance with the equation $f = P/E$.

Therefore at 550 W maximum output: f = 110 Hz for energy 5J, 55Hz for energy 10J, 27.5 Hz for energy 20J, 18.33 Hz for energy 30J and 9.16 Hz for energy 60J.

The maximum values in the graphs Figure 6.1 (100Hz), Figure 6.2 (50Hz) are close to the calculated values.

Fault condition error statements highlighted in Section 6.1 were encountered when the Average output power also given by Equation 1 exceeded the maximum specification of 550W on the laser thus exhibiting the message 'Laser Output over limit'. The graphs Figure 6.1 for 5J and Figure 6.2 for 10J also indicate the maximum calculated frequencies 110Hz and 55Hz respectively are relevant only at certain low pulse widths e.g. 2,6, 10ms. The frequency options reduce as pulse widths increase and the higher pulse widths of 18 and 20ms, the possible maximum frequency even dips below the calculated value (e.g. 55Hz for 10J Figure 6.2). In this case the laser gives the error message as 'Calculated Pump Power Limit', indicated that there is a maximum equipment limit for obtaining output at high pulse width parameters.

7.2. Effect of pulse parameters (pulse energy, pulse width and frequency) and speed on the beads.

7.2.1. Effect on bead width

It is seen from a general observation of the graphs in section 6.3.1.1 that there are certain clear trends especially at low to medium speeds 1mm/s (Figure 6.14

at 10J) and 5mm/s (Figure 6.8 at 5J) where the average width of a bead is seen to increase with increasing pulse widths (duration of the pulse) and increasing frequency. At higher speeds (10mm/s and beyond) the results are more random. The maximum number of beads were produced for 5 and 10 mm/s.

Pulse duration or the pulse width in tandem with pulse height determines the area for a rectangular pulse, hence its energy. For a single energy level, frequency determines the amount of mean (average) power, which is available for processing as can be seen in Equation 1.

It is well documented that short pulse durations are usually suited for operations such as cutting and drilling [58]. On a 1mm substrate covered with a 1mm powder layer, short pulse widths have the capacity to penetrate deeper into the surface of the powder bed and into the substrate, its extent depending on the energy level chosen. Its is therefore possible that packets of energy delivered within a shorter time as dictated by a low pulse width (duration) and a higher pulse height would distribute less heat to fuse the powder on the plate and produce a greater effect within the substrate. This would result in perhaps a smaller melt pool at the powder resulting in narrower beads. A higher pulse width (duration) would concentrate the heat on the surface and to the surrounding powder by conduction and less into the substrate, thus producing larger melt pools, fusing more powder and producing greater widths. This would account for the increase in average width (seen in section 6.3.1.1) with an increase in pulse duration (width) seen at various speed values.

Similarly, frequency with its increasing effect on the mean power delivered will supply more energy (heat) to the powder layer perhaps creating a larger molten

pool, fusing more metal powder into the bead. This in turn would increase the average width of the beads.

An increase in the slope of the lines seen in Figure 6.8 (5mm/s, 5J) as compared to Figure 6.7 (1mm/s, 5J) [at 1mm layer height] shows that an increase in speed increases the effect of pulse width (duration) on the bead width.

An increasing energy produces a small increase in the average bead width. This is expected due to the increased energy levels producing greater heat. The general ranges of average bead widths are seen not to change much across all results.

A reduction in layer height as observed in Section 6.3.1.2 is followed by a reduction in the general average widths of beads that are obtained. A possible reason could be due to the less mass of metal powder available on the substrate. The effect of the reduction in layer height can be seen in Figure 6.97.

Trends in graphs for 0.4 mm layer beads are not so distinct as in the case of 1mm layer heights with little increase in average bead width with increased pulse width.

For beads produced with a layer height of 0.4mm, a greater number are generally seen possible for all speeds up to 20mm/s. Smaller layer thickness will tend to permeate more heat to the substrate thus effecting surface tension effects and reducing balling. Hence a flatter bead would dominate. The beads in general have a more uniform definition as compared to those at 1mm layer height. This is seen in Figure 6.97.

At higher energy levels, the number of beads possible reduced compared to lower energy levels. One reason is the limit on the frequencies available for high

energy levels. Also the available combinations at high energy levels e.g. 20J, 30J and 60J tend to produce high heat due to the higher peak powers causing burnt welds, plasma, and blown powder at low frequencies and low speeds. At high speeds e.g. 10, 15 mm/s such energies tend to cause balling.

7.2.2.   Effect on bead height

Bead height has a similar trend as bead width, seen in Section 6.3.2. Thus, an increase in pulse width generally produces an increase in average height as does an increase in frequency. High frequency parameters are also seen to produce beads of lower average height when utilising very low pulse widths like 2ms (Figure 6.55). This is seen as possibly an effect of the high average powers e.g. 450W at 90Hz in combination with relatively high peak power at 2ms. The height is seen to increase for increasing pulse widths, hence reducing peak power.

As with 1mm layers, bead heights for 0.4 mm layer show an increasing trend of average height with an increase in pulse duration (pulse width) for certain values of frequency.

7.3. On the nature of beads and bead processing

The experiments show (see Appendix A) that out of a possible 400 parameter combinations that are possible for a single layer height, slightly greater than 35 % produce beads that are measurable and fused to the substrate. The choice of a

parameter combination for final use would require the bead to have sound physical qualities, with continuous nature, fused to substrate.

There could also be a greater heat affected zone (HAZ) causing burning or colouring of the zone adjacent to the bead (e.g. brownish colour). This may or may not be acceptable. There could be a thin ' gutter' area adjacent to the bead where there is a lack of powder material for a following overlapping scan. This could go on to cause porosity.

A classification of the effect of varying parameters are given as follows:

A. Physical (bead) attributes:

1. Formation of continuous bead

2. Beads that have surface waviness but continuous

3. Porous at the base where attached to the substrate (though appears continuous from above)

4. Balling (fused to plate or loosely attached to substrate)

5. Continuous or partially continuous bead loosely bonded to the substrate.

6. Formation of undercut.

7. Irregular bead shape following an unsteady molten pool.

B. Processing (region) attributes that are seen include:

- Excessive plasma formation at the interaction zone

- Blowing away of powder

- Wide heat affected zone

- Unsteady molten pool

- Many fumes

- Too much heat penetrating and affecting (burning) the substrate

- Coolant temperature at the laser head increasing beyond 28° C (especially at high energies)- this could damage the shutter assembly.

- Clean bead (without blown particles, no excessive heat fumes or plasma)

Figures in Section 6.4.2 show examples of such bead qualities.

The undesirable effects of incorrect scan parameters could be due to the combination of the following:

1. Low pulse width, low speed (Figure 6.101) (blown powder with undercut along bead path)

2. Low speed (Figure 6.102) (Surface waviness)

3. High frequency, high pulse width and low speed (Figure 6.103) (Irregular bead)

4. Low frequency, high speed (Regularly spaced balling fused to plate)

5. High speed (Balling like bead appearance with intermittent discontinuities)

6. Undercuts due to high energy and low layer height

.

8. Conclusions

1. A general increase in bead width and bead height appears to be present due to an increase in pulse width and pulse frequency and with decrease in speed.

2. There were more possible beads observed at lower layer thickness (0.4mm) especially at higher speeds (15, 20 mm/s)

3. Effect of frequency variations, are less clearer for beads at low layer thickness.

4. In general higher pulse widths result in smoother bead surface due to less tendency for the pulse to penetrate the plate (as could occur for a cutting, drilling process)

5. The process produces beads, at relatively moderate frequencies (10Hz, 30Hz), moderate pulse widths (10, 14ms), speeds of 5 and 10 mm/s and low to moderate energy levels (5J, 10J)

6. High energy levels, in combination with low speeds and/or low pulse widths or high frequency may not be suitable for producing beads. This could depend on the material chosen and the thickness of the substrate.

7. In general, speed was seen to have a greater effect on the bead formation (continuous, balling etc) than a change in frequency (hence average power) or energy levels.

8. There are undesirable effects such as undercuts, blown powder, overheating of substrate, HAZ etc seen at extreme values of parameter choice.

9. For higher energy settings e.g. 30J, bead geometry was affected by heating up of the substrate and showed improvement when subjected to a time gap between individual scans. Hence at high energy levels a wait time between scans could improve bead geometry.

10. In general a wide combination of pulse parameters are seen capable of producing continuous beads

9. Further Work

1. A parameter combination capable of producing a continuous bead could be further analysed by observing the physical properties of the bead.

2. A study of the stability and size of a moving molten material could be useful to determine the effect on the resulting bead geometry

3. The effect of gas flow rate on the bead formation, and focal length variation on the process window could be investigated.

4. The effect of varying hatch patterns and time delays between scans could be useful for producing beads of different shape.

5. The work on individual beads could further be extended to a horizontal layer composed of successive overlapping beads and followed by vertical layers to form blocks.

6. The effect of bead overlap for a single layer and the effect of substrate penetration for single layers could be studied for the effect on porosity.

7. The building of layers could induce thermal gradients in the block and hence a study of stresses would become necessary. Preheating of the platform or substrate to reduce thermal gradients and improve wetting will be useful for multiple layers. Also cooling techniques could minimise heat accumulation during part build which may cause distortion. A study of their effect on surface finish and interlayer bonding could be useful

8. A study of the microstructure and strength of the resultant part would be required to establish a possible usage for industrial applications.

10.References

[1] Sears, J.W., Direct Laser Powder Deposition, State-of-the-Art, Nov 1999, US Department of Energy's Website database, www.osti.gov/bridge (Accessed 29th June 2002)

[2] Boddu, R.M., Robert, G.L. and Liou, F.W., Control of Laser Cladding for Rapid Prototyping- A Review, Proceedings of Solid Freeform Fabrication Symposium, Aug 2001, Edited by Bourell, D.L., Beaman, J.J., Crawford, R.H., Marcus, H.L., Wood, K.L., Barlow, J.W., University of Texas, Austin, USA, pp. 460-466

[3] Vilar, R.M., Laser Cladding, Proceedings of the 2002 International conference on Metal Powder Deposition for Rapid Manufacturing, Editors: Keicher, D.M., Smugeresky, J.E. and Sears, J.W., San Antonio, Texas, USA, April 2002, pp. 9-24.

[4] Koch, J.L., Mazumder, J., " Rapid Prototyping by Laser Cladding", The International Society for Optical Engineering, Vol. 2306, pp. 556-562

[5] Keicher, D.M., Laser-Engineered Net-Shaping (LENS™) Enhances Repair and Overhaul methods, White Paper, Application Brief, Optomec® Inc, April 2001

[6] Nyrhilä, O., Direct Laser Sintering of Injection Moulds, Editor Dickens, P.M., Proceedings of the 5th European Conference on Rapid Prototyping and Manufacturing, Helsinki Finland, ISBN: 0 951 9759 51, June 1996, pp.185-194

[7] Das, S., Fuesting, T.P., Danyo, G., Brown, L., Beaman, J., Bourell, D.L., Sargent, K., Direct Laser Fabrication of a Gas Turbine Engine Component, Part I

and II, Proceedings of Solid Freeform Fabrication Symposium, Aug 1998, Edited by Bourell, D.L., Beaman.J.J, Crawford, R.H., Marcus, H.L., Barlow, J.W., University of Texas, Austin, USA, pp. 1-18

[8] Dickens, P.M., Rapid Tooling Research, Proceedings of the Time-Compression Technologies' Oct 1998, Nottingham UK, pp. 284-292

[9] Beaman, J.J., Lepson, L., Bourell, D.L., Wood, K.L., SLS processing of Functionally Graded Materials, Proceedings of Solid Freeform fabrication Symposium, University of Texas, Austin USA, August 1997, pp. 67-79

[10] Fessler, J.R., Nickel, A.H., Link, G.R., Prinz, F.B., Functionally Gradient Metallic prototypes through Shape Deposition Manufacturing, Proceedings of Solid Freeform Fabrication Symposium, Edited by Bourell, D.L., Beaman, J.J., Crawford, R.H., Marcus, H.L., Barlow, J.W., August 1997, University of Texas, Austin, Texas, USA, pp. 521-528

[11] Ashley, S., "Rapid Prototyping Systems", Mechanical Engineering, April 1991, pp. 36-43

[12] Beckert, B.A., Cutting it in Rapid Prototyping, Computer Aided Engineering, Sept. 1991, pp. 28-40

[13] Kruth, J.P., Material Incress Manufacturing by Rapid Prototyping Techniques, Annals of CIRP, Vol.40, no.2, ISSN: 0007- 8506, 1991, pp. 603-614

[14] Rapid Prototyping: Principles and Applications in Manufacturing, Kai, C.C. and Fai, L.K., John Wiley and Sons Inc. (Asia, Singapore), 1997, ISBN: 0-471-19004-7

[15] Nyrhilä, O., Direct Metal Laser Sintering: Industrialisation and Case Studies, Proceedings of the Time-Compression Technologies' Oct 1998, Nottingham UK, pp. 123-132

[16] Nyrhilä, O., Kotila, J., Lind, J.E., Syvänen, T., Industrial use of Direct Metal Laser Sintering, Proceedings of Solid Freeform Fabrication Symposium, Aug 1998, Edited by Bourell, D.L., Beaman, J.J., Crawford, R.H., Marcus, H.L., Barlow, J.W., University of Texas, Austin, USA, pp. 487-493

[17] Sindel, M., Pintat, T., Greul, M., Nyrhilä, O., Wilkening, C., Direct Laser Sintering of Metals and Metal Melt Infiltration for Near Net Shape Fabrication of Components, Proceedings of Solid Freeform Fabrication Symposium, Aug 1994, Edited by Bourell, D.L., Beaman, J.J., Crawford, R.H., Marcus, H.L., Barlow, J.W., University of Texas, Austin, USA, pp. 94-101

[18] Eyerer, P., Shen, J., Keller, B., LAPS- Laser Aided Powder Solidification-Technology for Direct Production of Metallic and polymer parts, Proceedings of Solid Freeform Fabrication Symposium, Edited by Marcus, H.L., Beaman, J.J., Bourell, D.L., Barlow, J.W., Crawford, R.H., University of Texas, Austin, Texas, USA, August 1994, pp. 82-93

[19] www.cs.hut.fi/~ado/rp/subsection3_6_3.html, Date: 09/09/2002

[20] Ravi, B., Rapid Prototyping and Tooling, An Overview of the emerging technology, Industry Seminar handout, Industrial Design Centre, Indian Institute of Technology, Bombay India, 18th April 1997

[21] Nutt, K., The Selective Laser Sintering Process, "Photonics Spectra, Vol. 25, n.9, Sept, 1991, ISSN: 0731-1230, pp. 102-104

[22] Badrinarayan, B., and Barlow, J.W., Metal Parts from Selective Laser Sintering of Metal-Polymer Powders, Proceedings of Solid Freeform Fabrication Symposium, Aug 1992, Edited by Bourell, D.L., Beaman, J.J., Crawford, R.H., Marcus, H.L., Barlow, J.W., University of Texas, Austin, USA, pp. 141-146

[23] Birch, J., Diecasting World, Vol. 175, Sept 2001, ISSN: 0965-6111, pp.6-12

[24] Hejmadi, U., Selective Laser Sintering of Metal Molds: The Rapid Tool™ Process, Proceedings of Solid Freeform Fabrication Symposium, Edited by Marcus, H.L., Beaman, J.J., Bourell, D.L., Barlow, J.W., Crawford, R.H., University of Texas, Austin, Texas, USA, August 1996, pp. 97-104

[25] Boivie, K., SLS Application of the Fe-Cu-C System for Liquid Phase Sintering, Proceedings of Solid Freeform Fabrication Symposium, Aug 2000, Edited by Bourell, D.L., Beaman, J.J., Crawford, R.H., Marcus, H.L., Barlow, J.W., University of Texas, Austin, USA, pp. 141-149

[26] Zong, G., Wu, Y., Tran, N., Lee, I., Bourell, D.L., Beaman, J.J., and Marcus, H.L., Direct Selective Laser Sintering of High Temperature Materials, Proceedings of Solid Freeform Fabrication Symposium, Aug 1992, Edited by Bourell, D.L., Beaman, J.J., Crawford, R.H., Marcus, H.L., Barlow, J.W., University of Texas, Austin, USA, pp. 72-85

[27] Knight, R., Wright, J., Beaman, J., Frietag, D., Metal processing using Selective Laser Sintering and Hot Isostatic Pressing (SLS/HIP), Proceedings of Solid Freeform Fabrication Symposium, Edited by Marcus, H.L., Beaman, J.J., Bourell, D.L., Barlow, J.W., Crawford, R.H., University of Texas, Austin, Texas, USA, August 1996, pp. 349-353

[28] Das, S., Harlan, N., Beaman, J.J., Bourell, D.L., Selective Laser Sintering of High Performance High Temperature Materials, Proceedings of Solid Freeform Fabrication Symposium, Edited by Marcus, H.L., Beaman, J.J., Bourell, D.L., Barlow, J.W., Crawford, R.H., University of Texas, Austin, Texas, USA, August 1996, pp. 89-95

[29] http://itri.loyola.edu/rp/06_02.htm, Date: 09/09/02

[30] Abe, F., Osakada, K., Fundamental Study of Rapid Prototyping of Metallic Parts, International Journal of the Japan Society for Precision Engineering, Vol.30, no.3, Sept 1996, ISSN: 0916-782X, pp. 278-279

[31] Hofmeister, W., Wert, M., Smugeresky, J., Philliber, J., Griffith, M., Ensz, M., Investigating Solidification with Laser Engineered Net Shaping (LENS)™ Process, JOM-e [electronic (web) equivalent of article published in JOM, Vol. 51, no.7, July 1999], www.tms.org/pubs/journals/JOM/9907/Hofmeister

[32] http://itri.loyola.edu/rp/06_03.htm, Date: 09/09/2002

[33] Jeng, J.Y., Peng, S.C., and Chou, C.J., Metal Rapid Prototyping Fabrication Using Selective Laser Cladding Technology, International Journal of Advanced Manufacturing Technology, Vol. 16, pp.681-687

[34] Keicher, D.M., Miller, W.D., Smugeresky, J.E., Romero, J.A., 1998, " Laser Engineered Net-Shaping LENS): Beyond Rapid Prototyping to Direct Fabrication, " Proceedings of the 1998 TMS Annual Meeting, San Antonio, Texas, pp. 369-377

[35] Atwood, C., Griffith, M., Harwell, L., Schlienger, E., Ensz, M., Smugeresky, J., Romero, T., Greene, D., Reckaway, D., Laser Engineered Net Shaping (LENS™): A Tool for Direct Fabrication of Metal Parts, Sandia

National Laboratories, Alburquerque USA, SAND98-2473C, 1998, US Department of Energy website database, www.osti.gov/bridge (Accessed 29th June 2002)

[36] Gorman, P.H., Keicher, D., Bullen, J., Grylls, R., Add value to existing moulds, published by Society of Manufacturing Engineers (SME) Rapid Prototyping Association (RPA), Fourth Quarter Vol. 7, No. 4, 2001

[37] Website, www.optomec.com, Optomec Inc., (accessed, July 2002)

[38] Lewis, G.K., Milewski, J.O., Thoma, D.B., Nemec, R.B., Properties of Near-Net Shape Metallic Components made by the Directed Light Fabrication Process, Proceedings of Solid Freeform Fabrication Symposium, Edited by Marcus, H.L., Beaman, J.J., Bourell, D.L., Barlow, J.W., Crawford, R.H., University of Texas, Austin, USA, August 1997, pp. 513-520

[39] Lewis, G.K., Nemec, R., Milewski, J., Thoma, D.J., Cremers, D., Barbe, M., Directed Light Fabrication, Proceedings of ICALEO, 1994, pp.17-26

[40] Thoma, D.J., Charbon, C., Lewis, G.K., Nemec, R.B., Directed Light Fabrication of Iron-Based Materials, Materials Research Society Symposium Proceedings, Vol. 397, 1996, pp. 341-346

[41] Mazumder, J., Choi, J., Nagarathnam, K., Koch, J., Hetzner, D., The Direct Metal Deposition of H13 tool steels for 3-D Components, JOM, v.49, n.5, May 1997, ISSN: 1047-4838, pp. 55-60

[42] Mazumder, J., Schiffer, A., Choi, J., " Direct Materials Deposition: Designed Macro and Microstructure, Materials Research Society Symposium Proceedings, v. 542, 1999, ISSN: 0272-9172, pp. 51-63

[43] www.pomgroup.com (POM Group Inc.), July 2002

[44] Klocke, F., Wirtz, H., Meiners, W., Direct Manufacturing of Metal Prototypes and Prototype tools, Proceedings of Solid Freeform Fabrication Symposium, Edited by Marcus, H.L., Beaman, J.J., Bourell, D.L., Barlow, J.W., Crawford, R.H., University of Texas, Austin, Texas, USA, August 1996, pp. 141-148

[45] Xue, L., Islam, M., Laser Consolidation- A Novel One-Step Manufacturing Process from CAD Models to Net-Shape Functional Components, Proceedings of the 2002 International conference on Metal Powder Deposition for Rapid Manufacturing, Edited by Keicher, D., Sears, J.W, Smugeresky, J., San Antonio, Texas, USA, April 2002, pp. 61-68

[46] Dave, V.R., Matz, J.E., Eager, T.W., Electron Beam Solid Freeform Fabrication of Metal Parts, Proceedings of Solid Freeform Fabrication Symposium, Aug 1995, Edited by Marcus, H.L., Beaman, J.J., Bourell, D.L., Barlow, J.W., Crawford, R.H., University of Texas, Austin, USA, pp. 64-71

[47] Technical brochure, www.arcam.com

[48] Riberio, A.F., Norrish, J, Rapid Prototyping Process Using Metal Directly, Proceedings of Solid Freeform Fabrication Symposium, Edited by Marcus, H.L., Beaman, J.J., Bourell, D.L., Barlow, J.W., Crawford, R.H., University of Texas, Austin, Texas, USA, August 1996, pp. 249-256

[49] Song, Y., Park, S., Hwang, K., Choi, D., Jee, H., 3D Welding and Milling for the Direct Prototyping of metallic parts, Proceedings of Solid Freeform Fabrication Symposium, Aug 1998, Edited by Bourell, D.L., Beaman, J.J., Crawford, R.H., Marcus, H.L., Barlow, J.W., University of Texas, Austin, USA, pp. 495-499

[50] Merz, R., Prinz, F.B., Ramaswami, K., Terk, M., Weiss, L.E., Shape Deposition Manufacturing, Proceedings of Solid Freeform Fabrication Symposium, Edited by Marcus, H.L., Beaman, J.J., Bourell, D.L., Barlow, J.W., Crawford, R.H., University of Texas, Austin, Texas, USA, August 1994, pp. 1-8

[51] Karunakaran, K.P., Bapat, V.P., Ravi, B., Rapid Prototyping and Tooling: New Paradigms in Design and Manufacturing, Seminar report, Industrial Design Centre, Indian Institute of Technology, Bombay, India, February 1998

[52] Fessler, J.R., Merz, R., Nickel, A.H., Prinz, F.B., Weiss, L.E., Laser Deposition of Metals for Shape Deposition Manufacturing, Proceedings of the Solid Freeform Fabrication Symposium, Aug 1996, University of Texas, Austin, USA, pp. 117-124

[53] Dickens, P.M., Pridham, M.S., Cobb, R.C., Gibson, I., Dixon, G., Rapid Prototyping using 3D-Welding, Proceedings of Solid Freeform Fabrication Symposium, Aug 1992, Edited by Bourell, D.L., Beaman, J.J., Crawford, R.H., Marcus, H.L., Barlow, J.W., University of Texas, Austin, USA, pp. 280-290

[54] Jackson, R.T., Patrikalakis, N.M., Sachs, E.M., Cima, M.J., Modeling and Designing Components with Locally Controlled Composition, Proceedings of Solid Freeform Fabrication Symposium, Aug 1998, Edited by Bourell, D.L., Beaman, J.J., Crawford, R.H., Marcus, H.L., Barlow, J.W., University of Texas, Austin, USA, pp. 259-266

[55] Karlsen, R., Consolidation of thin powder layers for layer manufacturing technology, NTNU 98001, 1998, ISBN: 82-471-0195-5

[56] Laser Materials Processing, 2nd Edition, Steen, W.M., Springer Verlag London Ltd., ISBN 3-540-76174-8

[57] Laser materials processing, introductory workshop, Laser Centre, Loughborough College, Loughborough University UK, Course Notes, 8th-12th November 1999

[58] GSI Lumonics, JK701 Manual for Operation and Maintenance, 1987

[59] Hayes, R.H., Laser Powder Fusion, World Aviation gas turbine engine overhaul and repair conference, 1997

[60] Jacobs, P.F., From Stereolithography to LENS: A brief history of laser fabrication, Conference Lecture, Proceedings of the 2002 International Conference on Metal Powder Deposition for Rapid Manufacturing, San Antonio, Texas, USA, April 2002

[61] Rapid Solidification of Metals and Alloys, Monograph No. 8, Jones, H., The Institution of Metallurgists, London 1982, ISBN: 0901 462 187

[62] Flinn, J.E., Kelly, T.F., Wolfer, W.G., Rapid Solidification processing: A new insight on producing high temperature microstructures and strengthening with powders, Advances in Powder Metallurgy, Vol. 1-3, Chapter 121, ISBN: 187-895400-8, pp. A65-A79

[63] De Hosson.J.Th.M., University of Groningen, Netherlands, Surface composites and functionally gradient materials with high power lasers,(part of a Ph.D. research project advert, published on the internet), March 16th 1998

[64] Suresh, S., Modelling and Design of Multilayered materials, Progress in Materials Science, Vol. 42, 1997, pp. 243-251.

[65] Neubrand, A., and Rödel, J., Gradient materials: an overview of a Novel concept, Zeitrift Fur Metallkunde, Vol 88, No. 5, pp. 358-371

[66] Tsuda, K., Ikegaya, A., Isobe, K., Kitagawa, N., Nomura, J., Development of functionally graded sintered hard materials, Powder Metallurgy, Vol. 39, No. 4, 1996, pp. 296-300

[67] Yoo, J., Cho, K., Bae, W.S., Cima, M., and Suresh, S., Transformation-Toughened Ceramic Multilayers with Compositional Gradients, Journal of American Ceramic Society, Vol. 81, n1, Jan 1998, pp. 21-32

[68] Wu, B., Borland, S., Giordano, R., Cima, L., Sachs, E., Cima, M., Solid Free-form fabrication of Drug Delivery Devices, Journal of Controlled Releases, 40(1-2), June 1996, pp. 77-87

[69] Rawlings, R., Tailoring Properties: Functionally graded materials, Materials World, Vol. 3, no. 10, October 1995, ISSN: 0967-8638, pp.474-475

[70] Shishkovsky, I., Synthesis of Functional gradient parts via RP methods, Rapid Prototyping Journal, Editor. Campbell, I., Vol. 7, No. 4, 2001, ISSN: 1355-2546, pp. 207-211.

[71] Aerospace Materials, Edited By Cantor, B., Assender, H., Grant, P., IOP Publishing Ltd 2001, ISBN: 0 7503 0742 0

[72] http://www.hut.fi/Units/LMP/tribograd.htm, 6th Oct 2002

[73] Dickens, P.M., Rapid Prototyping of Metal Parts and Tools, Proceedings of Competitive Advantages by Near-Net Shape Manufacturing, Symposium, Editor Kunze, H.D., April 14-16, 1997, Bremen, Germany, ISBN: 3-88355-246-1, pp. 311-317.

[74] Peterseim, J., Luck, J.M., Direct Metal Prototyping by Laser Fusion of Metal Powder, Proceedings of Competitive Advantages by Near-Net Shape

Manufacturing, Symposium, Editor Kunze, H.D., April 14-16, 1997, Bremen, Germany, ISBN: 3-88355-246-1, pp. 319-326

[75] Metal Printing- Approach to Processing Metals and Ceramics through Sintering of Powder layers, State-of-the-Art report for RAPTIA EU thematic network, Karlsen, R., June 2002

[76] Niu, H.J., Chang, T.H., Selective Laser Sintering of gas atomized M2 high speed steel powder, Journal of Materials Science, Vol 35, 2000, pp.31-38

[77] O'Neill, W., Sutcliffe, C.J., Morgan, R., Hon, K.K.B., Investigation of Short Pulse Nd:YAG laser Interaction with Stainless Steel Powder beds, Proceedings of the Time-Compression Technologies' Oct 1998, Nottingham UK, pp. 272-282

[78] Susan, D.F., Puskar, J.D., Brooks, J.A., Robino, C.V., Porosity in Stainless Steel Powders and Deposits, Proceedings of Solid Freeform Fabrication Symposium, Aug 2000, Edited by Bourell, D.L., Beaman, J.J., Crawford, R.H., Marcus, H.L., Barlow, J.W., University of Texas, Austin, USA, pp. 50-57

[79] Kobryn, P.A., Moore, E.H., Semiatin, S.L., The effect of Laser Power and Traverse Speed on Microstructure, Porosity and Build Height in Laser Deposited Ti-6Al-4V, Scripta Materialia, Elsevier Science limited, Vol 43, 2000, pp. 299-305

[80] Morgan, R., Papworth, A., Sutcliffe, C., Fox, P., O'Neill, W., Direct Metal Laser Re-melting of 316L Stainless Steel Powder, Part 2: Analysis of Cubic primitives, Proceedings of Solid Freeform Fabrication Symposium, Aug 2001, Edited by Bourell, D.L., Beaman, J.J., Crawford, R.H., Marcus, H.L., Wood, K.L., Barlow, J.W., University of Texas, Austin, USA, pp. 283-295

[81] Karapatis, N.P., Egger, G., Gygax, P.E., Glardon, R., Optimisation of Powder Layer Density in Selective Laser Sintering, Proceedings of Solid Freeform Fabrication Symposium, Aug 1999, Edited by Bourell, D.L., Beaman, J.J., Crawford, R.H., Marcus, H.L., Barlow, J.W., University of Texas, Austin, USA, pp. 255-263

[82] Karapatis, N.P., van Griethuysen, J-P.S., Glardon, R., Direct Rapid Tooling: a review of the current research, Rapid Prototyping Journal, Editor. Campbell, I., Vol.4, No.2, 1998, pp.77-89

[83] Griffith, M.L., Schlienger, M.E., Harwell, L.D., Oliver, M.S., Baldwin, M.D., Ensz, M.T., Hofmeister, W.H., Wert, M.J., Nelson, D.V., Proceedings of Solid Freeform Fabrication Symposium, Aug 1998, Edited by Bourell, D.L., Beaman, J.J., Marcus, H.L., Barlow, J.W., Crawford, R.H., University of Texas, Austin, USA, pp. 89-96

[84] Tikare, V., Griffith, M., Schlienger, E., Smugeresky, J., Simulation of Coarsening during Laser Engineered Net Shaping, Proceedings of Solid Freeform Fabrication Symposium, Aug 1997, University of Texas, Austin, USA, pp. 699-708

[85] Schwendner, I.K., Banerjee, R., Collins, P.C., Brice, C.A., Fraser, H.L., Direct laser deposition of alloys from elemental powder blends, Scripta Materialia, Elsevier Science Ltd., Vol. 45, 2001, pp. 1123-1129

[86] Deckard, C., Miller, D., Improved Energy delivery for Selective Laser Sintering, Proceedings of Solid Freeform Fabrication Symposium, Aug 1995, Edited by Marcus, H.L., Beaman, J.J., Bourell, D.L., Barlow, J.W., Crawford, R.H., University of Texas, Austin, USA, pp.151-158

[87] Karapatis, N.P., Guidoux, Y., Gygax, P.E., Glardon, R., Thermal Behaviour of Parts made by Direct Metal Laser Sintering, Proceedings of Solid Freeform Fabrication Symposium, Aug 1998, Edited by Bourell, D.L., Beaman, J.J., Marcus, H.L., Barlow, J.W., Crawford, R.H., University of Texas, Austin, USA, pp. 79-87

[88] Nickel, A., Barnett, D., Link, G., Prinz, F., Residual Stresses in Layered Manufacturing, Proceedings of Solid Freeform Fabrication Symposium, Aug 1999, Edited by Bourell, D.L., Beaman, J.J., Crawford, R.H., Marcus, H.L., Barlow, J.W., University of Texas, Austin, USA, pp. 239-246

[89] Hauser, C., Childs, T.H.C., Dalgarno, K.W., Selective Laser Sintering of Stainless Steel 314S HC processed using room temperature powder beds, Proceedings of Solid Freeform Fabrication Symposium, Aug 1999, Edited by Bourell, D.L., Beaman, J.J., Crawford, R.H., Marcus, H.L., Barlow, J.W., University of Texas, Austin, USA, pp. 273-280

[90] Hauser, C., Childs, T.H.C., Dalgarno, K.W., Eane, R.B., Atmospheric Control during Direct Selective Laser Sintering of Stainless Steel 314S powder, Proceedings of Solid Freeform Fabrication Symposium, Aug 1999, Edited by Bourell, D.L., Beaman,.J.J., Crawford, R.H., Marcus, H.L., Barlow, J.W., University of Texas, Austin, USA, pp. 265-272

[91] Carter, W.T., Jr and Jones, M.G., Direct Laser Sintering of Metals, Proceedings of Solid Freeform Fabrication Symposium, Aug 1993, Edited by Marcus, H.L., Beaman, J.J., Bourell, D.L., Barlow, J.W., Crawford, R.H., University of Texas, Austin, USA, pp. 51-59

[92] Ghose, A.K., Joarder, A., Dissimilar Metal Welding – A practical dossier, Tool Alloy Steels, Vol. 25, n 8, August 1991, pp. 289-294

[93] Kim, T.H., Development of Graded – Boundary materials by Laser beam, Journal of Laser Applications, Vol. 10, n 5, 1998, pp. 191-197

[94] Electron Beam Welding, Schultz, H., Ablington Publishing, Cambridge, England 1993, ISBN: 185573 0502

[95] The Materials Selector: Voll, Waterman and Ashby, 2nd Edition 1997, Edited by Waterman. Norman, A and Ashby, M. F., Publisher: Chapman & Hall, ISBN: 0 412 615509

[96] Engineering Metallurgy, Part 1: Applied Physical Metallurgy, Higgins, R.A., 6th Edition 1993, Edward Arnold, London, ISBN: 0 340 56830 5, p.32

[97] Copper: Selection of Wrought alloys: Encyclopaedia of Materials Science and Engineering. Editor-in-chief: Bever, M.B., Pergamon Press Ltd, Oxford UK, 1st Edition 1996, ISBN: 0-08-022158-0. p 867,868.

[98] Laser Welding, Christopher, D., New York: Mc-Graw-Hill Inc. 1992, ISBN: 0070161232, p.51, 52, 53, 86 and 87

[99] Laser Materials Processing, Steen, W. M., Springer Verlag London Limited, 1991, ISBN 3-540-19670-6

[100] Metallurgy for Engineers, Rollason, E.C., 3rd Edition, Edward Arnold (Publishers) Limited, 1970

[101] H13 data provided by Osprey Powders Group, Osprey Metals Ltd., UK

[102] Matweb: Online materials database, 2002, www.matweb.com

[103] PROMET: European Brite/Euram Project on Rapid Prototyping of Metallic Components, 1993-1997

11. Appendix A:

11.1.   Result Tables: 1mm layer

For 5J				Width in mm							Height in mm					
Vmm/s	width ms	freq(Hz)	Energy J	1	2	3	4	5	Avg.		h1	h2	h3	h4	h5	Avg.
1	0.5	30	5													
1	0.5	50	5													
1	0.5	70	5													
1	0.5	90	5													
1	0.5	100	5													
1	2	5	5	0.880	0.886	0.826	0.878	0.886	0.871		1.694	1.544	1.497	1.571	1.510	1.563
1	2	10	5	1.080	1.142	1.048	1.058	1.086	1.083		1.567	1.604	1.593	1.637	1.682	1.617
1	2	30	5													
1	2	50	5													
1	2	70	5													
1	2	90	5													
1	2	100	5													
1	6	5	5	0.904	0.910	0.874	0.854	0.866	0.882		1.330	1.333	1.309	1.279	1.317	1.314
1	6	10	5	1.132	1.060	1.100	1.080	1.046	1.084		1.686	1.662	1.506	1.488	1.490	1.566
1	6	30	5													
1	6	50	5													
1	6	70	5													
1	10	5	5	0.894	0.958	0.892	0.960	0.902	0.921		1.376	1.298	1.420	1.334	1.380	1.362
1	10	10	5	1.140	1.044	1.096	1.206	1.136	1.124		1.523	1.468	1.432	1.464	1.518	1.481
1	10	30	5													
1	10	50	5													
1	10	70	5													
1	14	5	5													
1	14	10	5	1.230	1.244	1.120	1.132	1.168	1.179		1.430	1.365	1.347	1.386	1.437	1.393
1	14	30	5													
1	14	50	5													
1	18	5	5													
1	18	10	5													
1	18	30	5													
1	20	5	5													
1	20	10	5	1.164	1.240	1.234	1.292	1.082	1.202		1.394	1.364	1.370	1.389	1.335	1.370
1	20	30	5													

Vmm/s	For 5J width ms	freq(Hz)	Energy J	Width in mm 1	2	3	4	5	Avg.		Height in mm h1	h2	h3	h4	h5	Avg.
5	0.5	30	5													
5	0.5	50	5													
5	0.5	70	5													
5	0.5	90	5													
5	0.5	100	5													
5	2	5	5													
5	2	10	5	0.653	0.690	0.688	0.668	0.792	0.698		0.678	0.621	0.636	0.685	0.711	0.666
5	2	30	5	0.832	0.836	0.780	0.824	0.806	0.816		1.019	0.924	0.920	0.950	0.956	0.954
5	2	50	5	1.050	1.044	0.996	1.068	0.990	1.030		1.380	1.242	1.314	1.331	1.366	1.327
5	2	70	5	1.126	1.262	1.156	1.380	1.374	1.260		1.137	0.873	0.922	1.040	0.997	0.994
5	2	90	5	1.228	1.296	1.330	1.437	1.556	1.369		0.911	0.809	0.790	0.797	0.773	0.816
5	2	100	5	1.312	1.484	1.418	1.462	1.368	1.409		1.000	0.962	1.057	0.996	1.029	1.009
5	6	5	5													
5	6	10	5													
5	6	30	5	0.997	1.115	1.061	1.110	1.066	1.070		1.162	1.107	1.064	1.351	1.186	1.174
5	6	50	5	1.270	1.342	1.330	1.385	1.372	1.340		1.456	1.570	1.536	1.495	1.509	1.513
5	6	70	5	1.456	1.478	1.544	1.476	1.456	1.482		1.408	1.389	1.366	1.346	1.308	1.363
5	10	5	5													
5	10	10	5													
5	10	30	5	1.262	1.156	1.230	1.262	1.236	1.229		1.230	1.122	1.156	1.178	1.179	1.173
5	10	50	5	1.546	1.612	1.490	1.454	1.442	1.509		1.389	1.390	1.392	1.404	1.387	1.392
5	10	70	5	1.360	1.360	1.442	1.434	1.346	1.388		1.288	1.301	1.311	1.321	1.373	1.319
5	14	5	5													
5	14	10	5													
5	14	30	5	1.234	1.212	1.242	1.258	1.254	1.240		1.158	1.177	1.198	1.255	1.249	1.207
5	14	50	5	1.646	1.528	1.496	1.528	1.502	1.540		1.475	1.435	1.449	1.438	1.452	1.450
5	18	5	5													
5	18	10	5													
5	18	30	5	1.558	1.410	1.294	1.336	1.256	1.371		1.358	1.271	1.211	1.187	1.155	1.236
5	20	5	5													
5	20	10	5													
5	20	30	5	1.440	1.322	1.264	1.324	1.324	1.335		1.252	1.226	1.268	1.229	1.225	1.240

For 5J				Width in mm								Height in mm					
Vmm/s	width ms	freq(Hz)	Energy J	1	2	3	4	5	Avg.		h1	h2	h3	h4	h5	Avg.
10	0.5	30	5	0.940	0.980	0.820	0.890	1.052	0.936		0.473	0.409	0.429	0.499	0.513	0.465
10	0.5	50	5	1.134	1.110	0.952	0.954	1.014	1.033		0.547	0.555	0.580	0.632	0.607	0.584
10	0.5	70	5	1.042	1.088	1.092	1.086	1.076	1.077		0.574	0.609	0.634	0.627	0.612	0.611
10	0.5	90	5	1.052	1.086	1.154	1.030	0.952	1.055		0.784	0.770	0.814	0.879	0.864	0.822
10	0.5	100	5	1.018	0.998	1.024	1.096	1.068	1.041		0.819	0.781	0.761	0.798	0.711	0.774
10	2	5	5													
10	2	10	5													
10	2	30	5	0.860	0.808	0.794	0.766	0.808	0.807		0.693	0.636	0.653	0.659	0.654	0.659
10	2	50	5	0.804	0.912	0.830	0.902	0.856	0.861		0.730	0.719	0.747	0.797	0.791	0.757
10	2	70	5	1.038	1.060	1.110	1.064	1.064	1.067		1.285	1.175	0.921	0.906	0.924	1.042
10	2	90	5	1.050	1.036	0.960	1.028	1.130	1.041		1.038	0.856	0.802	0.821	0.816	0.867
10	2	100	5	1.252	1.372	1.304	1.380	1.428	1.347		1.076	0.982	0.946	0.942	0.966	0.982
10	6	5	5													
10	6	10	5													
10	6	30	5													
10	6	50	5	1.158	1.120	1.196	1.184	1.174	1.166		1.233	1.104	1.116	1.067	1.068	1.118
10	6	70	5	1.328	1.346	1.598	1.440	1.484	1.439		1.735	1.586	1.442	1.339	1.272	1.475
10	10	5	5													
10	10	10	5													
10	10	30	5													
10	10	50	5	1.192	1.280	1.352	1.256	1.270	1.270		1.155	1.206	1.205	1.242	1.380	1.238
10	10	70	5	1.304	1.328	1.264	1.292	1.330	1.304		1.218	1.146	1.126	1.091	1.106	1.137
10	14	5	5													
10	14	10	5													
10	14	30	5													
10	14	50	5	1.160	1.186	1.152	1.138	1.210	1.169		1.085	1.046	1.058	1.105	1.130	1.085
10	18	5	5													
10	18	10	5													
10	18	30	5													
10	20	5	5													
10	20	10	5													
10	20	30	5													

Vmm/s	For 5J width ms	freq(Hz)	Energy J	Width in mm 1	2	3	4	5	Avg.		Height in mm h1	h2	h3	h4	h5	Avg.
15	0.5	30	5													
15	0.5	50	5	0.896	1.122	1.108	1.042	1.044	1.042		0.435	0.426	0.472	0.443	0.620	0.479
15	0.5	70	5	1.122	1.062	1.056	1.064	1.112	1.083		0.405	0.431	0.417	0.528	0.472	0.451
15	0.5	90	5	0.972	0.988	1.162	1.076	1.056	1.051		0.689	0.702	0.747	0.712	0.720	0.714
15	0.5	100	5	1.634	0.988	0.960	0.966	1.048	1.119		0.883	0.911	0.960	1.002	1.011	0.953
15	2	5	5													
15	2	10	5													
15	2	30	5													
15	2	50	5													
15	2	70	5													
15	2	90	5													
15	2	100	5	1.006	0.852	0.900	0.962	0.885	0.921		1.092	1.039	1.027	1.041	0.932	1.026
15	6	5	5													
15	6	10	5													
15	6	30	5													
15	6	50	5													
15	6	70	5													
15	10	5	5													
15	10	10	5													
15	10	30	5													
15	10	50	5													
15	10	70	5													
15	14	5	5													
15	14	10	5													
15	14	30	5													
15	14	50	5													
15	18	5	5													
15	18	10	5													
15	18	30	5													
15	20	5	5													
15	20	10	5													
15	20	30	5													

V mm/s	For 5J width ms	freq(Hz)	Energy J	Width in mm 1	2	3	4	5	Avg.		Height in mm h1	h2	h3	h4	h5	Avg.
20	0.5	30	5													
20	0.5	50	5	1.084	1.098	1.128	1.102	0.968	1.076		0.329	0.448	0.434	0.443	0.429	0.417
20	0.5	70	5	1.298	1.222	1.232	1.140	1.192	1.217		0.366	0.424	0.069	0.492	0.465	0.363
20	0.5	90	5	0.986	1.014	1.044	1.070	0.970	1.017		0.656	0.788	0.749	0.809	0.734	0.747
20	0.5	100	5	0.982	1.074	1.050	0.996	0.978	1.016		0.736	0.721	0.626	0.769	0.697	0.710
20	2	5	5													
20	2	10	5													
20	2	30	5													
20	2	50	5													
20	2	70	5	1.120	1.058	0.992	0.970	0.937	1.015		1.338	1.173	1.229	1.210	1.115	1.213
20	2	90	5	1.200	1.164	1.158	1.130	1.146	1.160		1.430	1.337	1.351	1.382	1.386	1.377
20	2	100	5	1.152	1.210	1.100	1.160	1.166	1.158		1.419	1.385	1.377	1.346	1.472	1.400
20	6	5	5													
20	6	10	5													
20	6	30	5													
20	6	50	5													
20	6	70	5													
20	10	5	5													
20	10	10	5													
20	10	30	5													
20	10	50	5													
20	10	70	5													
20	14	5	5													
20	14	10	5													
20	14	30	5													
20	14	50	5													
20	18	5	5													
20	18	10	5													
20	18	30	5													
20	20	5	5													
20	20	10	5													
20	20	30	5													

AT 10J				Result (Width) in mm						Height in mm					
V mm/sec	width ms	freq(Hz)	Energy(J)	1	2	3	4	5	AV	h1	h2	h3	h4	h5	AV
1	2	5	10												
1	2	10	10	0.982	0.938	0.894	0.980	1.026	0.964	0.640	0.725	0.648	0.728	0.632	0.675
1	2	30	10												
1	2	50	10												
1	6	5	10	0.958	1.000	0.998	1.038	1.092	1.017	1.629	1.420	1.406	1.459	1.395	1.462
1	6	10	10	1.128	1.111	1.134	1.138	1.224	1.147	1.373	1.266	1.427	1.476	1.432	1.395
1	6	30	10												
1	6	50	10												
1	10	5	10	0.988	0.990	0.966	0.946	1.000	0.978	1.370	1.381	1.370	1.270	1.410	1.360
1	10	10	10	1.326	1.316	1.318	1.258	1.300	1.304	1.513	1.434	1.494	1.436	1.410	1.458
1	10	30	10												
1	10	50	10												
1	14	5	10	1.142	1.132	1.146	1.154	1.144	1.144	1.656	1.680	1.619	1.619	1.523	1.619
1	14	10	10	1.204	1.278	1.248	1.382	1.344	1.291	1.564	1.474	1.549	1.582	1.556	1.545
1	14	30	10	1.718	1.730	1.903	1.778	1.680	1.762	1.149	1.511	1.514	1.098	1.545	1.364
1	18	5	10	1.108	1.096	1.148	1.170	1.208	1.146	1.445	1.504	1.522	1.554	1.608	1.527
1	18	10	10	1.298	1.322	1.360	1.464	1.374	1.364	1.523	1.425	1.430	1.494	1.519	1.478
1	18	30	10												
1	20	5	10	1.038	1.076	1.104	1.110	1.074	1.080	1.378	1.317	1.338	1.418	1.385	1.367
1	20	10	10	1.344	1.462	1.318	1.366	1.402	1.378	1.565	1.551	1.554	1.600	1.618	1.578
1	20	30	10												

AT 10J				Result (Width) in mm						Height in mm					
V mm/sec	width ms	freq(Hz)	Energy(J)	1	2	3	4	5	AV	h1	h2	h3	h4	h5	AV
5	2	5	10							0.487	0.536	0.493	0.571	0.592	0.536
5	2	10	10	0.884	0.900	0.872	0.784	0.900	0.868	0.534	0.652	0.534	0.631	0.644	0.599
5	2	30	10	1.120	1.152	1.174	1.218	1.156	1.164	1.068	1.076	1.001	1.142	1.070	1.071
5	2	50	10	1.322	1.374	1.436	1.350	1.438	1.384	1.501	1.485	1.275	1.202	1.142	1.321
5	6	5	10												
5	6	10	10							1.390	1.274	1.342	1.359	1.276	1.328
5	6	30	10	1.130	1.228	1.304	1.176	1.120	1.192	0.973	1.029	1.066	1.086	1.134	1.058
5	6	50	10	1.416	1.498	1.414	1.510	1.476	1.463	1.364	1.339	1.323	1.399	1.415	1.368
5	10	5	10												
5	10	10	10							1.408	1.300	1.283	1.333	1.378	1.340
5	10	30	10	1.366	1.378	1.384	1.450	1.352	1.386	1.304	1.273	1.306	1.396	0.955	1.247
5	10	50	10	1.430	1.502	1.488	1.434	1.504	1.472	1.258	1.302	1.324	1.281	1.290	1.291
5	14	5	10												
5	14	10	10												
5	14	30	10	1.670	1.498	1.556	1.606	1.492	1.564	1.242	1.185	1.203	1.213	1.231	1.215
5	18	5	10												
5	18	10	10												
5	18	30	10	1.622	1.602	1.482	1.524	1.544	1.555	1.461	1.396	1.431	1.370	1.372	1.406
5	20	5	10												
5	20	10	10												
5	20	30	10	1.300	1.352	1.330	1.346	1.358	1.337	1.186	1.161	1.206	1.175	1.219	1.190

V mm/sec	AT 10J width ms	freq(Hz)	Energy(J)	Result (Width) in mm 1	2	3	4	5	AV	Height in mm h1	h2	h3	h4	h5	AV
10	2	5	10												
10	2	10	10	0.824	0.714	0.714	0.766	0.788	0.761	0.608	0.615	0.657	0.564	0.548	0.598
10	2	30	10	0.932	0.874	0.874	0.946	0.900	0.905	0.697	0.614	0.617	0.651	0.766	0.669
10	2	50	10	0.918	1.040	1.058	1.054	1.012	1.016	1.038	0.900	0.785	0.917	0.857	0.899
10	6	5	10												
10	6	10	10												
10	6	30	10	0.912	0.996	0.962	0.946	0.936	0.950	0.919	0.878	0.916	0.841	0.773	0.865
10	6	50	10	1.126	1.202	1.214	1.236	1.218	1.199	0.902	0.888	0.898	0.930	1.013	0.926
10	10	5	10												
10	10	10	10												
10	10	30	10	1.474	1.112	1.280	1.276	1.316	1.292	1.774	1.580	1.606	1.602	1.476	1.608
10	10	50	10	1.254	1.286	1.252	1.382	1.276	1.290	1.126	1.128	1.102	1.212	1.134	1.141
10	14	5	10												
10	14	10	10												
10	14	30	10	1.203	1.170	1.164	1.294	1.226	1.211	1.264	1.235	1.216	1.194	1.277	1.237
10	18	5	10												
10	18	10	10												
10	18	30	10	1.198	1.284	1.272	1.318	1.264	1.267	1.241	1.193	1.178	1.225	1.168	1.201
10	20	5	10												
10	20	10	10												
10	20	30	10	1.246	1.286	1.230	1.318	1.292	1.274	1.181	1.305	1.432	1.271	1.257	1.289

AT 10J				Result (Width) in mm						Height in mm					
V mm/sec	width ms	freq(Hz)	Energy(J)	1	2	3	4	5	AV	h1	h2	h3	h4	h5	AV
15	2	5	10												
15	2	10	10												
15	2	30	10	0.926	0.812	0.952	0.984	1.022	0.939	0.593	0.557	0.485	0.520	0.454	0.522
15	2	50	10	0.934	0.932	1.018	0.982	0.896	0.952	0.896	1.034	0.951	1.050	0.925	0.971
15	6	5	10												
15	6	10	10												
15	6	30	10												
15	6	50	10	1.090	1.026	1.110	1.076	1.126	1.086	1.225	1.007	0.939	1.078	1.124	1.075
15	10	5	10												
15	10	10	10												
15	10	30	10												
15	10	50	10	1.212	1.142	1.258	1.150	1.260	1.204	1.303	1.296	1.172	1.345	1.454	1.314
15	14	5	10												
15	14	10	10												
15	14	30	10												
15	18	5	10												
15	18	10	10												
15	18	30	10												
15	20	5	10												
15	20	10	10												
15	20	30	10												

	AT 10J			Result (Width) in mm						Height in mm					
V mm/sec	width ms	freq(Hz)	Energy(J)	1	2	3	4	5	AV	h1	h2	h3	h4	h5	AV
20	2	5	10												
20	2	10	10												
20	2	30	10	0.702	0.788	0.764	0.774	0.784	0.762	0.682	0.678	0.674	0.784	0.770	0.718
20	2	50	10	0.974	0.914	0.868	0.822	0.976	0.911	0.667	0.777	0.761	0.764	0.764	0.747
20	6	5	10												
20	6	10	10												
20	6	30	10												
20	6	50	10	1.332	1.288	1.218	1.128	1.188	1.231	1.387	1.324	1.293	1.369	1.522	1.379
20	10	5	10												
20	10	10	10												
20	10	30	10												
20	10	50	10												
20	14	5	10												
20	14	10	10												
20	14	30	10												
20	18	5	10												
20	18	10	10												
20	18	30	10												
20	20	5	10												
20	20	10	10												
20	20	30	10												

	AT 20J			Result (Width) in mm						Height in mm					
Vmm/s	width ms	freq Hz	Energy J	1	2	3	4	5	AV	h1	h2	h3	h4	h5	AV
1	2	5	20												
1	2	10	20												
1	6	5	20	1.056	1.056	1.010	1.034	1.022	1.036	0.868	0.914	0.859	0.847	0.841	0.866
1	6	10	20	1.328	1.358	1.400	1.420	1.382	1.378	1.190	1.057	1.008	1.020	1.042	1.063
1	10	5	20	1.074	1.086	1.062	1.068	1.180	1.094	1.111	1.083	1.168	1.100	1.183	1.129
1	10	10	20	1.408	1.570	1.452	1.340	1.354	1.425	1.458	1.339	1.380	1.272	1.334	1.356
1	14	5	20	1.110	1.142	1.122	1.180	1.050	1.121	1.240	1.149	1.222	1.303	1.249	1.233
1	14	10	20	1.452	1.430	1.558	1.736	1.447	1.525	1.491	1.361	1.452	1.390	1.589	1.457
1	18	5	20	1.294	1.256	1.206	1.254	1.232	1.248	1.614	1.466	1.330	1.465	1.397	1.454
1	18	10	20	1.494	1.437	1.507	1.320	1.430	1.438	1.563	1.452	1.505	1.586	1.397	1.501
1	20	5	20	1.246	1.242	1.282	1.310	1.324	1.281	1.381	1.310	1.497	1.506	1.521	1.443
1	20	10	20	1.416	1.488	1.542	1.530	1.463	1.488	1.487	1.498	1.495	1.587	1.559	1.525

	AT 20J			Result (Width) in mm						Height in mm					
Vmm/s	width ms	freq Hz	Energy J	1	2	3	4	5	AV	h1	h2	h3	h4	h5	AV
5	2	5	20												
5	2	10	20												
5	6	5	20							0.865	0.813	0.773	0.760	0.825	0.807
5	6	10	20	0.972	0.948	0.882	0.882	0.974	0.932	0.919	0.887	0.841	0.760	0.792	0.840
5	10	5	20												
5	10	10	20	0.912	0.956	0.940	0.948	0.968	0.945	0.946	0.882	0.918	0.882	0.901	0.906
5	14	5	20												
5	14	10	20	1.098	1.108	1.122	1.040	1.124	1.098	1.121	1.116	1.058	1.071	1.091	1.091
5	18	5	20												
5	18	10	20	1.144	1.128	1.128	1.146	1.134	1.136	1.091	1.059	1.059	1.036	1.105	1.070
5	20	5	20												
5	20	10	20	1.050	1.130	1.152	1.084	1.020	1.087	1.118	1.126	1.036	1.120	1.240	1.128

AT 20J				Result (Width) in mm						Height in mm					
Vmm/s	width ms	freq hz	Energy J	1	2	3	4	5	AV	h1	h2	h3	h4	h5	AV
10	2	5	20												
10	2	10	20												
10	6	5	20												
10	6	10	20	0.898	0.964	0.984	1.024	1.020	0.978	0.793	0.794	0.792	0.892	0.915	0.837
10	10	5	20												
10	10	10	20												
10	14	5	20												
10	14	10	20												
10	18	5	20												
10	18	10	20												
10	20	5	20												
10	20	10	20												

AT 20J				Result (Width) in mm						Height in mm					
Vmm/s	width ms	freq hz	Energy J	1	2	3	4	5	AV	h1	h2	h3	h4	h5	AV
15	2	5	20												
15	2	10	20												
15	6	5	20												
15	6	10	20												
15	10	5	20												
15	10	10	20												
15	14	5	20												
15	14	10	20												
15	18	5	20												
15	18	10	20												
15	20	5	20												
15	20	10	20												

	AT 20J			Result (Width) in mm						Height in mm					
Vmm/s	width ms	freq Hz	Energy J	1	2	3	4	5	AV	h1	h2	h3	h4	h5	AV
20	2	5	20												
20	2	10	20												
20	6	5	20												
20	6	10	20												
20	10	5	20												
20	10	10	20												
20	14	5	20												
20	14	10	20												
20	18	5	20												
20	18	10	20												
20	20	5	20												
20	20	10	20												

	AT 30J			Width in mm						Height in mm					
V(mm/s)	width ms	freqHz	Energy J	1	2	3	4	5	AV	h1	h2	h3	h4	h5	AV
1	6	5	30	1.256	1.204	1.160	1.266	1.216	1.220	1.032	0.918	0.878	0.974	0.817	0.924
1	6	10	30							1.360	1.264	1.328	1.353	1.363	1.334
1	10	5	30	1.172	1.282	1.166	1.172	1.250	1.208	1.222	1.275	1.292	1.271	1.309	1.274
1	10	10	30							1.562	1.393	1.382	1.469	1.366	1.434
1	14	5	30	1.452	1.478	1.618	1.524	1.546	1.524	0.933	0.896	0.910	1.020	1.069	0.966
1	14	10	30												
1	18	5	30	1.374	1.318	1.352	1.342	1.368	1.351	1.115	1.054	1.025	1.067	1.068	1.066
1	18	10	30	1.842	1.996	1.966	1.864	1.808	1.895	1.530	1.456	1.339	1.347	1.430	1.420
1	20	5	30	1.450	1.420	1.408	1.426	1.364	1.414	1.453	1.402	1.316	1.251	1.268	1.338
1	20	10	30												

	AT 30J			Width in mm						Height in mm					
V(mm/s)	width ms	freqHz	Energy J	1	2	3	4	5	AV	h1	h2	h3	h4	h5	AV
5	6	5	30	0.888	0.956	0.902	0.984	1.018	0.950	0.773	0.729	0.758	0.814	0.819	0.779
5	6	10	30	1.064	1.044	1.136	1.112	1.050	1.081	0.675	0.637	0.806	0.764	0.865	0.749
5	10	5	30	0.872	1.016	1.050	1.030	1.028	0.999	0.735	0.713	0.692	0.734	0.776	0.730
5	10	10	30	1.232	1.294	1.320	1.274	1.294	1.283	0.955	0.865	0.869	0.843	0.819	0.870
5	14	5	30	1.086	1.098	1.148	1.142	1.106	1.116	0.892	0.909	0.916	0.870	0.873	0.892
5	14	10	30	1.256	1.210	1.252	1.238	1.272	1.246	0.979	0.843	0.889	0.820	0.798	0.866
5	18	5	30	1.146	1.110	1.126	1.234	1.206	1.164	0.933	0.902	0.923	0.951	0.971	0.936
5	18	10	30	1.162	1.228	1.246	1.326	1.256	1.244	0.959	0.918	0.875	0.929	0.905	0.917
5	20	5	30	1.222	1.280	1.270	1.232	1.186	1.238	1.023	1.045	1.050	1.071	1.024	1.043
5	20	10	30	1.230	1.270	1.306	1.278	1.292	1.275	0.921	0.884	0.929	0.985	0.976	0.939

AT 30J				Width in mm						Height in mm					
V(mm/s)	width ms	freqHz	Energy J	1	2	3	4	5	AV	h1	h2	h3	h4	h5	AV
10	6	5	30												
10	6	10	30	0.890	0.926	0.948	0.890	0.924	0.916	0.686	0.643	0.637	0.682	0.675	0.665
10	10	5	30							1.020	1.007	0.967	0.988	0.945	0.985
10	10	10	30	1.098	1.152	1.134	1.136	1.130	1.130	0.680	0.660	0.696	0.690	0.706	0.686
10	14	5	30	1.272	1.130	1.244	1.238	1.224	1.222	0.896	0.901	0.865	0.949	0.971	0.916
10	14	10	30	1.054	1.118	1.086	1.068	1.036	1.072	0.893	0.853	0.845	0.867	0.873	0.866
10	18	5	30												
10	18	10	30	1.118	1.088	1.034	1.028	1.112	1.076	1.037	1.007	1.011	0.993	1.015	1.012
10	20	5	30												
10	20	10	30	1.260	1.280	1.172	1.146	1.164	1.204	1.314	1.116	1.085	1.113	1.030	1.132

AT 30J				Width in mm						Height in mm					
V(mm/s)	width ms	freqHz	EnergyJ	1	2	3	4	5	AV	h1	h2	h3	h4	h5	AV
15	6	5	30												
15	6	10	30												
15	10	5	30												
15	10	10	30							0.823	0.831	0.915	0.879	0.865	0.863
15	14	5	30												
15	14	10	30												
15	18	5	30												
15	18	10	30												
15	20	5	30												
15	20	10	30												

	AT 30J			Width in mm						Height in mm					
V(mm/s)	width ms	freqHz	EnergyJ	1	2	3	4	5	AV	h1	h2	h3	h4	h5	AV
20	6	5	30												
20	6	10	30												
20	10	5	30												
20	10	10	30												
20	14	5	30												
20	14	10	30												
20	18	5	30												
20	18	10	30												
20	20	5	30												
20	20	10	30												

AT 60 J Energy				width in mm						height in mm					
Vmm/sec	width ms	freq Hz	EnergyJ	1	2	3	4	5	AV	h1	h2	h3	h4	h5	AV
1	6	5	60												
1	10	5	60												
1	14	5	60	2.470	2.384	2.460	2.542	2.466	2.464						
1	18	5	60												
1	20	5	60												

AT 60 J Energy				width in mm						height in mm					
Vmm/sec	width ms	freq Hz	EnergyJ	1	2	3	4	5	AV	h1	h2	h3	h4	h5	AV
5	6	5	60												
5	10	5	60	1.126	1.114	1.112	1.148	1.132	1.126	0.726	0.798	0.705	0.766	0.762	0.751
5	14	5	60	1.172	1.250	1.222	1.202	1.172	1.204	0.777	0.775	0.826	0.883	0.915	0.835
5	18	5	60	1.270	1.186	1.166	1.160	1.176	1.192	0.781	0.764	0.744	0.782	0.711	0.756
5	20	5	60	1.262	1.232	1.234	1.270	1.180	1.236	0.915	0.895	0.781	0.778	0.742	0.822

AT 60 J Energy				width in mm						height in mm					
Vmm/sec	width ms	freq Hz	EnergyJ	1	2	3	4	5	AV	h1	h2	h3	h4	h5	AV
10	6	5	60												
10	10	5	60												
10	14	5	60												
10	18	5	60												
10	20	5	60												

AT 60 J Energy				width in mm						height in mm					
Vmm/sec	width ms	freq Hz	EnergyJ	1	2	3	4	5	AV	h1	h2	h3	h4	h5	AV
15	6	5	60												
15	10	5	60												
15	14	5	60												
15	18	5	60												
15	20	5	60												

AT 60 J Energy				width in mm						height in mm					
Vmm/sec	width ms	freq hz	EnergyJ	1	2	3	4	5	AV	h1	h2	h3	h4	h5	AV
20	6	5	60												
20	10	5	60												
20	14	5	60												
20	18	5	60												
20	20	5	60												

11.2. Tables for 0.4 mm layer

AT 5J				Width (mm)						Height (mm)					
Vmm /s	width ms	freq(Hz)	Energy J	1	2	3	4	5	AV	h1	h2	h3	h4	h5	AV
1	0.5	30	5												
1	0.5	50	5												
1	0.5	70	5												
1	0.5	90	5												
1	0.5	100	5												
1	2	5	5	0.698	0.680	0.726	0.712	0.718	0.707	0.616	0.611	0.672	0.680	0.733	0.662
1	2	10	5	0.670	0.580	0.622	0.720	0.610	0.640	0.499	0.413	0.495	0.540	0.567	0.503
1	2	30	5												
1	2	50	5												
1	2	70	5												
1	2	90	5												
1	2	100	5												
1	6	5	5	0.696	0.622	0.630	0.692	0.652	0.658	0.385	0.304	0.358	0.425	0.494	0.393
1	6	10	5	0.844	0.760	0.726	0.794	0.770	0.779	0.620	0.572	0.528	0.646	0.877	0.649
1	6	30	5												
1	6	50	5												
1	6	70	5												
1	10	5	5	0.886	0.740	0.742	0.762	0.754	0.777	0.734	0.644	0.678	0.717	0.683	0.691
1	10	10	5	0.834	0.790	0.758	0.826	0.892	0.820	0.888	0.827	0.822	0.832	0.929	0.860
1	10	30	5												
1	10	50	5												
1	10	70	5												
1	14	5	5	0.730	0.816	0.826	0.804	0.776	0.790	0.771	0.677	0.708	0.713	0.788	0.731
1	14	10	5	0.916	0.866	0.826	0.902	0.882	0.878	0.958	0.888	0.847	0.891	0.927	0.902
1	14	30	5												
1	14	50	5												
1	18	5	5	0.670	0.692	0.606	0.512	0.634	0.623	0.863	0.703	0.619	0.640	0.683	0.702
1	18	10	5	0.640	0.600	0.614	0.680	0.716	0.650	0.877	0.860	0.841	0.908	0.927	0.883
1	18	30	5												
1	20	5	5	0.736	0.740	0.746	0.606	0.680	0.702	0.906	0.728	0.691	0.700	0.758	0.757
1	20	10	5												
1	20	30	5												

AT 5J				Width (mm)						Height (mm)					
Vmm/s	width ms	freq(Hz)	Energy J	1	2	3	4	5	AV	h1	h2	h3	h4	h5	AV
5	0.5	30	5												
5	0.5	50	5	0.820	0.776	0.864	0.840	0.806	0.821	0.282	0.201	0.193	0.201	0.251	0.226
5	0.5	70	5	0.904	0.970	0.944	0.997	0.917	0.946	0.541	0.489	0.464	0.427	0.313	0.447
5	0.5	90	5												
5	0.5	100	5	0.990	1.116	1.162	1.296	1.356	1.184	0.553	0.452	0.528	0.676	0.844	0.611
5	2	5	5												
5	2	10	5	0.664	0.648	0.714	0.674	0.718	0.684	0.321	0.308	0.290	0.326	0.327	0.314
5	2	30	5	0.794	0.744	0.778	0.826	0.804	0.789	0.330	0.324	0.309	0.327	0.317	0.321
5	2	50	5	0.882	0.688	0.832	0.864	0.872	0.828	0.411	0.330	0.314	0.458	0.527	0.408
5	2	70	5	0.878	0.882	0.884	0.826	0.810	0.856	0.756	0.690	0.693	0.610	0.458	0.641
5	2	90	5	1.374	1.374	1.436	1.572	1.596	1.470	0.354	0.265	0.334	0.459	0.564	0.395
5	2	100	5												
5	6	5	5												
5	6	10	5	0.632	0.624	0.598	0.682	0.666	0.640	0.697	0.636	0.673	0.684	0.693	0.677
5	6	30	5	0.754	0.760	0.842	0.848	0.826	0.806	0.573	0.617	0.625	0.615	0.699	0.626
5	6	50	5	0.920	0.924	0.854	0.896	0.836	0.886	0.809	0.706	0.725	0.702	0.744	0.737
5	6	70	5	0.888	0.976	1.002	1.008	0.956	0.966	0.797	0.707	0.657	0.679	0.692	0.706
5	10	5	5												
5	10	10	5	0.730	0.718		0.640	0.734	0.706	0.850	0.981	0.988	0.640	0.939	0.880
5	10	30	5	0.810	0.818	0.836	0.874	0.826	0.833	0.525	0.437	0.488	0.427	0.542	0.484
5	10	50	5	0.914	0.932	0.894	0.888	0.910	0.908	0.600	0.538	0.545	0.649	0.697	0.606
5	10	70	5	0.884	0.828	0.838	0.854	0.926	0.866	0.685	0.640	0.645	0.649	0.743	0.672
5	14	5	5												
5	14	10	5	0.638	0.638	0.678	0.690	0.595	0.648	0.506	0.559	0.539	0.480	0.436	0.504
5	14	30	5	0.824	0.842	0.820	0.800	0.792	0.816	0.687	0.579	0.505	0.636	0.650	0.611
5	14	50	5	1.040	0.948	0.962	0.874	0.948	0.954	0.829	0.763	0.674	0.755	0.811	0.766
5	18	5	5												
5	18	10	5	0.630	0.562	0.592	0.600	0.637	0.604	0.597	0.505	0.536	0.562	0.663	0.573
5	18	30	5	0.758	0.736	0.814	0.862	0.850	0.804	0.729	0.665	0.744	0.781	0.813	0.746
5	20	5	5												
5	20	10	5	0.620	0.580	0.702	0.678	0.793	0.675	0.470	0.449	0.486	0.639	0.785	0.566
5	20	30	5							0.683	0.619	0.575	0.630	0.581	0.618

AT 5J				Width (mm)						Height (mm)					
Vmm/s	width ms	freq(Hz)	Energy J	1	2	3	4	5	AV	h1	h2	h3	h4	h5	AV
10	0.5	30	5												
10	0.5	50	5												
10	0.5	70	5												
10	0.5	90	5												
10	0.5	100	5												
10	2	5	5												
10	2	10	5												
10	2	30	5	0.662	0.660	0.602	0.586	0.610	0.624						
10	2	50	5	0.752	0.748	0.780	0.780	0.752	0.762	0.546	0.517	0.529	0.542	0.521	0.531
10	2	70	5	0.866	0.822	0.840	0.842	0.776	0.829	0.515	0.413	0.372	0.423	0.642	0.473
10	2	90	5	0.802	0.862	0.864	0.894	0.844	0.853	0.451	0.448	0.465	0.522	0.506	0.478
10	2	100	5	0.794	0.772	0.800	0.822	0.908	0.819	0.449	0.413	0.489	0.527	0.569	0.489
10	6	5	5												
10	6	10	5												
10	6	30	5	0.602	0.684	0.720	0.726	0.692	0.685	0.565	0.508	0.570	0.603	0.575	0.564
10	6	50	5	0.764	0.702	0.868	0.776	0.754	0.773	0.567	0.579	0.687	0.655	0.607	0.619
10	6	70	5	0.888	0.846	0.902	0.986	0.834	0.891	0.607	0.618	0.579	0.597	0.695	0.619
10	10	5	5												
10	10	10	5												
10	10	30	5	0.754	0.750	0.788	0.732	0.748	0.754	0.674	0.601	0.654	0.689	0.723	0.668
10	10	50	5	0.970	0.932	0.870	0.920	0.834	0.905	0.735	0.651	0.641	0.661	0.680	0.674
10	10	70	5	0.834	0.868	0.882	0.912	0.938	0.887	0.675	0.697	0.680	0.772	0.818	0.728
10	14	5	5												
10	14	10	5												
10	14	30	5	0.754	0.804	0.730	0.746	0.732	0.753	0.650	0.545	0.472	0.477	0.559	0.541
10	14	50	5	0.810	0.804	0.864	0.840	0.936	0.851	0.702	0.537	0.542	0.651	0.720	0.630
10	18	5	5												
10	18	10	5												
10	18	30	5	0.710	0.762	0.774	0.848	0.865	0.792	0.477	0.530	0.714	0.777	0.811	0.662
10	20	5	5												
10	20	10	5												
10	20	30	5	0.736	0.802	0.736	0.838	0.880	0.798	0.717	0.672	0.695	0.672	0.666	0.684

AT 5J				Width (mm)						Height (mm)					
Vmm/s	width ms	freq(Hz)	Energy J	1	2	3	4	5	AV	h1	h2	h3	h4	h5	AV
15	0.5	30	5												
15	0.5	50	5												
15	0.5	70	5												
15	0.5	90	5												
15	0.5	100	5												
15	2	5	5												
15	2	10	5												
15	2	30	5	0.740	0.770	0.704	0.674	0.722	0.722	0.263	0.256	0.267	0.371	0.367	0.305
15	2	50	5	0.716	0.710	0.656	0.692	0.700	0.695	0.354	0.361	0.391	0.406	0.345	0.371
15	2	70	5	0.720	0.690	0.702	0.790	0.758	0.732	0.417	0.394	0.400	0.460	0.466	0.427
15	2	90	5	0.662	0.596	0.704	0.686	0.724	0.674	0.332	0.286	0.366	0.421	0.520	0.385
15	2	100	5	0.864	0.912	0.798	0.848	0.804	0.845	0.540	0.582	0.499	0.497	0.563	0.536
15	6	5	5												
15	6	10	5												
15	6	30	5	0.596	0.566	0.598	0.596	0.646	0.600	0.583	0.522	0.490	0.497	0.572	0.533
15	6	50	5	0.784	0.740	0.658	0.740	0.724	0.729	0.643	0.561	0.382	0.400	0.548	0.507
15	6	70	5	0.864	0.784	0.846	0.852	0.816	0.832	0.599	0.637	0.590	0.585	0.680	0.618
15	10	5	5												
15	10	10	5												
15	10	30	5	0.632	0.658	0.634	0.616	0.634	0.635	0.535	0.520	0.562	0.606	0.604	0.565
15	10	50	5	0.720	0.814	0.740	0.772	0.828	0.775	0.470	0.440	0.470	0.417	0.465	0.452
15	10	70	5												
15	14	5	5												
15	14	10	5												
15	14	30	5	0.628	0.744	0.548	0.716	0.660	0.659	0.875	0.735	0.581	0.631	0.681	0.701
15	14	50	5	0.818	0.812	0.798	0.820	0.800	0.810	0.636	0.539	0.523	0.558	0.635	0.578
15	18	5	5												
15	18	10	5												
15	18	30	5	0.714	0.730	0.708	0.634	0.712	0.700	0.661	0.623	0.612	0.497	0.448	0.568
15	20	5	5												
15	20	10	5												
15	20	30	5	0.638	0.754	0.712	0.694	0.652	0.690						

AT 5J				Width (mm)						Height (mm)					
Vmm/s	width ms	freq(Hz)	Energy J	1	2	3	4	5	AV	h1	h2	h3	h4	h5	AV
20	0.5	30	5												
20	0.5	50	5												
20	0.5	70	5												
20	0.5	90	5												
20	0.5	100	5												
20	2	5	5												
20	2	10	5												
20	2	30	5	0.622	0.562	0.536	0.726	0.636	0.616	0.289	0.272	0.316	0.356	0.437	0.334
20	2	50	5	0.782	0.768	0.702	0.656	0.732	0.728	0.338	0.406	0.375	0.333	0.408	0.372
20	2	70	5	0.666	0.698	0.632	0.760	0.732	0.698	0.391	0.348	0.327	0.308	0.302	0.335
20	2	90	5	0.722	0.670	0.672	0.722	0.716	0.700	0.412	0.363	0.387	0.421	0.526	0.422
20	2	100	5	0.660	0.766	0.776	0.752	0.762	0.743	0.467	0.390	0.308	0.385	0.396	0.389
20	6	5	5												
20	6	10	5												
20	6	30	5	0.612	0.610	0.620	0.616	0.600	0.612	0.642	0.535	0.526	0.468	0.419	0.518
20	6	50	5	0.660	0.670	0.644	0.634	0.690	0.660	0.612	0.548	0.437	0.553	0.627	0.555
20	6	70	5	0.794	0.868	0.878	0.706	0.854	0.820	1.134	0.828	0.691	0.598	0.636	0.777
20	10	5	5												
20	10	10	5												
20	10	30	5												
20	10	50	5	0.758	0.744	0.694	0.758	0.730	0.737	0.608	0.584	0.504	0.533	0.713	0.588
20	10	70	5	0.778	0.786	0.830	0.728	0.834	0.791	0.645	0.577	0.603	0.590	0.648	0.613
20	14	5	5												
20	14	10	5												
20	14	30	5												
20	14	50	5	0.700	0.662	0.730	0.788	0.820	0.740	0.641	0.597	0.716	0.755	0.841	0.710
20	18	5	5												
20	18	10	5												
20	18	30	5												
20	20	5	5												
20	20	10	5												
20	20	30	5												

AT Energy 10J				Width (mm)						Height (mm)					
Vmm/sec	width ms	freq(Hz)	Energy(J)	w1	w2	w3	w4	w5	AV	h1	h2	h3	h4	h5	AV
1	2	5	10												
1	2	10	10												
1	2	30	10												
1	2	50	10												
1	6	5	10	0.716	0.666	0.688	0.700	0.752	0.704	0.352	0.287	0.294	0.418	0.448	0.360
1	6	10	10	0.764	0.732	0.814	0.880	0.924	0.823	0.407	0.251	0.193	0.274	0.368	0.299
1	6	30	10												
1	6	50	10												
1	10	5	10	0.848	0.680	0.664	0.658	0.746	0.719	0.624	0.405	0.305	0.304	0.573	0.442
1	10	10	10	0.776	0.734	0.760	0.826	0.822	0.784	0.671	0.500	0.594	0.598	0.729	0.618
1	10	30	10												
1	10	50	10												
1	14	5	10	0.862	0.812	0.868	0.902	0.930	0.875	0.870	0.811	0.911	1.063	1.140	0.959
1	14	10	10	0.928	0.978	1.084	0.986	1.038	1.003	0.857	0.857	0.869	1.000	1.019	0.920
1	14	30	10												
1	18	5	10	0.812	0.822	0.814	0.738	0.846	0.806	0.854	0.873	0.899	0.759	0.725	0.822
1	18	10	10												
1	18	30	10												
1	20	5	10	0.742	0.796	0.930	0.814	0.830	0.822	0.751	0.699	0.736	0.940	0.934	0.812
1	20	10	10	0.830	0.774	0.838	0.916	0.802	0.832	0.827	0.590	0.612	0.668	0.747	0.689
1	20	30	10												

AT Energy 10J				Width (mm)						Height (mm)					
Vmm/sec	width ms	freq(Hz)	Energy(J)	w1	w2	w3	w4	w5	AV	h1	h2	h3	h4	h5	AV
5	2	5	10												
5	2	10	10												
5	2	30	10	0.980	1.072	1.120	1.166	0.940	1.056	0.358	0.282	0.291	0.337	0.343	0.322
5	2	50	10	1.034	1.036	0.967	0.900	1.222	1.032	0.384	0.416	0.379	0.472	0.518	0.434
5	6	5	10												
5	6	10	10	0.702	0.660	0.676	0.716	0.706	0.692	0.671	0.635	0.570	0.599	0.607	0.616
5	6	30	10	0.932	0.904	1.040	0.976	0.918	0.954	0.674	0.695	0.671	0.816	0.793	0.730
5	6	50	10	0.884	1.068	1.226	1.318	1.154	1.130	0.420	0.160	0.228	0.329	0.417	0.311
5	10	5	10												
5	10	10	10	0.932	0.850	0.826	0.848	0.852	0.862	0.876	0.911	0.863	0.871	0.821	0.868
5	10	30	10	0.816	0.876	0.840	0.868	0.850	0.850	0.594	0.512	0.432	0.524	0.487	0.510
5	10	50	10												
5	14	5	10												
5	14	10	10	0.850	0.846	0.848	0.824	0.864	0.846	0.941	0.819	0.871	0.878	0.984	0.899
5	14	30	10	0.996	0.994	0.958	1.074	1.000	1.004						
5	18	5	10												
5	18	10	10	0.704	0.770	0.660	0.712	0.690	0.707	0.516	0.510	0.474	0.425	0.486	0.482
5	18	30	10	1.082	1.068	1.076	1.020	1.080	1.065	0.913	0.882	0.837	0.824	0.917	0.875
5	20	5	10												
5	20	10	10	0.612	0.636	0.744	0.862	0.850	0.741	0.434	0.279	0.563	0.742	0.742	0.552
5	20	30	10	0.838	0.860	0.798	0.822	0.866	0.837	0.584	0.506	0.558	0.572	0.585	0.561

AT Energy 10J				Width (mm)						Height (mm)					
Vmm/sec	width ms	freq(Hz)	Energy(J)	w1	w2	w3	w4	w5	AV	h1	h2	h3	h4	h5	AV
10	2	5	10												
10	2	10	10												
10	2	30	10	0.690	0.864	0.830	0.814	0.846	0.809	0.556	0.446	0.485	0.574	0.434	0.499
10	2	50	10	0.972	0.996	0.970	0.896	0.916	0.950	0.512	0.547	0.582	0.727	0.649	0.603
10	6	5	10												
10	6	10	10												
10	6	30	10	0.752	0.802	0.814	0.814	0.818	0.800	0.512	0.498	0.493	0.452	0.445	0.480
10	6	50	10	0.856	0.874	0.894	0.858	0.854	0.867	0.546	0.604	0.505	0.380	0.463	0.500
10	10	5	10												
10	10	10	10												
10	10	30	10	0.766	0.698	0.692	0.726	0.724	0.721	0.338	0.223	0.228	0.280	0.355	0.285
10	10	50	10	0.930	0.820	0.770	0.852	0.888	0.852	0.558	0.458	0.418	0.414	0.441	0.458
10	14	5	10												
10	14	10	10												
10	14	30	10	0.924	0.856	0.884	0.886	0.826	0.875	0.708	0.729	0.700	0.693	0.687	0.703
10	18	5	10												
10	18	10	10												
10	18	30	10	0.734	0.798	0.832	0.852	0.862	0.816	0.473	0.457	0.567	0.667	0.674	0.568
10	20	5	10												
10	20	10	10												
10	20	30	10	0.836	0.882	0.858	0.914	0.876	0.873	0.626	0.585	0.621	0.674	0.777	0.657

AT Energy 10J				Width (mm)						Height (mm)					
Vmm/sec	width ms	freq(Hz)	Energy(J)	w1	w2	w3	w4	w5	AV	h1	h2	h3	h4	h5	AV
15	2	5	10												
15	2	10	10												
15	2	30	10	0.790	0.838	0.688	0.804	0.774	0.779	0.260	0.239	0.296	0.369	0.448	0.322
15	2	50	10	0.802	0.904	0.838	0.874	0.782	0.840	0.558	0.512	0.613	0.581	0.754	0.604
15	6	5	10												
15	6	10	10												
15	6	30	10	0.746	0.774	0.702	0.698	0.718	0.728	0.417	0.213	0.230	0.299	0.307	0.293
15	6	50	10	0.832	0.900	0.826	0.982	1.018	0.912	0.622	0.601	0.641	0.685	0.731	0.656
15	10	5	10												
15	10	10	10												
15	10	30	10	0.832	0.852	0.848	0.814	0.828	0.835						
15	10	50	10	0.908	0.960	1.004	0.978	0.962	0.962	0.722	0.712	0.760	0.824	0.934	0.790
15	14	5	10												
15	14	10	10												
15	14	30	10	0.602	0.644	0.676	0.738	0.726	0.677	0.403	0.478	0.390	0.419	0.601	0.458
15	18	5	10												
15	18	10	10												
15	18	30	10	0.682	0.712	0.790	0.750	0.738	0.734	0.522	0.454	0.420	0.379	0.458	0.447
15	20	5	10												
15	20	10	10												
15	20	30	10	0.688	0.692	0.640	0.596	0.614	0.646	0.495	0.439	0.446	0.267	0.317	0.393

AT Energy 10J				Width (mm)						Height (mm)					
Vmm/sec	width ms	freq(Hz)	Energy(J)	w1	w2	w3	w4	w5	AV	h1	h2	h3	h4	h5	AV
20	2	5	10												
20	2	10	10												
20	2	30	10												
20	2	50	10	0.652	0.726	0.586	0.730	0.748	0.688	0.540	0.451	0.447	0.406	0.389	0.447
20	6	5	10												
20	6	10	10												
20	6	30	10	0.720	0.582	0.618	0.600	0.592	0.622	0.404	0.314	0.334	0.313	0.321	0.337
20	6	50	10	0.764	0.748	0.794	0.794	0.738	0.768	0.637	0.562	0.574	0.540	0.523	0.567
20	10	5	10												
20	10	10	10												
20	10	30	10	0.736	0.698	0.668	0.646	0.728	0.695	0.654	0.617	0.454	0.610	0.661	0.599
20	10	50	10	0.732	0.764	0.762	0.840	0.754	0.770	0.665	0.670	0.626	0.660	0.657	0.656
20	14	5	10												
20	14	10	10												
20	14	30	10	0.704	0.748	0.796	0.824	0.826	0.780	0.586	0.708	0.805	0.812	0.858	0.754
20	18	5	10												
20	18	10	10												
20	18	30	10	0.914	0.746	0.652	0.714	0.762	0.758	0.000	0.471	0.412	0.405	0.370	0.332
20	20	5	10												
20	20	10	10												
20	20	30	10	0.714	0.668	0.660	0.702	0.750	0.699	0.602	0.638	0.531	0.563	0.479	0.563

AT 20J				Width (mm)						Height (mm)					
V mm/s	width ms	freq hz	Energy J	1	2	3	4	5	AV	h1	h2	h3	h4	h5	AV
1	2	5	20												
1	2	10	20												
1	6	5	20												
1	6	10	20												
1	10	5	20	1.046	1.006	1.124	1.170	1.258	1.121	0.483	0.369	0.356	0.319	0.406	0.387
1	10	10	20	1.466	1.510	1.510	1.572	1.550	1.522	0.472	0.482	0.447	0.449	0.451	0.460
1	14	5	20	0.964	0.958	1.160	1.266	1.164	1.102	0.391	0.393	0.244	0.198	0.177	0.281
1	14	10	20												
1	18	5	20	0.754	0.752	0.754	0.852	0.828	0.788						
1	18	10	20												
1	20	5	20	0.902	0.840	0.882	0.952	0.944	0.904	0.747	0.628	0.545	0.563	0.465	0.590
1	20	10	20												

AT 20J				Width (mm)						Height (mm)					
V mm/s	width ms	freq hz	Energy J	1	2	3	4	5	AV	h1	h2	h3	h4	h5	AV
5	2	5	20												
5	2	10	20												
5	6	5	20	0.676	0.786	0.826	0.778	0.718	0.757	0.423	0.393	0.399	0.370	0.355	0.388
5	6	10	20	0.874	0.846	0.946	0.964	0.986	0.923	0.659	0.560	0.422	0.416	0.411	0.494
5	10	5	20	0.780	0.724	0.854	0.816	0.828	0.800	0.431	0.368	0.306	0.311	0.276	0.338
5	10	10	20	0.914	0.916	0.910	0.920	0.920	0.916	0.457	0.444	0.485	0.477	0.473	0.467
5	14	5	20	0.842	0.752	0.814	0.756	0.812	0.795	0.650	0.603	0.581	0.601	0.652	0.617
5	14	10	20	0.874	0.808	0.800	0.844	0.800	0.825	0.575	0.483	0.402	0.397	0.479	0.467
5	18	5	20	0.858	0.780	0.764	0.860	0.922	0.837						
5	18	10	20	0.824	0.924	0.856	0.830	0.830	0.853						
5	20	5	20												
5	20	10	20	0.908	0.890	0.732	0.820	0.778	0.826	0.754	0.655	0.625	0.579	0.518	0.626

AT 20J				Width (mm)						Height (mm)					
Vmm/s	width ms	freq hz	Energy J	1	2	3	4	5	AV	h1	h2	h3	h4	h5	AV
10	2	5	20												
10	2	10	20												
10	6	5	20												
10	6	10	20	0.702	0.774	0.846	0.912	0.854	0.818	0.257	0.312	0.298	0.302	0.405	0.315
10	10	5	20												
10	10	10	20	0.724	0.760	0.742	0.754	0.682	0.732	0.540	0.499	0.421	0.498	0.536	0.499
10	14	5	20												
10	14	10	20												
10	18	5	20												
10	18	10	20	0.682	0.726	0.760	0.736	0.732	0.727						
10	20	5	20												
10	20	10	20	0.860	0.826	0.752	0.742	0.742	0.784	0.857	0.782	0.660	0.643	0.734	0.735

AT 20J				Width (mm)						Height (mm)					
Vmm/s	width ms	freq hz	Energy J	1	2	3	4	5	AV	h1	h2	h3	h4	h5	AV
15	2	5	20												
15	2	10	20												
15	6	5	20												
15	6	10	20												
15	10	5	20												
15	10	10	20												
15	14	5	20												
15	14	10	20												
15	18	5	20												
15	18	10	20												
15	20	5	20												
15	20	10	20												

AT 20J				Width (mm)						Height (mm)					
Vmm/s	width ms	freq hz	Energy J	1	2	3	4	5	AV	h1	h2	h3	h4	h5	AV
20	2	5	20												
20	2	10	20												
20	6	5	20												
20	6	10	20												
20	10	5	20												
20	10	10	20												
20	14	5	20												
20	14	10	20												
20	18	5	20												
20	18	10	20												
20	20	5	20												
20	20	10	20												

AT 30J				Width in mm						Height in mm					
V(mm/sec)	width ms	freq hz	Energy(J)	1	2	3	4	5	AV	h1	h2	h3	h4	h5	AV
1	6	5	30												
1	6	10	30	1.13	1.12	1.16	1.16	1.16	1.14						
1	10	5	30												
1	10	10	30	0.94	0.91	0.91	1.03	1.01	0.96	0.62	0.6	0.64	0.65	0.64	0.63
1	14	5	30												
1	14	10	30	0.87	0.85	0.9	0.86	0.92	0.88	0.65	0.5	0.49	0.49	0.6	0.55
1	18	5	30												
1	18	10	30	1.47	1.39	1.42	1.44	1.4	1.42						
1	20	5	30												
1	20	10	30												

AT 30J				Width in mm						Height in mm					
V(mm/sec)	width ms	freq hz	Energy(J)	1	2	3	4	5	AV	h1	h2	h3	h4	h5	AV
5	6	5	30	0.94	1.12	1.05	1.15	1.02	1.05						
5	6	10	30	0.84	0.87	0.85	0.85	0.88	0.86	0.5	0.5	0.44	0.41	0.38	0.45
5	10	5	30	1.14	1.25	1.14	1.09	1.06	1.13	0.34	0.28	0.27	0.29	0.32	0.3
5	10	10	30	1.24	0.97	0.86	0.94	0.9	0.98	0.33	0.32	0.3	0.35	0.35	0.33
5	14	5	30	1.27	1.32	1.36	1.35	1.31	1.32	0.26	0.26	0.24	0.28	0.29	0.27
5	14	10	30	0.84	0.8	0.83	0.87	0.8	0.83						
5	18	5	30	0.98	1.01	1.02	1.06	1.06	1.03						
5	18	10	30	0.84	0.82	0.91	0.84	0.84	0.85						
5	20	5	30	0.92	0.97	1.06	1	0.95	0.98						
5	20	10	30												

AT 30J				Width in mm						Height in mm					
V(mm/sec)	width ms	freq hz	Energy(J)	1	2	3	4	5	AV	h1	h2	h3	h4	h5	AV
10	6	5	30	0.79	0.73	0.84	0.77	0.76	0.78						
10	6	10	30												
10	10	5	30	0.78	0.8	0.8	0.81	0.78	0.8						
10	10	10	30												
10	14	5	30	1	1.13	1.1	0.99	1	1.04	0.34	0.32	0.27	0.34	0.41	0.34
10	14	10	30												
10	18	5	30	0.82	0.89	0.88	0.94	0.95	0.89	0.47	0.45	0.48	0.37	0.36	0.42
10	18	10	30												
10	20	5	30												
10	20	10	30												

AT 30J				Width in mm						Height in mm					
V(mm/sec)	width ms	freq hz	Energy(J)	1	2	3	4	5	AV	h1	h2	h3	h4	h5	AV
15	6	5	30	0.81	0.83	0.96	0.98	0.92	0.9						
15	6	10	30												
15	10	5	30												
15	10	10	30												
15	14	5	30	0.9	0.97	0.92	0.83	0.97	0.92	0.52	0.51	0.51	0.44	0.48	0.49
15	14	10	30												
15	18	5	30												
15	18	10	30												
15	20	5	30												
15	20	10	30												

V(mm/sec)	AT 30J width ms	freq hz	Energy(J)	Width in mm						Height in mm					
				1	2	3	4	5 AV	h1	h2	h3	h4	h5	AV	
20	6	5	30												
20	6	10	30												
20	10	5	30												
20	10	10	30												
20	14	5	30												
20	14	10	30												
20	18	5	30												
20	18	10	30												
20	20	5	30												
20	20	10	30												

AT 60J				Width in mm						Height in mm					
Vmm/sec	width ms	freq hz	Energy(J)	1	2	3	4	5	AV	h1	h2	h3	h4	h5	AV
1	6	5	60												
1	10	5	60												
1	14	5	60												
1	18	5	60												
1	20	5	60												

AT 60J				Width in mm						Height in mm					
Vmm/sec	width ms	freq hz	Energy(J)	1	2	3	4	5	AV	h1	h2	h3	h4	h5	AV
5	6	5	60												
5	10	5	60												
5	14	5	60	1.04	1.15	1.09	1.16	1.22	1.13						
5	18	5	60	1.21	1.35	1.26	1.41	1.23	1.29						
5	20	5	60												

AT 60J				Width in mm						Height in mm					
Vmm/sec	width ms	freq hz	Energy(J)	1	2	3	4	5	AV	h1	h2	h3	h4	h5	AV
10	6	5	60												
10	10	5	60												
10	14	5	60												
10	18	5	60												
10	20	5	60												

AT 60J				Width in mm						Height in mm					
Vmm/sec	width ms	freq hz	Energy(J)	1	2	3	4	5	AV	h1	h2	h3	h4	h5	AV
15	6	5	60												
15	10	5	60												
15	14	5	60							0.29	0.26	0.29	0.27	0.37	0.3
15	18	5	60							0.35	0.29	0.33	0.37	0.39	0.34
15	20	5	60												

AT 60J				Width in mm						Height in mm					
Vmm/sec	width ms	freq hz	Energy(J)	1	2	3	4	5	AV	h1	h2	h3	h4	h5	AV
20	6	5	60												
20	10	5	60												
20	14	5	60												
20	18	5	60												
20	20	5	60												